NAVAL POSTGRADUATE SCHOOL
Monterey, California

THESIS

EVALUATION OF THE CMARC PANEL CODE SOFTWARE SUITE FOR THE DEVELOPMENT OF A UAV AERODYNAMIC MODEL

by

Stephen J. Pollard

June, 1997

Thesis Advisor: Max F. Platzer
Co-Advisor: Ismail H. Tuncer

Approved for public release; distribution is unlimited.

REPORT DOCUMENTATION PAGE

Form Approved OMB No. 0704-0188

1. AGENCY USE ONLY *(Leave blank)*	2. REPORT DATE	3. REPORT TYPE AND DATES COVERED
	June 1997	Master's Thesis

4. TITLE AND SUBTITLE
EVALUATION OF THE CMARC PANEL CODE SOFTWARE SUITE FOR THE DEVELOPMENT OF A UAV AERODYNAMIC MODEL

5. FUNDING NUMBERS

6. AUTHOR(S)
Pollard, Stephen J.

7. PERFORMING ORGANIZATION NAME(S) AND ADDRESS(ES)
Naval Postgraduate School
Monterey, CA 93943-5000

8. PERFORMING ORGANIZATION REPORT NUMBER

9. SPONSORING / MONITORING AGENCY NAME(S) AND ADDRESS(ES)

10. SPONSORING / MONITORING AGENCY REPORT NUMBER

11. SUPPLEMENTARY NOTES
The views expressed in this thesis are those of the author and do not reflect the official policy or position of the Department of Defense or the U.S. Government.

12a. DISTRIBUTION / AVAILABILITY STATEMENT
Approved for public release; distribution unlimited.

12b. DISTRIBUTION CODE

13. ABSTRACT *(maximum 200 words)*

The CMARC panel code is evaluated to verify its accuracy and suitability for the development of an aerodynamic model of the Naval Postgraduate School (NPS) FROG Unmanned Air Vehicle (UAV). CMARC is a DOS personal computer based version of the NASA Panel Method Ames Research Center (PMARC) panel code. The core processing algorithms in CMARC are equivalent to PMARC. CMARC enhancements include improved memory management and command line functionality. Both panel codes solve for inviscid, incompressible flow over complex three-dimensional bodies using potential flow theory. Emphasis is first placed on verifying CMARC against the PMARC and NPS Unsteady Potential Flow (UPOT) panel codes. CMARC boundary layer calculations are then compared to experimental data for an inclined prolate spheroid. Finally, a complex three-dimensional panel model is developed for aerodynamic modeling of the FROG UAV. CMARC off-body flow field calculations are used to generate static-source and angle-of-attack vane position corrections. Position corrections are provided in look-up table and curve fit formats. Basic longitudinal and lateral-directional stability derivatives are also developed with CMARC data. CMARC derived stability derivatives are sufficiently accurate for incorporation into an initial aerodynamic model. Adjustments through analysis of flight test data may be required. Future CMARC studies should concentrate on the development of the damping and control power derivatives.

14. SUBJECT TERMS
Unmanned Aerial Vehicles, UAV, CMARC, PMARC, UPOT, Panel Code, Stability Derivatives, Boundary Layer Code, Computational Fluid Dynamics, CFD

15. NUMBER OF PAGES 151

16. PRICE CODE

17. SECURITY CLASSIFICATION OF REPORT	18. SECURITY CLASSIFICATION OF THIS PAGE	19. SECURITY CLASSIFICATION OF ABSTRACT	20. LIMITATION OF ABSTRACT
Unclassified	Unclassified	Unclassified	UL

NSN 7540-01-280-5500

Standard Form 298 (Rev. 2-89)
Prescribed by ANSI Std. 239-18

EVALUATION OF THE CMARC PANEL CODE SOFTWARE SUITE FOR THE DEVELOPMENT OF A UAV AERODYNAMIC MODEL

Stephen J. Pollard
Lieutenant Commander, United States Navy
B.S., United States Naval Academy, 1982

Submitted in partial fulfillment of the
requirements for the degree of

MASTER OF SCIENCE IN AERONAUTICAL ENGINEERING

from the

NAVAL POSTGRADUATE SCHOOL

June 1997

Author: S J Pollard
Stephen J. Pollard

Approved by: Max F. Platzer
Max F. Platzer, Thesis Advisor

Ismail H. Tuncer
Ismail H. Tuncer, Co-Advisor

Daniel J. Collins
Daniel J. Collins, Chairman
Department of Aeronautics and Astronautics

ABSTRACT

The CMARC panel code is evaluated to verify its accuracy and suitability for the development of an aerodynamic model of the Naval Postgraduate School (NPS) FROG Unmanned Air Vehicle (UAV). CMARC is a DOS personal computer based version of the NASA Panel Method Ames Research Center (PMARC) panel code. The core processing algorithms in CMARC are equivalent to PMARC. CMARC enhancements include improved memory management and command line functionality. Both panel codes solve for inviscid, incompressible flow over complex three-dimensional bodies using potential flow theory. Emphasis is first placed on verifying CMARC against the PMARC and NPS Unsteady Potential Flow (UPOT) panel codes. CMARC boundary layer calculations are then compared to experimental data for an inclined prolate spheroid. Finally, a complex three-dimensional panel model is developed for aerodynamic modeling of the FROG UAV. CMARC off-body flow field calculations are used to generate static-source and angle-of-attack vane position corrections. Position corrections are provided in look-up table and curve fit formats. Basic longitudinal and lateral-directional stability derivatives are also developed with CMARC data. CMARC derived stability derivatives are sufficiently accurate for incorporation into an initial aerodynamic model. Adjustments through analysis of flight test data may be required. Future CMARC studies should concentrate on the development of the damping and control power derivatives.

TABLE OF CONTENTS

I. INTRODUCTION

A. BACKGROUND

Computational fluid dynamics (CFD) is increasingly used as a design and analysis tool. As the price of computer hardware drops and computational power increases, CFD becomes more attractive to a larger audience. CFD tools range from the high end three-dimensional (3D) Navier-Stokes solvers for compressible, viscous fluids to potential flow solvers for incompressible, inviscid flows. This paper discusses the development of a DOS personal computer hosted panel code model for the Naval Postgraduate School (NPS) Fiber Optic Guided (FROG) Unmanned Air Vehicle (UAV) program.

The Personal Simulation Works software suite, consisting of LOFTSMAN, CMARC and POSTMARC, is used for all aspects of the study. The software provides for panel model development, input file processing and the visualization of results. Emphasis is placed on verifying both the accuracy and suitability of the CFD programs for aerodynamic modeling.

Until recently, personal computers (PC) did not have the computational power or memory to be practical for panel code CFD programs. Things have changed with the introduction of the Pentium class PC and low cost RAM. AeroLogic capitalized on the power of the Pentium class PC and developed Personal Simulation Works (PSW). PSW is centered around the 3D low order, inviscid potential flow solver named CMARC. CMARC is a re-hosted version of NASA's Panel Method Ames Research Code (PMARC). PMARC was re-written in the C language and compiled for IBM compatible PCs. CMARC runs under the DOS operating system. CMARC will also run in a DOS window under the WINDOWS 3.x, 95 or NT operating systems. CMARC has enhanced capabilities that include; improved memory management, an expanded set of command line switches and provisions for expanded boundary layer post-processing capabilities. However, the core processing algorithms remain the same as implemented in PMARC.

LOFTSMAN, the PSW pre-processing program, is used to mesh complex 3D bodies and create input file patches. The program runs under the DOS operating system and allows the user to loft conics based 3D surfaces. The program automatically creates CMARC, PMARC or VSAERO input patches based on desired panel densities and distribution.

POSTMARC is used for flow visualization and integration of resultant forces. It runs under the Windows 3.x, 95 and NT operating systems. POSTMARC reads CMARC or PMARC output files and provides for the visualization of model geometry, wake stepping, on and off-body streamlines and surface phenomena.

B. REQUIREMENTS

The Naval Postgraduate School Aeronautics Department is integrating UAV hardware and software to demonstrate autonomous flight, trajectory tracking and automatic landing. A core requirement for flight control development is a valid aerodynamic truth model for the UAV airframe. The introduction of each new airframe requires the development of a new aerodynamic truth model. Most recently, Papageorgiou [Ref. 1] developed and tested an aerodynamic model for the NPS FROG UAV based on classical methods. His model produced a close match to flight test results in the longitudinal axis. However, the lateral-directional axis required modifications based on measured flight test data to produce acceptable results. With the availability of low cost panel code CFD capabilities, it is suggested that a panel code model of the FROG UAV is an alternative for estimating many of the stability derivatives required for an aerodynamic truth model.

Accurate pitot-static and angle-of-attack sensors are required for highly augmented flight control systems. CMARC is well suited for solving on-body static pressure distributions and off-body flow velocities over the predominately attached flow fields of fuselage fore bodies. This proves particularly useful for generating pitot static and angle of attack correction curves and look-up tables.

C. STATEMENT OF OBJECTIVES

The Naval Postgraduate School Aeronautics Department has both active CFD research and avionics development programs. The primary purpose of this investigation is to verify the accuracy and suitability of the PSW software suite while developing a panel code model for the NPS FROG UAV program. Specific objectives are as follows:

- Demonstrate panel code modeling, processing and visualization on a Pentium PC using the PSW software package.

- Verify CMARC results against PMARC.
- Investigate the CMARC integral boundary layer calculations through comparison to validated 2D CFD codes and 3D experimental data.
- Develop and analyze a panel code model for the NPS FROG UAV using PSW to estimate basic stability derivatives and produce angle-of-attack vane and pitot-static correction curves.
- Compare relative speed of CMARC hosted on 150 MHz Pentium personal computer to PMARC hosted on a Silicon Graphics Indigo^2 workstation.

II. OVERVIEW OF PERSONAL SIMULATION WORKS

A. GENERAL

Personal Simulation Works is a PC based software suite that provides for the three primary CFD requirements; 3D modeling of an aircraft (LOFTSMAN), panel code flow solver (CMARC), and post-processing of the computed flow field (POSTMARC). The software package contains three applications hosted on the IBM compatible personal computer. Each software program is discussed separately.

B. LOFTSMAN

LOFTSMAN is a 3D modeling tool that generates surface panel distributions for CMARC or PMARC input files. The program is based on conics, which allows rapid lofting of streamlined bodies such as aircraft fuselages and engine nacelles. In addition, wing and control surfaces can be designed with the extensive library of airfoil templates or with user specified coordinates. The software is well documented, including a tutorial, in the Personal Simulation Works User Guide [Ref. 2]. LOFTSMAN is primarily designed for creating new objects, but an existing airframe can be matched quite closely with just a detailed three-view drawing that includes frame cross sections.

1. Streamlined Bodies

LOFTSMAN functionality is divided into Body Objects and Wing Objects. In general, they remain separate unless the intersection between a wing and body is required.

Body Objects are created using a family of curves called second-degree conics. Circles, ellipses, parabolas and hyperbolas are among this group. An entire fuselage is described by specifying just four lines. These are the top waterline (TW), bottom waterline (BW), the maximum breadth line (MB) and the waterline of the maximum breadth line (WW). For each line, the beginning, ending and a few points along the line are specified. Control points are also specified with a curvature factor that allows LOFTSMAN to generate a smooth conic between the points. The power of conic lofting will become evident when discussing the modeling of the complex FROG UAV fuselage in Chapter V.

2. Wings and Control Surfaces

Wings and control surfaces are easily specified in LOFTSMAN using a short input file created with any text editor. The file specifies root, intermediate and tip rib section, location, axis, chord and incidence. LOFTSMAN then fairs a smooth surface through the rib sections. Washout is specified by varying the incidence of the root and tip ribs. Sweep-back is controlled by staggering the tip rib location with respect to the root rib. Once the general wing surface is specified, control surfaces such as ailerons, flaps and elevators can be deflected and meshed.

3. Patches

LOFTSMAN automatically meshes 3D surfaces and creates patches for CMARC/PMARC input files. The distinction between a mesh and a patch is important. A mesh is a set of quadrilateral and triangular panels that represent the surface of a wing or body. When the set of panels is organized and formatted to create a sub-component portion of a CMARC or PMARC input file, it is called a patch.

A body or wing surface is first meshed at a density specified by the user. Cosine and half-cosine spacing are among the compression options. After meshing the object, one saves it to a text file as a formatted patch. One then opens the patch file with any text editor and copies/pastes the patch text into the appropriate location in the CMARC input file.

Each control surface deflection requires a separate mesh and formatted patch. For instance, to evaluate roll performance one needs to separately mesh an upward aileron deflection on the right wing and a downward deflection on the left wing. If multiple deflections of a single control surface are required, each deflection must be meshed separately.

C. CMARC

CMARC is the C version of the Panel Method NASA Ames Research Center (PMARC) low order, 3D panel code. Inviscid, irrotational, incompressible, potential flow is assumed. Low order means that source and doublet strength distribution is constant across a panel. There is no attempt to match the source or doublet strength of an adjacent

panel at a common edge. Advanced features include internal flow modeling and time stepping wake models.

PMARC version 12.19 was released as FORTRAN 77 source code in 1992. CMARC was rewritten in the C language and compiled for hosting on IBM compatible personal computers by AeroLogic, Inc. The program runs under the DOS operating system. It will also run in a DOS window from Windows 3.1, 95 or NT. Enhanced features include command line options and flexible memory management. Command line options simplify batch processing by adding an extensive set of switches that can be set external to the CMARC input file. Flexible memory management provides for the automatic sizing of arrays without having to recompile the source code.

D. POSTMARC

POSTMARC is a Windows post-processing program for the visualization of CMARC and PMARC output files. Capabilities include body geometry, wake stepping, surface pressure and streamline visualization. POSTMARC also provides the capability to integrate pressure and skin friction forces over the model geometry. This proves particularly useful when one desires to recalculate loads around a different center of gravity.

An interesting feature for design work integrates panel surface area to obtain total wetted area. After lofting a new geometry in LOFTSMAN, a quick check of geometry is made by running CMARC with the -g command line toggle. The total wetted area is then checked in POSTMARC. This function is particularly useful when working to reduce skin friction drag.

Versions 1.17.3 and later of POSTMARC include the capability to integrate skin friction drag coefficient over the model geometry. It is important to note that a key piece of the drag equation is missing from a POSTMARC solution. CMARC provides induced drag from the surface pressure distribution and skin friction drag from the 2D boundary layer code. Skin friction is only calculated up to the point of boundary layer separation. Pressure drag due to separation, a major portion of the drag equation, is missing from a CMARC/POSTMARC solution.

In fact, if one isn't careful, POSTMARC drag calculations can be misleading. Take for instance two similar model configurations with only minor geometry differences that do not affect wetted area. It is possible for the model with more flow separation to

have less skin friction drag because there is no CMARC output for skin friction coefficient after the boundary layer code predicts separation. During iterative design work, this could lead to the incorrect conclusion that the design team is reducing overall drag. Perhaps a better function for LOFTSMAN than integrated skin friction drag would be a function that predicts the percentage of attached flow and laminar flow. Iterative design changes could be made that maximize laminar flow and minimize separated flow.

III. CMARC PANEL CODE THEORY

A. POTENTIAL FLOW PANEL CODE THEORY (CMARC/PMARC)

Potential flow theory involves the superposition of sources and doublets to generate the desired flow field around a 3D body. It assumes inviscid, irrotational and incompressible flow. As such, valid solutions are only obtained at low Mach numbers and for flow fields without large areas of separation.

The basic concept of panel methods, as outlined by Bertin and Smith [Ref. 3], requires the modeling of the desired 3D configuration with a large number of quadrilateral and triangular panels representing the surface of the aircraft. A series of sources, doublets and vortices is then distributed on each panel. Superposition allows the simultaneous computation of the singularity strengths required to satisfy flow tangency on the surface. The inviscid, irrotational and incompressible flow field represented by the superposition of sources and doublets satisfies the Laplace equation:

$$\nabla^2\Phi = 0 \qquad 3.1$$

Using Green's Theorem, the potential at any point P in the flow is represented by:

$$\Phi_P = \frac{1}{4\pi}\iint_{S+W}(\Phi - \Phi_i)\bar{n}\nabla\left(\frac{1}{r}\right)dS - \frac{1}{4\pi}\iint_{S+W}\left(\frac{1}{r}\right)\bar{n}\cdot(\nabla\Phi - \nabla\Phi_i)dS \qquad 3.2$$

Where $(\Phi - \Phi_i)$ represents the potential from the doublet distribution and $\bar{n}\cdot(\nabla\Phi - \nabla\Phi_i)$ represents the potential from the source distributions.

CMARC is a low order panel code that assumes constant source and doublet strength distributions across each panel. Figure 3.1 shows a panel layout for a generic 3D wing fuselage configuration. It is important to note that for a 3D solution, there is an equivalence to surface doublet and surface vortex distributions. CMARC implements source and doublet distributions.

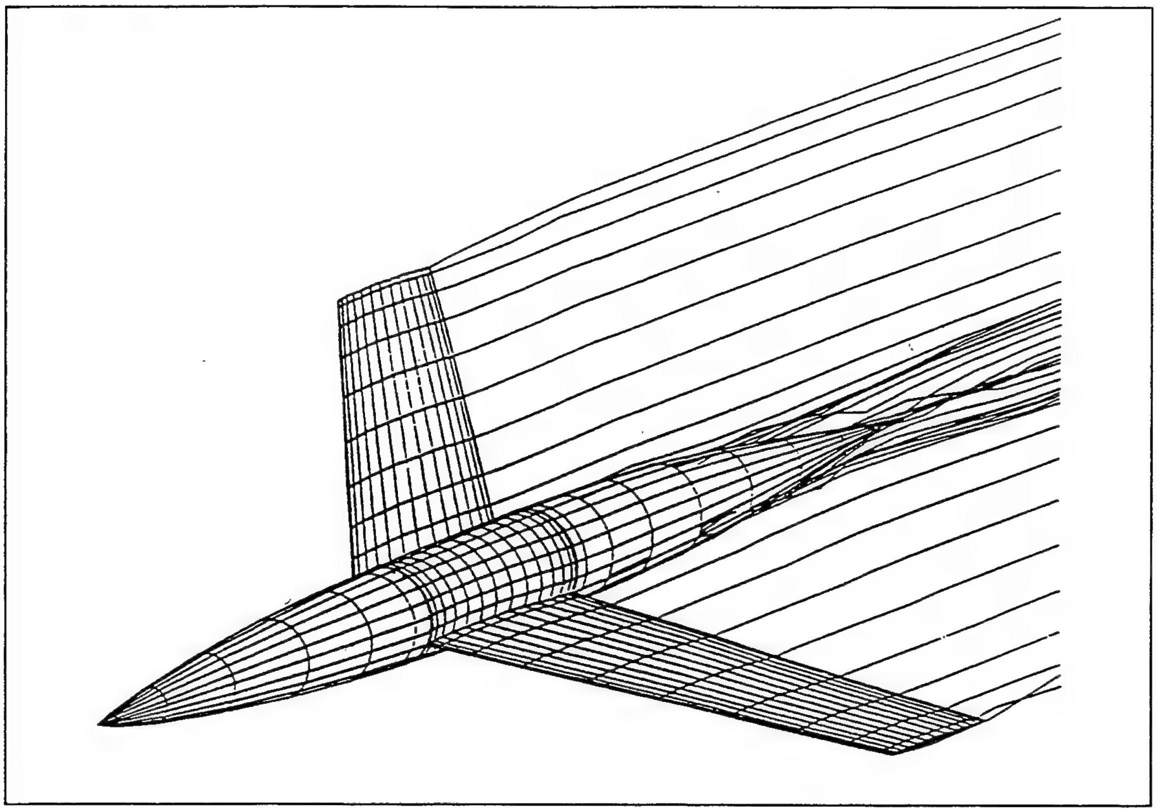

Figure 3.1 Typical Wing-Body Panel Code Configuration, from Ref. [4].

As mentioned previously, the general boundary condition imposed is tangential flow at the surface. CMARC, as outlined in Ref. [2], allows the modification of this boundary condition on individual panels or groups of panels. A normal surface velocity distribution may be specified to simulate flow into or out of ducts.

In order to produce lift, a potential flow panel code requires a method to implement the Kutta condition. As noted in Anderson [Ref. 5], the Kutta condition at the trailing edge implies that the circulation, Γ, around an airfoil is such that the flow exits the trailing edge smoothly. In addition, the velocities leaving the top and bottom surfaces are finite and equal in magnitude and direction.

Panel codes impose the Kutta condition by the shedding of wake panels along the trailing edges or separation lines. Wake panels are similar to a surface panel with only a doublet distribution. The doublet strength of the attached wake panel equals the difference in doublet strengths of the two adjacent surface panels.

The CMARC core panel code processing engine is functionally equivalent to the PMARC panel code module. The implemented equations are well documented by Ashby et al. [Ref. 4]. The PMARC documentation includes a wing-body combination, shown in Figure 3.1, evaluated by PMARC with good correlation to experimental data. The results are shown in Figures 3.2 and 3.3. In addition, Lambert [Ref. 6] compared PMARC panel code results to several theoretical and experimental test cases with good correlation at low angle-of-attack. Sensitivity to wake placement is highlighted by his studies.

Wake positioning can have a large influence on potential flow solutions. A wake is obviously attached to the trailing edge of wings and control surfaces with sharp, thin trailing edges to produce the Kutta condition. However, wake positioning on streamlined fuselages, missile airframes and nacelles is more of an art than science. Recently, Tuncer and Platzer [Ref. 7] investigated generalized wake placement techniques for cylindrical bodies of revolution with good correlation to experimental data at up to 20 degrees angle-of-attack. The techniques are used in this study with success for the verification of CMARC calculations for flow over an inclined 6:1 prolate spheroid.

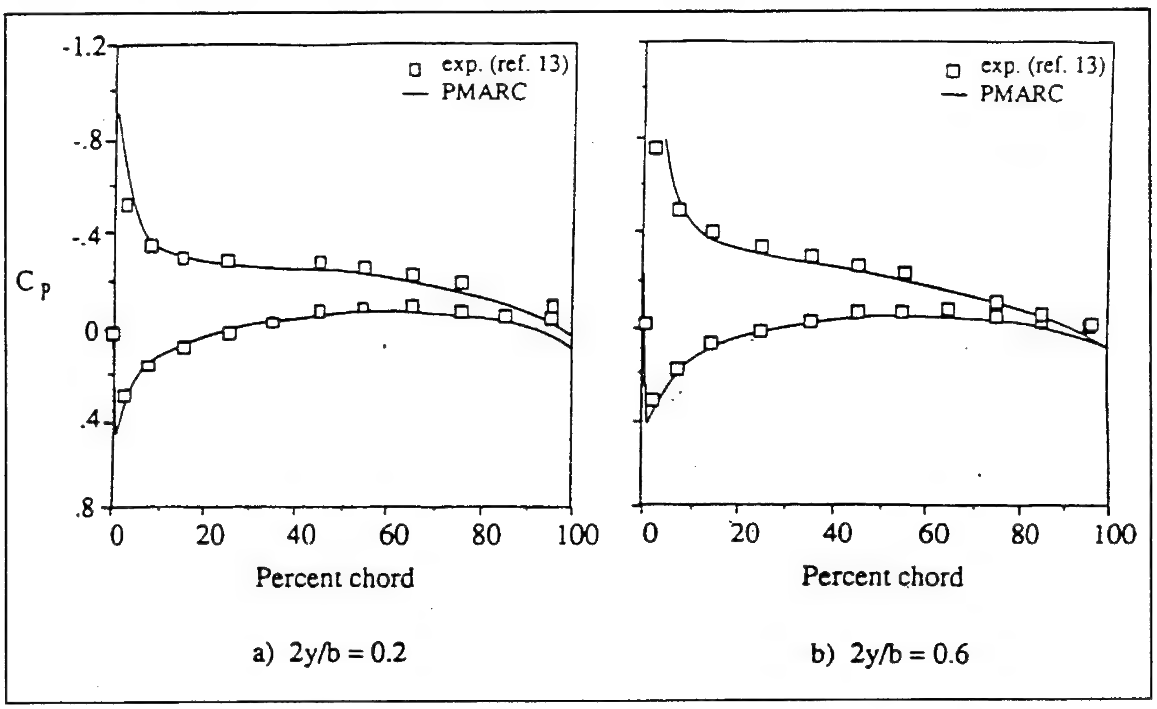

Figure 3.2 Comparison of Experimental Data and PMARC Results for Two Spanwise Stations of the Wing/Body ($\alpha = 4°$), from Ref. [4].

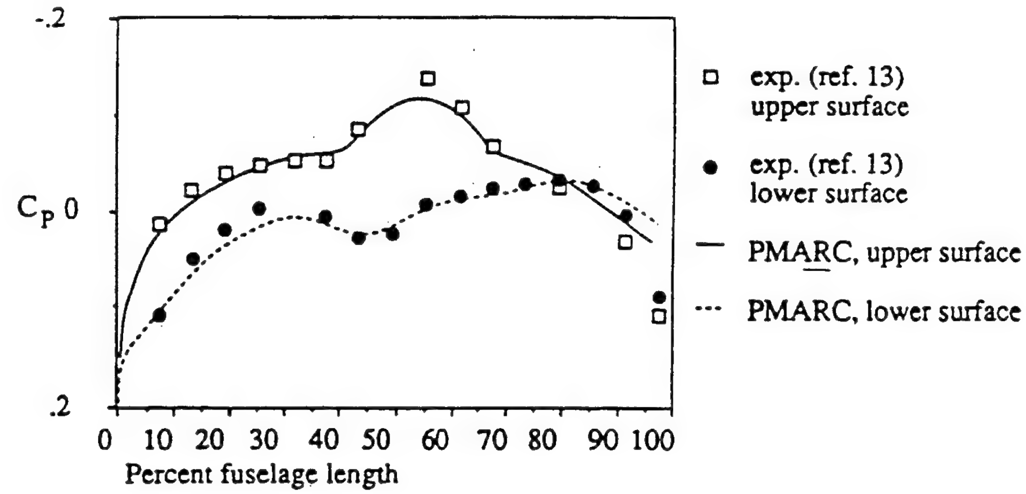

Figure 3.3 Comparison of Experimental Data and PMARC Along the Fuselage Centerline of the Wing/Body Configuration ($\alpha = 4°$), from Ref. [4].

B. CMARC BOUNDARY LAYER ANALYSIS THEORY

CMARC and PMARC use the same two-dimensional integral method to calculate boundary layer characteristics along a surface streamline. A transition model automatically switches from laminar to turbulent calculations. The developers of the PMARC code chose a 2D integral routine over a 3D finite difference grid method due to speed and robustness of the calculations [Ref. 4]. Building a finite difference grid is a difficult and time consuming process requiring the user to develop grids over complex 3D surfaces. In addition, boundary layer calculation times can easily exceed that required for the basic potential flow solution. Reference [8] gives a good outline of three-dimensional finite difference methods.

The CMARC and PMARC User's Guides [Refs. 2 and 4] contain detailed discussions on the development of the CMARC/PMARC boundary layer code starting from the two-dimensional momentum equation:

$$\frac{d\theta}{d\eta} + (2+H)*\frac{\theta}{U}\frac{dU}{d\eta} = \frac{1}{2}C_f \tag{3.3}$$

The momentum integral equation is numerically integrated along a surface streamline. The derivation leading to Equation 3.3 is developed in Appendix A for completeness.

The laminar region of the boundary layer is modeled by numerically integrating the following exact differential equation. The equation is solved iteratively through numerical integration along a streamline starting at a stagnation point [Ref. 4]:

$$\theta(\eta)^2 = \frac{0.45\nu}{U(\eta)^6}\int_0^\eta \left(1 + 2.222g(K,\mu)\right)U(\eta)^5\,d\eta + \theta(0)^2\left(\frac{U(0)}{U(\mu)}\right)^6 \tag{3.4}$$

Where: U - velocity at outer edge of boundary layer

θ - momentum thickness

$K = \frac{\theta^2}{\nu}\frac{dU}{d\eta}$

η - generalized coordinate along a streamline

The value g(K,u) is based on exact solutions for a number of pressure distributions. Initial work was conducted by Thwaites with improvements by Curle [Ref. 9]:

$$g(K,\mu) = F_0(K) - \mu G_0(K) - 0.45 + 6K \tag{3.5}$$

CMARC uses an empirical transition model based on the average pressure gradient, $\overline{K}$, for predicting laminar to turbulent transition. The following relations are used to calculate the transition point [Ref. 4]:

$$\overline{K} = \frac{\int_{\eta_{ins}}^{\eta} K d\eta}{\eta - \eta_{ins}} \tag{3.6}$$

Where η_{ins} is the streamline coordinate at instability. And, K is the local pressure gradient at boundary layer instability [Ref. 4]:

$$K = -0.4709 + 0.11066 * \ln(\mathrm{Re}_\theta) + 0.0058591 * \ln^2(\mathrm{Re}_\theta) \qquad (0 \le \mathrm{Re}_\theta \le 650)$$
$$K = 0.69412 - 0.23992 * \ln(\mathrm{Re}_\theta) + 0.0205 * \ln^2(\mathrm{Re}_\theta) \qquad (650 < \mathrm{Re}_\theta \le 10000) \tag{3.7}$$

The local Reynolds number at transition is correlated to $\overline{K}$ with the following expressions [Ref. 4]:

$$\overline{K} = -0.0925 + 0.00007 * \mathrm{Re}_\theta \qquad (0 \le \mathrm{Re}_\theta \le 750)$$
$$\overline{K} = -0.12571 + 0.000114286 * \mathrm{Re}_\theta \qquad (750 < \mathrm{Re}_\theta \le 1100) \tag{3.8}$$
$$\overline{K} = 1.59381 - 0.45543 * \ln(\mathrm{Re}_\theta) + 0.032534 * \ln^2(\mathrm{Re}_\theta) \qquad (1100 < \mathrm{Re}_\theta \le 3000)$$

At transition, the initial turbulent shape factor, H, is given by the following empirical formula that is a fit to data developed by Coles [Ref. 9]:

$$H = \frac{1.4754}{\log_{10}(\mathrm{Re}_\theta)} + 0.9698 \tag{3.9}$$

Provisions are made to check for turbulent reattachment if laminar separation is encountered. At laminar separation, a point calculation is made to determine if the boundary layer will reattach. If reattachment is predicted, the boundary layer code immediately switches to turbulent calculations. No attempt is made to model the laminar separation bubble or provide a transition length. After laminar separation is predicted, the following empirical relations are used to determine if reattachment occurs [Ref. 4]:

$$K = 0.0227 - 0.007575 * \mathrm{Re}_\theta - 0.000001157 * \mathrm{Re}_\theta^{\,2} \qquad (\mathrm{Re}_\theta \geq 125)$$

$$K = -0.09 \qquad (\mathrm{Re}_\theta < 125) \qquad 3.10$$

The boundary layer code in CMARC uses a point transition model. No attempt is made to model a more representative transition length. Turbulent calculations begin at transition using the Nash-Hicks model [Ref. 4]. Calculations continue along the streamline until turbulent separation is predicted or the end of the streamline is reached. No boundary layer data is available after separation.

The authors of PMARC caveat that their boundary layer calculations are quite accurate for predominately 2D flow but break down in regions of large cross flow near separation. This premise will be first tested by comparing predominately 2D flow over the inboard region of a high aspect ratio wing to the finite difference calculations performed by the Naval Postgraduate School Unsteady Potential Flow Code (UPOT). Then a comparison is made to experimental data for flow over an inclined prolate spheroid. The 6:1 prolate spheroid is chosen because of the availability of extensive experimental data. In addition, three-dimensional flow around the prolate spheroid is similar to flow around a streamlined slender fuselage.

IV. CMARC VERIFICATION

A. VERIFICATION OF CMARC AGAINST PMARC

The first step in CMARC verification is comparison with NASA's PMARC panel code. CMARC is PMARC-12 rewritten in C from FORTRAN. Additionally, CMARC is compiled for hosting on an IBM compatible PC. Other than some added command line functionality and significant memory management improvements, the CMARC basic panel code and boundary layer routines are equivalent to PMARC and should produce the same results. However, due to the recent fielding of CMARC, the author felt it prudent to spot check the solutions to verify equivalency.

CMARC and PMARC were both fed an identical input file for a straight NACA 2415 wing with a 6.4 aspect ratio at 5 degrees angle of attack. The input file is listed in full in Appendix C. Figures 4.1 and 4.2 show CMARC and PMARC pressure coefficients cross-plotted for chordwise and spanwise wing stations respectively. The results overlay as an identical match. Figure 4.3 and 4.4 display the boundary layer calculations for skin friction coefficient and displacement thickness. Again the results overlay. Integrated forces and moment listings were also identical. From this, it is inferred that CMARC and PMARC produce equivalent results.

Although both programs produce equivalent results, it is worthy to note that there are occasionally small, insignificant differences in floating point calculations and rounding. Some results differ by a digit in the sixth decimal place. In addition, with identical input files, there can be a difference in convergence likelihood. Occasionally, PMARC failed to converge when CMARC did. Again, floating point differences are the most likely source of the disparity. Regardless, difference in the rates of convergence were slight and relatively transparent to the user. However, in all cases CMARC was better behaved with a higher likelihood of convergence. It is concluded that CMARC and PMARC results are interchangeable.

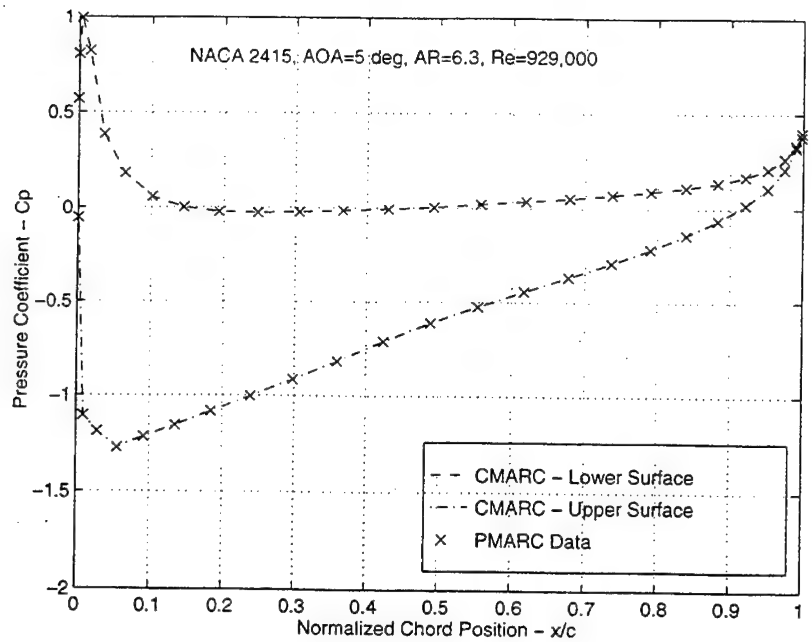

Figure 4.1 **Comparison of CMARC and PMARC Pressure Coefficients For a Chordwise Wing Station.**

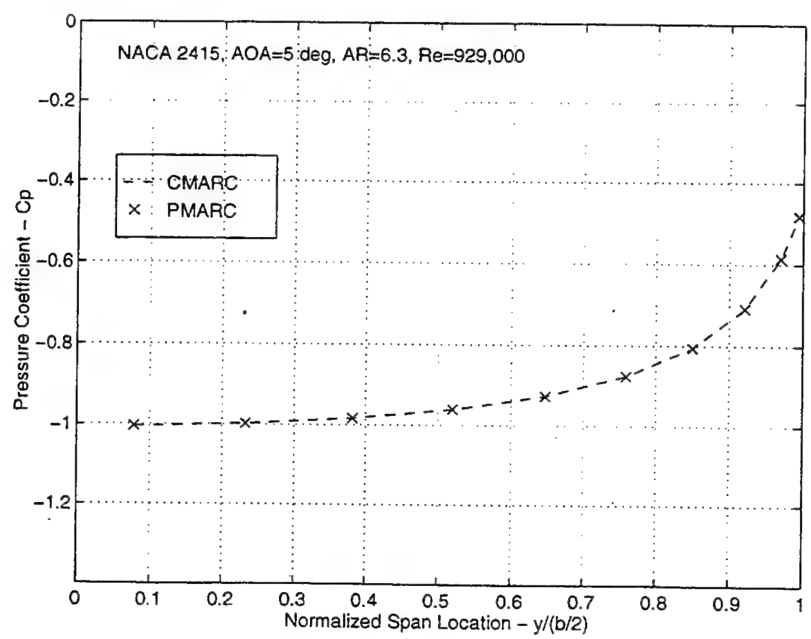

Figure 4.2 **Comparison of CMARC and PMARC Pressure Coefficients For a Spanwise Wing Station.**

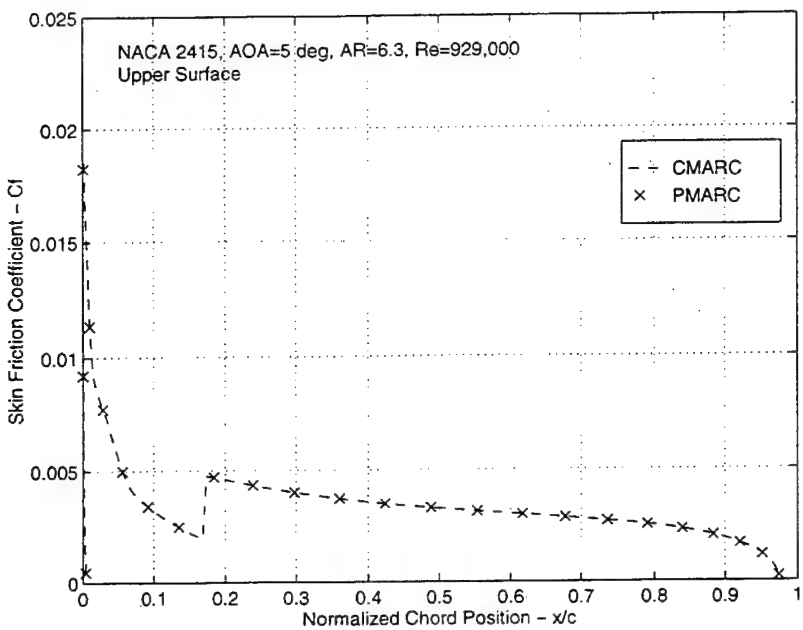

Figure 4.3 Comparison of CMARC and PMARC Skin Friction Coefficient for an Upper Wing Surface Streamline.

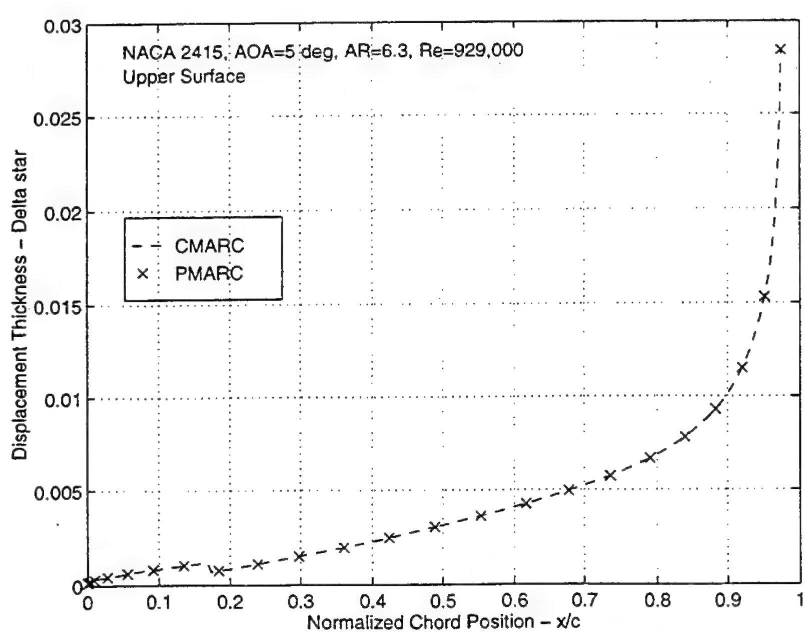

Figure 4.4 Comparison of CMARC and PMARC Boundary Layer Displacement Thickness for an Upper Wing Surface Streamline.

B. COMPARISON OF CMARC AND PMARC PROCESSING TIMES

One of the primary metrics in determining suitability of a panel code hosted on an inexpensive PC is processing time. CMARC's processing speed should be within an order of magnitude of PMARC hosted on the NPS Aeronautics Department Silicon Graphics (SGI) workstations to be of much utility. To this end, processing times were compared for identical input models ranging from 200 to 1600 panels. Comparisons were performed between a 150 MHz/48 MB Pentium PC and two configurations of networked SGI Indigo^2 workstations. One workstation was the 150 MHz/64 MB Indigo^2 (Viper) running the IRIX 5.3 operating system and the other a 250 MHz/128 MB SGI Indigo^2 (Aurora) workstation running IRIX 6.2. With both workstations, file input/output is addressed through the network to the server.

Three versions of PMARC were tested. The first version, "pmarc12" located in the local/usr/bin, was compiled in FORTRAN to run on the older IRIX 5.3 operating system. The second version, "pmarc-inram," was compiled with Dynamic Linked Libraries (DLLs) to run on the new IRIX 6.2 operating system. These first two PMARC executable codes were compiled with the "in RAM" flag selected for matrix storage. This considerably reduced hard disk accessing time. PMARC either keeps all the matrices in RAM or all on the file server depending on whether the RAM flag is when compiled. Flexible memory management allows CMARC to fill available RAM and then automatically spill over to the hard drive. This reduces user memory management requirements.

A third version, "pmarc_dll," was compiled with DLLs, but the matrix storage flag was inadvertently set to hard drive instead of RAM. Processing times were considerably longer with this option selected. It is not recommended unless the computer is RAM limited.

The input model used was a NACA 2415 finite wing with four time steps. The panel density was varied to obtain the desired panel count. Appendix D contains a representative input file.

The processing benchmarks showed that CMARC, hosted on a PC, is significantly faster than all three versions of PMARC hosted on the networked SGI workstations. Table 4.1 summarizes results for identical models ranging from 200 - 1600 panels.

Figure 4.5 is a plot of processing time vs. panel count for models ranging from 200 to 1600 panels. For small sized models, all configurations are relatively close to the

same speed. As the model size increases, processing time increases roughly as the square of model size. However, as model size increases, all versions of PMARC on the networked SGI workstations become significantly slower than CMARC on the PC. This is most likely due to the slower file read/write access times to the file server. The version of PMARC with the matrix storage flag set to hard drive required considerably more processing time than the two versions with RAM selected.

Platform	Pentium PC	SGI Indigo^2		SGI Indigo^2	
CPU / RAM	150 MHz / 48 MB	150 MHz / 64 MB		250 MHz / 128 MB	
Program	CMARC	PMARC	PMARC-DLL	PMARC	PMARC-DLL
Panel Count	min:sec	min:sec	min:sec	min:sec	min:sec
200	0:11	0:12	0:15	N/A	0:13
400	0:27	0:43	0:53	N/A	0:29
800	1:29	2:46	3:10	N/A	1:51
1600	5:54	9:31	17:30	N/A	10:04

Table 4.1 CMARC and PMARC Processing Times for Models Ranging from 200 to 1600 Panels.

It is important to note that the models compared in this study only differed in panel count. Panel count is not the only factor in determining processing time. The number of time steps selected, solution resolution, convergence rate and boundary layer calculations will all impact processing speed. As a result, the times presented should only be viewed as representative of the relative impact of panel density and not as the time required to process any other model geometry.

In conclusion, CMARC hosted on a dedicated 150 MHz Pentium PC is significantly faster than PMARC hosted on a similar or faster networked SGI workstation. In some cases, over twice as fast. Clearly, executing the CMARC panel code on the PC is a suitable alternative to running PMARC on the SGI workstations. Low cost 200-300 MHz Pentium II PCs are now available which will allow further reductions in CMARC processing times.

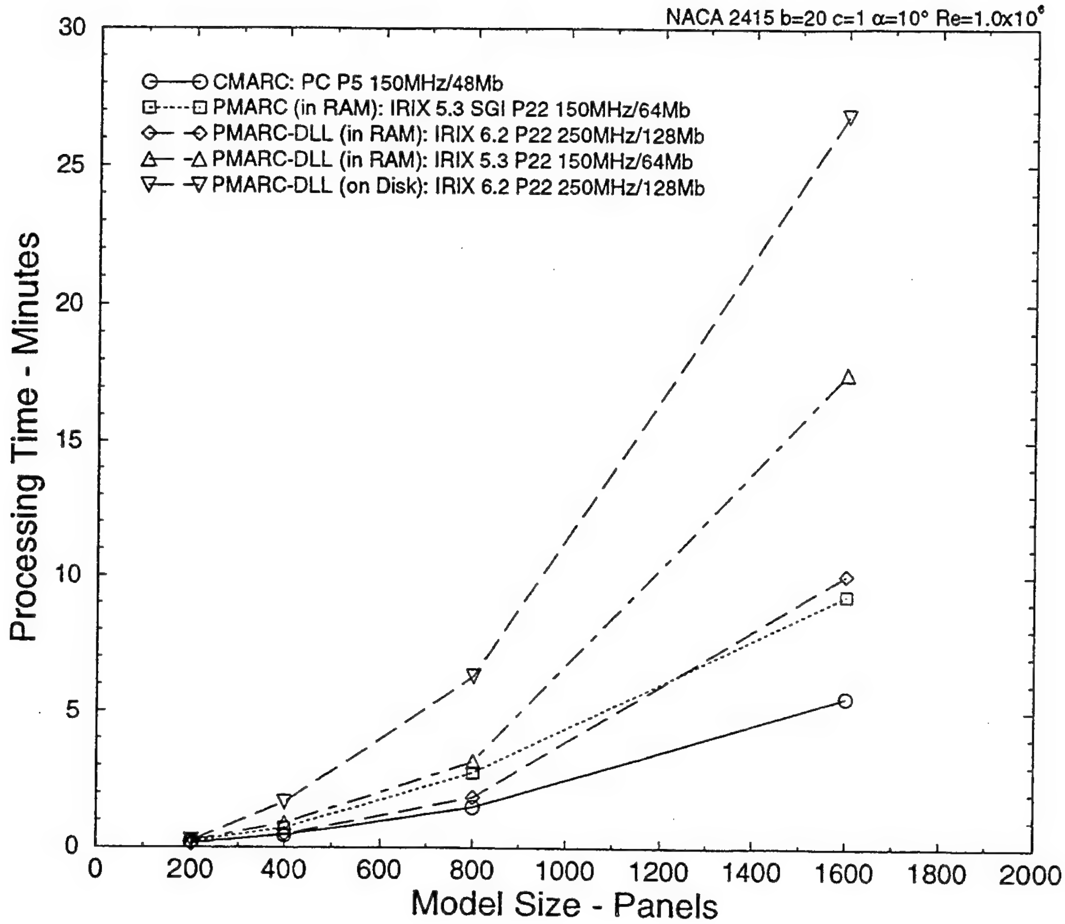

Figure 4.5 Comparison of CMARC and PMARC Processing Times for Similar Finite Wing Models Ranging from 200 to 1600 Panels.

C. COMPARISON OF CMARC TO THE UPOT BOUNDARY LAYER CODE

As a first step in investigating CMARC boundary layer calculations and utility, CMARC results are compared to 2D calculations from the NPS Unsteady Potential Flow Code (UPOT). Although the potential flow solution used by CMARC for the boundary layer calculations is strictly a 3D solution, 2D flow can be approximated with the proper choice of geometry. In this case, flow over the inboard portion of a high aspect ratio (AR) wing is selected. A straight NACA 2415 wing with AR=20 is chosen for the comparison. The NACA 2415 is the same section used in the FROG UAV. Boundary layer transition and separation points are compared at angles-of-attack ranging from 0 to 20 degrees. In addition, boundary layer solution sensitivity is investigated over four Reynolds numbers ranging from 5.0×10^5 to 6.0×10^6.

1. UPOT Boundary Layer Calculations

The NPS UPOT panel code was developed as a tool to assist in unsteady flow visualization over two-dimensional airfoils. It features an excellent interactive graphical user interface and rapid modeling capabilities [Ref. 10]. Unlike the integral momentum equations used by CMARC and PMARC, UPOT implements the Cebeci-Keller finite difference boundary layer code. The algorithm is documented by Nowak [Ref. 11]. The UPOT code has been compared to experimental data for a range of airfoils with favorable results. As such, it is considered to be acceptable to benchmark CMARC results.

2. High AR Wing Model

A high aspect ratio NACA 2415 wing is modeled to evaluate the boundary layer over the inboard section to approximate 2D flow. CMARC's built-in modeling capability was used to generate a finite wing with dimensions of 20 ft wingspan (b) and unit chord (c) yielding an aspect ratio of 20. Fifty chordwise panels are distributed over the top and bottom surface in a full cosine distribution and 10 panel sections in a spanwise direction with half cosine distribution. There are 600 panels total, including the enclosed wing tip, over the semi-span. Figure 4.6 displays a semi-planform view of this configuration. Streamlines are placed on the upper and lower surfaces of the inboard root panels. The root area is chosen as the area where the flow is nearly two-dimensional flow.

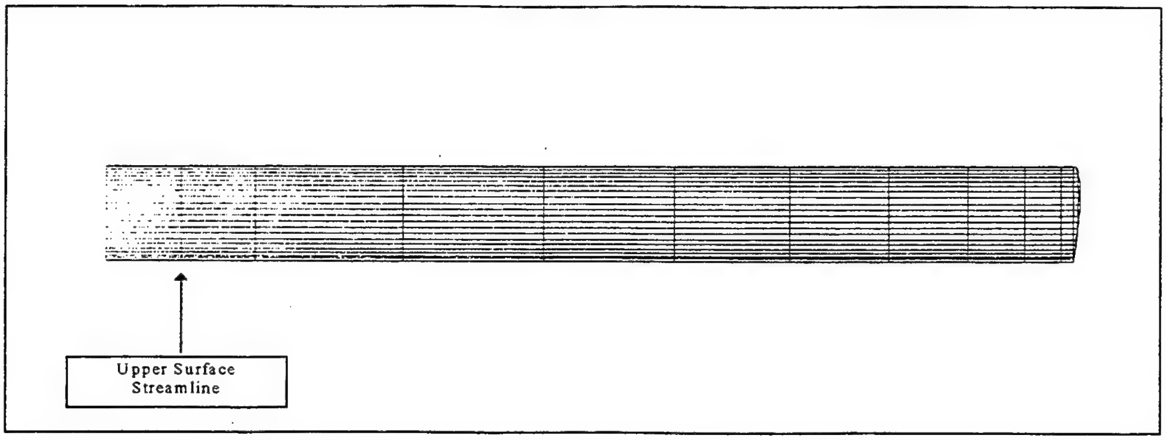

Figure 4.6 Semi-Span of Finite Wing for the Approximation of Two-Dimensional Flow Near the Root (AR=20). 50 Chordwise x 10 Spanwise Panels.

3. Boundary Layer Results and Analysis (CMARC vs. UPOT)

CMARC and UPOT boundary layer calculations are compared for the FROG UAV NACA 2415 airfoil. Two angles-of-attack were chosen for comparison. The first, -2° or zero lift, is used to compare transition models. The second angle-of-attack, 10° is selected for comparison to the 10° incidence of the inclined spheroid discussed in a later section. A comparison for Reynolds numbers ranging from $0.5\text{x}10^6$ to $6.0\text{x}10^6$ is also performed at 10° to investigate boundary layer calculation sensitivity to Reynolds number. In addition, boundary layer transition and separation locations are compared at angles-of-attack ranging from 0° to 20° at $Re=1.0\text{x}10^6$.

a. *Boundary Layer Transition*

The shortcomings of the point boundary layer transition model coded in CMARC is evident when compared to the more sophisticated transition length model implemented in UPOT. UPOT uses the Michel transition onset and the Chen-Thyson transition length models [Ref. 11]. Figures 4.7 through 4.14 display skin friction coefficient as a function of chordwise location (x/c) for the upper and lower surfaces of a NACA 2415 airfoil. Results for four Reynolds numbers ranging from $0.5\text{x}10^6$ to $6.0\text{x}10^6$ are plotted at zero lift (-2°) and 10° angle-of-attack. Boundary layer transition will be

discussed first, followed by boundary layer separation. Finally, differences in modeling at the stagnation point will be discussed.

In almost all cases, CMARC predicts an early transition. The transition from laminar to turbulent boundary layer occurs in CMARC as a sudden jump or point transition. The UPOT transition length model provides for a more realistic representation of the boundary layer physics. Combined, early and point transition result in higher total skin friction drag predicted by CMARC. The difference is most pronounced at the lower Reynolds numbers associated with the FROG UAV. At $Re=0.5x10^6$ and zero lift, CMARC overpredicts skin friction drag by approximately 40% on the upper surface and 20% on the lower surface. Although skin friction drag may be a relatively small portion of the total drag, airframe manufacturers go to great lengths to refine models to accurately predict it. A few percentage points of error can cause the aircraft to meet or miss performance goals.

Despite the differences in transition modeling, CMARC accurately predicts the skin friction coefficient with respect to UPOT. When comparing laminar to laminar and turbulent to turbulent regions in Figures 4.7 through 4.10 (zero lift plots), the skin friction coefficients are a close match. This indicates that an adjustment in the CMARC model delaying transition could provide more accurate results.

As another comparison of boundary layer calculations, displacement thickness (δ^*) is displayed in Figures 4.15 through 4.22 as a function of chord position (x/c) for zero lift (-2°) and 10° angle-of-attack. In general, CMARC and UPOT predict similar trends in δ^*. The final displacement thickness is a good relative indication of total skin friction drag. CMARC always predicts a greater δ^* and thus more drag. This is in keeping with the previous observations indicating higher integrated skin friction forces.

b. Separation

Boundary layer separation is indicated in Figures 4.7 through 4.14 by a zero or negative skin friction coefficient. In all cases, CMARC slightly overpredicts the extent of attached flow. Again, the differences are most significant at the lower Reynolds numbers.

Figures 4.23 and 4.24 display transition and separation points for the NACA 2415 as a function of angles-of-attack ranging from 0° to 20°. The data is for $Re=1.0x10^6$ which is close to the FROG UAV high speed cruise at Re=929,000. On both

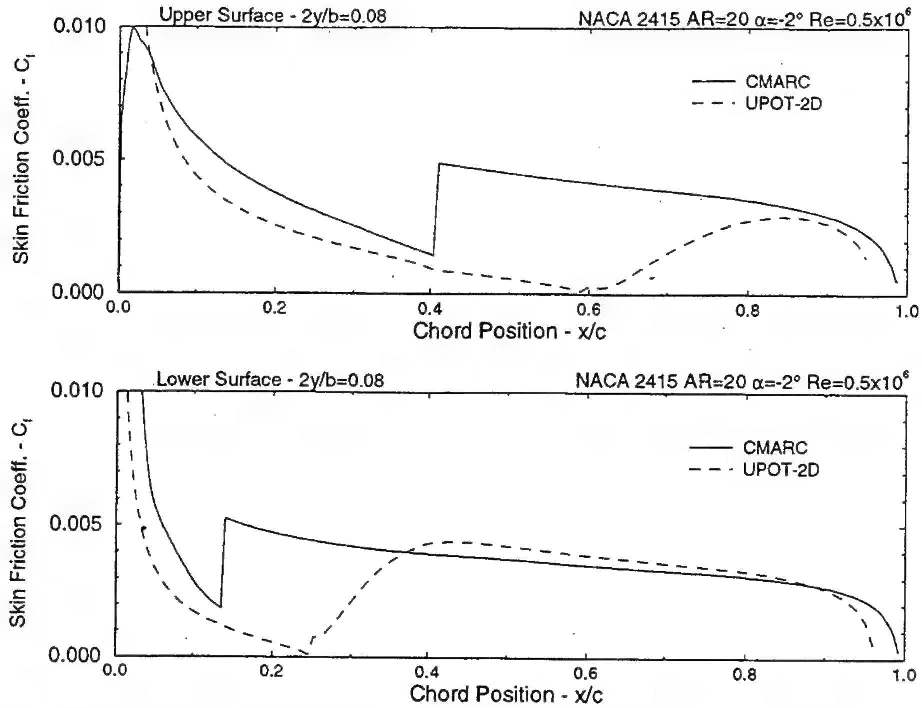

Figure 4.7 Comparison of CMARC and UPOT Skin Friction Coefficient (C_f) for NACA 2415 at zero lift (α=-2°) and Re=$0.5\text{x}10^6$.

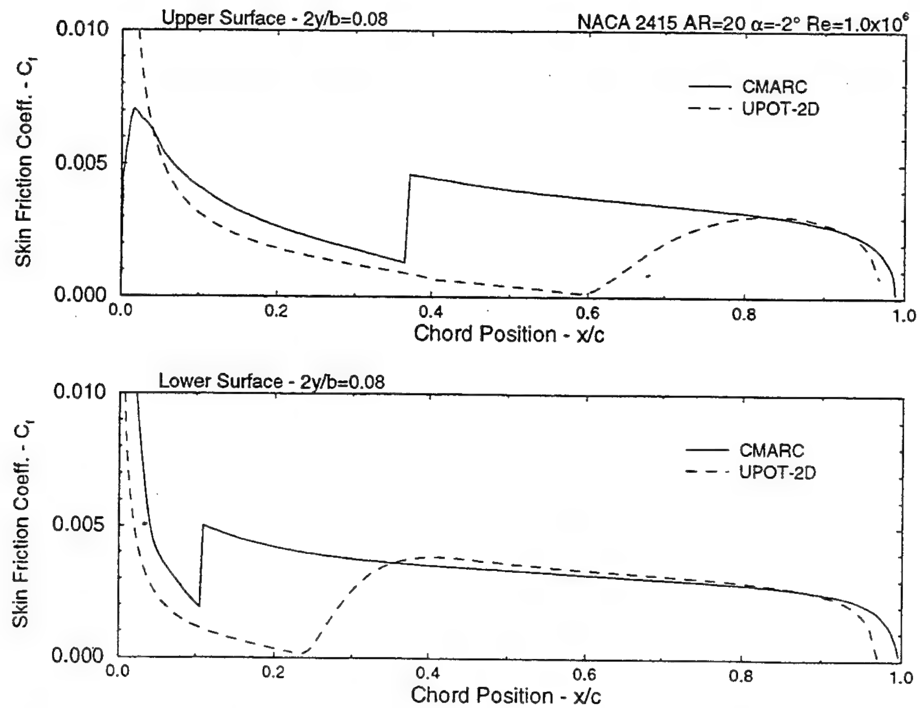

Figure 4.8 Comparison of CMARC and UPOT Skin Friction Coefficient (C_f) for NACA 2415 at zero lift (α=-2°) and Re=$1.0\text{x}10^6$.

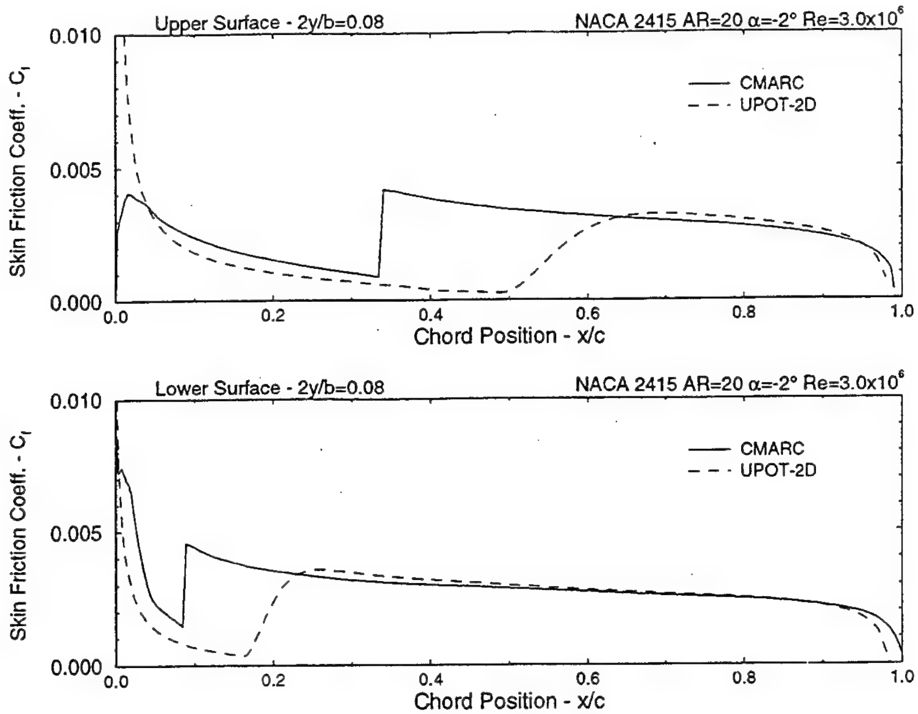

Figure 4.9 Comparison of CMARC and UPOT Skin Friction Coefficient (C_f) for NACA 2415 at zero lift (α=-2°) and Re=$3.0\text{x}10^6$.

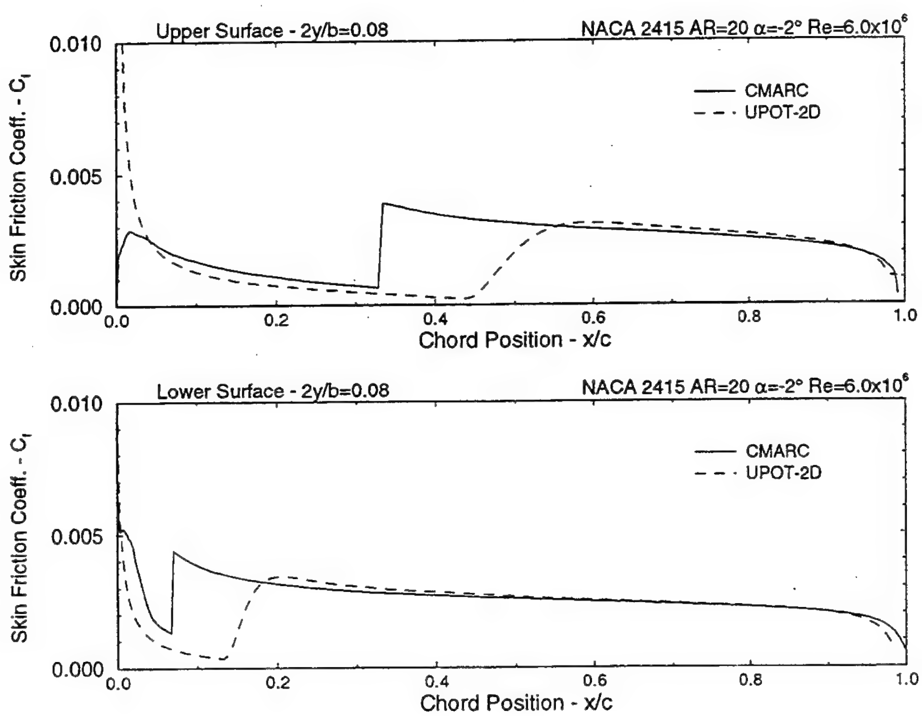

Figure 4.10 Comparison of CMARC and UPOT Skin Friction Coefficient (C_f) for NACA 2415 at zero lift (α=-2°) and Re=$6.0\text{x}10^6$.

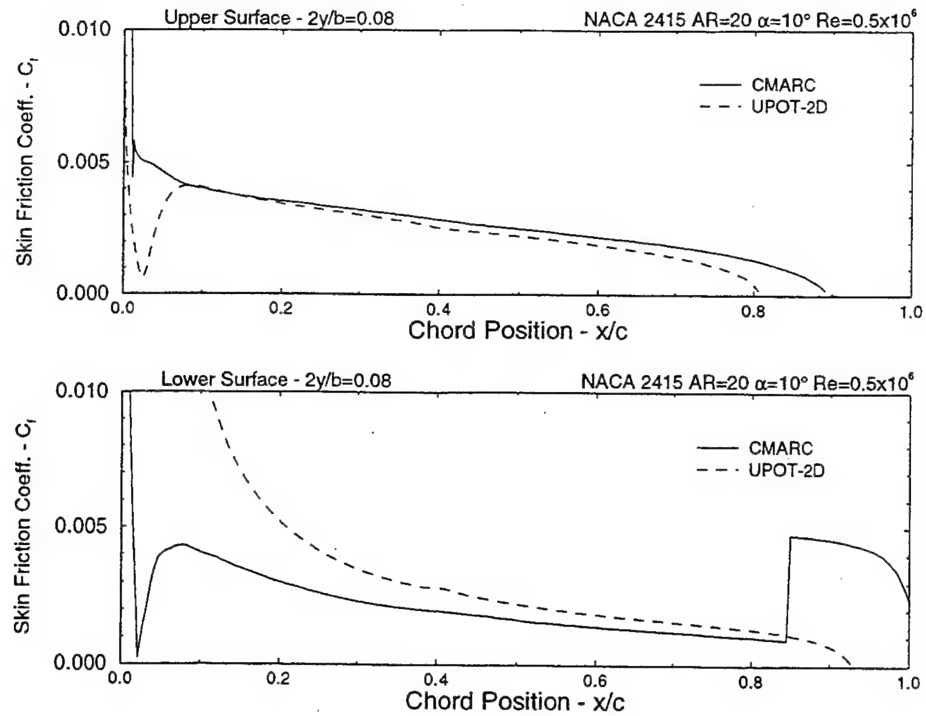

Figure 4.11 Comparison of CMARC and UPOT Skin Friction Coefficient (C_f) for NACA 2415 at α=10° and Re=0.5x10^6.

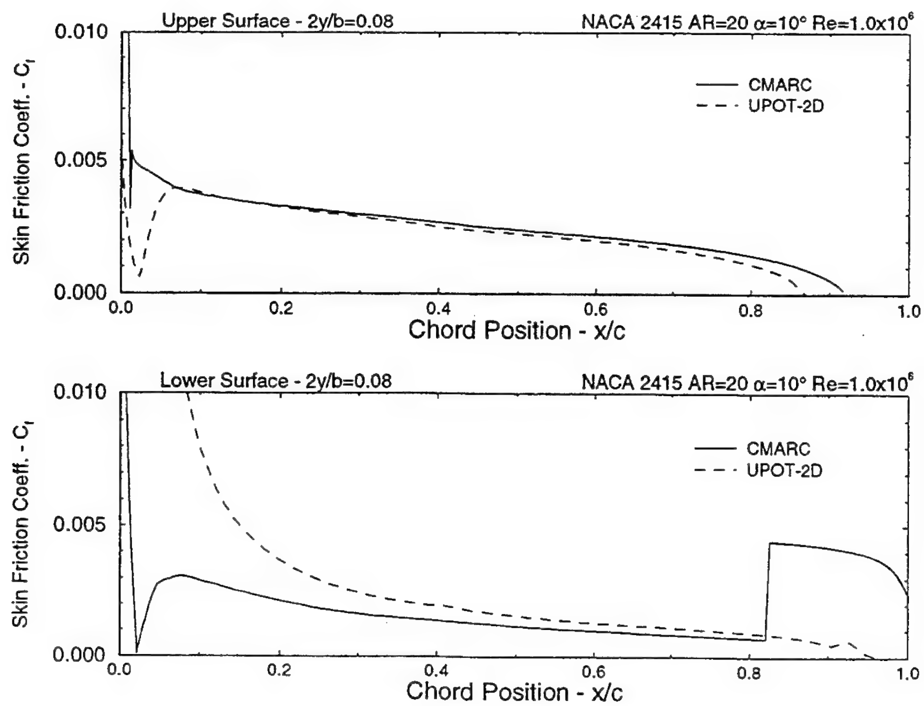

Figure 4.12 Comparison of CMARC and UPOT Skin Friction Coefficient (C_f) for NACA 2415 at α=10° and Re=1.0x10^6.

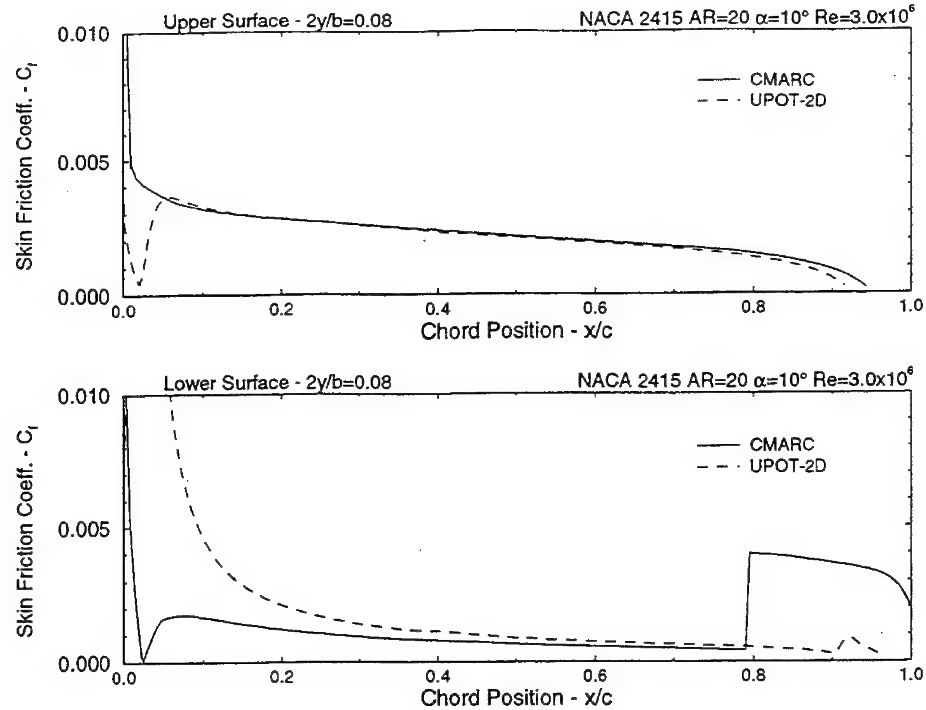

Figure 4.13 Comparison of CMARC and UPOT Skin Friction Coefficient (C_f) for NACA 2415 at α=10° and Re=3.0x10^6.

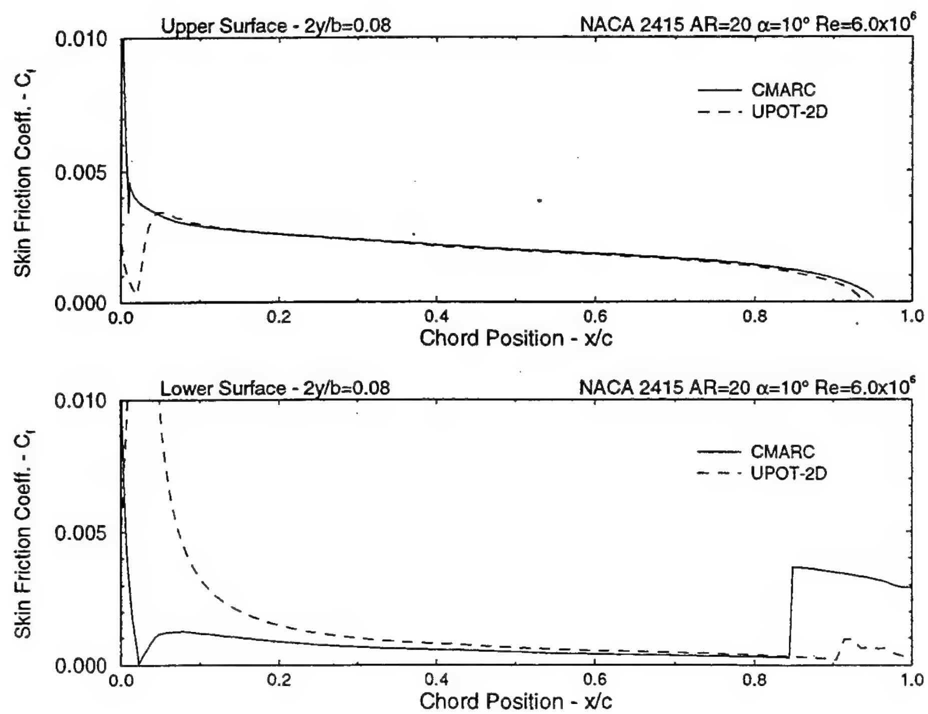

Figure 4.14 Comparison of CMARC and UPOT Skin Friction Coefficient (C_f) for NACA 2415 at α=10° and Re=6.0x10^6.

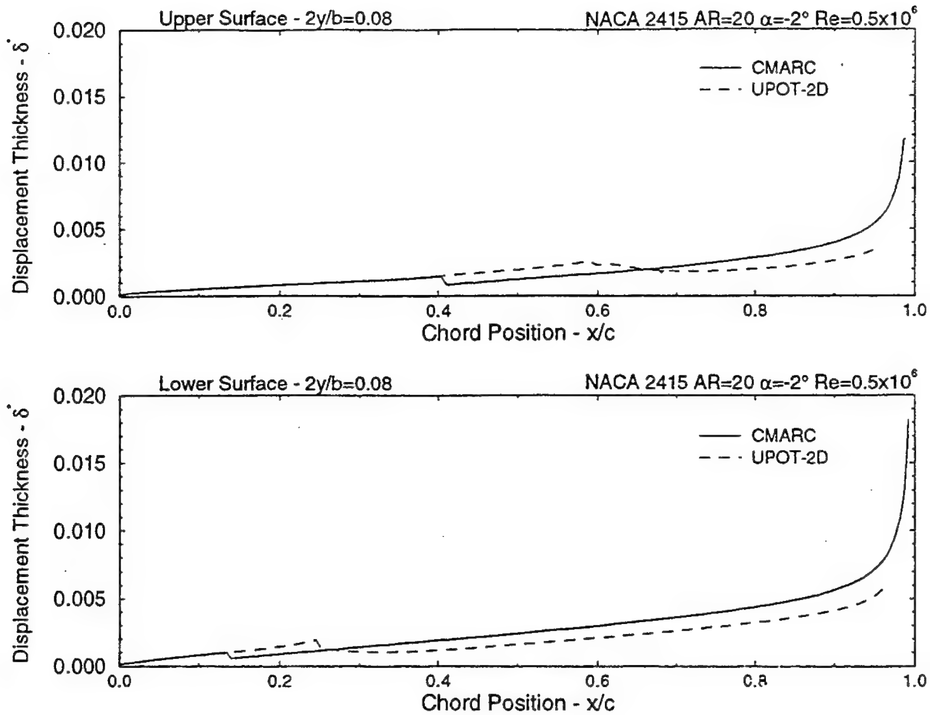

Figure 4.15 Comparison of CMARC and UPOT Boundary Layer Displacement Thickness (δ*) for NACA 2415 at zero lift (α=-2°) and Re=0.5x10^6.

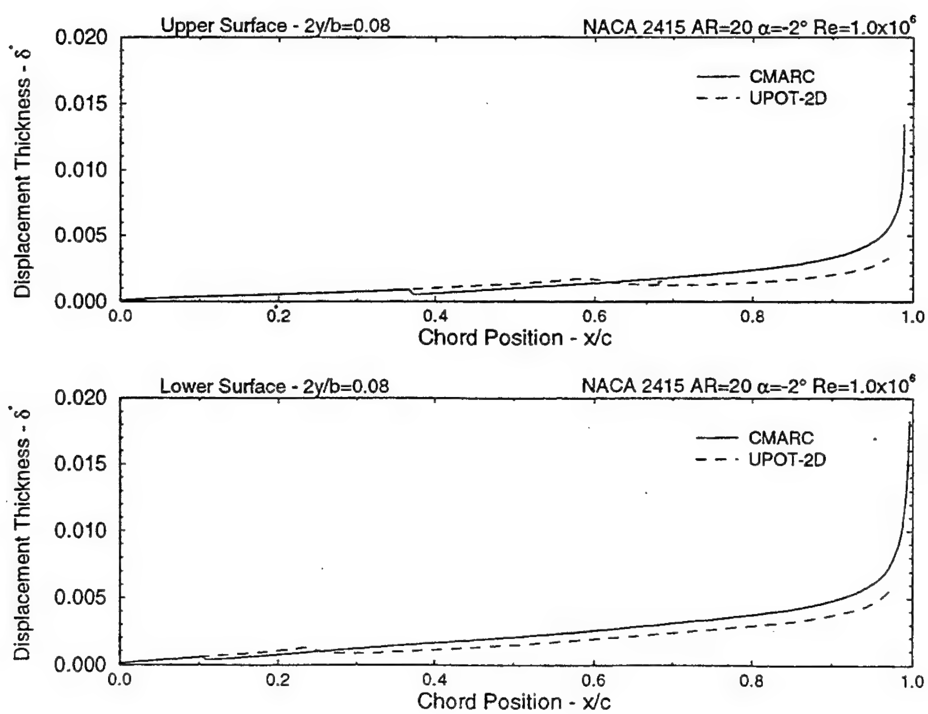

Figure 4.16 Comparison of CMARC and UPOT Boundary Layer Displacement Thickness (δ*) for NACA 2415 at zero lift (α=-2°) and Re=1.0x10^6.

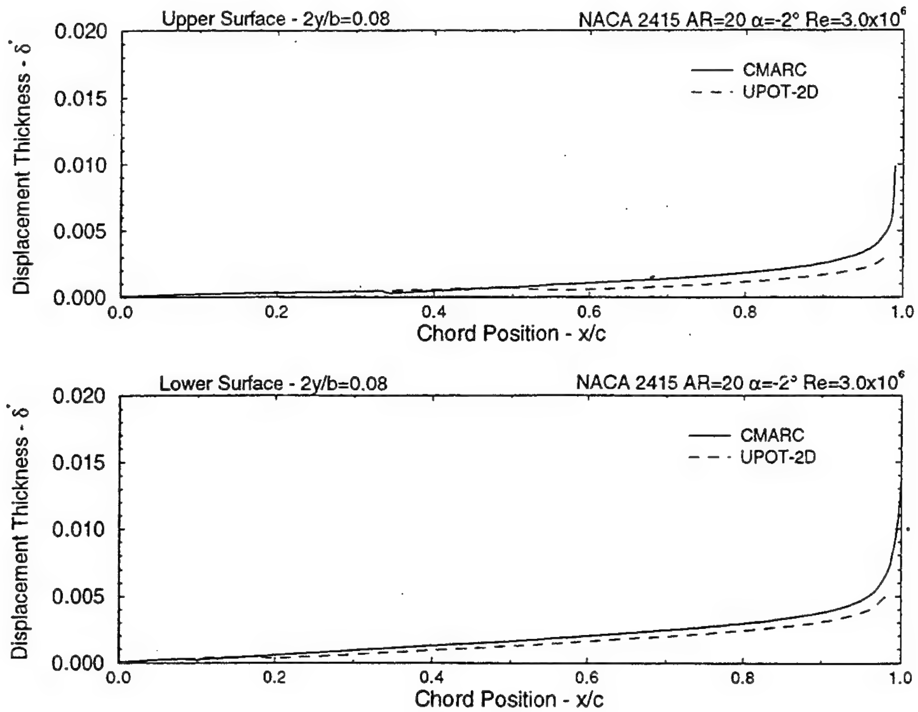

Figure 4.17 Comparison of CMARC and UPOT Boundary Layer Displacement Thickness (δ^*) for NACA 2415 at zero lift (α=-2°) and Re=3.0x10^6.

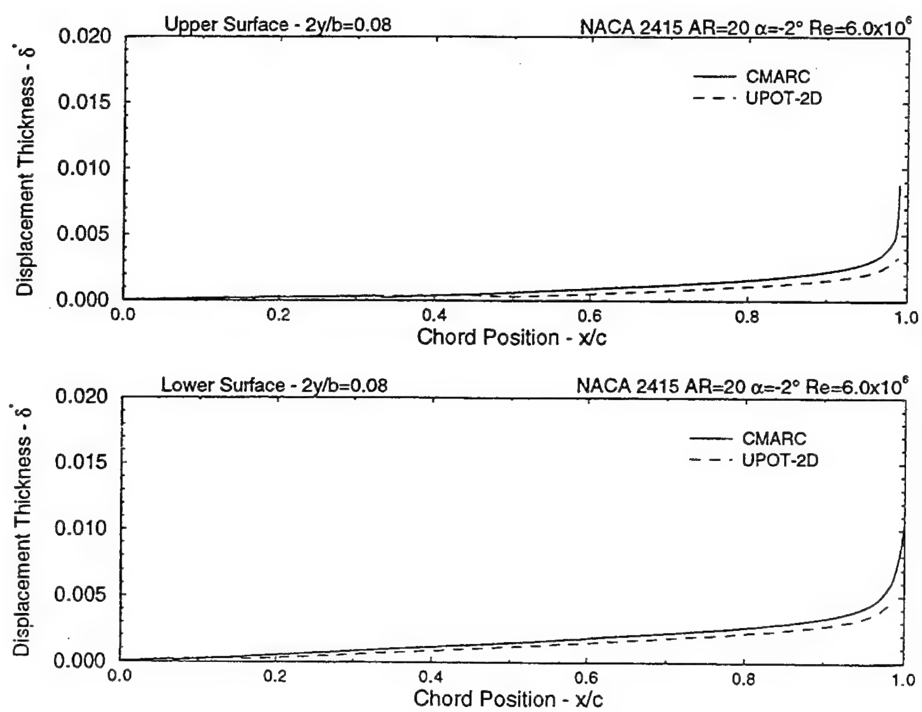

Figure 4.18 Comparison of CMARC and UPOT Boundary Layer Displacement Thickness (δ^*) for NACA 2415 at zero lift (α=-2°) and Re=6.0x10^6.

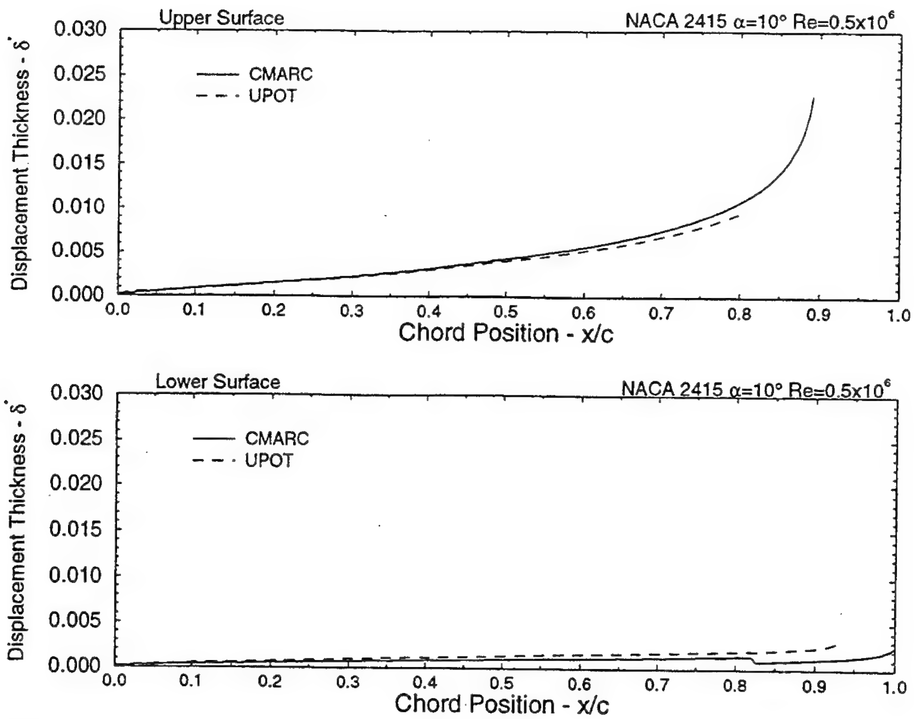

Figure 4.19 Comparison of CMARC and UPOT Boundary Layer Displacement Thickness (δ^*) for NACA 2415 at α=10° and Re=0.5×10^6.

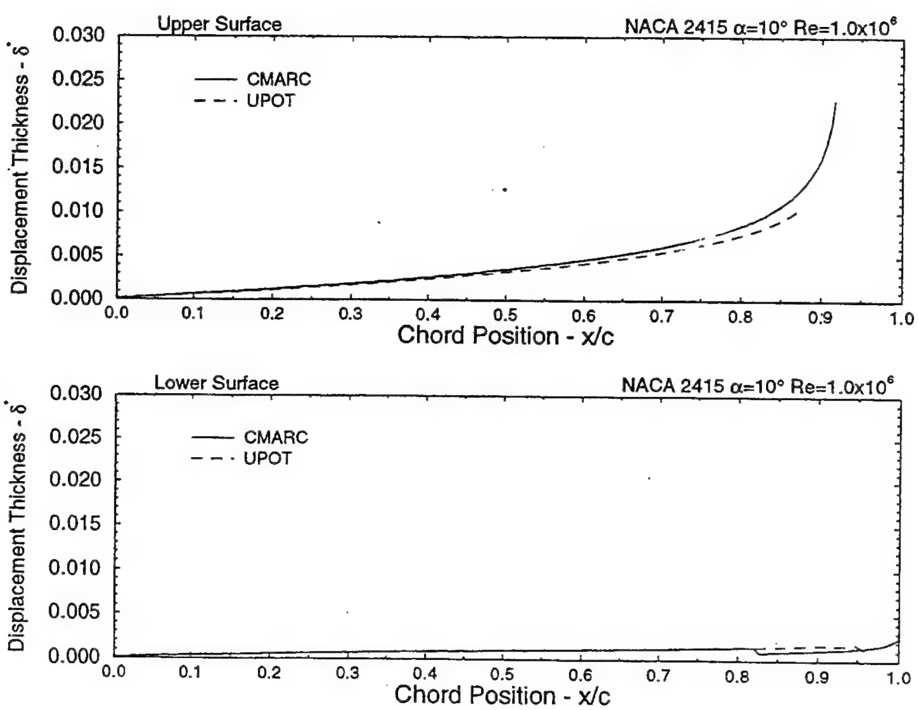

Figure 4.20 Comparison of CMARC and UPOT Boundary Layer Displacement Thickness (δ^*) for NACA 2415 at α=10° and Re=1.0×10^6.

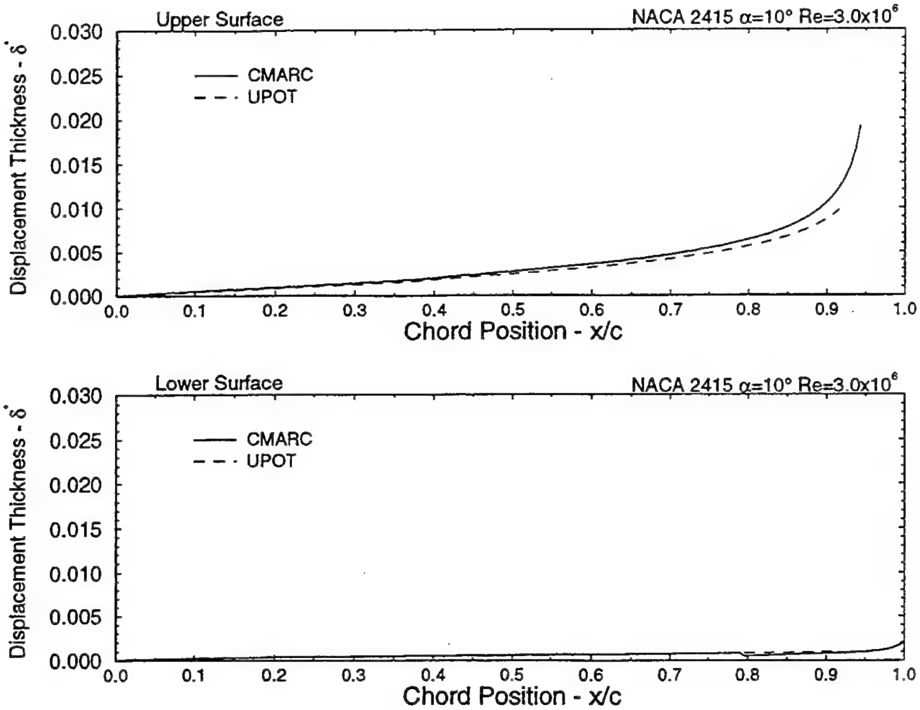

Figure 4.21 Comparison of CMARC and UPOT Boundary Layer Displacement Thickness (δ^*) for NACA 2415 at α=10° and Re=3.0x10^6.

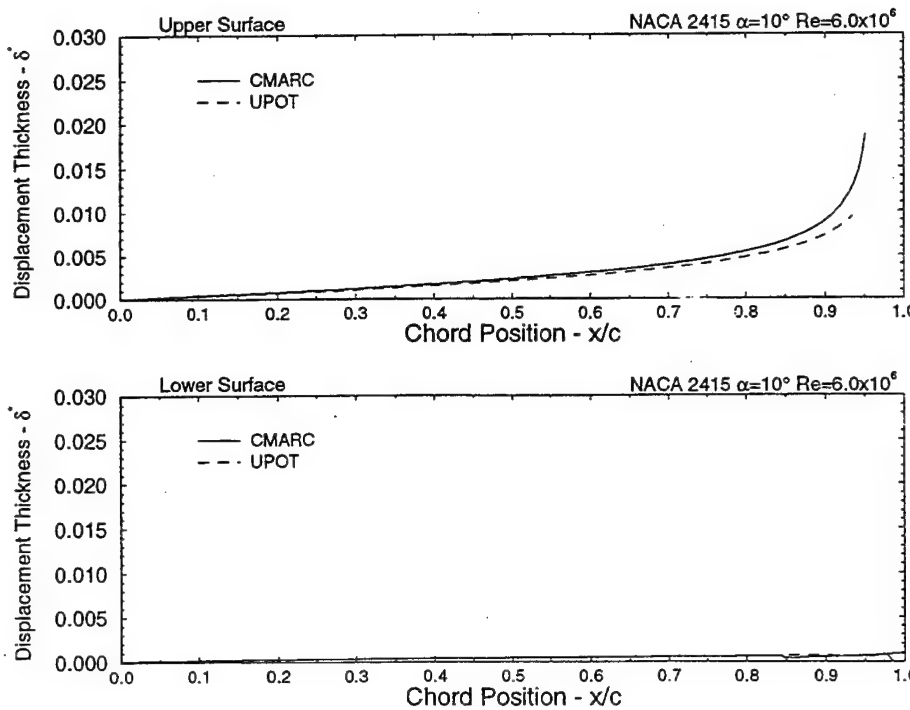

Figure 4.22 Comparison of CMARC and UPOT Boundary Layer Displacement Thickness (δ^*) for NACA 2415 at α=10° and Re=6.0x10^6.

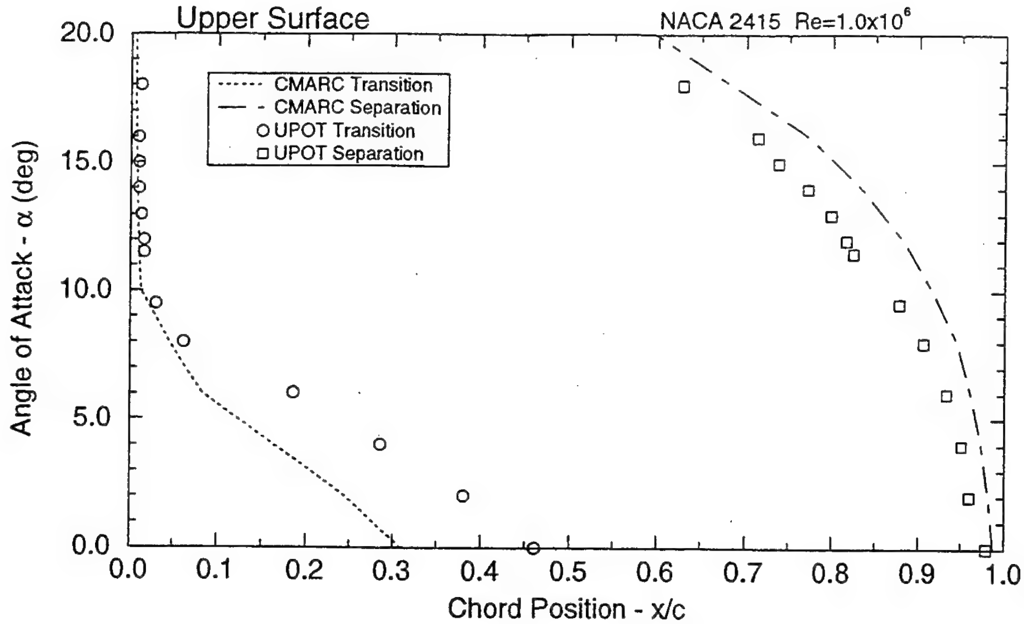

Figure 4.23 **Comparison of CMARC and UPOT Boundary Layer Transition and Separation Points for the Upper Surface of a NACA 2415 Airfoil at Re=1.0x10^6 from 0° to 20° AOA.**

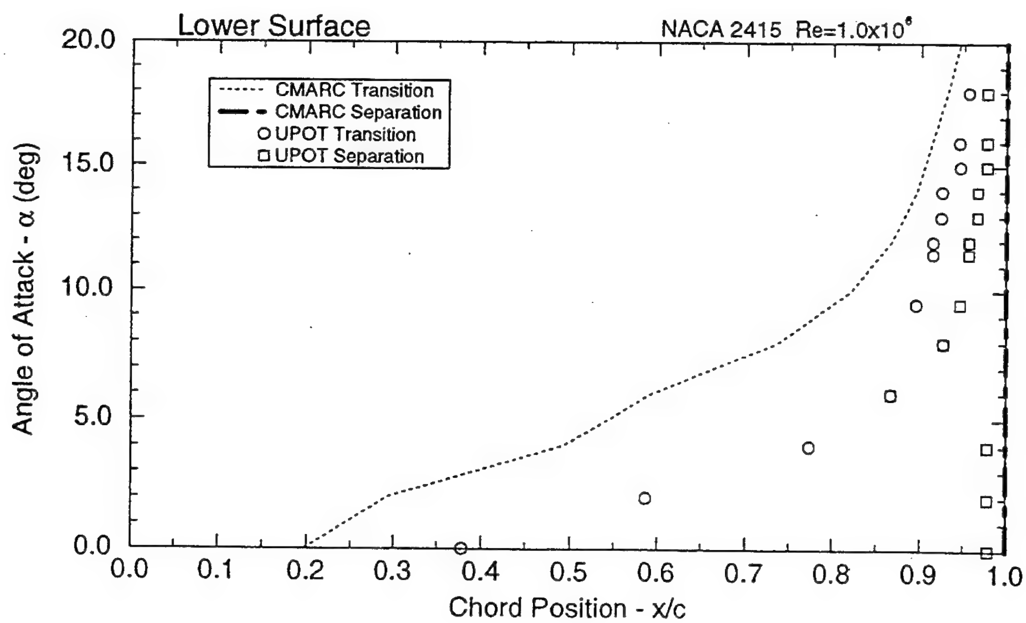

Figure 4.24 **Comparison of CMARC and UPOT Boundary Layer Transition and Separation Points for the Lower Surface of a NACA 2415 Airfoil at Re=1.0x10^6 from 0° to 20° AOA.**

the upper and lower surface, CMARC clearly provides correct trends for both the transition and separation points. However, as seen at zero lift in Figures 4.7 through 4.10, CMARC always predicts an early transition and late separation.

Despite the inaccuracies in transition and separation points, CMARC boundary layer calculations remain useful. A low order panel code is unlikely going to be used for performance calculations. Instead, it is more useful as a design tool. It allows for rapidly visualizing the trend in transition and separation points with minor changes in configuration.

A word of caution is advised when total skin friction drag is integrated. A design change could be implemented that reduces overall skin friction drag but neglects large increases in pressure drag. In other words, one could reduce skin friction drag, but fail to realize earlier separation is taking place. The net result is a small reduction in skin friction drag that is more than offset by a large increase in separation pressure drag. Extending the extent of attached flow should always be considered preferable to reducing overall integrated skin friction drag.

c. *Skin Friction Coefficient near the Stagnation Point*

Another major difference between the integral boundary layer code in CMARC and the finite difference code in UPOT is highlighted at the stagnation point. In Figure 4.11, both codes locate the stagnation point on the lower surface at x/c=0.025 for the NACA 2415 airfoil at 10 degrees angle-of-attack. However, it is clear that the CMARC skin friction coefficient starts at 0.0002, a small number approaching zero asymptotically, while the UPOT skin friction shoots out of the top of the chart in excess 0.7, a relatively large number approaching $+\infty$ asymptotically.

From boundary layer theory, it is know that the skin friction coefficient is inversely proportional to the square root of the local Reynolds number or:

$$C_f = \frac{1}{\sqrt{\mathrm{Re}_x}} \qquad 4.1$$

At the stagnation point, C_f approaches $+\infty$. The finite difference code in UPOT correctly models this trend. On the other hand, CMARC implements a discrete

integration of the following exact differential laminar skin friction calculation:

$$\theta(\eta)^2 = \frac{0.45\nu}{U(\eta)^6}\int_0^{\eta}\left(1+2.222g(K,\mu)\right)U(\eta)^5 d\eta + \theta(0)^2\left(\frac{U(0)}{U(\mu)}\right)^6 \qquad 4.2$$

Where: U - velocity at outer edge of boundary layer

θ - momentum thickness

g - empirical parameter

$K=\dfrac{\theta^2}{\nu}\dfrac{dU}{d\eta}$

η - generalized coordinate along a streamline

At η=0, the momentum thickness starts at zero and builds rapidly from the stagnation point. Thus, the momentum integral equation reduces to:

$$\frac{d\theta}{d\eta}=\frac{1}{2}C_f=0,\ \text{ at the stagnation point.} \qquad 4.3$$

The integral solution for C_f starts at zero and rises quickly until the integral portion of Equation 4.2 dominates.

The incorrect modeling of C_f near the stagnation point is considered minor due to its local nature at the stagnation point. When skin friction is integrated over the entire surface the differences are bound to be relatively small. In addition, when integrated into a force, the errors in C_f at the stagnation point tend to cancel out. Close to the stagnation point on either side, skin friction forces are opposite in direction.

D. COMPARISON OF CMARC TO INCLINED PROLATE SPHEROID EXPERIMENTAL DATA

In the previous section, model geometry was selected to produce predominantly two-dimensional flow. In this section, CMARC pressure distributions and integral

boundary layer data are investigated for a model geometry that produces largely three-dimensional flow. For comparison, a suitable experimental test case was found in AGARD AR-303: A Selection of Experimental Test Cases for the Validation of CFD Codes [Ref. 12]. Case number C-2, entitled "Three-Dimensional Boundary Layer and Flow Field Data of an Inclined Prolate Spheroid" was selected. A 6:1 prolate spheroid approximates a typical streamlined fuselage. The data set was ordered from AGARD through the NASA Center for Aerospace Information (CASI).

A complete data set for all test cases in AGARD AR-303 was available for a nominal charge of $59.00 through NASA's CASI publications office. Ordering information inside the rear cover of the publication proved to be accurate and useful. The data arrived on nine PC formatted high density disks. After copying the desired data sets to the hard drive, each file is self extracting through a built-in DOS decompression program. Detailed instructions are printed in the back section of AR-303.

1. Inclined 6:1 Prolate Spheroid - AGARD AR-303 Case C-2

AGARD AR-303 test case number C-2 contains pressure coefficient and skin friction distributions for a 6:1 prolate spheroid inclined to the flow field. Table 4.2 lists the test conditions for which data are available.

Test case I was chosen for comparison to CMARC output. At 10° angle-of-attack, some separated flow was expected which would provide a good comparison to CMARC integral boundary layer separation points. The only drawback to this test case is the forced transition at $X/2a = 0.20$. Natural transition would have been more desirable for comparison to the CMARC transition model. The test cases at 30° angle-of-attack are deemed to have too much separated flow to provide a meaningful comparison to a CMARC potential flow solution.

a. Wind Tunnel Experimental Set-up

Figure 4.25 contains a diagram of the experimental set-up for the 6:1 prolate spheroid performed by Kreplin in the DLR Göttingen three meter Low Speed Wind Tunnel (NWG). Of note, the wind tunnel test section is of the Göttingen type with closed return and open test section. No corrections are applied to the data.

PARAMETER	CASE I	CASE II	CASE III
Mach Number	0.16	0.13	0.23
Reynolds Number	7.7×10^6	6.5×10^6	43.0×10^6
Incidence	10.0°	29.7°	30.0°
Transition	tripped at X/2a =0.20	free	free

Table 4.2 AGARD AR-303 Test Conditions, from Ref. [12].

Figure 4.26 shows the configuration for the 6:1 prolate spheroid wind tunnel model. The 2.4 meter long model contains 42 pressure taps located along an axial meridian. The model can be rotated axially in 50 steps through just over 180 degrees providing in excess of 2000 pressure readings over half the surface. With yaw angle set to zero, symmetry is assumed for the other half. In addition to pressure ports, surface hot film sensors are located at 12 axial positions for the measurement of wall shear stress. Wall shear stress is normalized by dynamic pressure to provide skin friction coefficient (C_f). Once again, the measurements are provided for approximately 50 rotation angles, providing coverage of half the surface.

In addition to pressure and skin friction coefficients, boundary layer velocity profiles and flow field mean velocity vectors are available at several axial locations. Although not used in this investigation, the data would prove useful for more detailed studies.

Unfortunately, the wind tunnel set-up was not instrumented for loads. As will be discussed in the next section, the number of pressure and skin friction measurements was deemed to be sufficient to allow the integration of local forces to provide a reasonable calculation of lift, drag and pitching moments.

b. Experimental Data

Two data files from test case C-2 at α=10.0° are used for comparison to CMARC data. The first file, "cp10nwg.dat," contains pressure coefficient listed as a function of axial location (X/2a) and circumferential angle (ϕ). For each circumferential

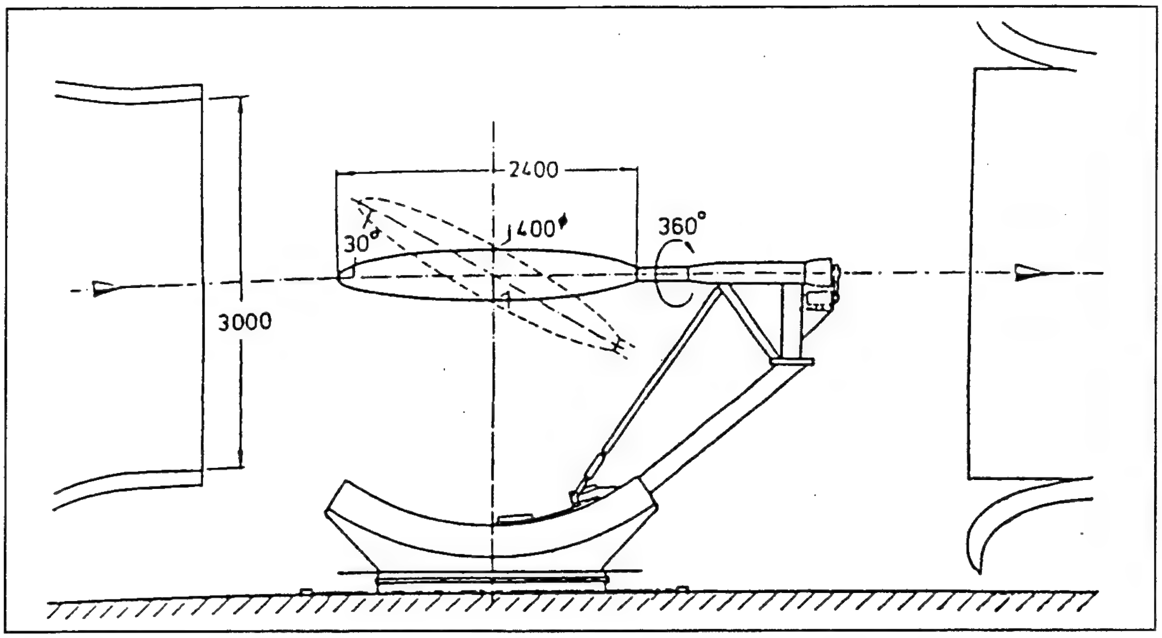

Figure 4.25 Inclined 6:1 Prolate Spheroid Model in the DLR Göttingen Three Meter Low Speed Wind Tunnel (NWG) , from Ref. [12].

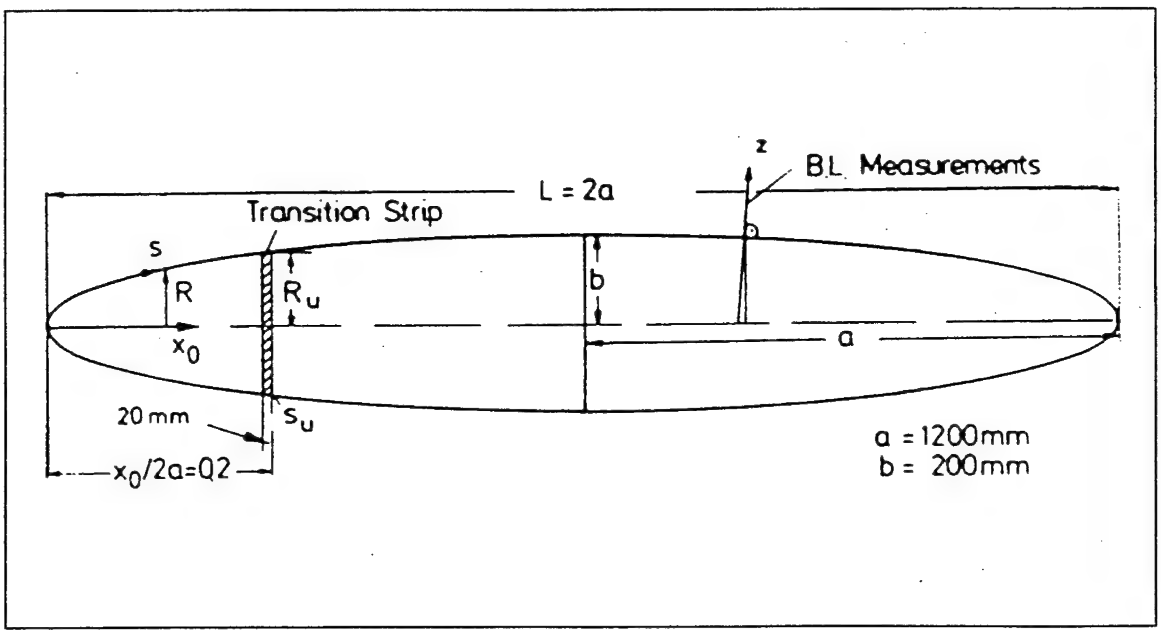

Figure 4.26 Prolate Spheroid Wind Tunnel Model Configuration, from Ref. [12].

angle all the successive axial location pressure coefficients were listed. It is more common to plot pressure distribution as a function of circumferential angle at a given axial station. The data file was rearranged using the MATLAB M-file listed in Appendix E.

The second data file, "cf10nwg.dat," contains skin friction listed as a function of axial location (X/2a) and circumferential angle (ϕ). The data, listed in two columns, were reordered to one column for ease of plotting.

c. *Integration of Local Forces to Provide Lift Drag and Pitching Moment*

The experimental set-up did not include balance measurement of forces. However, it was deemed that the 2000+ pressure and 500+ skin friction measurements would be sufficient to allow the integration of measurements over the surface of the prolate spheroid for an approximation of total force and moment coefficients. The following equations were developed to provide integrated pressure and friction force coefficients. Symmetry is assumed. Appendix B outlines the development of these relations. Appendix C lists the MATLAB program which implements the discrete integration.

The pressure force coefficients normalized by $S = \pi b^2$ and $\bar{c} = 2b$ are yielded by discretely integrating the following equations in a cylindrical coordinate system:

$$C_{N_P} = \frac{N_P}{q_\infty S}, \qquad N_P = 2\sum_{i=1}^{m}\sum_{j=1}^{n} -\left(q_\infty C_P r\bar{n}\right)\cdot \bar{k}\Delta\phi j\Delta x_i / 2a \qquad 4.3$$

$$C_{A_P} = \frac{A_P}{q_\infty S}, \qquad A_P = 2\sum_{i=1}^{m}\sum_{j=1}^{n} -\left(q_\infty C_P r\bar{n}\right)\cdot \bar{i}\Delta\phi_j \Delta xi / 2a \qquad 4.4$$

$$C_{M_P} = \frac{M_P}{q_\infty S\bar{c}}, \qquad M_P = 2\sum_{i=1}^{m}\sum_{j=1}^{n}\left[\left(q_\infty C_P r\bar{n}\right)\cdot\left(x_i / 2a\cdot\bar{k} - z_i / 2a\cdot\bar{i}\right)\right]\Delta\phi_j\Delta x_i / 2a \qquad 4.5$$

Where the surface unit normal is given by:

Unit Normal: $$\bar{n} = -\frac{m}{\sqrt{m^2+1}}\bar{i} + \frac{\sin(\phi)}{\sqrt{m^2+1}}\bar{j} - \frac{\cos(\phi)}{\sqrt{m^2+1}}\bar{k} \qquad 4.6$$

The skin friction coefficients normalized by $S=\pi b^2$ and $\bar{c}=2b$ are yielded by discretely integrating the following equations in a cylindrical coordinate system:

$$C_{N_{SF}}=\frac{N_{SF}}{q_\infty S},\qquad N_{SF}=2\sum_{i=1}^{m}\sum_{j=1}^{n}\left(q_\infty C_f r\bar{v}\right)\cdot\bar{k}\Delta\phi_j\Delta x_i/2a \qquad 4.7$$

$$C_{A_{SF}}=\frac{A_{SF}}{q_\infty S},\qquad A_{SF}=2\sum_{i=1}^{m}\sum_{j=1}^{n}\left(q_\infty C_f r\bar{v}\right)\cdot\bar{i}\Delta\phi_j\Delta x_i/2a \qquad 4.8$$

$$C_{M_{SF}}=\frac{M_{SF}}{q_\infty S\bar{c}},\quad M_{SF}=2\sum_{i=1}^{m}\sum_{j=1}^{n}\left[\left(q_\infty C_f r\bar{v}\right)\cdot\left(-x_i/2a\cdot\bar{k}+z_i/2a\cdot\bar{i}\right)\right]\Delta\phi_j\Delta x_i/2a \quad 4.9$$

Where the unit surface velocity vector is given by:

$$\bar{v}=\frac{\cos(\gamma)}{\sqrt{m^2+1}}\bar{i}+\left[\frac{m\sin(\phi)\cos(\gamma)}{\sqrt{m^2+1}}+\cos(\phi)\sin(\gamma)\right]\bar{j}+\left[-\frac{m\cos(\phi)\cos(\gamma)}{\sqrt{m^2+1}}+\sin(\phi)\sin(\gamma)\right]\bar{k}$$

4.10

The surface and local slope of a prolate spheroid comes from the following relations:

$$\text{Prolate Spheroid:}\quad \frac{x^2}{a^2}+\frac{r^2}{b^2}=1 \qquad \Rightarrow \qquad slope \quad m=\frac{dr}{dx}=-\frac{bx}{a^2\sqrt{1-\frac{x^2}{a^2}}}$$

4.11

Note: The forces are summed over half the spheroid, $\phi=0\rightarrow 180^\circ$, and doubled. The y-direction forces and the roll and yaw moments are neglected zero due to symmetry.

2. CMARC Model of 6:1 Prolate Spheroid

A 40x20 panel model of the 2.4 meter 6:1 prolate spheroid wind tunnel model was created with LOFTSMAN. The right half surface was modeled with symmetry around the y=0 plane. Appendix F contains a printout of the LOFTSMAN input file which includes a fore/aft wake. The patch was created with 40 axial and 20 semi-circumferential panels. Full cosine compression was used to bunch panels at the leading and trailing edge.

After creating the patch in LOFTSMAN, it was decided that a doubling of circumferential panel count would increase wake placement flexibility. The CMARC input file was modified to create 40 circumferential panels by setting TNPC=40 in the break point input field for each cross section.

Figure 4.27 is a POSTMARC rendering of the final 1600 (40x40) panel configuration. The input file takes advantage of the plane of symmetry capability built into CMARC. It calculates just half a model symmetric around the y=0 plane of symmetry provided there is zero side slip.

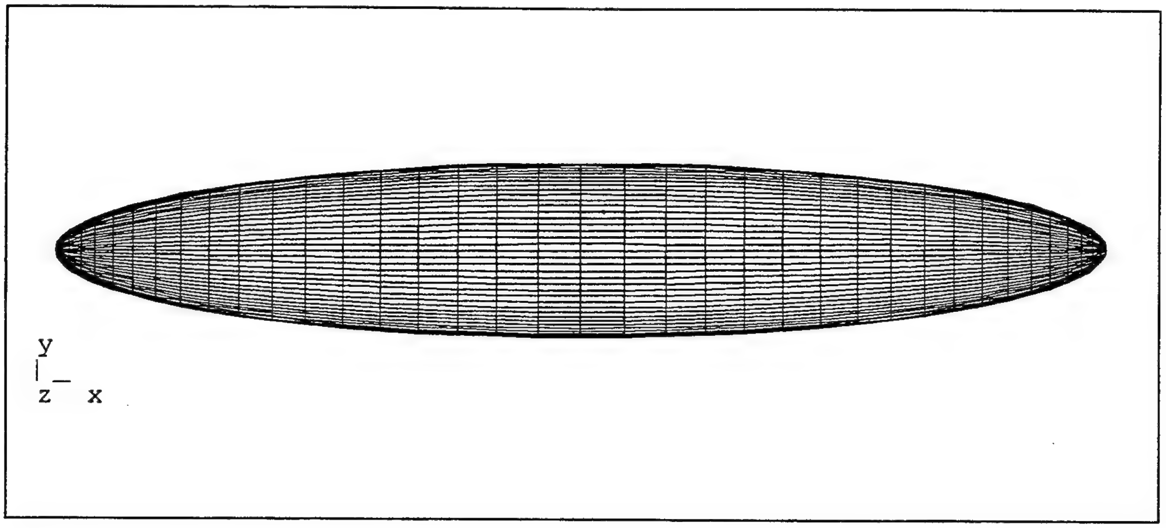

Figure 4.27 CMARC 40x40 Prolate Spheroid Model Rendered with POSTMARC.

3. Data Extraction

Pressure coefficient data are extracted using the "postprolate.exe" FORTRAN file listed in Appendix G. This program extracts data from a CMARC or PMARC output file (DATA6) for a range of panel numbers and places them in a separate plot input file. CMARC output files are transferred to the SGI workstations for data extraction using the Windows 3.1 FTP program. Results are then plotted against experimental data with any x-y plotting program (xmgr).

4. Prolate Spheroid Pressure Distribution

CMARC and experimental pressure coefficients are compared at 10 degrees angle-of-attack and Re=7.7×10^6. Results are displayed as a function of axial station, x/2a, and circumferential angle, ϕ, in Figure 4.28. Circumferential angle is measured starting from the lower centerline of the model. CMARC generated potential flow pressure coefficients over the forward 60% of the prolate spheroid closely match experimental results. Of note, there is a constant bias between the two sets of data.

The divergence between CMARC and experimental results aft of x/2a=0.60 indicates flow separation over the top portion of the prolate spheroid. It is clear that a potential flow solution without wakes does a poor job of predicting pressure distribution over regions with separated flow.

To model the flow separation, wakes were added to the CMARC model. Tuncer and Platzer's research [Ref. 7] indicates that proper wake placement can produce a close match between panel code and experimental results for slender bodies of revolution for angles-of-attack up to 20 degrees. They concluded that a circumferential wake placement angle of 144 degrees on an ogive cylinder body provides the closest match for force and moment coefficients.

A series of wakes were placed at several circumferential angles ranging from 117 to 162 degrees. The wakes run fore-aft from x/2a=0.50 to a wake separation ring at x/2a=0.99. Results are plotted in Figure 4.29. A wake angle of 117 degrees produced the closest average match to the experimental results. Figure 4.30 shows the final wake configuration.

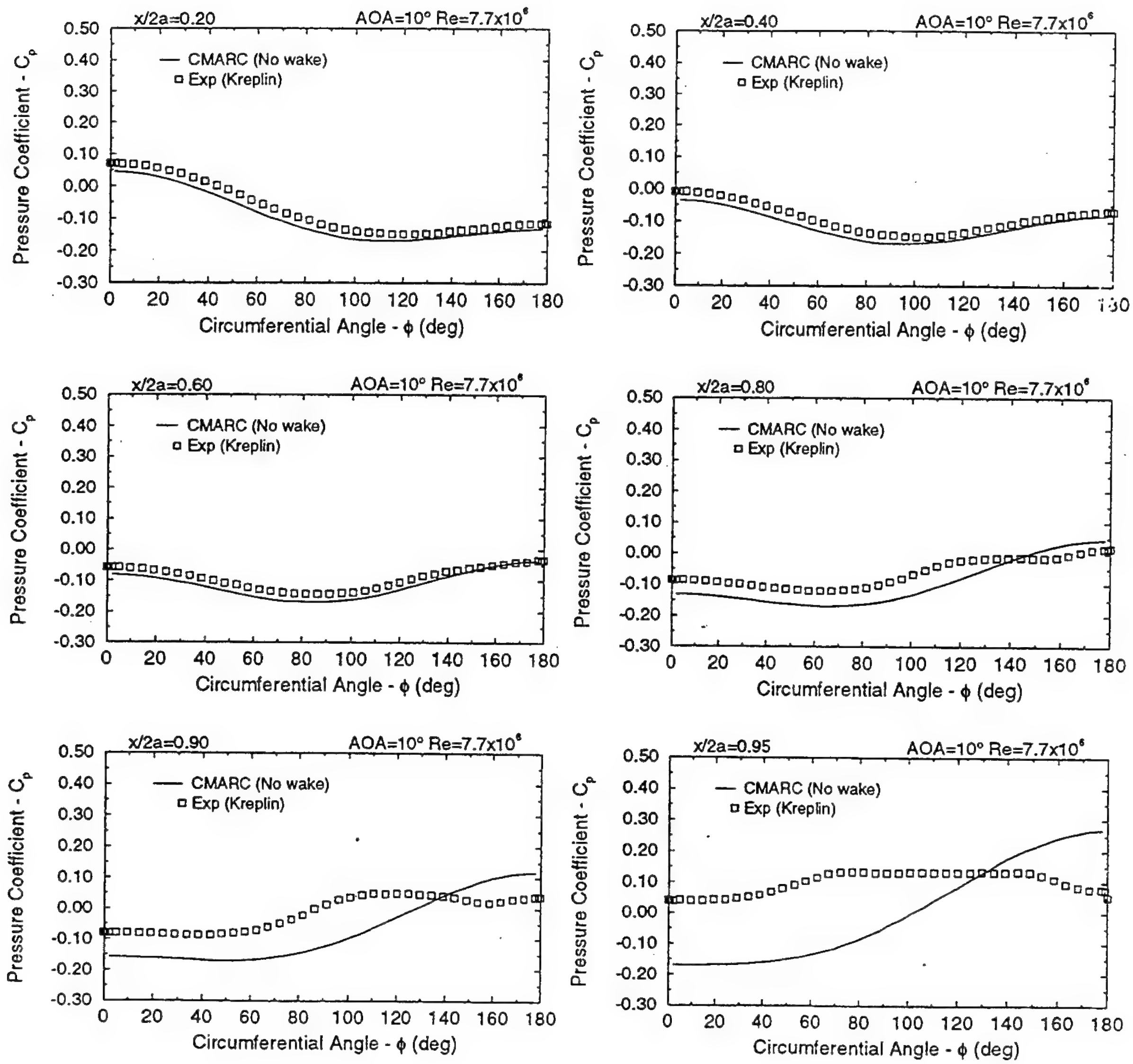

Figure 4.28 CMARC Potential Flow (No Wakes) Pressure Distribution Compared to Experimental Data, after Ref. [12].

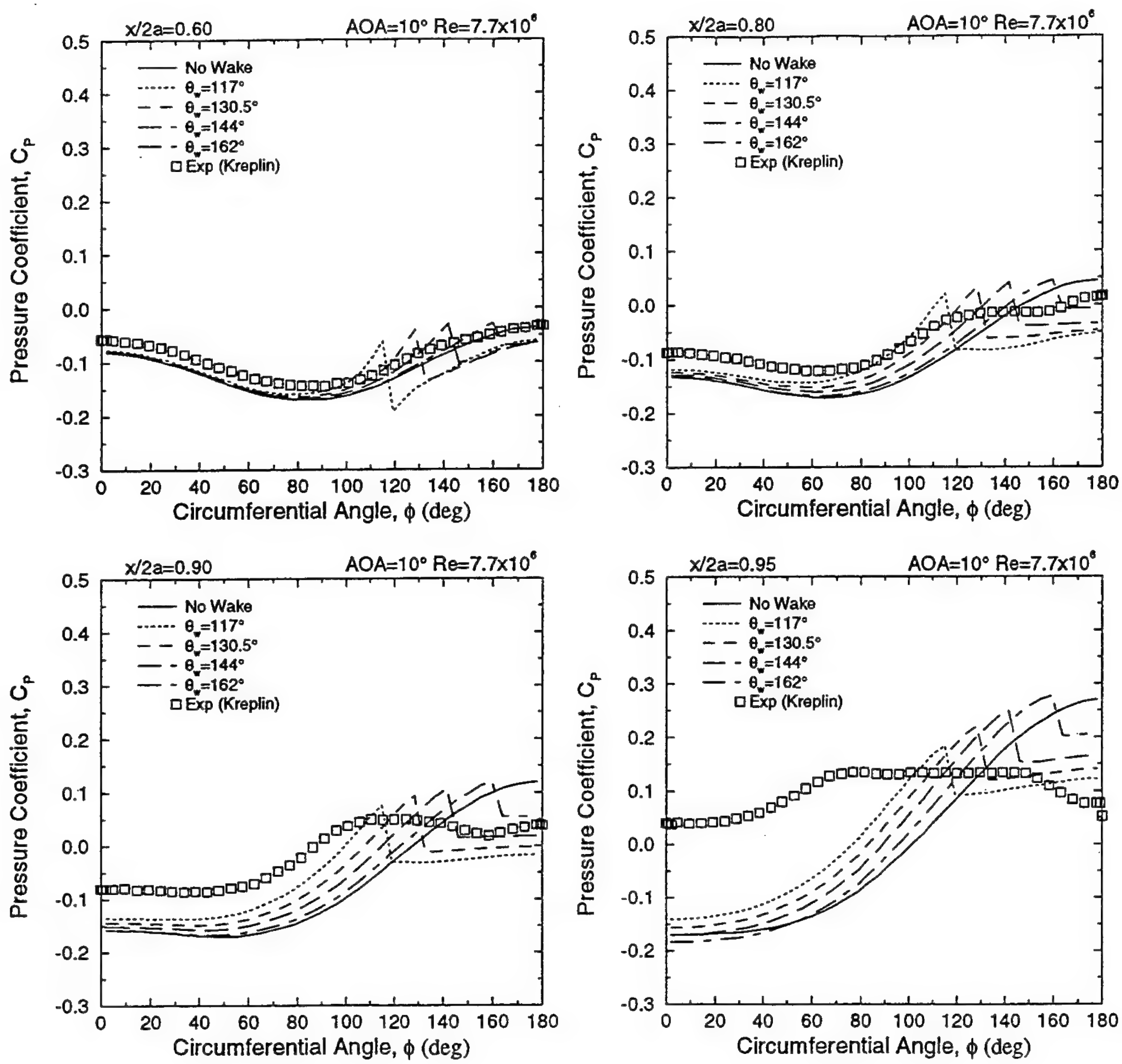

Figure 4.29 CMARC Pressure Distribution with Wake Angles Ranging from 117° to 162° Compared to Experimental Data, after Ref. [12].

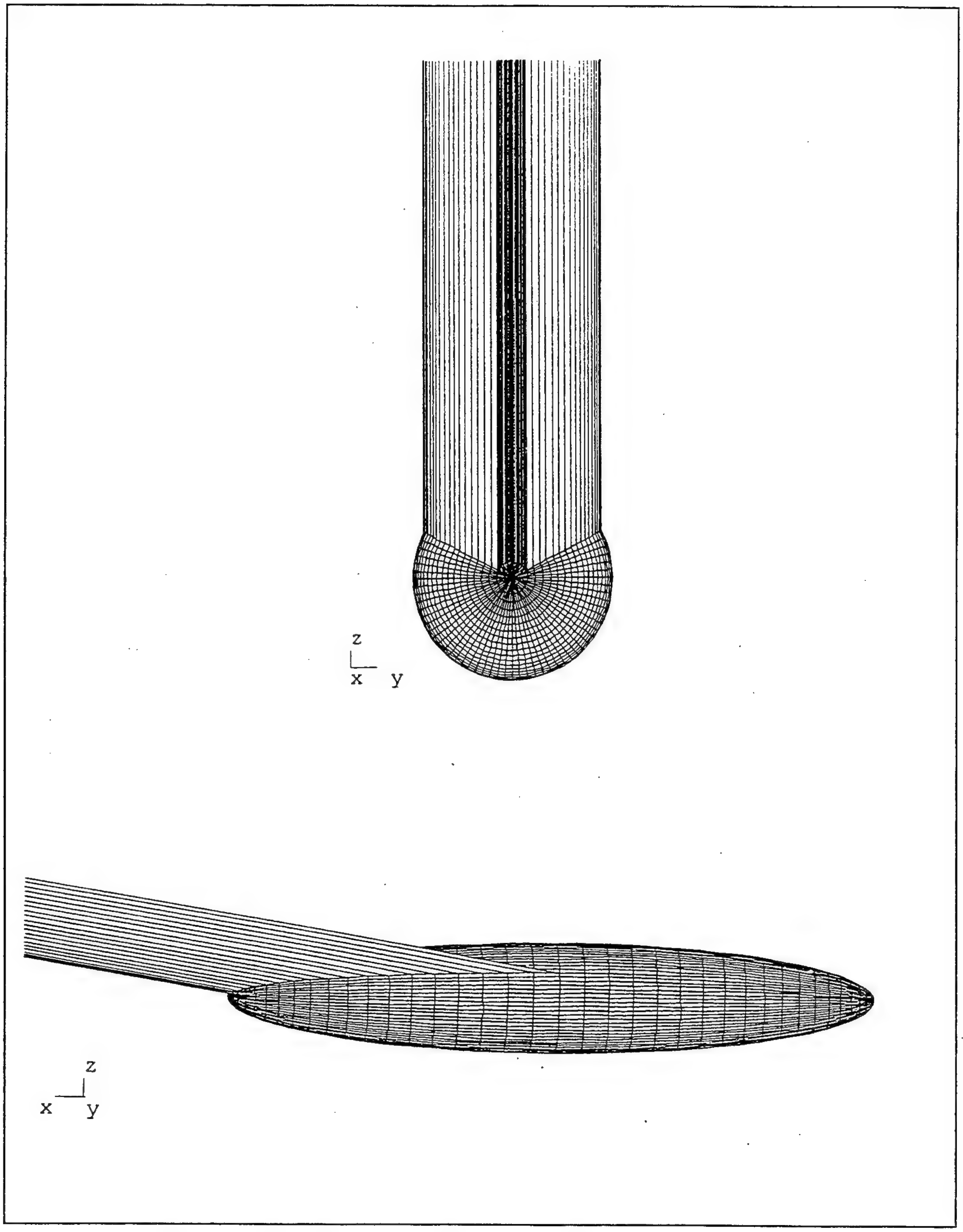

Figure 4.30 POSTMARC Views of CMARC Model with 117° Wake Separation Line Running Aft from x/2a=0.5 to x/2a=0.99.

Coefficients for normal (C_N), axial (C_A), lift (C_L), drag (C_D), and pitching moment (C_m) are compared to experimental forces in Table 4.3 for a circumferential wake angle of 117 degrees. CMARC automatically outputs the pressure load coefficients in both wind and body axes. Skin friction forces are calculated using POSTMARC and will be discussed in a later section. The experimental results are from integrated pressure forces using the method outlined in Appendix B. The coefficients are normalized by maximum diameter and cross sectional area. A wake angle of 117 degrees produces a close match to experimental results for C_N, C_L and C_m. As expected, the axial and drag coefficients are off considerably from experimental data.

Force Origin	Force/Moment Coefficient	Experimental AGARD 303-Kreplin	CMARC θ_w=117°	% Difference (CMARC-exp)/exp
Pressure Forces	C_N	0.1924	0.1816	-5.6%
	C_A	0.0026	0.0411	1480.8%
	C_L	0.1890	0.1717	-9.2%
	C_D	0.0359	0.0720	100.6%
	C_m	0.9009	0.9003	-0.1%

Table 4.3 Comparison of Integrated Experimental Pressure Forces to the CMARC Model with 117° Wake Placement Angle, after Ref. [12].

It is concluded that a pure potential flow solution over a streamlined body at 10° angle-off-attack will fail to predict substantial regions of flow separation. However, pressure distributions over bodies with substantial flow separation can be approximated by proper wake distribution. As outlined by Tuncer and Platzer [Ref. 7], a wake separation angle of 144° is a good starting point.

5. Boundary Layer Separation Locations

Next, CMARC boundary layer calculations were visualized to see how well CMARC predicted separation points for the inclined prolate spheroid. As reported in the section on the NACA 2415 finite wing, predicted boundary layer separation points from CMARC matched those predicted by the NPS UPOT code fairly well, especially at higher

Reynolds numbers. In this case, the boundary layer points are compared to experimental data at the same 10° angle-of-attack over the three-dimensional prolate spheroid.

Sixty-six streamlines for boundary layer calculations were placed on the CMARC model at locations corresponding to experimental data points. Appendix F contains the input file. CMARC only predicted separation over the very aft end of the body. A separation point is best visualized with POSTMARC by selecting the on-body streamline boundary layer thickness or shape factor functions. The separation point is indicated at the last downstream point on the streamline. It is important to note that if one visualizes streamline pressure coefficient, velocity or Mach number, the streamline will travel all the way to the aft stagnation point. In other words, to visualize a separation point, phenomena derived from the boundary layer calculations and not the streamline calculations must be selected for visualization.

Figure 4.31 displays the streamline separation points on the aft end of the prolate spheroid. CMARC boundary layer separation points are compared to experimental data as a function of axial location and circumferential angle in Figure 4.32. It is to be expected that the 2D code implemented in CMARC fails to accurately predict separation regions over streamlined bodies of revolution with large cross flow velocities. Nevertheless, these results help to quantify the differences.

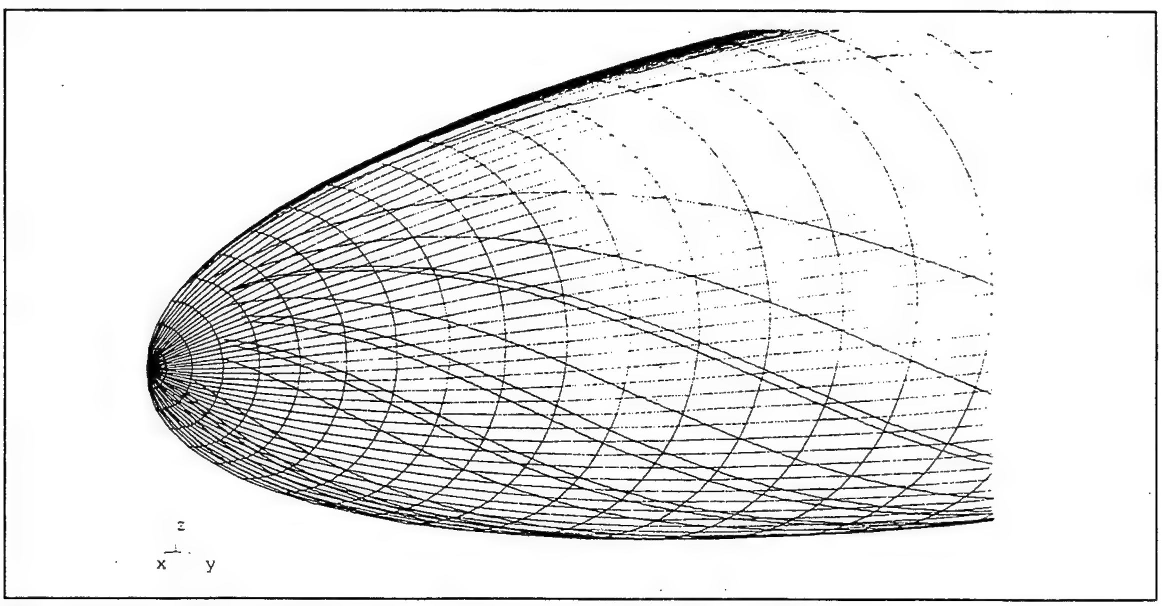

Figure 4.31 POSTMARC Visualization of CMARC Predicted Separation Points on the Aft End of the Prolate Spheroid Model (No Wakes).

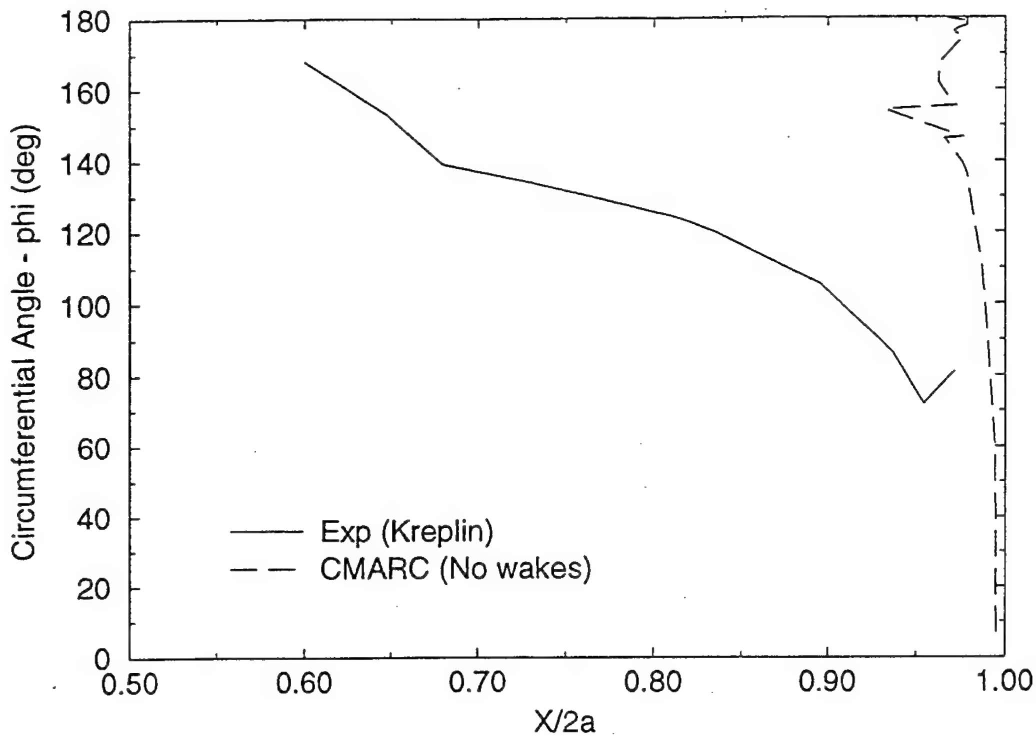

Figure 4.32 Comparison of CMARC Predicted Separation Line to Experimental Data, after Ref. [12].

6. Boundary Layer Skin Friction Coefficient

CMARC-computed skin friction coefficients were compared to experimental data obtained from hot film sensors [Ref. 12]. Sixty-six streamlines were placed through panels on the CMARC model corresponding to skin friction data pints. Data were extracted manually from the CMARC output filew. Data are plotted at six axial locations as a function of circumferential angle in Figure 4.33. The wind tunnel model has a transition strip located at x/2a=0.20. All CMARC boundary layer calculations are based on a built-in transition model. There are no provisions for specifying the transition location in CMARC.

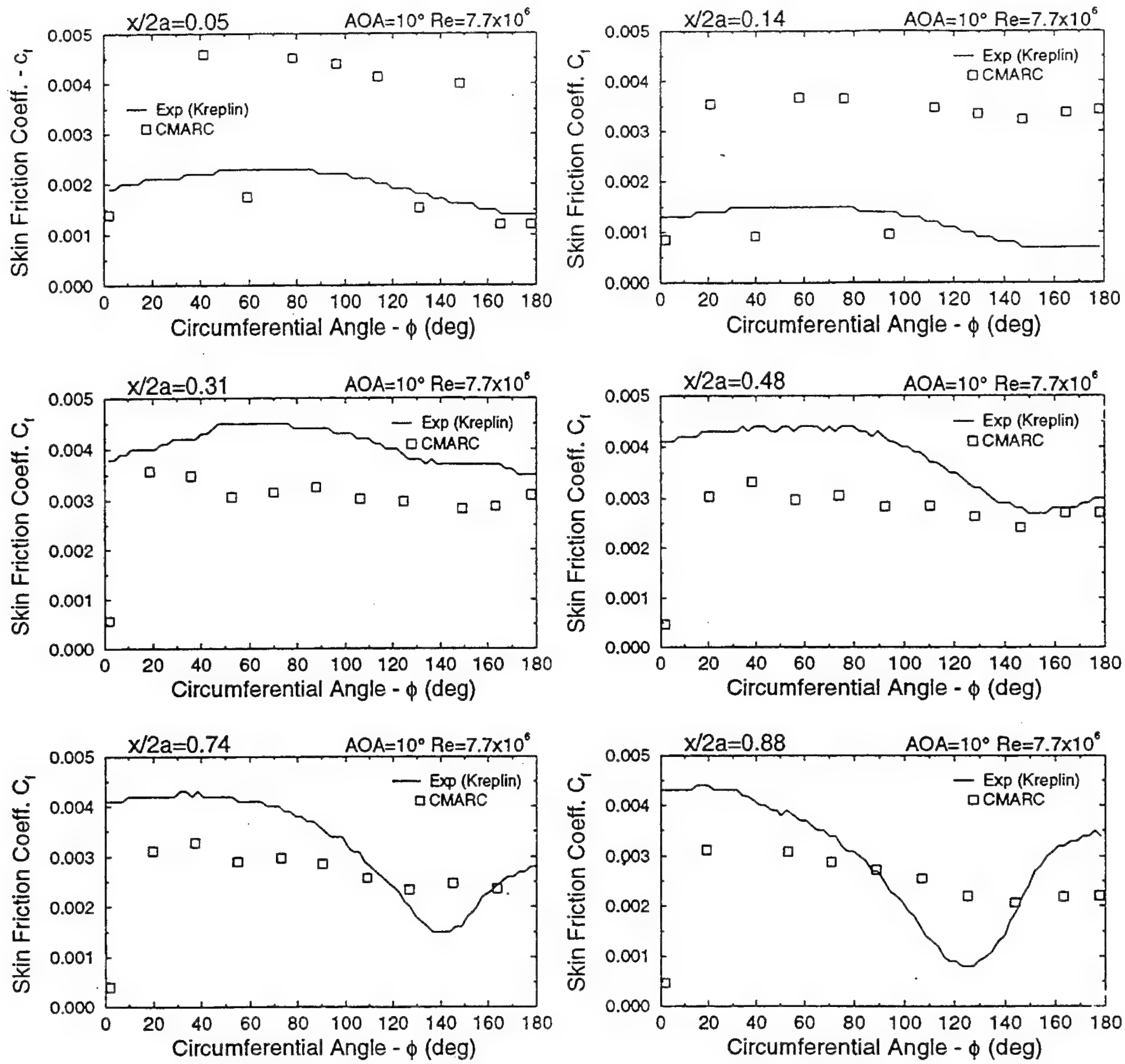

Figure 4.33 Comparison of CMARC Predicted Skin Friction Coefficient to Experimental Data, after Ref. [12].

For the two axial locations in front of the transition strip, x/2a=0.05 and 0.14, CMARC predicts a mix of laminar and turbulent flow. A laminar boundary layer is indicated by the data points where $C_f < 0.002$. Experimental data indicate strictly laminar flow for these axial locations. CMARC streamlines passing through each circumferential location travel a unique path across different panel geometry from the forward stagnation point to the point of interest. Being an integral two-dimensional boundary layer method, CMARC's empirical transition formula predicts separation for some of the streamlines and laminar flow for the others. In general, CMARC over-predicts skin friction drag in this region due to the mixed flow. If CMARC correctly predicted all laminar flow, the results would be close to experimental results.

Aft of the transition strip at x/2a=0.20, experimental data indicate fully turbulent flow as expected. CMARC predicts turbulent flow for all but the lower streamline which has a low adverse pressure gradient. At x/2a=0.31 and 0.48, computed skin friction is accurate to within 25%. Aft of x/2a=0.48, CMARC results are less meaningful due to the large region of separated flow.

7. Integrated Skin Friction Forces

POSTMARC version 1.17.3 contains functionality for performing integrated skin friction calculations. When a CMARC model is processed with the "-p" command line switch, a file with a ".pm" extension is created with the information necessary for POSTMARC to perform boundary layer calculations. POSTMARC then places streamlines on every panel, performs boundary layer calculations and integrates the skin friction loads. Experimental data is integrated as outlined in Appendix B.

Integrated skin friction forces for the prolate spheroid model without wakes are compared to experimental data in Table 4.4. Normal, axial, drag and pitching moment coefficients were all within 40% of the rough estimate provided by integrating the experimental data. This is in keeping with the observations from Figure 4.33. The lift coefficient produced due to skin friction is so small that comparisons between experimental and CMARC data are meaningless.

Force Origin	Force/Moment Coefficient	Experimental AGARD 303-Kreplin	CMARC θ_w=117°	% Difference (CMARC-exp)/exp
Skin Friction Forces	C_N	0.0102	0.0071	-30.6%
	C_A	0.0610	0.0376	-38.4%
	C_L	-0.0006	0.0004	-166.7%
	C_D	0.0618	0.0376	-39.2%
	C_m	0.0022	0.0019	-12.4%

Table 4.4 Comparison of Integrated Experimental Skin Friction Forces to the CMARC Model without Wakes, after Ref. [13].

8. Total Integrated Forces

As a final comparison of CMARC results to experimental data, the summed pressure and skin friction force coefficients are presented in Table 4.5. A simple fore/aft wake running from x/2a=0.5 to a partial ring wake at x/2a=0.99 provides good results for all but the axial and drag coefficients. It is concluded that CMARC, with proper wake selection, will provide meaningful force and moment coefficients for the development of stability derivative data. Results for drag coefficient are less meaningful and should be avoided for performance calculations.

Force Origin	Force/Moment Coefficient	Experimental AGARD 303-Kreplin	CMARC θ_w=117°	% Difference (CMARC-exp)/exp
Pressure Forces	C_N	0.1924	0.1816	-5.6%
	C_A	0.0026	0.0411	1480.8%
	C_L	0.1890	0.1717	-9.2%
	C_D	0.0359	0.0720	100.6%
	C_m	0.9009	0.9003	-0.1%
Skin Friction Forces	C_N	0.0102	0.0060	-41.2%
	C_A	0.0610	0.0379	-37.9%
	C_L	-0.0006	-0.0017	180.0%
	C_D	0.0618	0.0388	-37.2%
	C_m	0.0022	0.0017	-23.5%
Total Forces	C_N	0.2026	0.1876	-7.4%
	C_A	0.0635	0.0790	24.4%
	C_L	0.1884	0.1700	-9.8%
	C_D	0.0977	0.1108	13.4%
	C_m	0.9031	0.9020	-0.1%

Table 4.5 Comparison of Integrated Experimental Forces to the CMARC Model with 117° Wake Placement Angle, after Ref. [12].

V. AERODYNAMIC MODEL OF THE FROG UAV

A. BACKGROUND

The Naval Postgraduate School Aeronautics Department is integrating UAV hardware and software to demonstrate autonomous flight, trajectory tracking and automatic landing. A core requirement for flight control law development is a valid aerodynamic truth model for the UAV airframe. A panel code model of the FROG UAV is one method for estimating many of the stability derivatives required for an aerodynamic truth model. This development effort concentrates on finding the $C_{L\alpha}$ and $C_{m\alpha}$ longitudinal stability derivatives followed by the $C_{Y\beta}$, $C_{l\beta}$ and $C_{n\beta}$ lateral-directional stability derivatives. A future study will continue the development for rate damping and control effectiveness derivatives.

Panel code modeling utility goes beyond the development of aerodynamic coefficients. Flight control systems require accurate pitot-static and angle-of-attack sensor inputs. CMARC accurately solves on-body static pressure distributions and off-body flow velocities over the predominately attached flow fields of fuselage fore bodies. In this study, correction curves are generated for static-pressure source and angle-of-attack probe position errors.

B. FROG UAV DESCRIPTION

The FROG UAV is a small single engine flight test vehicle used for autonomous flight research by the Naval Postgraduate School Aeronautics Department. The aircraft was originally designated the FOG-R by the U. S. Army. It was designed as a small lightweight, battlefield observation platform that could be guided by a fiber optic data link. Table 5.1 presents the basic aircraft specifications.

The aircraft is somewhat unconventional in that the engine is mounted in a nacelle tractor style above the fuselage and wing. The aft fuselage consists of a 1.75 in. diameter aluminum tube which connects the tail surfaces to the main fuselage. Figure 5.1 displays a three view drawing of the FROG UAV.

PARAMETER	MEASUREMENT/UNITS	
Length	8.125 ft	97.5 in
Height	1.75 ft	21 in
Weight	67.7 lbs	
Power Plant	12 Hp / 2 Cycle	
Wing Airfoil	NACA 2415	
Horiz. Stab. Airfoil	NACA 0006 (Approx.)	
$S_w (S_{ref})$	17.57 ft^2	2530 in^2
S_t	3.174 ft^2	457.1 in^2
S_v	0.9818 ft^2	141.4 in^2
c	1.66 ft	20 in
c_t	0.958 ft	11.5 in
b_w	10.54 ft	126.5 in
b_t	3.313 ft	39.75 in
b_v	1.25 ft	15.0 in
l_t	4.44 ft	53.25 in
l_v	4.44 ft	53.25 in
AR_w	6.32	
AR_t	3.46	
AR_v	1.59	
V_H	0.49	
V_v	0.02	

Table 5.1 FROG UAV Characteristics, after Ref. [1].

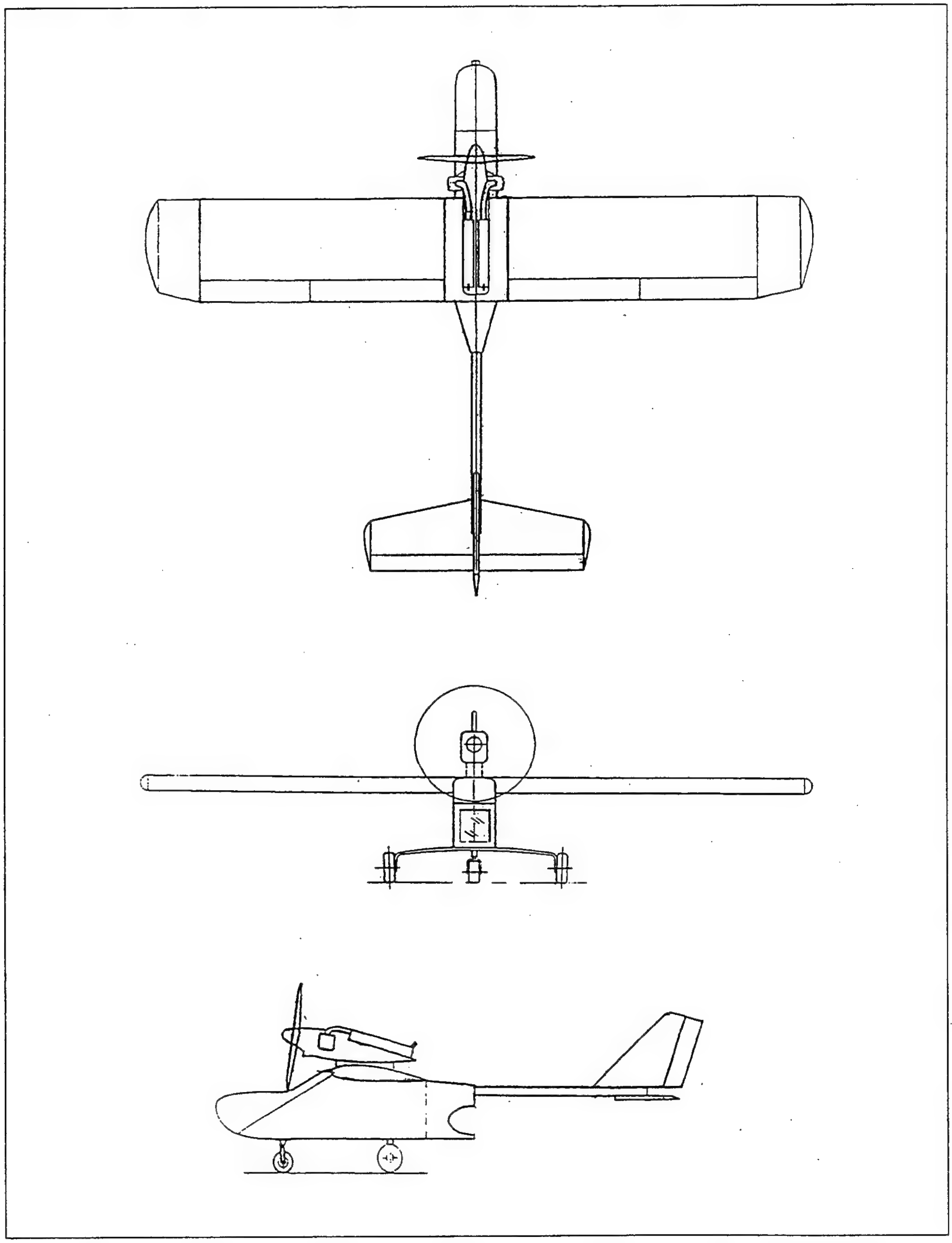

Figure 5.1 FROG UAV Three-View Drawing.

The FROG UAV, as operated by NPS, is equipped with airspeed, angle-of-attack, altitude and control surface sensors. In addition, a miniature Inertial Measurement Unit (IMU) captures aircraft attitude, acceleration and body rates. Data is down linked to a mobile SGI workstation through a spread spectrum modem. Onboard GPS provides differential GPS navigation capability with the ground station used as a reference. The aircraft can be flown by conventional radio control or by up-linking flight control commands from the computer workstation.

Current flight control development revolves around the cruise trim point of 60 m.p.h. or 88 ft/s. This flight condition is selected for the development of stability derivative data. Table 5.2 lists the aircraft parameters for the trim flight condition.

PARAMETER	MEASUREMENT	UNITS
Weight	67.73	lbs
IXX	12.52	slug-ft^2
IYY	8.43	slug-ft^2
IZZ	18.55	slug-ft^2
Airspeed	60/88	mph and ft/s
Altitude	800	ft MSL
Air Density	0.002327	slug/ft$_3$
Center of Gravity	34.5%	M.A.C
$C_{L\ trim}$	0.4295	n/a
$\alpha_{trim\ (est)}$	-1.3	degrees
δ_{Etrim}	5.1	degrees

Table 5.2 FROG UAV Trim Flight Condition, after Ref.[1].

C. FROG UAV MODELING

1. General

LOFTSMAN is utilized for the creation of all CMARC input file patches except for wing tips. In some cases, CMARC's more efficient built-in capability to model standard NACA 4-digit wing surfaces could have been used. However, future studies will

require flight control surface patches meshed with LOFTSMAN. Therefore, with growth provisions in mind, all patches were created with LOFTSMAN from the start. Figure 5.2 displays the complete FROG UAV model with all patches and wakes activated.

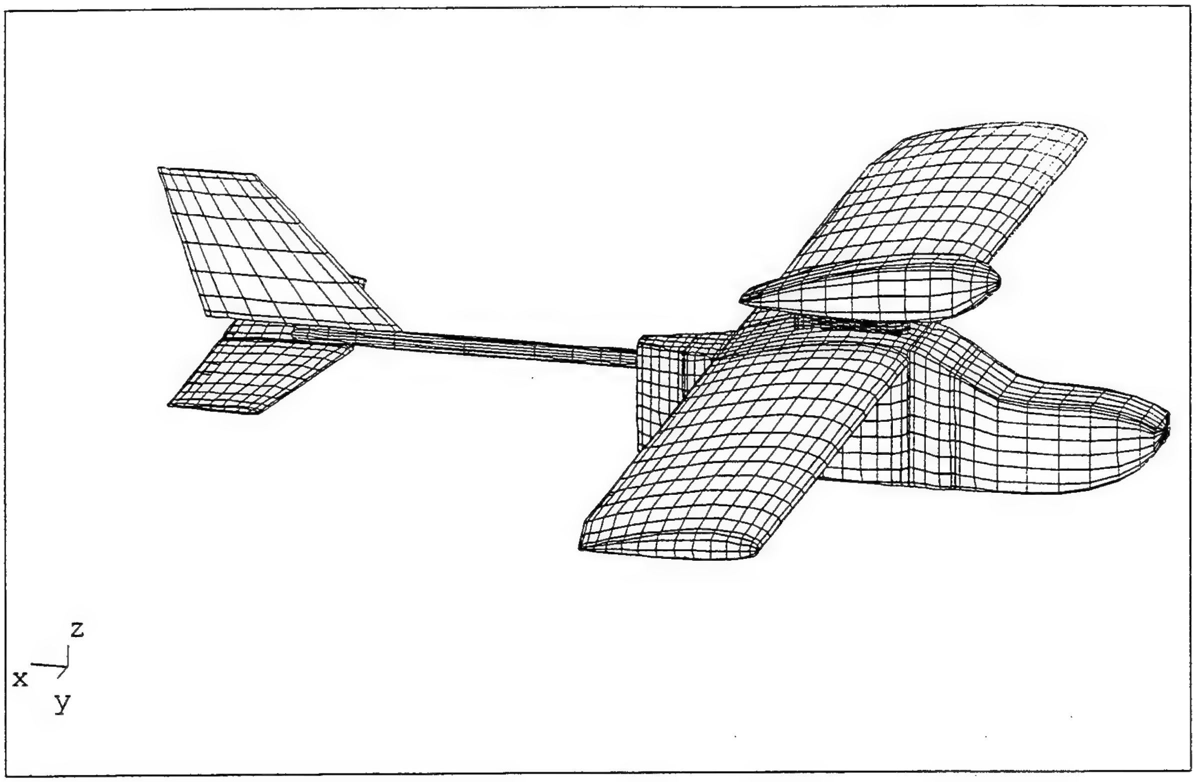

Figure 5.2 FROG UAV Panel Code Model.

Some assumptions are made to simplify the modeling process. First, the horizontal and vertical stabilizers are modeled with a NACA 0006 section. The actual surfaces are constructed with a flat section, rounded at the nose and tapered starting at the control surface hinge line to a sharp trailing edge. The NACA 0006 provides a close approximation and allows the use of LOFTMAN's built-in wing lofting capability. For a potential flow solution, this simplification is considered minor.

A second simplification is made regarding the vertical stabilizer's tip rib orientation. The actual rib is canted down 5° with respect to the longitudinal waterline.

LOFTSMAN will only model a chord line that is parallel to the waterline (constant BL). The vertical tail tip rib is modeled with a constant BL, but the span is adjusted to maintain the same overall surface area.

Finally, there is no attempt to model the tricycle landing gear struts or wheel assemblies. The landing gear components do not contribute significantly to the aerodynamic stability derivatives. However, they certainly need to be taken into account when measuring moments of inertia for a dynamic model.

2. Modeling Coordinate System

The model is developed using a coordinate system selected to simplify fuselage measurements. The +x-axis starts even with the nose and runs aft along the bottom of the fuselage, parallel with the tail boom. The bottom of the fuselage is used as the waterline with +z-axis in the up direction. This allows for easy vertical measurements when the aircraft is placed flat on a horizontal surface. The +y-axis runs from centerline outboard parallel to the right wing. Figure 5.3, which displays static-pressure source and alpha vane locations, also shows the location and origin of the modeling coordinate system.

3. LOFTSMAN Patches

LOFTSMAN is used to generate all the model patches except for wing tips. CMARC's built-in capability is used to create wing tip patches. Appendix H contains listings of all the LOFTSMAN input files. Once a surface is meshed, the mesh is saved to a file as a CMARC/PMARC patch. The resulting text file is then opened, and the text is copied and pasted with any text editor into the patch definition section of the CMARC input file. LOFTSMAN patch files are not listed because they are redundant with the patches in the final CMARC input file listed in Appendix I.

When saving a patch, LOFTSMAN automatically takes care of all CMARC input file formatting except for the TNODS patch continuation or final patch toggle. A patch, as formatted by LOFTSMAN, assumes additional patches will follow in the CMARC input file. Therefore, the last segment's TNODS variable is set TNODS=3. When the patch is the last patch in the input file, the TNODS variable must be manually set to TNODS=5. If CMARC hangs up while reading in geometry information, most likely TNODS=5 is missing on the last patch.

a. Fuselage Model

The fuselage is lofted as a B-type body. A B-type body is used when major portions of the fuselage have a circular or oval cross section. The input file is listed in Appendix H. Only the right side is meshed, with a symmetric left side created by toggling the IPATSYM variable to IPATSYM=1. LOFTSMAN assumes that B-type bodies converge to a specific point at the fore and aft ends. The flat aft fuselage face does not provide this single point. A slight modification was made to the aft face to allow automatic meshing as a B-type body. The center of the aft face is extended very slightly, approximately 1/8 inch, to provide a convergence point for the final rear triangular panels. This small deviation is assumed not affect the aerodynamic fidelity of the model for a potential flow solution.

The right side was originally meshed separately from the wing as a 20 x 20 panel patch. This created a low order fit when the wing patch was butted to the side of the fuselage, resulting in overlapping panels. A final mesh was created that flowed around the wing root and fuselage intersection for a high order fit. All the fuselage panels at the wing root join with the adjacent wing panels. This mesh requires that the fuselage be broken up into six separate panels per side. They are the nose patch, the forward transition patch, the top and bottom wing root patches, the aft transition patch and finally the rear fuselage patch. Some manual editing is required to straighten out panels on the upper fuselage patch. When the six patches are added together, the final configuration is modeled with a 44x15 panel patch.

b. Main Wing Patch

The NACA 2415 wing is created with four separate patches to allow the addition of an aileron mesh at a later date. CMARC comes with a broad selection of "*.SD" airfoil template files that are automatically loaded during installation. The "NACA2415.SD" file is used for this model. The inboard patch runs from the wing root, past the flaps, to the start of the aileron. The mid patch covers the portion of the wing spanned by the aileron. The outboard patch creates the tapered wing extension. Finally, a semi-circular wing tip patch is added in the input file using CMARC's built-in wing tip functionality. The wing is set to a 4.5° incidence in the LOFTSMAN input file. Alternatively, the patch could be created with zero incidence and then the patch

coordinate system could be rotated in the CMARC input file. Together, the four wing patches add to make a 20 x 30 panel wing model.

c. *Horizontal Stabilizer Patch*

The horizontal stabilizer patch is created with a single 10 x 22 mesh using the "NACA0006.SD" airfoil template. No special modifications are required. A tip patch is not added because some of the resulting panels would be too small. In particular, the triangular panels closing out the aft end of the tip are too small in proportion to the other panels. An attempt was made to model horizontal and vertical stabilizer wing tips, but the model will not converge with them. Leaving off tip patches will not significantly influence results according to the CMARC User's Guide [Ref. 2].

d. *Vertical Stabilizer Patch*

The vertical stabilizer patch is created with a single 8 x 18 mesh using the "NACA0006.SD" airfoil template. The LOFTSMAN input file is different in that a vertical wing surface requires a modification to the rib axis. The rib axis must be specified with an x-axis rotation of 90°, a y-axis rotation of 0° and an unspecified (999.0) z-axis rotation. No symmetry is selected for the vertical stabilizer because the patch is already symmetric about the y=0 plane. As with the horizontal stabilizer, a tip patch is not added because some of the resulting panels would be too small.

e. *Tail Boom Patch*

The tail boom patch is created as a single 12 x 10 mesh using a B-type body. Again, only the right side is meshed due to symmetry. The LOFTSMAN input file requires modifications at both ends in a similar fashion to the aft fuselage. A single point is added to allow convergence of the triangular panels at either end. With this point, the tail boom has the appearance of being tapered at both ends. The point is then manually edited out in the CMARC input file by replacing the "x" coordinate of the beginning and ending section panels with the correct value. In most cases, the tail boom is left out of solution to aid in convergence. This is due to the small overlapping panels at the fuselage tail boom junction. Being a slender, round tube directly in the fuselage slip stream, the tail boom should have little influence on the stability derivatives.

f. Engine Pod Patch

The engine pod patch, or nacelle, is created as a single 15 x 10 mesh using a B-type body. Only the right side is meshed due to symmetry. The prop spinner is an integral part of the patch. No attempt is made to model the prop, engine heads or exhaust system.

g. Engine Pylon Patch

The engine pylon patch is modeled with a single 15 x 10 mesh using an A-type body. A-type bodies are used to model surfaces similar to boat hulls with cornered surfaces or sharp chines. In addition, A-type bodies do not require the body to be completely enclosed. As a result, an A-body was selected to model just the sides of the pylon. Only the right side is meshed due to symmetry. A low order fit is achieved with the adjacent fuselage and engine pod panels. This results in questionable pressure distributions. As a result, the pylon patch was turned off for most configurations. A future attempt will be made to create a high order fit between the other patches. This will probably require manual editing of the intersecting patches.

4. Common CMARC Input File Errors

The patches created in LOFTSMAN are assembled into a single CMARC input file with any text editor. A default minimum input file comes with CMARC or any old file may be modified. There are many errors that will cause CMARC to hang up without an error message. The two most common errors are forgetting to designate the last patch and incorrectly numbering the wake patches.

The last patch must be designated by including a TNODS=5 setting in the last section of the last patch. If it is not included, CMARC hangs up when reading in the geometry. In a similar manner, the last wake must be designated with a NODEW=5 setting. If the last wake is not designated, CMARC hangs up while reading in the wake information.

Another common error involves incorrect wake to patch number association. Patch numbering changes whenever patches are disabled or reordered. The KWPACH field for each wake definition must be checked to make sure it reflects the current patch numbering.

D. STATIC-PRESSURE SOURCE AND YAW VANE CORRECTIONS THROUGH OFF-BODY FLOW ANALYSIS

CMARC is ideally suited for off-body flow analysis. Off-body streamlines may be placed through a point anywhere in the flow field. CMARC will then follow the streamline up and downstream the distance designated in the input file. This is particularly useful for flow visualization. In addition, CMARC calculates pressure coefficient and velocity at each point along the streamline. For this study, two streamlines are placed through the locations of the static-pressure source and alpha probe locations. Pressure coefficient is used to quantify static source position error and velocity is used to calculate alpha probe position error as a function of FROG UAV angle-of-attack. Both static pressure and AOA are digitized for down link to the ground station allowing the values to be easily corrected. Either a look-up table or curve fit correction can be applied subsequent to being passed to the flight control routines.

1. Description of the FROG UAV Pitot-Static and AOA Systems

The pitot-static system and angle-of-attack probe share a common flight test boom extending from the nose of the UAV. The boom contains both the total and static pressure ports. Figure 5.3 depicts the general dimensions of the flight test boom installation and the modeling coordinate system.

2. Modeling Off-Body Streamlines

Streamlines are placed at the two locations indicated in Figure 5.3 which correspond to the static source and alpha probe locations. Two off body streamlines were activated in CMARC by setting NSTLIN=2 in the &SLIN1 line. Only a short distance of 2 inches is selected up and downstream in the SU and SD fields to reduce the size of the output file. Figure 5.4 is a POSTMARC rendering of the two off-body streamlines used for sensor corrections. With the model at α_t=0°, notice that the streamline is curving up at the angle-of-attack vane location 6.5 inches in front of the aircraft nose.

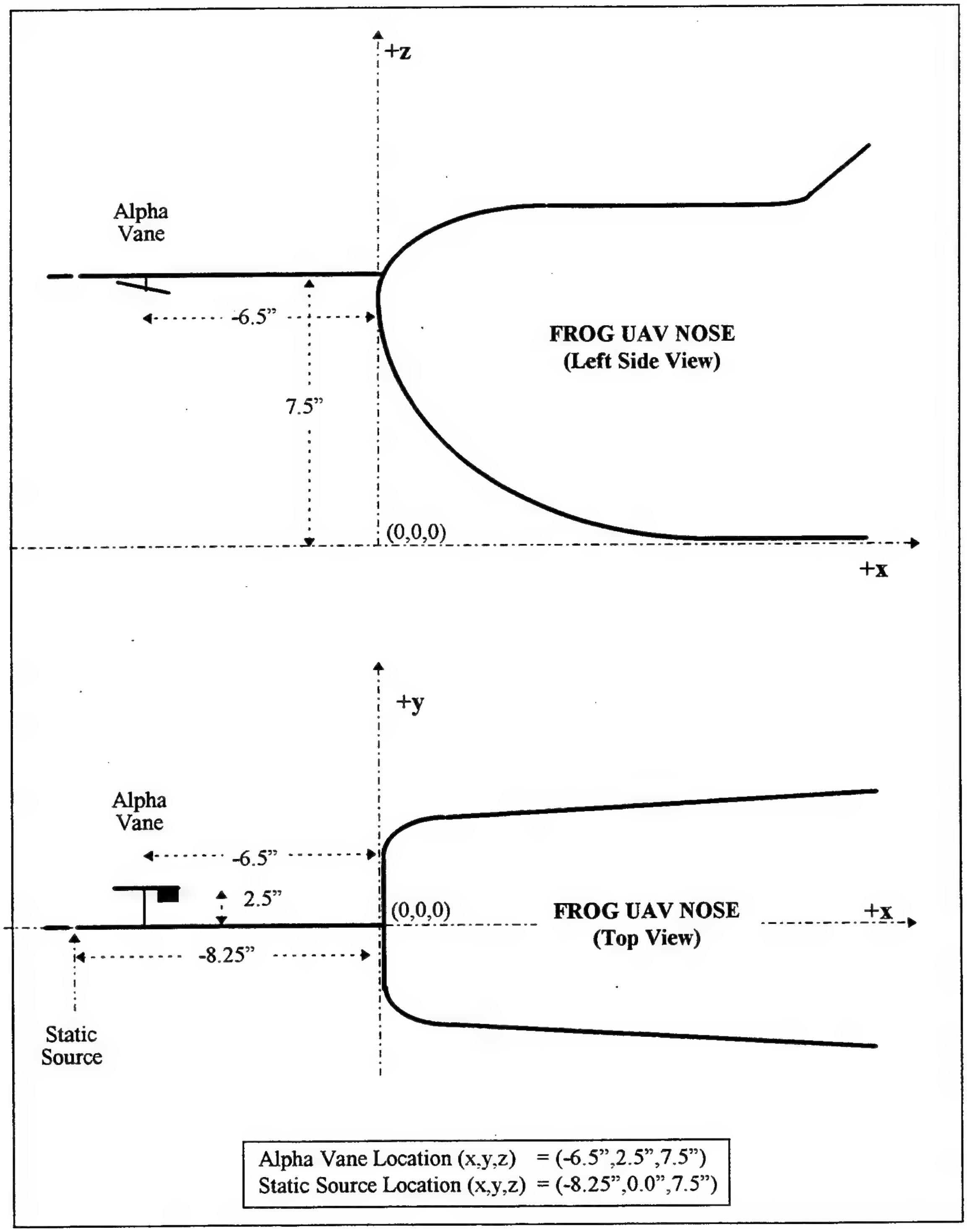

Figure 5.3 Diagram of the FROG UAV Pitot-Static and AOA Systems.

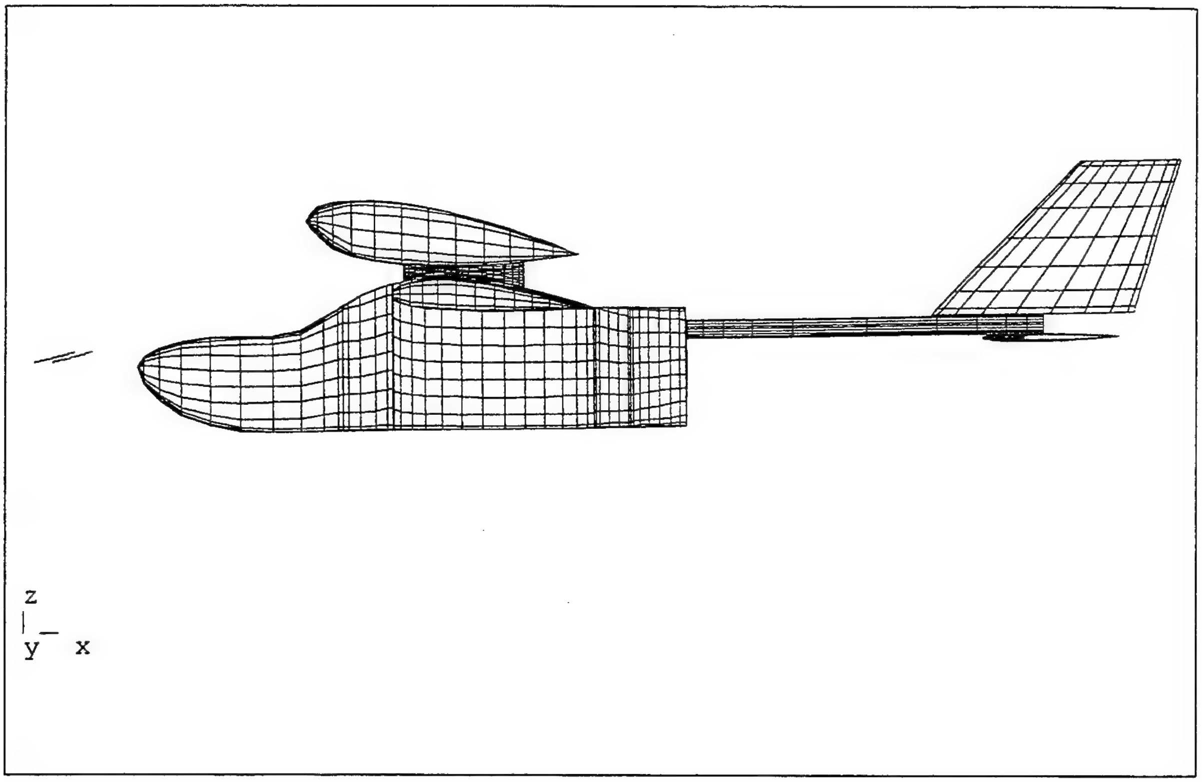

Figure 5.4 FROG UAV Off-Body Streamline visualization with POSTMARC (α_t=10°).

3. Analysis of Static Source Position Errors

In general, the position error pressure coefficient, $\Delta C_{P\,pc}$ or $\Delta P_p/q_c$, is a function of freestream Mach number and angle-of-attack provided that the static source is located outside of a thick boundary layer and sideslip is minimized [Ref. 13]. In the case of the FROG UAV with incompressible flow, $\Delta P_p/q_c$ becomes a function of angle-of-attack only. As a result, the corrections can be simply defined as a function of measured angle-of-attack.

A DOS batch file was executed to step the CMARC model through angles-of-attack ranging from -8° to 20°. The batch file incremented the angle-of-attack using CMARC's command line override feature. In addition, a new output file name was designated for each angle-of-attack. Position error pressure coefficient is then read from the off-body streamline listing of the output file at the location corresponding to the static

source. Table 5.3 lists the values of $\Delta P_p/q_c$ calculated from CMARC data. Figure 5.5 displays $\Delta C_{P\,pc}$ as a function of indicated angle-of-attack. The second order influence of angle-of-attack is clear with the second order curve fitting tightly through the data points. Of note, the error is relatively constant for a ±8° band around trim angle-of-attack. For incompressible flow, position error pressure coefficient is independent of airspeed and altitude.

Position error pressure coefficient can be turned into position corrections for airspeed and altitude. The following relations were developed which assume small errors and incompressible flow:

$$\Delta V_{pc} = \frac{V_i \Delta C_p}{2} \quad \text{and} \quad \Delta V_{pc} = V_c - V_i \tag{5.1}$$

$$\Delta H_{pc} = \frac{\Delta V_{pc} V_i}{\sigma_{std} g_o} \quad \text{and} \quad \Delta H_{pc} = H_c - H_i \tag{5.2}$$

Where:

ΔH_{pc} is the altitude position correction.

ΔV_{pc} is the velocity position correction.

$\Delta C_p = \dfrac{\Delta P_p}{q_c}$ or position error pressure coefficient.

σ_{std} is standard day density ratio.

g_o is the gravitational constant.

Table 5.3 displays corrections calculated for both airspeed and altitude at the FROG UAV trim condition of 88 ft/s and 800 ft MSL. The corrections are added to the indicated value to obtain the corrected value. Figures 5.6 and 5.7 display the corrections as a function of indicated angle-of-attack. Again, a second order curve fits nicely through the data points. Equations 5.1 and 5.2 can be used to implement a correction algorithm based on airspeed and altitude.

UAV AOA α_T (deg)	ΔCp_{pc} $\Delta P/q_c$	V Correction $\Delta V_{pc}=V_c-V_i$ (ft/s)	H Correction $\Delta H_{pc}=H_c-H_i$ (ft)
-8	0.1092	4.8	13.5
-6	0.1120	4.9	13.8
-3	0.1141	5.0	14.1
-2	0.1140	5.0	14.1
-1	0.1137	5.0	14.1
0	0.1132	5.0	14.0
1	0.1123	5.0	13.9
2	0.1111	4.9	13.7
3	0.1096	4.8	13.5
4	0.1078	4.8	13.3
5	0.1057	4.7	13.1
6	0.1034	4.6	12.8
8	0.0977	4.3	12.1
10	0.0909	4.0	11.2
12	0.0831	3.7	10.3
14	0.0741	3.3	9.2
16	0.0641	2.8	7.9
18	0.0530	2.3	6.6
20	0.0410	1.8	5.1

Table 5.3 Position Error Corrections for the NPS FROG UAV at V=88 ft/s and H=800 ft MSL. Derived from CMARC Panel Code Off-Body Flow Field Analysis.

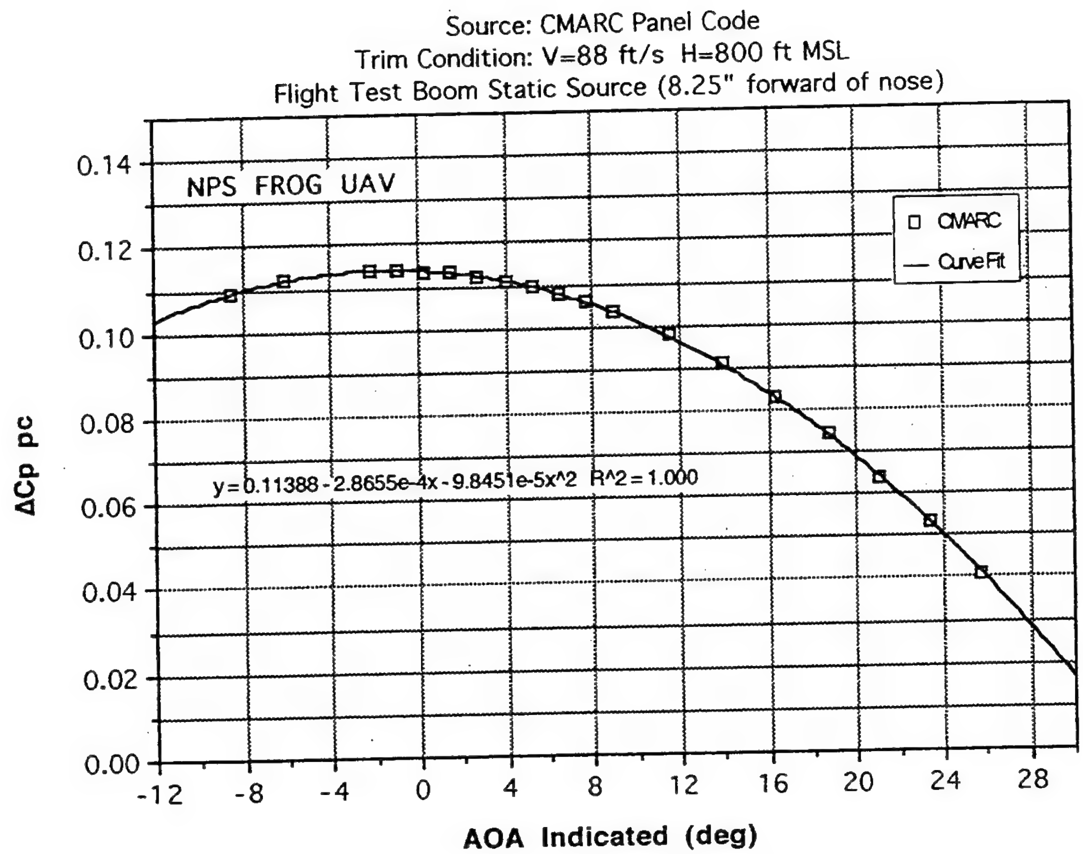

Figure 5.5 Position Error Pressure Coefficient, $\Delta C_{P\ pc}$, for the NPS FROG UAV. Derived from CMARC Panel Code Off-Body Flow Field Analysis.

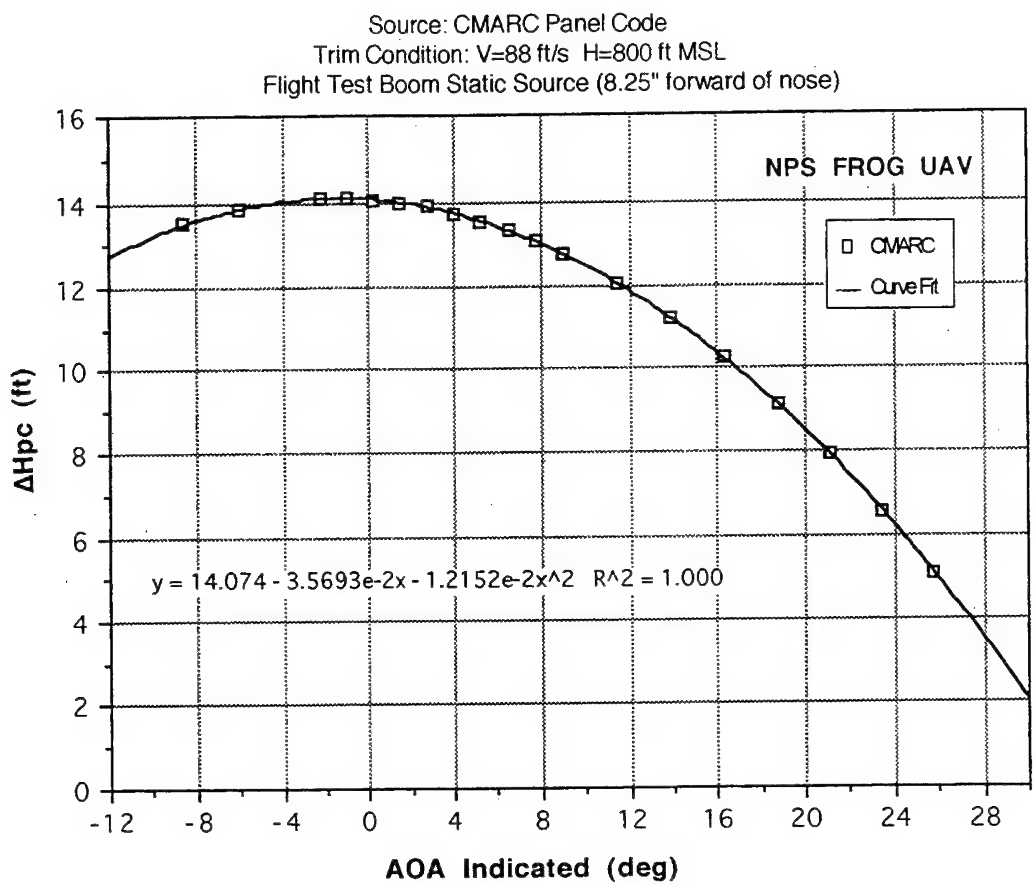

Figure 5.6 Altitude Position Error, ΔH_{pc}, for the NPS FROG UAV at V=88 ft/s and H=800 ft MSL. Derived from CMARC Panel Code Off-Body Flow Field Analysis.

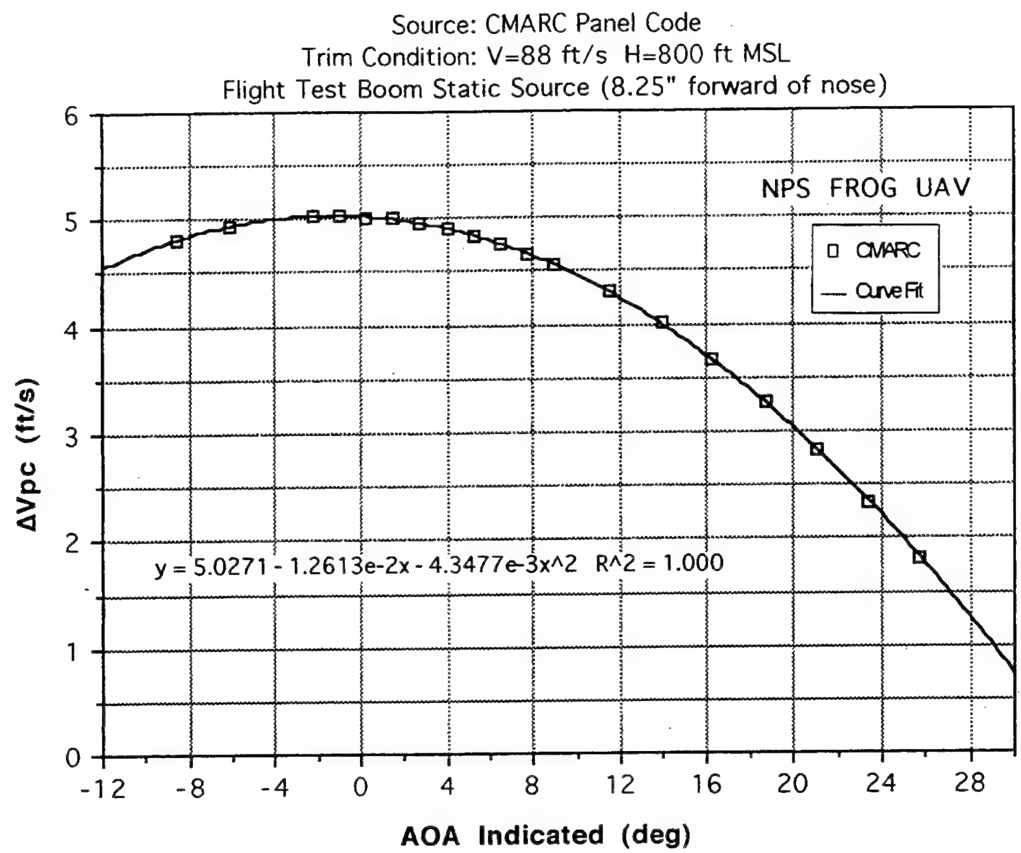

Figure 5.7 Airspeed Position Error, ΔVpc, for the NPS FROG UAV at V=88 ft/s and H=800 ft MSL. Derived from CMARC Panel Code Off-Body Flow Field Analysis.

4. Analysis of Alpha Vane Position Error

Local flow field velocity is extracted from the off-body streamline listing to obtain local angle-of-attack. The alpha vane is assumed to capture the x-z component of the local velocity field and ignore cross flow in the y direction. Flow field velocity is turned into indicated angle-of-attack and angle-of-attack position correction with the following equations:

$$\alpha_i{}^\circ = a\tan\left(\frac{V_z}{V_x}\right) * \frac{180}{\pi} \text{ degrees} \qquad 5.3$$

$$\Delta\alpha^\circ_{pc} = \alpha_t - \alpha_i \text{ degrees} \qquad 5.4$$

A DOS batch file is executed to step the CMARC model, with an off-body streamline located at the vane position, through angles-of-attack ranging from -8° to 20°. Local velocity components are then read from the location corresponding to the alpha vane. Table 5.4 lists the values of $\Delta\alpha_{pc}$ calculated from CMARC data. Figure 5.8 displays $\Delta\alpha_{pc}$ as a function of indicated angle-of-attack. Linear and second order curve fit equations are also indicated on Figure 5.8. Angle-of-attack correction is fairly linear through the FROG operating envelope, with approximately -1.25 degrees of position error at the FROG cruise trim condition. The corrections apply at all incompressible airspeeds and all altitudes.

5. Summary of Off-Body Flow Field Analysis

CMARC proved useful for both static-pressure source and alpha vane position corrections. Measured data may be corrected using look-up tables with the values in Table 5.3 and 5.4 or by using the curve fits in Figures 5.5 through 5.8. Flight testing is recommended for validation of sensor corrections obtained from this CMARC off-body flow field analysis.

UAV AOA	Velocity at Alpha Vane			AOA $_{Correction}$	AOA $_{Indicated}$
α_T (deg)	V_x (ft/s)	V_y (ft/s)	V_z (ft/s)	$\Delta\alpha=\alpha_T-\alpha_i$ (deg)	α_i (deg)
-8	80.92	1.66	-12.23	0.60	-8.60
-6	81.27	1.65	-8.65	0.08	-6.08
-3	81.60	1.64	-3.21	-0.75	-2.25
-2	81.67	1.63	-1.47	-0.97	-1.03
-1	81.71	1.63	0.28	-1.20	0.20
0	81.73	1.62	2.13	-1.49	1.49
1	81.73	1.61	3.93	-1.75	2.75
2	81.70	1.60	5.72	-2.00	4.00
3	81.66	1.59	7.51	-2.25	5.25
4	81.58	1.58	9.30	-2.50	6.50
5	81.48	1.57	11.08	-2.75	7.75
6	81.37	1.56	12.88	-2.99	8.99
8	81.07	1.53	16.43	-3.46	11.46
10	80.67	1.51	19.98	-3.91	13.91
12	80.17	1.48	23.50	-4.34	16.34
14	79.61	1.46	26.99	-4.73	18.73
16	78.93	1.43	30.47	-5.11	21.11
18	78.18	1.39	33.90	-5.44	23.44
20	77.34	1.36	37.31	-5.75	25.75

Table 5.4 Angle-of Attack Vane Position Error Corrections for the NPS FROG UAV. Derived from CMARC Panel Code Off-Body Flow Field Analysis.

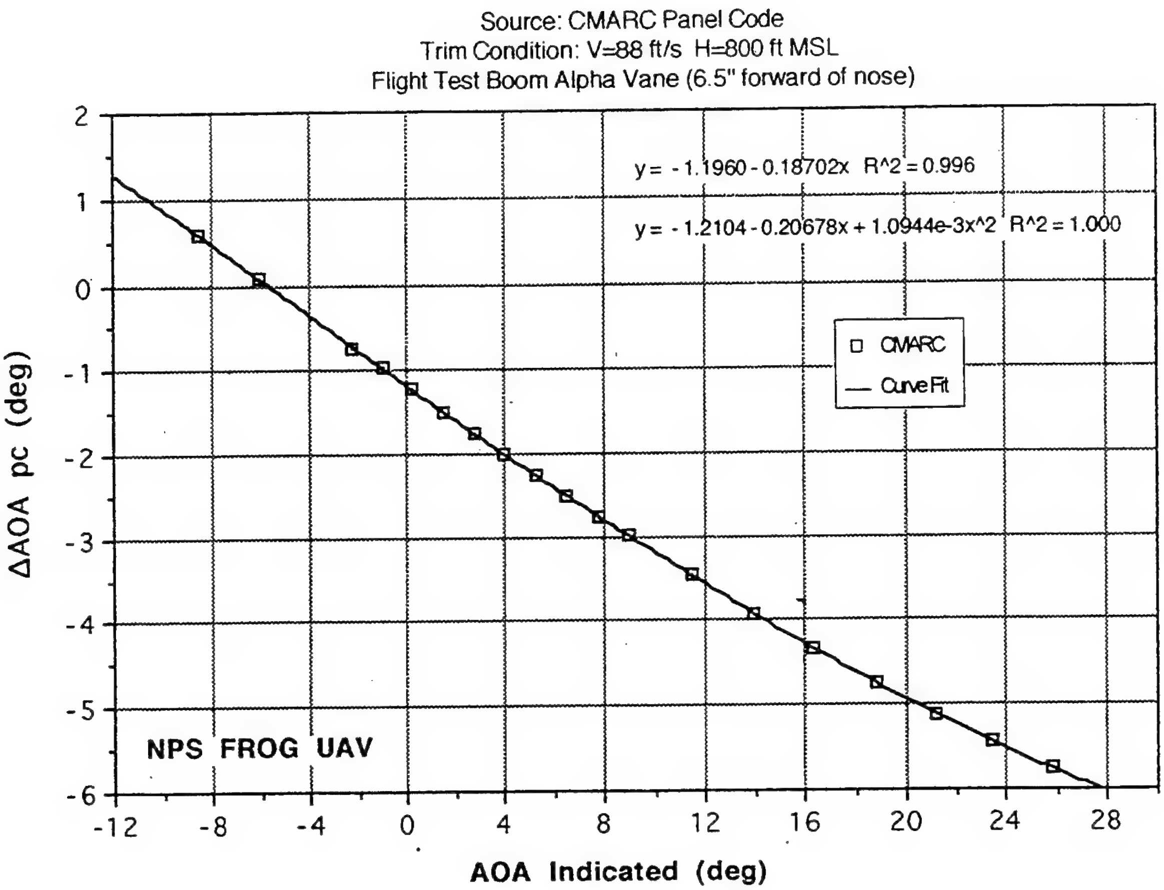

Figure 5.8 Angle-of-Attack Vane Position Error, $\Delta\alpha_{pc}$, for the NPS FROG UAV. Derived from CMARC Panel Code Off-Body Flow Field Analysis.

E. DEVELOPMENT OF BASIC STABILITY DERIVATIVES

In this section, CMARC is used to develop some of the basic longitudinal and lateral-directional stability derivatives for the FROG UAV. The development effort focuses on finding the $C_{L\alpha}$ and $C_{m\alpha}$ longitudinal stability derivatives followed by the $C_{Y\beta}$, $C_{l\beta}$ and $C_{n\beta}$ lateral-directional stability derivatives. Control power and rate damping derivatives will be the focus of ongoing research.

CMARC contains built-in functionality to integrate forces and moments in all axes over the surface of a body. Forces and moments are automatically normalized into non-dimensional coefficients based on the mean aerodynamic chord, reference wing area, semi-span and center of gravity location in the CMARC BINP9 input line. Coefficients are presented in both wind and body axes. The CMARC model is run at two different angles-of-attack and one sideslip angle. The slope of the force and moment coefficients is then taken to produce the $C_{L\alpha}$ and $C_{m\alpha}$ longitudinal derivatives and the $C_{Y\beta}$, $C_{l\beta}$ and $C_{n\beta}$ lateral-directional derivatives.

The CMARC model must be analyzed in the linear slope regions of α and β for valid results. A potential flow solution will not produce satisfactory results for bodies with significant areas of flow separation.

1. Longitudinal Stability Derivatives

a. Longitudinal Stability Derivative Methods

Three basic longitudinal stability derivatives can be measured with just two runs of the CMARC model. The model is first analyzed at an angle-of-attack corresponding to the estimated trim condition. In this case, α_t=0° is selected for the first run. A second CMARC run is conducted with angle-of attack incremented one or two degrees. C_L and C_m are then extracted manually from the data files. The slope of C_L and C_m versus angle-of-attack provide the $C_{L\alpha}$ and $C_{m\alpha}$ longitudinal derivatives. For this study, several angles-of-attack were analyzed to check consistency of the slope. In addition, α_{trim} is calculated from the lift curve slope and trim lift coefficient. Equations 5.5 through 5.7 are used for these calculations. For the longitudinal analysis, only half the model is analyzed. The symmetric calculation mode is selected by setting both RSYM=0.0 and IPATSYM=0 in the CMARC input file.

$$C_{L_\alpha} = \frac{\left(C_{L_2} - C_{L_1}\right)}{\left(\alpha_2 - \alpha_1\right)} * \frac{180}{\pi} \text{ per radian} \qquad 5.5$$

$$C_{m_\alpha} = \frac{\left(C_{m_2} - C_{m_1}\right)}{\left(\alpha_2 - \alpha_1\right)} * \frac{180}{\pi} \text{ per radian} \qquad 5.6$$

$$\alpha^\circ{}_{trim} = \alpha^\circ{}_1 + \frac{\left(C_{L_{trim}} - C_{L_1}\right)}{C_{L_\alpha}} * \frac{180}{\pi} \text{ degrees} \qquad 5.7$$

Several FROG UAV model configurations were analyzed in a build-up approach to check results against classical calculations and flight test data. Figure 5.9 shows the simplified CMARC models. First, just the wing and horizontal tail were considered. The patches for all other surfaces and wakes were turned off and the wing root was extended to centerline. The FROG fuselage was then analyzed separately and the results were added to the simplified wing and horizontal tail combination. Next, the original butted (low order fit) wing/fuselage and horizontal tail were considered. Finally, the blended wing/fuselage and horizontal tail were analyzed. Values of $C_{L\alpha}$ and $C_{m\alpha}$ for these four configurations are presented in Table 5.5.

Classical design calculations are also performed to estimate $C_{m\alpha}$ for comparison to CMARC results. Equation 5.8 is used for the calculation of $C_{m\alpha}$. In classical design, the horizontal tail downwash derivative, $d\varepsilon/d\alpha$, is generally selected from empirical data. Using a taper ratio of TR=1:1 and aspect ratio of AR=6, $d\varepsilon/d\alpha=0.4$ is selected from empirical charts in Ref. [14] for the FROG UAV configuration. A few other values of the horizontal tail downwash derivative, $d\varepsilon/d\alpha$, are selected to see how well CMARC models downwash effects. Classical design estimates of $C_{m\alpha}$ for values of $d\varepsilon/d\alpha$ ranging from 0 to 0.4 are presented in Table 5.5 for comparison with CMARC results.

$$C_{m_\alpha} = a_w\left[\left(h - h_{ac}\right) - V_H \frac{a_t}{a_w}\left(1 - \frac{d\varepsilon}{d\alpha}\right)\right] \qquad 5.8$$

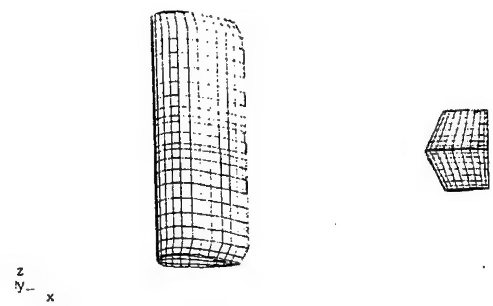

Simplified Wing and Horizontal Tail

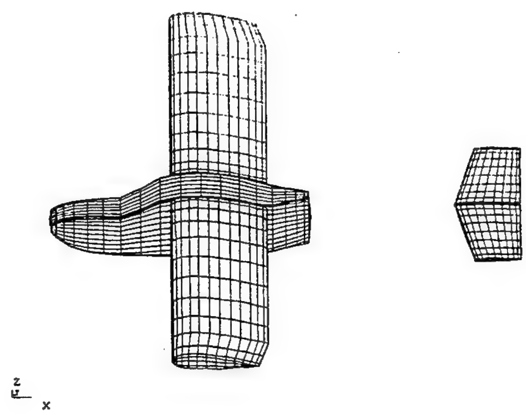

Butted Wing and Fuselage with Horizontal Tail

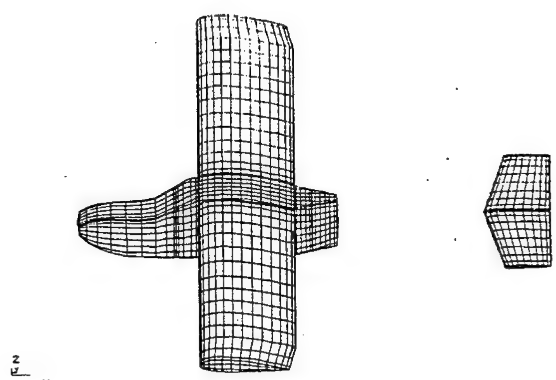

Blended Wing and Fuselage with Horizontal Tail

Figure 5.9 Simplified CMARC Models of the FROG UAV for the Determination of Longitudinal Stability Derivatives.

Flight test data for the short period and phugoid modes were used for longitudinal parameter estimation. Values for $C_{L\alpha}$ and $C_{m\alpha}$ based on preliminary parameter estimation work by Engdahl [pending publication] are presented in Table 5.5. Caution is advised against making definitive comparisons until the work is published.

METHOD	CONFIGURATION[1]	LONGITUDINAL PARAMETERS α_{trim}[2] (deg)	$C_{L\alpha}$ (per rad)	$C_{m\alpha}$ (per rad)
CMARC Panel Code	Wing/Horiz Tail	-0.87	4.86	-0.835
	Wing/Horiz Tail + Fuselage	-0.86	4.78	-0.608
	Blended Wing-Fuselage/Horiz Tail	-0.01	4.72	-1.105
	Butted Wing-Fuselage/Horiz Tail	-0.8	5.37	-1.348
Classical Design[3]	Wing/Horiz Tail - $\delta\varepsilon/\delta\alpha$=0	-0.78	4.89	-1.50
	Wing/Horiz Tail - $\delta\varepsilon/\delta\alpha$=0.25	-0.81	4.85	-1.00
	Wing/Horiz Tail - $\delta\varepsilon/\delta\alpha$=0.35	-0.82	4.83	-0.80
	Wing/Horiz Tail - $\delta\varepsilon/\delta\alpha$=0.40	-0.82	4.82	-0.70
Parameter Estimation[4]	Flying Aircraft	n/a	4.09	-0.42

NOTES: 1) CG_x=34.5% M.A.C. / CG_z=8.6" from bottom of fuselage.
2) Zero lift wing incidence is +6.5° from the longitudinal reference line.
3) Classical Design after Ref. [14].
4) Unpublished parameter estimation from flight test data by Engdahl.

Table 5.5 Comparison of FROG UAV Longitudinal Stability Derivatives.

b. Analysis of Longitudinal Stability Data

The first three configurations in Table 5.5 produce good results for $C_{L\alpha}$ and reasonable values for $C_{m\alpha}$. However, the fourth configuration, the butted wing root and fuselage, produces excessively large values of both $C_{L\alpha}$ and $C_{m\alpha}$. This configuration should be avoided in future models. It is recommended that CMARC model developers spend the time up front to produce the higher fidelity model from the start.

The values produced for $C_{m\alpha}$ from CMARC are somewhat high when compared with to the classical design calculations. Clearly, some downwash is sensed by the horizontal tail in the CMARC analysis because all values for $C_{m\alpha}$ are considerably less

than the classical calculation with $d\varepsilon/d\alpha$=0. Still, high values compared to flight test data indicates that CMARC has a difficult time capturing the complete $d\varepsilon/d\alpha$ downwash effect. This could be due to the requirement to select rigid wakes to prevent the wing wake from impacting the horizontal tail. A more careful wake definition may help capture the tail downwash derivative with more fidelity. A study by Walden et al. [Ref. 15] studied wake turbulence by modeling an aircraft flying in trail of a wake generating wing. A horizontal tail trailing the main wing is a similar configuration. The study found that a streamline-based wake is the best method for modeling downwash effects. This wake definition should be investigated for modeling the $C_{m\alpha}$ derivative. Of note, the wake diffusion process is neglected ia a potential flow analysis.

In summary, CMARC produced accurate values for $C_{L\alpha}$ and slightly high values of $C_{m\alpha}$. Difficulties were encountered trying to model the horizontal tail downwash derivative. A more careful study of the effects of wing wake placement on the downwash derivative is recommended.

2. Lateral Directional Stability Derivatives

a. Lateral-Directional Stability Derivative Methods

Development of the lateral-directional stability derivatives is more straight forward than for the longitudinal derivatives because the vertical tail sidewash angle plays a lesser role. However, both sides must be modeled by setting both RSYM=1.0 and IPATSYM=1. This creates symmetric patches around the y=0 plane allowing CMARC to perform asymmetric calculations around the entire body and significantly increases processing times.

For the lateral-directional axis, the aircraft is modeled with the blended wing and fuselage in combination with the vertical and horizontal stabilizers as shown in Figure 5.10. The engine nacelle and pylon are left off because their wakes impact the vertical tail. In addition, the pylon/fuselage and pylon/nacelle junctions were meshed with a low order, butted fit. This type of junction was found to produce poor results during the longitudinal stability study.

The model is first checked for lateral directional balance at zero yaw angle. The side force, rolling and yawing coefficients should be zero when a trial run is

performed at zero yaw angle. If lateral-directional forces or moments are present, the model and wake geometry should be checked for symmetry.

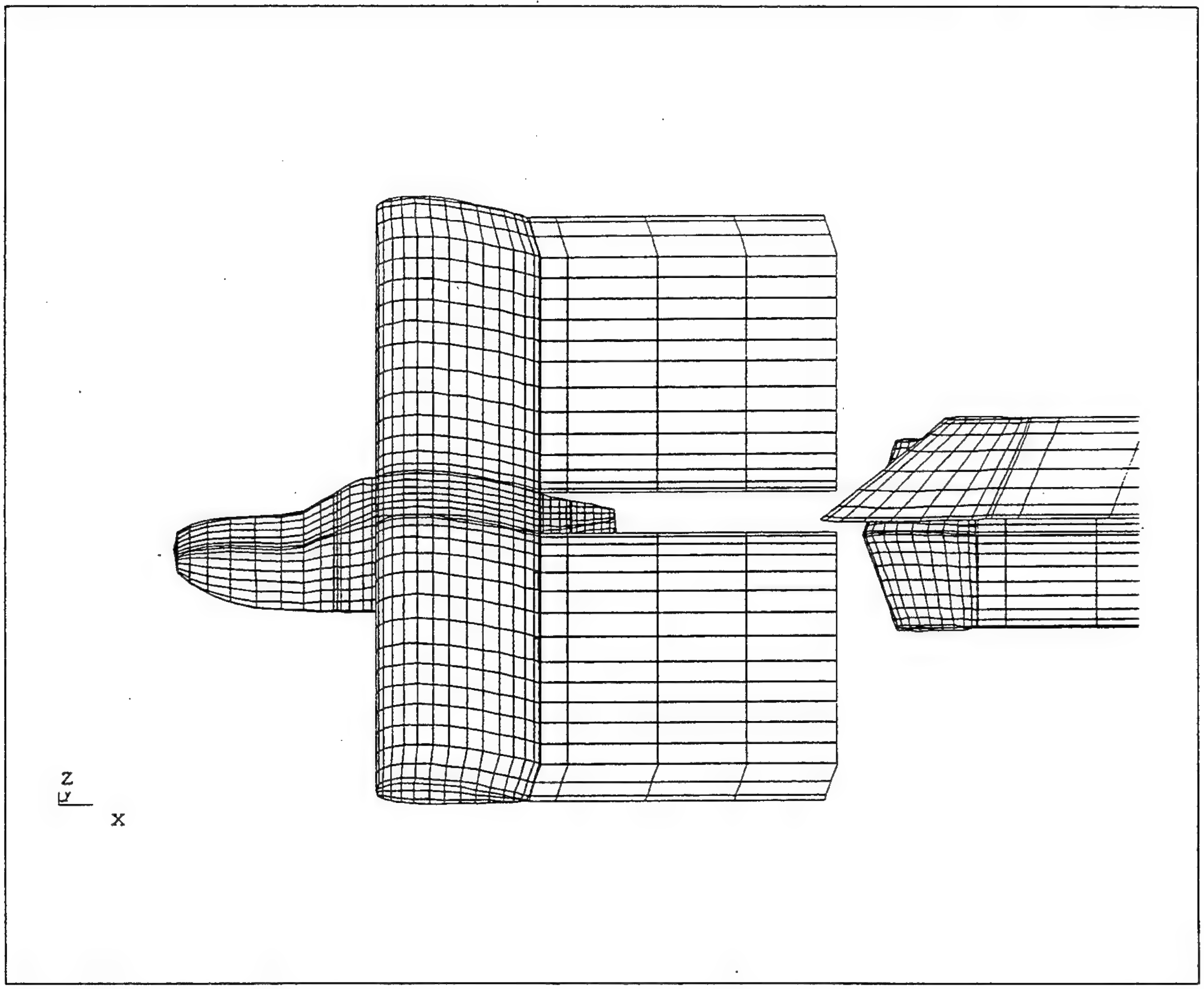

Figure 5.10 Simplified CMARC Model of the FROG UAV for the Determination of Lateral-Directional Stability Derivatives.

Next, a single CMARC run is performed with $\alpha = \alpha_{trim}$ and yaw angle set to one degree. The lateral-directional derivatives, $C_{Y\beta}$, $C_{l\beta}$ and $C_{n\beta}$, are then obtained directly with equations 5.9 through 5.11:

$$C_{Y_\beta} = \frac{C_Y}{\Delta\beta^\circ} * \frac{180}{\pi} \text{ per radian} \qquad 5.9$$

$$C_{l_\beta} = \frac{C_l}{\Delta\beta^\circ} * \frac{180}{\pi} \text{ per radian} \qquad 5.10$$

$$C_{n_\beta} = \frac{C_n}{\Delta\beta^\circ} * \frac{180}{\pi} \text{ per radian} \qquad 5.11$$

It should be noted that the stability axis as modeled (x-aft and z-up) differs from the standard flight dynamics stability axis. Care must be taken to reverse the signs of the appropriate coefficients to convert from a CMARC model's stability axis into the flight dynamics stability axes

b. Analysis of Lateral-Directional Stability Data

Lateral-directional stability derivatives obtained from CMARC are presented in Table 5.6. For comparison three other sets of data are also presented. The first comes from the classical analysis presented by Papageorgiou in Ref. [1]. The second set comes from estimates based on data recorded from flight test static sideslip maneuvers, also published in Ref. [1]. The third set comes from parameter estimation by Engdahl based on dynamic flight test data. It is unpublished and should be considered preliminary. In all cases, the CMARC lateral-directional stability derivatives produce a closer match to flight test data than those derived from classical methods. It is concluded that CMARC is a good tool for lateral-directional stability analysis.

3. Summary of CMARC Stability Derivative Analysis

In summary, for the longitudinal axis, CMARC produces accurate values for α_{trim} and $C_{L\alpha}$ and slightly high values of $C_{m\alpha}$. Difficulties may be encountered while trying to model the horizontal tail downwash derivative. A more careful study of the effects wing wake placement on the downwash derivative is recommended. Specifically, modeling should include streamline-based wake placement techniques [Ref. 15]. Analysis of the lateral-directional axis proves more straightforward. Lateral-directional derivatives from CMARC for $C_{Y\beta}$, $C_{l\beta}$ and $C_{n\beta}$ provide a closer match to flight test data than the classical estimates. The engine nacelle and pylon should be re-meshed and included in future studies.

Overall, CMARC derived stability derivatives are sufficiently accurate for entry into an initial aerodynamic model. Adjustments through analysis of flight test data will still be required. Future CMARC studies should concentrate on developing the rate damping and control power derivatives.

METHOD	CONFIGURATION[1]	LAT-DIR PARAMETERS		
		$C_{Y\beta}$ (per rad)	$C_{l\beta}$ (per rad)	$C_{n\beta}$ (per rad)
CMARC Panel Code	Blended Wing-Fuselage/Horz/Vert Tails	-0.573	-0.063	0.120
Classical Design[2]	Wing/Fuselage/Vert Tail	-0.310	-0.051	0.058
Flight Test[3]	Flying Aircraft	-0.700	-0.053	0.057
Parameter Estimation[4]	Flying Aircraft	-0.987	-0.094	0.176

NOTES: 1) CG_x=34.5% M.A.C. / CG_z=8.6" from bottom of fuselage.
2) Classical Design calculations by Papageorgio, from Ref. [1].
3) Flight test results from Steady Heading Sideslip, from Ref. [1]
4) Unpublished parameter estimation from flight test data by Engdahl.

Table 5.6 Comparison of FROG UAV Lateral-Directional Stability Derivatives.

VI. CONCLUSIONS AND RECOMMENDATIONS

CMARC is a DOS personal computer hosted panel code adopted from the NASA Ames PMARC code. AeroLogic, Inc., created CMARC by converting PMARC FORTRAN 77 source code into the C language. Significant memory management and command line enhancements were also added. CMARC solves for inviscid, incompressible flow over complex three-dimensional bodies. Emphasis in this study is first placed on verifying CMARC against the PMARC and Naval Postgraduate School Unsteady Potential Flow (UPOT) panel codes. CMARC pressure distributions and boundary layer calculations are then compared to experimental data for an inclined prolate spheroid. Finally, a complex three-dimensional panel model of the Naval Postgraduate School FROG UAV is developed which successfully generates static-pressure source position corrections, alpha vane correction curves and basic stability derivatives.

CMARC results are found to be equivalent to the NASA-Ames PMARC panel code. As expected, pressure distribution and boundary layer calculations from CMARC match exactly those obtained with PMARC. The following enhancements are noteworthy. CMARC, hosted on a Pentium class PC, processes input files significantly faster than PMARC hosted on a networked SGI Indigo^2 UNIX workstation. CMARC's extensive command line functionality greatly enhances batch file processing capabilities. On the other side, CMARC's poor error flagging capability leaves the user frequently spending much time searching for input file mistakes. Improved input file error checking should be incorporated into CMARC functionality.

CMARC integral boundary layer calculations are compared to the two-dimensional finite difference methods implemented in the UPOT code. In general, CMARC provides correct trends for both the transition and separation points. However, in all cases, CMARC predicts early transition and late flow separation. As expected, the differences are greatest at lower Reynolds numbers where boundary layer thickness is larger. An adjustment of the empirical transition and separation models contained in CMARC may prove useful.

CMARC calculations are also compared to wind tunnel data for a 6:1 inclined prolate spheroid model at 10 degrees angle-of-attack. With proper wake placement, CMARC can produce accurate normal force and pitching moment coefficients. Over the three dimensional body, CMARC boundary layer calculations also predict early transition

and late flow separation. Despite inaccuracies, CMARC boundary layer calculations remain useful when used as a design tool for visualizing the trend in transition and separation points with configuration changes.

CMARC integrated skin friction forces are compared to prolate spheroid wind tunnel data. Normal, axial, and pitching moment coefficients for skin friction forces are underpredicted by CMARC, but remain within 40% of integrated experimental data.

The LOFTSMAN and POSTMARC portions of the Personal Simulation Works software suite are used exclusively for the pre-process modeling and post-process visualization of CMARC files. The LOFTSMAN capability to automatically format and generate CMARC input patches is an enhancing characteristic. Functionality should be added to allow the modeling of wing tip ribs that are not parallel to the aircraft butt line.

POSTMARC is an excellent tool for visualizing CMARC output files. The capability to create streamlines and perform boundary layer calculations external to CMARC is extremely useful. However, much time could be saved if POSTMARC maintained previous settings and selections following translations, rotations and re-scaling. Additionally, a capability to overlay multiple data types is desired.

CMARC off-body flow field analysis is useful for both static-pressure source and alpha vane position corrections. Measured data may be corrected using look-up tables or through curve fits of CMARC derived data. Flight testing is recommended for validation of sensor corrections obtained from the CMARC off-body analysis.

For the longitudinal analysis, CMARC produces accurate values for α_{trim} and $C_{L\alpha}$ and slightly high values of $C_{m\alpha}$. Some difficulties are encountered trying to model the horizontal tail downwash derivative. A more careful study of the effects of wing wake placement on the downwash derivative is recommended.

Analysis of the lateral-directional axis proves more straightforward. Lateral-directional derivatives from CMARC for $C_{Y\beta}$, $C_{l\beta}$ and $C_{n\beta}$ provide a closer match to flight test data than classical design calculations. Adjustments through analysis of flight test data may still be required. The engine nacelle and pylon should be re-meshed and included in future studies.

Overall, the CMARC panel code is found to be suitable for aerodynamic modeling of the Naval Postgraduate School FROG UAV. CMARC derived stability derivatives are sufficiently accurate for incorporation into an initial aerodynamic model. Future CMARC studies should concentrate on the development of the rate damping and control power derivatives.

APPENDIX A.

DEVELOPMENT OF THE MOMENTUM INTEGRAL EQUATION

The CMARC and PMARC User's Guides contain the development of the implemented boundary layer equations starting from the two-dimensional momentum integral equation. For completeness, the momentum integral equation is developed here to provide continuity.

The development of the momentum boundary layer equations is outlined by Young in Ref. [9]. In 1904 Prandtl first presented his *Boundary Layer Theory* based on the following observations:

1) However small the viscosity of a fluid , it cannot be ignored. At the surface, the fluid is at rest compared to the body (no slip condition).
2) Shear stresses are directly proportional to the rates of strain.
3) The ratio of inertial forces to viscous forces, or Reynolds number, is important in characterizing flow phenomena.
4) The full non-linear viscous Navier-Stokes equations are difficult to solve directly. Prandtl observed that simplifications could made when assuming a thin boundary layer. Viscosity can be ignored outside the boundary layer allowing the use of classical inviscid methods.

Thin boundary layer theory also assumes that the pressure distribution outside the thin boundary layer is transmitted normally through the boundary layer to the surface without loss. CMARC takes advantage of this assumption by neglecting the thickness of the boundary layer and imposes a potential flow solution over the surface.

The momentum integral equation for two-dimensional incompressible flow is the starting point for the boundary layer analysis outlined in References [2] and [4]. It is obtained through the following total energy integral analysis as outlined by Young in Ref. [9].

Figure A.1 depicts an incremental portion of a two-dimensional boundary layer. The mass flow rate ($\dot{m}$) across each side is given by:

$$\dot{m}_{AD} = 0$$

$$\dot{m}_{DC} - \dot{m}_{AB} = \frac{d}{dx}\left[\int_0^h \rho u dz\right]\Delta x + O\left(\Delta x^2\right)$$

$$\dot{m}_{BC} = \rho_e w_h \Delta x \quad \text{and} \quad \dot{m}_{DC} - \dot{m}_{AB} = \dot{m}_{BC} \quad \text{from continuity.} \qquad \text{A.1}$$

$$\therefore \; \rho_e w_h = \frac{d}{dx}\left[\int_0^h \rho u dz\right] + O(\Delta x)$$

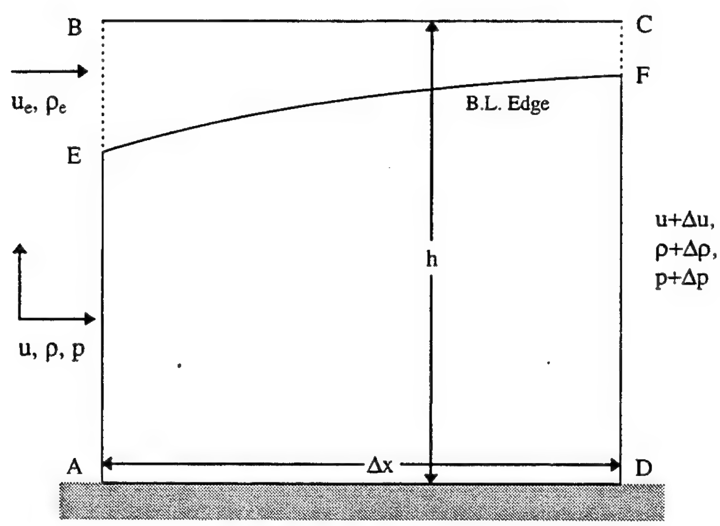

Figure A.1 Elementary boundary layer section for deriving the momentum integral equation for two-dimensional flow, after Ref. [9].

Similarly, the rate of momentum transport across each boundary is given by:

$$AD: \quad = 0$$

$$DC - AB: \quad = \frac{d}{dx}\left[\int_0^h \rho u^2 dw\right] + O\left(\Delta x^2\right) \qquad \text{A.2}$$

$$BC: \quad = \rho w_h \cdot u_e \Delta x = u_e \frac{d}{dx}\left[\int_0^h \rho u dz\right]\Delta x + O\left(\Delta x^2\right)$$

The force due to pressure on the sectional boundary layer element is given by:

$$= -h\Delta p = -h\left(\frac{dp}{dx}\right)\Delta x + O\left(\Delta x^2\right) \qquad \text{A.3}$$

And, the friction force exerted by the wall is:

$$= -\tau_w \cdot \Delta x \qquad \text{A.4}$$

Summing the momentum terms and equating them to the forces while taking the limit as $\Delta x \to 0$ yields the momentum integral equation:

$$\frac{d}{dx}\left(\int_0^h \rho u dz\right) = -h\frac{dp}{dx} - \tau_w \qquad \text{A.5}$$

It is more convenient to express the relation in terms of displacement and momentum thickness by substituting the following:

$$-\frac{dp}{dx} = \rho_e u_e \frac{du_e}{dx} \qquad \text{A.6}$$

The momentum integral is then reduced to:

$$\frac{d}{dx}\left[\int_0^h \rho u\left(u - u_e\right)dz\right] + \frac{du_e}{dx}\left[\int_0^h \rho u dz\right] = h\rho_e u_e \frac{du_e}{dx} - \tau_w \;\rightarrow\; \frac{d}{dx}\left[\int_0^h \rho u\left(u - u_e\right)dz\right] + \frac{du_e}{dx}\left[\int_0^h \left(\rho u - \rho u_e\right)dz\right] = -\tau_w$$

$$or \quad \frac{d}{dx}\left(\rho_e u_e^2 \theta\right) + \frac{du_e}{dx}\rho_e u_e \delta^* = \tau_w$$

A.7

Where $d^* = \int_0^h \left(1 - \frac{ru}{r_e u_e}\right) dz \quad and \quad q = \int_0^h \frac{ru}{r_e u_e}\left(1 - \frac{u}{u_e}\right) dz$ A.8

Substituting $H = \delta^* / \theta$, where H is the boundary layer shape factor, and rearranging after the chain rule, the momentum integral can be written in as:

$$\frac{d\theta}{dx} + \frac{1}{u_e}\frac{du_e}{dx}\theta(H+2) + \frac{\theta}{\rho_e}\frac{dp_e}{dx} = \frac{\tau_w}{\rho_e u_e^2} \quad \text{A.9}$$

And finally, by substituting $C_f = \frac{\tau_w}{\frac{1}{2} q_\infty} = \frac{2\tau_w}{\rho_e u_e^2}$, one obtains Equation 16 in References [2] and [4]:

$$\frac{d\theta}{dx} + \frac{1}{u_e}\frac{du_e}{dx}\theta(H+2) + \frac{\theta}{\rho_e}\frac{dp_e}{dx} = \frac{C_f}{2} \quad \text{A.10}$$

From here, the CMARC or PMARC guides provide a detailed development of the implemented boundary layer models.

APPENDIX B.

INTEGRATION OF AERODYNAMIC FORCES OVER THE SURFACE OF A PROLATE SPHEROID

The experimental set-up in Ref. [12] did not include measurement of forces. However, it was deemed that the 2000+ pressure and 500+ skin friction measurements would be sufficient to allow the integration of measurements over the surface of the prolate spheroid for a good approximation of total force and moment coefficients. The following technique is developed to provide an estimate of integrated pressure and friction forces. Symmetry is assumed. Appendix C lists the entire MATLAB program which implements the technique that follows.

In general the pressure force is given by:

$$\overline{F}_P = \iint_S P\overline{n}dS \text{, } \overline{n} \text{ is a unit surface normal} \qquad \text{B.1}$$

However, the test data is provided discreetly in cylindrical coordinates, resulting in the following discrete double summation:

$$\overline{F}_P = \sum_{x/2a}\sum_{\phi} P\overline{n}r\Delta d\phi\Delta x / 2a \text{, where dS}=r\Delta d\phi\Delta x/2\text{a} \qquad \text{B.2}$$

Figure B.1 shows a diagram of the pressure and skin friction acting over the incremental surface areas, ΔS. The pressure and skin friction coefficients, scalars, are assumed to be constant over the incremental surface.

$$\Delta\overline{F}_p = P\overline{n}r\Delta\phi\Delta x / 2a = \left(qCp + p_\infty \right)\overline{n}\Delta S \text{,} \qquad \text{B.3}$$

$$\text{where } Cp = \frac{P - P_\infty}{q} \Rightarrow \quad P = Cp \cdot q + P_\infty \qquad \text{B.4}$$

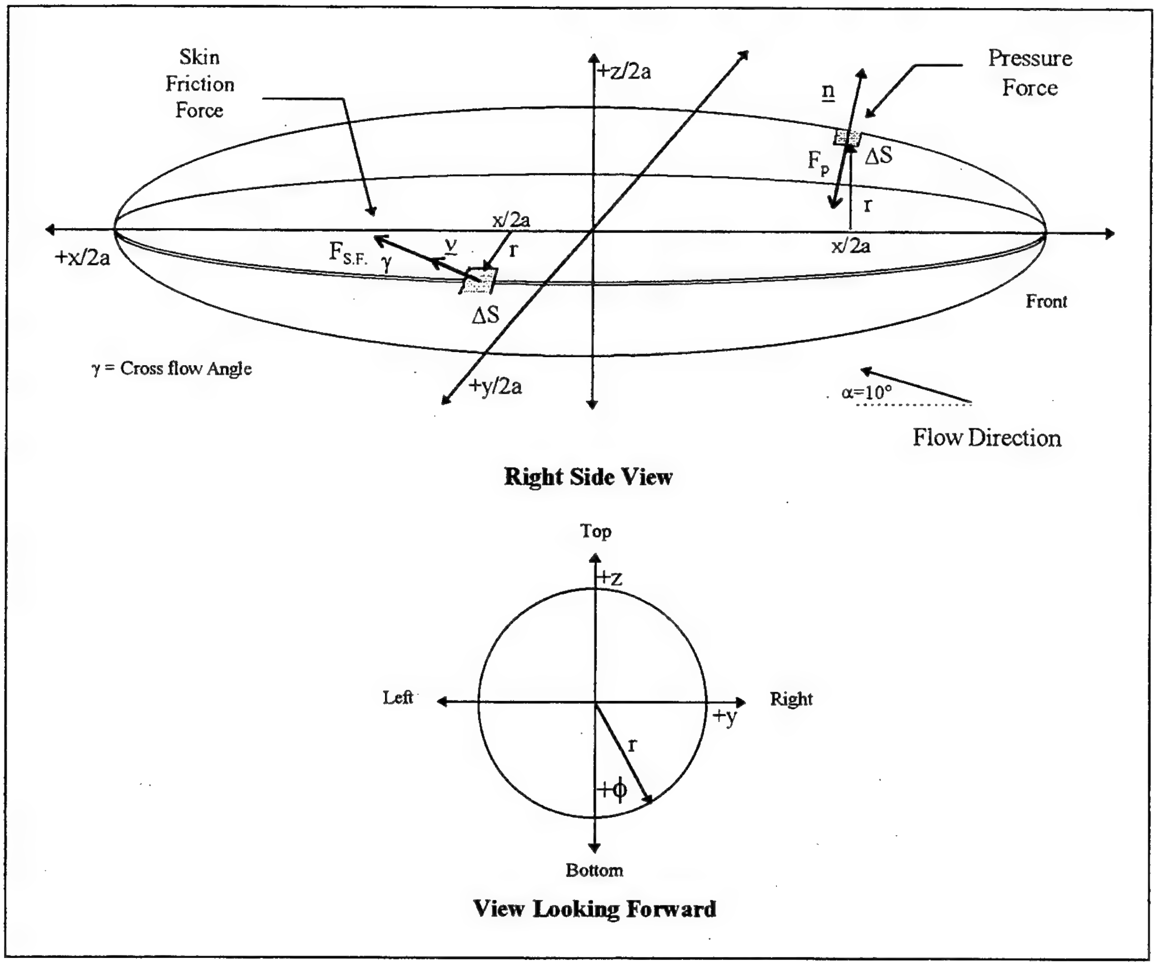

Figure B.1 Prolate Spheroid Geometry and Forces

Free stream pressure (P_∞), assumed to be constant, can be dropped from the integration due to symmetry. This leaves the following relation:

$$F_P = \sum_{x/2a=0}^{1} \sum_{\phi=0}^{360} qCp\bar{n}r\Delta\phi\Delta x / 2a \qquad \text{B.5}$$

Likewise, skin friction can also be integrated using the following relations:

$$\Delta F_{SF} = qC_f\bar{v}\Delta S = qC_f\bar{v}r\Delta\phi\Delta x / 2a, \text{ where } \bar{v} \text{ is a unit velocity vector} \qquad \text{B.6}$$

$$F_{SF} = \sum_{x/2a=0}^{1} \sum_{\phi=0}^{360} qC_f r\bar{v}\Delta\phi\Delta x / 2a$$

B.7

The pressure force coefficients, normalized by $S = \pi b^2$ and $\bar{c} = 2b$, are yielded by discretely integrating the following equations in a cylindrical coordinate system:

$$C_{N_P} = \frac{N_P}{q_\infty S}, \qquad N_P = 2\sum_{i=1}^{m}\sum_{j=1}^{n} -\left(q_\infty C_P r\bar{n}\right)\cdot \bar{k}\Delta\phi j\Delta x_i / 2a \qquad \text{B.8}$$

$$C_{A_P} = \frac{A_P}{q_\infty S}, \qquad A_P = 2\sum_{i=1}^{m}\sum_{j=1}^{n} -\left(q_\infty C_P r\bar{n}\right)\cdot \bar{i}\Delta\phi_j \Delta xi / 2a \qquad \text{B.9}$$

$$C_{M_P} = \frac{M_P}{q_\infty S\bar{c}}, \qquad M_P = 2\sum_{i=1}^{m}\sum_{j=1}^{n}\left[\left(q_\infty C_P r\bar{n}\right)\cdot\left(x_i / 2a\cdot\bar{k} - z_i / 2a\cdot\bar{i}\right)\right]\Delta\phi_j\Delta x_i / 2a$$

B.10

Where the surface unit normal is given by:

Unit Normal: $$\bar{n} = -\frac{m}{\sqrt{m^2+1}}\bar{i} + \frac{\sin(\phi)}{\sqrt{m^2+1}}\bar{j} - \frac{\cos(\phi)}{\sqrt{m^2+1}}\bar{k} \qquad \text{B.11}$$

The skin friction coefficients, normalized by $S = \pi b^2$ and $\bar{c} = 2b$, are yielded by discretely integrating the following equations in a cylindrical coordinate system:

$$C_{N_{SF}} = \frac{N_{SF}}{q_\infty S}, \qquad N_{SF} = 2\sum_{i=1}^{m}\sum_{j=1}^{n}\left(q_\infty C_f r\bar{v}\right)\cdot\bar{k}\Delta\phi_j\Delta x_i / 2a \qquad \text{B.12}$$

$$C_{A_{SF}} = \frac{A_{SF}}{q_\infty S}, \qquad A_{SF} = 2\sum_{i=1}^{m}\sum_{j=1}^{n}\left(q_\infty C_f r\bar{v}\right)\cdot\bar{i}\Delta\phi_j\Delta x_i / 2a \qquad \text{B.13}$$

$$C_{M_{SF}} = \frac{M_{SF}}{q_\infty S\bar{c}}, \quad M_{SF} = 2\sum_{i=1}^{m}\sum_{j=1}^{n}\left[\left(q_\infty C_f r\bar{v}\right)\cdot\left(-x_i / 2a\cdot\bar{k} + z_i / 2a\cdot\bar{i}\right)\right]\Delta\phi_j\Delta x_i / 2a \qquad \text{B.14}$$

Where the unit surface velocity vector is given by:

$$\bar{v} = \frac{\cos(\gamma)}{\sqrt{m^2+1}}\bar{i} + \left[\frac{m\sin(\phi)\cos(\gamma)}{\sqrt{m^2+1}} + \cos(\phi)\sin(\gamma)\right]\bar{j} + \left[-\frac{m\cos(\phi)\cos(\gamma)}{\sqrt{m^2+1}} + \sin(\phi)\sin(\gamma)\right]\bar{k}$$

B.15

The surface and local slope of a prolate spheroid comes from the following relations:

Prolate Spheroid: $\frac{x^2}{a^2}+\frac{r^2}{b^2}=1 \quad \Rightarrow \quad slope \quad m=\frac{dr}{dx}=-\frac{bx}{a^2\sqrt{1-\frac{x^2}{a^2}}}$ B.16

Note: The forces are summed over half the spheroid, $\phi = 0 \rightarrow 180°$, and doubled.

The y-direction forces and the roll and yaw moments are neglected zero due to symmetry.

APPENDIX C.

MATLAB PROGRAMS TO INTEGRATE AERODYNAMIC FORCES OVER THE SURFACE OF A PROLATE SPHEROID

Jun 4 1997 02:18 **icp_prolate.m** Page 1

```
%  This Matlab M-file script performs a first order (linear approximation)
%  integration of pressure forces over a 6:1 prolate spheroid. Central Differencing
%  of location is used for the first order integration routine. Data is input from
%  AGARD AR-303 Test C-2 as rotation angle, x/c, and Cp. Data is for two test
%  conditions, AOA = 10 and 29.7 degrees.

clear
%  Load in experimental data for AOA = 10 degrees, Re = 7.7x10e6, Vinf = 55 m/s:
%  M = 0.162
load cp10data
fid1=fopen('icp10raw','r+');  %open file for prining step data for error checking
fprintf(fid1,'i          j         l       phi    dphi      x         M       r        dx        Cp
nx        ny        nz        dS        dN        dA        dm \n');
data = [cp10data(:,2) cp10data(:,4) cp10data(:,5)]; % Extract columns 2,4,5
nphi = 40; nxc = 42;                 %Initialize # of rotation steps and pressure ports
m = 0; N = 0;A = 0; Si=0;                 % Initialize summed forces to zero
a = 0.5; b = 0.5/6;                  % a and b for 6:1 Prolate Spheroid
S = pi*b^2;                           % Reference area - max cross section
for i = 1:nphi
     for j = 1:nxc
       l = (i-1)*nxc+j;
         phi = data(l,1);
         x = data(l,2)-a;
         Cp = data(l,3);
         r = b*sqrt(1-x^2/a^2);
         M = -b*x/(a^2*sqrt(1-x^2/a^2+.000001));
         z = -r*cos(phi);
         nx = -M/sqrt(M^2+1);
         ny = sin(phi/57.296)/sqrt(M^2+1);
         nz = -cos(phi/57.296)/sqrt(M^2+1);
         nt=sqrt(nx^2+ny^2+nz^2);
             if j == 1
                 dx = data(l+1,2)/2;                      % dx at first pressure port
             elseif j == nxc
                 dx = (2*a-data(l-1,2))/2;                  % dx at last pressure port
             else
                 dx = (data(l+1,2)-data(l-1,2))/2; % central differencing at interme
diate pressure ports
             end
             if i == 1
                 dphi = data((i*nxc+1),1)/2;
             elseif i == nphi
                 dphi = (180-data(((i-1)*nxc),1))/2;
             else
                 dphi = (data((i*nxc+1),1)-data(((i-1)*nxc),1))/2;
             end
             dS = r*dphi/57.296*dx*sqrt(M^2+1);
             dN = 2*(-Cp)*dS*nz;
             dA = 2*(-Cp)*dS*nx;
             dm = 2*(-Cp)*dS*(-x*nz+z*nx);
             N = N+dN;
             A = A+dA;
             m = m+dm;
             raw(l,:)=[i  j   l   phi  dphi  x   M  r   dx  Cp  nx  ny   nz  dS  dN
  dA   dm];
             Si=Si+2*dS;
       end
end
CN_AOA10 = N/S
CA_AOA10 = A/S
CM_AOA10 = m/(S*2*b)
Si
fprintf(fid1,'%3.0f  %3.0f  %5.0f  %5.2f  %6.4f   %4.3f  %5.2f  %6.3f  %6.4f  %4.3f
  %4.3f   %4.3f   %4.3f %8.7f %8.7f %8.7f %8.7f\n ',raw');
fprintf(fid1,'i          j         l       phi    dphi      x         M       r        dx        Cp
nx        ny        nz        dS        dN        dA        dm \n');
fclose('all');
```

```
%  This Matlab M-file script performs a first order (linear approximation)
%  integration of skin friction over a 6:1 prolate spheroid. Central Differencing
%  of location is used for the first order integration routine. Data is input from
%  AGARD AR-303 Test C-2 as rotation angle, x/c, Cf and gamma (crossflow angle). Dat
a is for two test
%  conditions, AOA = 10
clear
%  Load in experimental data for AOA = 10 degrees, Re = 7.7x10e6, Vinf = 55 m/s:
%  M = 0.162
load cf10reorder
%fid1=fopen('icf10raw','r+');
%fprintf(fid1,'i       j       l      phi    dphi      x       r       m        dx        Cf
gamma     vx        vy        vz       dS        dN        dA        dm \n');

data = [cf10reorder(:,2) cf10reorder(:,1) cf10reorder(:,3) cf10reorder(:,4)]; % Extr
act columns 2,4,5
nphi = 74; nxc = 12;               %Initialize # of rotation steps and pressure ports
Nsf=0; Asf=0; msf=0;
m = 0; N = 0;A = 0; Si=0;            % Initialize summed forces to zero
a = 0.5; b = 0.5/6;                % a and b for 6:1 Prolate Spheroid
S = pi*b^2;                         % Reference area - max cross section
for i = 1:nxc
     for j = 1:nphi
        l = (i-1)*nphi+j;
          phi = data(l,1);
          x = data(l,2)-a;
          Cf = data(l,3);
          gamma = data(l,4);
          r = b*sqrt(1-x^2/a^2);
          M = -b*x/(a^2*sqrt(1-x^2/a^2+.000001));
          z = -r*cos(phi);
          vx = cos(gamma/57.3)/sqrt(M^2+1);
          vy = M*sin(phi/57.296)*cos(gamma/57.3)/sqrt(M^2+1)+cos(phi/57.3)*sin(gamma/
57.3);
          vz = -M*cos(phi/57.296)*cos(gamma/57.3)/sqrt(M^2+1)+sin(phi/57.3)*sin(gamma
/57.3);
          nt=sqrt(vx^2+vy^2+vz^2);
              if i == 1
                  dx = data(nphi+1,2)/2;                % dx at first hot film sensor
              elseif i == nxc
                  dx = (2*a-data(((i-1)*nphi),2))/2 ;         % dx at last hot film
sensor
              else
                  dx = (data((i*nphi+1),2)-data(((i-1)*nphi),2))/2 ;
              end
              if j == 1
                  dphi = data((l+1),1)/2;
              elseif j == nphi
                  dphi = (180-data(l-1,1))/2;
              else
                  dphi = (data(l+1,1)-data(l-1,1))/2;
              end
              dS = r*dphi/57.296*dx*sqrt(M^2+1);
              dN = 2*(Cf)*dS*vz;
              dA = 2*(Cf)*dS*vx;
              dm = 2*(Cf)*dS*(-x*vz+z*vx);
              Nsf = Nsf+dN;
              Asf = Asf+dA;
              msf = msf+dm;
%             raw(l,:)=[i  j    l   phi  dphi  x   M  r   dx  Cf   gamma vx  vy   vz
 dS  dN  dA    dm];
       end
end
CNsf_AOA10 = Nsf/S
CAsf_AOA10 = Asf/S
CMsf_AOA10 = msf/(S*2*b)
%fprintf(fid1,'%3.0f  %3.0f  %5.0f  %5.2f  %6.4f   %4.3f  %5.2f  %6.3f  %6.4f  %6.5f
  %4.1f   %4.3f    %4.3f    %4.3f %8.7f %8.7f %8.7f %8.7f\n ',raw');
%fclose('all');
```

APPENDIX D. REPRESENTATIVE CMARC/PMARC SPEED TEST FILE

Printed by pollard from hawkeye

Jun 20 1997 04:39 — 24p1600.in — Page 1

```
NACA2415 RECTANGULAR WING - 1600 Panels for CMARC/PMARC Time Trials
b=20 FT, cbar=1.00 FT, AR = 20 Re = 1,000,000 Vinf = 157.23 FT/S
File purpose:  For comparison of CMARC / PMARC processing times.

Created: 5/18 by Steve Pollard

&BINP2   LSTINP=2,    LSTOUT=0,    LSTFRQ=0,    LENRUN=0,    LPLTYP=1,       &END
&BINP3   LSTGEO=0,    LSTNAB=0,    LSTWAK=0,    LSTCPV=0,                    &END
&BINP4   MAXIT=500,    SOLRES=0.0005,                                        &END
&BINP5   NTSTPS= 10,  DTSTEP=0.5,                                            &END
&BINP6   RSYM=0.0,    RGPR=0.0,    RFF=5.0,  RCORES=0.0080, RCOREW=0.0080,   &END
&BINP7   VINF=157.23,  VSOUND=1116.0,                                        &END
&BINP8   ALDEG= 10.00, YAWDEG=0.0,  PHIDOT=0.0,  THEDOT=0.0,  PSIDOT=0.0,    &END
&BINP8A  PHIMAX= 0.0, THEMAX= 0.0, PSIMAX=0.0,
         WRX=0.0,     WRY=0.0,     WRZ=0.0,                                  &END
&BINP8B  DXMAX=0.0,   DYMAX=0.0,   DZMAX=0.0,
         WTX=0.0,     WTY=0.0,     WTZ=0.0,                                  &END
&BINP9   CBAR=1.00,   SREF=20,  SSPAN= 10,
         RMPX=0.25,   RMPY=0.00,   RMPZ=0.00,                                &END
&BINP10  NORSET=0,    NBCHGE=0,    NCZONE=0,
         NCZPCH=0,    CZDUB=0.0,   VREF=0.0,                                 &END
&BINP11  NORPCH=0,    NORF=0,      NORL=0,
         NOCF=0,      NOCL=0,      VNORM=0.0,                                &END
&BINP12  KPAN=0,      KSIDE=0,     NEWNAB=0,    NEWSID=0,                    &END
&BINP13  NBLIT=0,                                                            &END

&ASEM1   ASEMX=0.00,       ASEMY=0.00,       ASEMZ=0.00,
         ASCAL=1.00,       ATHET=0.00,       NODEA=5,                        &END
&ASEM2   APXX=0.00,        APYY=0.00,        APZZ=0.00,
         AHXX=0.00,        AHYY=1.00,        AHZZ=0.00,                      &END

&COMP1   COMPX= 0.0000,    COMPY= 0.0000,    COMPZ= 0.0000,
         CSCAL=  1.000,    CTHET=   0.0,     NODEC= 5,                       &END
&COMP2   CPXX= 0.0000,     CPYY= 0.0000,     CPZZ= 0.0000,
         CHXX= 0.0000,     CHYY=  1.000,     CHZZ= 0.0000,                   &END

&PATCH1  IREV=  0, IDPAT= 1, MAKE=   0, KCOMP= 1, KASS= 1, IPATSYM=0,
         IPATCOP=0,                                                          &END
          WING
&SECT1   STX=     0.0000, STY= 0.0000,    STZ= 0.0000,    SCALE=  1.00 ,
         ALF=    0.0,  THETA=    0.0,
         INMODE=  5,  TNODS= 0,    TNPS=  0,    TINTS= 3,                    &END
&SECT2   RTC=    0.1500, RMC= 0.0200,    RPC= 0.4000,
         IPLANE=  2,  TNPC= 40,    TINTC= 3,                                 &END
&SECT1   STX=    0.00, STY= 10,    STZ= 0.0000,    SCALE=  1.00,
         ALF=    0.0,  THETA=    0.0,
         INMODE=  0,  TNODS= 5,    TNPS= 20,    TINTS= 3,                    &END

&PATCH1  IREV=  0, IDPAT= 1, MAKE=   1, KCOMP= 1, KASS= 1, IPATSYM=0,
         IPATCOP=0,                                                          &END
          WING_TIP
&PATCH2  ITYP=  2,     TNODS= 5,    TNPS=   4,    TINTS= 3,                  &END

&WAKE1   IDWAK=1,          IFLXW=0,          ITRFTZ= 0,        INTRW= 0,     &END
 WING_WAKE
&WAKE2   KWPACH=2,         KWSIDE=4,         KWLINE=0,         KWPAN1=0,
         KWPAN2=0,         NODEW=0,          INITIAL=0,                      &END
&WAKE2   KWPACH=1,         KWSIDE=2,         KWLINE=0,         KWPAN1=0,
         KWPAN2=0,         NODEW=5,          INITIAL=0,                      &END

&ONSTRM  NONSL =0,  KPSL = 1,50,                                             &END

&BLPARAM RN =1000000,     VISC = 0.00015723, NSLBL = 1,2,                    &END

&VS1     NVOLR= 0,         NVOLC= 0,                                         &END
&VS2     XO=     -0.1000,  YO=     1.5000,  ZO=     -0.1000,  INTVSR= 1,     &END
```

Jun 20 1997 04:39 — 24p1600.in — Page 2

```
&VS3     X1=    -0.1000, Y1=     1.5000, Z1=     0.1000, NPT1=  0,           &END
&VS4     X2=    -0.1000, Y2=     1.5000, Z2=     0.1000, NPT2= 20,           &END
&VS5     X3=     1.1000, Y3=     1.5000, Z3=    -0.1000, NPT3= 25,           &END

&VS6     XR0=    2.0000, YR0=    2.0000, ZR0=    0.0000, INTVSC= 1,          &END
&VS7     XR1=    4.0000, YR1=    2.0000, ZR1=    0.0000,                     &END
         XR2=    2.0000, YR2=    2.0000, ZR2=    1.0000,                     &END
&VS8     R1=     0.1000, R2=     1.0000, PHI1=  0.0,      PHI2=360.0,        &END
&VS9     NRAD=   5,      NPHI=  12,      NLEN=  3,

&SLIN1   NSTLIN=0,                                                           &END
&SLIN2   SX0=   -2.0000, SY0=    1.0000, SZ0=   -0.5000,
         SU=     0.0000, SD=    10.0000, DS=     0.2500, INTSL= 1,           &END
```

APPENDIX E. MATLAB PROGRAM FOR REORDERING AGARD DATA FILE

Jun 20 1997 04:42 **reorder.m** Page 1

```
% This Matlab M-file transforms AGARD Prolate Spheroid Cp data listed
% in a chordwise direction and converts it into slices for a given x/c location.

% Created by:  Steve Pollard

load cwcp10;
load cwcp30;
fid1=fopen('swcp10','r+');
fid2=fopen('swcp30','r+');
fprintf(fid1,'#  DPN    PHI  I    X0/L     CP    \n');
fprintf(fid2,'#  DPN    PHI  I    X0/L     CP    \n');
for i=1:42
    for j=1:42
      swcp10((i-1)*42+j,:)=cwcp10((j-1)*42+i,:);
    end
end
for i=1:42
    for j=1:51
      swcp30((i-1)*51+j,:)=cwcp30((j-1)*42+i,:);
    end
end
fprintf(fid1,'%6.0f  %7.2f  %3.1f %8.5f  %8.5f \n',swcp10');
fprintf(fid2,'%6.0f  %7.2f  %3.1f %8.5f  %8.5f \n',swcp30');
fclose('all');
```

APPENDIX F. CMARC PROLATE SPHEROID INPUT FILE

```
Jun 11 1997 05:33                 pr10w117.in                      Page 1

Test Case #1:  AOA=10 deg, Uo=55 m/s Re=7.7e6, v=1.71429e-5 m^2/s

Geometry: 6:1 Prolate Spheroid, L=2.4 meters, W = 0.4 meters
Patch:       40 bands X 40 panels per semi band = 1600 panels Created in Loftsman
Wake:        1) Wake separation from partial trailing ring at X/C=0.99
             2)  for-aft at 117 deg from X/C=0.50 to 0.99

Created:   5/7    Steve Pollard
Modified:  6/3    Wakes changed to 117 deg


 &BINP2   LSTINP=0,     LSTOUT=0,     LSTFRQ=0,     LENRUN=0,     LPLTYP=1,       &END
 &BINP3   LSTGEO=0,     LSTNAB=0,     LSTWAK=0,     LSTCPV=0,                     &END
 &BINP4   MAXIT=400,     SOLRES=0.0005,                                           &END
 &BINP5   NTSTPS= 4,   DTSTEP=0.5,                                                &END
 &BINP6   RSYM=0.0,     RGPR=0.0,     RFF=5.0,  RCORES=0.0080, RCOREW=0.0080,     &END
 &BINP7   VINF=55,   VSOUND=340.3,                                                &END
 &BINP8   ALDEG= 10.00, YAWDEG=0.0,   PHIDOT=0.0,   THEDOT=0.0,   PSIDOT=0.0,     &END
 &BINP8A  PHIMAX= 0.0, THEMAX= 0.0,  PSIMAX=0.0,
          WRX=0.0,      WRY=0.0,      WRZ=0.0,                                    &END
 &BINP8B  DXMAX=0.0,    DYMAX=0.0,    DZMAX=0.0,
          WTX=0.0,      WTY=0.0,      WTZ=0.0,                                    &END
 &BINP9   CBAR=0.4,   SREF=0.1257,  SSPAN= .2,
          RMPX=1.2,    RMPY=0.00,    RMPZ=0.00,                                   &END
 &BINP10  NORSET=0,     NBCHGE=0,     NCZONE=0,
          NCZPCH=0,     CZDUB=0.0,    VREF=0.0,                                   &END
 &BINP11  NORPCH=0,     NORF=0,       NORL=0,
          NOCF=0,       NOCL=0,       VNORM=0.0,                                  &END
 &BINP12  KPAN=0,       KSIDE=0,      NEWNAB=0,     NEWSID=0,                     &END
 &BINP13  NBLIT=1,                                                                &END


 &ASEM1   ASEMX=0.00,       ASEMY=0.00,       ASEMZ=0.00,
          ASCAL=1.00,       ATHET=0.00,       NODEA=5,                            &END
 &ASEM2   APXX=0.00,        APYY=0.00,        APZZ=0.00,
          AHXX=0.00,        AHYY=1.00,        AHZZ=0.00,                          &END


 &COMP1   COMPX= 0.0000,     COMPY= 0.0000,     COMPZ= 0.0000,
          CSCAL=   1.000,    CTHET=    0.0,     NODEC= 5,                         &END
 &COMP2   CPXX= 0.0000,      CPYY= 0.0000,      CPZZ= 0.0000,
          CHXX= 0.0000,      CHYY=  1.000,      CHZZ= 0.0000,                     &END

 &PATCH1 IREV=0, IDPAT=2, MAKE=0, KCOMP=1, KASS=1, IPATSYM=0, IPATCOP=0,          &END
 Prolate_Spheroid
 &SECT1 STX=0.0, STY=0.0, STZ=0.0, SCALE=1.0, ALF=0.0, THETA=0.0, INMODE=4,
  TNODS=0, TNPS=0, TINTS=0, &END
    0.0000      0.0000      0.0000
    0.0000      0.0000      0.0000
    0.0000      0.0000      0.0000
    0.0000      0.0000      0.0000
    0.0000      0.0000      0.0000
    0.0000      0.0000      0.0000
    0.0000      0.0000      0.0000
    0.0000      0.0000      0.0000
    0.0000      0.0000      0.0000
    0.0000      0.0000      0.0000
    0.0000      0.0000      0.0000
    0.0000      0.0000      0.0000
    0.0000      0.0000      0.0000
    0.0000      0.0000      0.0000
    0.0000      0.0000      0.0000
    0.0000      0.0000      0.0000
    0.0000      0.0000      0.0000
    0.0000      0.0000      0.0000
    0.0000      0.0000      0.0000
    0.0000      0.0000      0.0000
    0.0000      0.0000      0.0000
 &BPNODE TNODE=3, TNPC=40, TINTC=3, &END
 &SECT1 STX=0.0, STY=0.0, STZ=0.0, SCALE=1.0, ALF=0.0, THETA=0.0, INMODE=4,
  TNODS=0, TNPS=0, TINTS=0, &END
    0.0037      0.0000     -0.0157
    0.0037      0.0028     -0.0154
    0.0037      0.0052     -0.0148
    0.0037      0.0074     -0.0138
    0.0037      0.0094     -0.0126
```



```
Jun 11 1997 05:33                 pr10w117.in                      Page 2
    0.0037      0.0110     -0.0111
    0.0037      0.0126     -0.0094
    0.0037      0.0139     -0.0073
    0.0037      0.0148     -0.0052
    0.0037      0.0154     -0.0028
    0.0037      0.0157     -0.0003
    0.0037      0.0154      0.0032
    0.0037      0.0147      0.0055
    0.0037      0.0137      0.0077
    0.0037      0.0124      0.0096
    0.0037      0.0110      0.0112
    0.0037      0.0090      0.0128
    0.0037      0.0071      0.0140
    0.0037      0.0049      0.0149
    0.0037      0.0025      0.0155
    0.0037      0.0000      0.0157
 &BPNODE TNODE=3, TNPC=40, TINTC=3, &END
 &SECT1 STX=0.0, STY=0.0, STZ=0.0, SCALE=1.0, ALF=0.0, THETA=0.0, INMODE=4,
  TNODS=0, TNPS=0, TINTS=0, &END
    0.0148      0.0000     -0.0313
    0.0148      0.0055     -0.0308
    0.0148      0.0104     -0.0295
    0.0148      0.0149     -0.0275
    0.0148      0.0188     -0.0250
    0.0148      0.0221     -0.0221
    0.0148      0.0252     -0.0185
    0.0148      0.0277     -0.0145
    0.0148      0.0296     -0.0100
    0.0148      0.0308     -0.0051
    0.0148      0.0313      0.0000
    0.0148      0.0308      0.0055
    0.0148      0.0295      0.0104
    0.0148      0.0275      0.0149
    0.0148      0.0250      0.0188
    0.0148      0.0221      0.0221
    0.0148      0.0185      0.0252
    0.0148      0.0145      0.0277
    0.0148      0.0100      0.0296
    0.0148      0.0051      0.0308
    0.0148      0.0000      0.0313
 &BPNODE TNODE=3, TNPC=40, TINTC=3, &END
 &SECT1 STX=0.0, STY=0.0, STZ=0.0, SCALE=1.0, ALF=0.0, THETA=0.0, INMODE=4,
  TNODS=0, TNPS=0, TINTS=0, &END
    0.0332      0.0000     -0.0467
    0.0332      0.0081     -0.0460
    0.0332      0.0155     -0.0440
    0.0332      0.0222     -0.0410
    0.0332      0.0282     -0.0372
    0.0332      0.0332     -0.0328
    0.0332      0.0374     -0.0278
    0.0332      0.0412     -0.0219
    0.0332      0.0441     -0.0151
    0.0332      0.0460     -0.0077
    0.0332      0.0467      0.0000
    0.0332      0.0460      0.0081
    0.0332      0.0440      0.0155
    0.0332      0.0410      0.0222
    0.0332      0.0372      0.0282
    0.0332      0.0328      0.0332
    0.0332      0.0278      0.0374
    0.0332      0.0219      0.0412
    0.0332      0.0151      0.0441
    0.0332      0.0077      0.0460
    0.0332      0.0000      0.0467
 &BPNODE TNODE=3, TNPC=40, TINTC=3, &END
 &SECT1 STX=0.0, STY=0.0, STZ=0.0, SCALE=1.0, ALF=0.0, THETA=0.0, INMODE=4,
  TNODS=0, TNPS=0, TINTS=0, &END
    0.0587      0.0000     -0.0618
    0.0587      0.0106     -0.0609
    0.0587      0.0203     -0.0583
    0.0587      0.0293     -0.0544
    0.0587      0.0371     -0.0494
    0.0587      0.0437     -0.0436
    0.0587      0.0496     -0.0368
    0.0587      0.0546     -0.0289
    0.0587      0.0584     -0.0200
```

```
   0.0587    0.0609   -0.0102
   0.0587    0.0618    0.0000
   0.0587    0.0609    0.0106
   0.0587    0.0583    0.0203
   0.0587    0.0544    0.0293
   0.0587    0.0494    0.0371
   0.0587    0.0436    0.0437
   0.0587    0.0368    0.0496
   0.0587    0.0289    0.0546
   0.0587    0.0200    0.0584
   0.0587    0.0102    0.0609
   0.0587    0.0000    0.0618
&BPNODE TNODE=3, TNPC=40, TINTC=3, &END
&SECT1 STX=0.0, STY=0.0, STZ=0.0, SCALE=1.0, ALF=0.0, THETA=0.0, INMODE=4,
 TNODS=0, TNPS=0, TINTS=0, &END
   0.0913    0.0000   -0.0765
   0.0913    0.0130   -0.0754
   0.0913    0.0251   -0.0722
   0.0913    0.0362   -0.0674
   0.0913    0.0459   -0.0612
   0.0913    0.0541   -0.0541
   0.0913    0.0614   -0.0456
   0.0913    0.0676   -0.0359
   0.0913    0.0724   -0.0248
   0.0913    0.0754   -0.0127
   0.0913    0.0765    0.0000
   0.0913    0.0754    0.0130
   0.0913    0.0722    0.0251
   0.0913    0.0674    0.0362
   0.0913    0.0612    0.0459
   0.0913    0.0541    0.0541
   0.0913    0.0456    0.0614
   0.0913    0.0359    0.0676
   0.0913    0.0248    0.0724
   0.0913    0.0127    0.0754
   0.0913    0.0000    0.0765
&BPNODE TNODE=3, TNPC=40, TINTC=3, &END
&SECT1 STX=0.0, STY=0.0, STZ=0.0, SCALE=1.0, ALF=0.0, THETA=0.0, INMODE=4,
 TNODS=0, TNPS=0, TINTS=0, &END
   0.1308    0.0000   -0.0908
   0.1308    0.0154   -0.0894
   0.1308    0.0298   -0.0857
   0.1308    0.0429   -0.0799
   0.1308    0.0545   -0.0726
   0.1308    0.0642   -0.0641
   0.1308    0.0728   -0.0541
   0.1308    0.0801   -0.0426
   0.1308    0.0858   -0.0294
   0.1308    0.0895   -0.0150
   0.1308    0.0908    0.0000
   0.1308    0.0894    0.0154
   0.1308    0.0857    0.0298
   0.1308    0.0799    0.0429
   0.1308    0.0726    0.0545
   0.1308    0.0641    0.0642
   0.1308    0.0541    0.0728
   0.1308    0.0426    0.0801
   0.1308    0.0294    0.0858
   0.1308    0.0150    0.0895
   0.1308    0.0000    0.0908
&BPNODE TNODE=3, TNPC=40, TINTC=3, &END
&SECT1 STX=0.0, STY=0.0, STZ=0.0, SCALE=1.0, ALF=0.0, THETA=0.0, INMODE=4,
 TNODS=0, TNPS=0, TINTS=0, &END
   0.1768    0.0000   -0.1045
   0.1768    0.0177   -0.1029
   0.1768    0.0343   -0.0987
   0.1768    0.0495   -0.0920
   0.1768    0.0628   -0.0835
   0.1768    0.0739   -0.0737
   0.1768    0.0837   -0.0624
   0.1768    0.0922   -0.0491
   0.1768    0.0988   -0.0339
   0.1768    0.1030   -0.0174
   0.1768    0.1045    0.0000
   0.1768    0.1029    0.0177
   0.1768    0.0987    0.0343
```

Printed by pollard from hawkeye


```
   0.1768    0.0920    0.0495
   0.1768    0.0835    0.0628
   0.1768    0.0737    0.0739
   0.1768    0.0624    0.0837
   0.1768    0.0491    0.0922
   0.1768    0.0339    0.0988
   0.1768    0.0174    0.1030
   0.1768    0.0000    0.1045
&BPNODE TNODE=3, TNPC=40, TINTC=3, &END
&SECT1 STX=0.0, STY=0.0, STZ=0.0, SCALE=1.0, ALF=0.0, THETA=0.0, INMODE=4,
 TNODS=0, TNPS=0, TINTS=0, &END
   0.2292    0.0000   -0.1175
   0.2292    0.0198   -0.1158
   0.2292    0.0385   -0.1110
   0.2292    0.0556   -0.1035
   0.2292    0.0705   -0.0940
   0.2292    0.0831   -0.0831
   0.2292    0.0942   -0.0702
   0.2292    0.1037   -0.0552
   0.2292    0.1111   -0.0382
   0.2292    0.1159   -0.0195
   0.2292    0.1175    0.0000
   0.2292    0.1158    0.0198
   0.2292    0.1110    0.0385
   0.2292    0.1035    0.0556
   0.2292    0.0940    0.0705
   0.2292    0.0831    0.0831
   0.2292    0.0702    0.0942
   0.2292    0.0552    0.1037
   0.2292    0.0382    0.1111
   0.2292    0.0195    0.1159
   0.2292    0.0000    0.1175
&BPNODE TNODE=3, TNPC=40, TINTC=3, &END
&SECT1 STX=0.0, STY=0.0, STZ=0.0, SCALE=1.0, ALF=0.0, THETA=0.0, INMODE=4,
 TNODS=0, TNPS=0, TINTS=0, &END
   0.2875    0.0000   -0.1298
   0.2875    0.0219   -0.1280
   0.2875    0.0426   -0.1227
   0.2875    0.0614   -0.1144
   0.2875    0.0780   -0.1038
   0.2875    0.0919   -0.0917
   0.2875    0.1041   -0.0776
   0.2875    0.1146   -0.0611
   0.2875    0.1228   -0.0422
   0.2875    0.1280   -0.0216
   0.2875    0.1298    0.0000
   0.2875    0.1280    0.0219
   0.2875    0.1227    0.0426
   0.2875    0.1144    0.0614
   0.2875    0.1038    0.0780
   0.2875    0.0917    0.0919
   0.2875    0.0776    0.1041
   0.2875    0.0611    0.1146
   0.2875    0.0422    0.1228
   0.2875    0.0216    0.1280
   0.2875    0.0000    0.1298
&BPNODE TNODE=3, TNPC=40, TINTC=3, &END
&SECT1 STX=0.0, STY=0.0, STZ=0.0, SCALE=1.0, ALF=0.0, THETA=0.0, INMODE=4,
 TNODS=0, TNPS=0, TINTS=0, &END
   0.3515    0.0000   -0.1414
   0.3515    0.0239   -0.1393
   0.3515    0.0464   -0.1336
   0.3515    0.0669   -0.1245
   0.3515    0.0850   -0.1130
   0.3515    0.1001   -0.0998
   0.3515    0.1132   -0.0846
   0.3515    0.1247   -0.0666
   0.3515    0.1337   -0.0460
   0.3515    0.1394   -0.0235
   0.3515    0.1414    0.0000
   0.3515    0.1393    0.0239
   0.3515    0.1336    0.0464
   0.3515    0.1245    0.0669
   0.3515    0.1130    0.0850
   0.3515    0.0998    0.1001
   0.3515    0.0846    0.1132
```

```
   0.3515    0.0666    0.1247
   0.3515    0.0460    0.1337
   0.3515    0.0235    0.1394
   0.3515    0.0000    0.1414
&BPNODE TNODE=3, TNPC=40, TINTC=3, &END
&SECT1 STX=0.0, STY=0.0, STZ=0.0, SCALE=1.0, ALF=0.0, THETA=0.0, INMODE=4,
 TNODS=0, TNPS=0, TINTS=0, &END
   0.4207    0.0000   -0.1520
   0.4207    0.0257   -0.1499
   0.4207    0.0499   -0.1436
   0.4207    0.0720   -0.1339
   0.4207    0.0914   -0.1215
   0.4207    0.1077   -0.1073
   0.4207    0.1217   -0.0910
   0.4207    0.1341   -0.0717
   0.4207    0.1437   -0.0495
   0.4207    0.1499   -0.0253
   0.4207    0.1520    0.0000
   0.4207    0.1499    0.0257
   0.4207    0.1436    0.0499
   0.4207    0.1339    0.0720
   0.4207    0.1215    0.0914
   0.4207    0.1073    0.1077
   0.4207    0.0910    0.1217
   0.4207    0.0717    0.1341
   0.4207    0.0495    0.1437
   0.4207    0.0253    0.1499
   0.4207    0.0000    0.1520
&BPNODE TNODE=3, TNPC=40, TINTC=3, &END
&SECT1 STX=0.0, STY=0.0, STZ=0.0, SCALE=1.0, ALF=0.0, THETA=0.0, INMODE=4,
 TNODS=0, TNPS=0, TINTS=0, &END
   0.4947    0.0000   -0.1618
   0.4947    0.0273   -0.1595
   0.4947    0.0530   -0.1528
   0.4947    0.0765   -0.1425
   0.4947    0.0972   -0.1293
   0.4947    0.1145   -0.1143
   0.4947    0.1296   -0.0968
   0.4947    0.1427   -0.0762
   0.4947    0.1530   -0.0526
   0.4947    0.1595   -0.0269
   0.4947    0.1618    0.0000
   0.4947    0.1595    0.0273
   0.4947    0.1528    0.0530
   0.4947    0.1425    0.0765
   0.4947    0.1293    0.0972
   0.4947    0.1143    0.1145
   0.4947    0.0968    0.1296
   0.4947    0.0762    0.1427
   0.4947    0.0526    0.1530
   0.4947    0.0269    0.1595
   0.4947    0.0000    0.1618
&BPNODE TNODE=3, TNPC=40, TINTC=3, &END
&SECT1 STX=0.0, STY=0.0, STZ=0.0, SCALE=1.0, ALF=0.0, THETA=0.0, INMODE=4,
 TNODS=0, TNPS=0, TINTS=0, &END
   0.5730    0.0000   -0.1705
   0.5730    0.0287   -0.1681
   0.5730    0.0558   -0.1611
   0.5730    0.0806   -0.1502
   0.5730    0.1023   -0.1364
   0.5730    0.1206   -0.1205
   0.5730    0.1366   -0.1020
   0.5730    0.1504   -0.0802
   0.5730    0.1612   -0.0554
   0.5730    0.1681   -0.0283
   0.5730    0.1705    0.0000
   0.5730    0.1681    0.0287
   0.5730    0.1611    0.0558
   0.5730    0.1502    0.0806
   0.5730    0.1364    0.1023
   0.5730    0.1205    0.1206
   0.5730    0.1020    0.1366
   0.5730    0.0802    0.1504
   0.5730    0.0554    0.1612
   0.5730    0.0283    0.1681
   0.5730    0.0000    0.1705
```



```
&BPNODE TNODE=3, TNPC=40, TINTC=3, &END
&SECT1 STX=0.0, STY=0.0, STZ=0.0, SCALE=1.0, ALF=0.0, THETA=0.0, INMODE=4,
 TNODS=0, TNPS=0, TINTS=0, &END
   0.6552    0.0000   -0.1782
   0.6552    0.0300   -0.1756
   0.6552    0.0584   -0.1683
   0.6552    0.0843   -0.1569
   0.6552    0.1071   -0.1424
   0.6552    0.1261   -0.1258
   0.6552    0.1427   -0.1067
   0.6552    0.1571   -0.0840
   0.6552    0.1685   -0.0580
   0.6552    0.1757   -0.0297
   0.6552    0.1782    0.0000
   0.6552    0.1756    0.0300
   0.6552    0.1683    0.0584
   0.6552    0.1569    0.0843
   0.6552    0.1424    0.1071
   0.6552    0.1258    0.1261
   0.6552    0.1067    0.1427
   0.6552    0.0840    0.1571
   0.6552    0.0580    0.1685
   0.6552    0.0297    0.1757
   0.6552    0.0000    0.1782
&BPNODE TNODE=3, TNPC=40, TINTC=3, &END
&SECT1 STX=0.0, STY=0.0, STZ=0.0, SCALE=1.0, ALF=0.0, THETA=0.0, INMODE=4,
 TNODS=0, TNPS=0, TINTS=0, &END
   0.7408    0.0000   -0.1848
   0.7408    0.0311   -0.1821
   0.7408    0.0604   -0.1746
   0.7408    0.0873   -0.1628
   0.7408    0.1109   -0.1478
   0.7408    0.1306   -0.1306
   0.7408    0.1480   -0.1105
   0.7408    0.1630   -0.0870
   0.7408    0.1747   -0.0601
   0.7408    0.1822   -0.0307
   0.7408    0.1848    0.0000
   0.7408    0.1821    0.0311
   0.7408    0.1746    0.0604
   0.7408    0.1628    0.0873
   0.7408    0.1478    0.1109
   0.7408    0.1306    0.1306
   0.7408    0.1105    0.1480
   0.7408    0.0870    0.1630
   0.7408    0.0601    0.1747
   0.7408    0.0307    0.1822
   0.7408    0.0000    0.1848
&BPNODE TNODE=3, TNPC=40, TINTC=3, &END
&SECT1 STX=0.0, STY=0.0, STZ=0.0, SCALE=1.0, ALF=0.0, THETA=0.0, INMODE=4,
 TNODS=0, TNPS=0, TINTS=0, &END
   0.8292    0.0000   -0.1902
   0.8292    0.0320   -0.1875
   0.8292    0.0623   -0.1797
   0.8292    0.0900   -0.1675
   0.8292    0.1143   -0.1520
   0.8292    0.1346   -0.1343
   0.8292    0.1523   -0.1139
   0.8292    0.1677   -0.0897
   0.8292    0.1798   -0.0620
   0.8292    0.1875   -0.0317
   0.8292    0.1902    0.0000
   0.8292    0.1875    0.0320
   0.8292    0.1797    0.0623
   0.8292    0.1675    0.0900
   0.8292    0.1520    0.1143
   0.8292    0.1343    0.1346
   0.8292    0.1139    0.1523
   0.8292    0.0897    0.1677
   0.8292    0.0620    0.1798
   0.8292    0.0317    0.1875
   0.8292    0.0000    0.1902
&BPNODE TNODE=3, TNPC=40, TINTC=3, &END
&SECT1 STX=0.0, STY=0.0, STZ=0.0, SCALE=1.0, ALF=0.0, THETA=0.0, INMODE=4,
 TNODS=0, TNPS=0, TINTS=0, &END
   0.9199    0.0000   -0.1945
```

```
      0.9199     0.0327    -0.1917
      0.9199     0.0637    -0.1837
      0.9199     0.0920    -0.1713
      0.9199     0.1168    -0.1554
      0.9199     0.1377    -0.1373
      0.9199     0.1557    -0.1165
      0.9199     0.1715    -0.0917
      0.9199     0.1838    -0.0633
      0.9199     0.1917    -0.0324
      0.9199     0.1945     0.0000
      0.9199     0.1917     0.0327
      0.9199     0.1837     0.0637
      0.9199     0.1713     0.0920
      0.9199     0.1554     0.1168
      0.9199     0.1373     0.1377
      0.9199     0.1165     0.1557
      0.9199     0.0917     0.1715
      0.9199     0.0633     0.1838
      0.9199     0.0324     0.1917
      0.9199     0.0000     0.1945
&BPNODE TNODE=3, TNPC=40, TINTC=3, &END
&SECT1 STX=0.0, STY=0.0, STZ=0.0, SCALE=1.0, ALF=0.0, THETA=0.0, INMODE=4,
 TNODS=0, TNPS=0, TINTS=0, &END
      1.0123     0.0000    -0.1975
      1.0123     0.0332    -0.1947
      1.0123     0.0646    -0.1867
      1.0123     0.0934    -0.1741
      1.0123     0.1185    -0.1580
      1.0123     0.1397    -0.1396
      1.0123     0.1582    -0.1182
      1.0123     0.1742    -0.0930
      1.0123     0.1868    -0.0643
      1.0123     0.1948    -0.0328
      1.0123     0.1975     0.0000
      1.0123     0.1947     0.0332
      1.0123     0.1867     0.0646
      1.0123     0.1741     0.0934
      1.0123     0.1580     0.1185
      1.0123     0.1396     0.1397
      1.0123     0.1182     0.1582
      1.0123     0.0930     0.1742
      1.0123     0.0643     0.1868
      1.0123     0.0328     0.1948
      1.0123     0.0000     0.1975
&BPNODE TNODE=3, TNPC=40, TINTC=3, &END
&SECT1 STX=0.0, STY=0.0, STZ=0.0, SCALE=1.0, ALF=0.0, THETA=0.0, INMODE=4,
 TNODS=0, TNPS=0, TINTS=0, &END
      1.1058     0.0000    -0.1994
      1.1058     0.0335    -0.1965
      1.1058     0.0653    -0.1884
      1.1058     0.0943    -0.1756
      1.1058     0.1198    -0.1594
      1.1058     0.1411    -0.1408
      1.1058     0.1596    -0.1194
      1.1058     0.1758    -0.0940
      1.1058     0.1885    -0.0649
      1.1058     0.1966    -0.0332
      1.1058     0.1994     0.0000
      1.1058     0.1965     0.0335
      1.1058     0.1884     0.0653
      1.1058     0.1756     0.0943
      1.1058     0.1594     0.1198
      1.1058     0.1408     0.1411
      1.1058     0.1194     0.1596
      1.1058     0.0940     0.1758
      1.1058     0.0649     0.1885
      1.1058     0.0332     0.1966
      1.1058     0.0000     0.1994
&BPNODE TNODE=3, TNPC=40, TINTC=3, &END
&SECT1 STX=0.0, STY=0.0, STZ=0.0, SCALE=1.0, ALF=0.0, THETA=0.0, INMODE=4,
 TNODS=0, TNPS=0, TINTS=0, &END
      1.2000     0.0000    -0.2000
      1.2000     0.0336    -0.1971
      1.2000     0.0655    -0.1890
      1.2000     0.0946    -0.1762
      1.2000     0.1201    -0.1599
```



```
      1.2000     0.1415    -0.1413
      1.2000     0.1601    -0.1198
      1.2000     0.1764    -0.0943
      1.2000     0.1891    -0.0651
      1.2000     0.1972    -0.0333
      1.2000     0.2000     0.0000
      1.2000     0.1971     0.0336
      1.2000     0.1890     0.0655
      1.2000     0.1762     0.0946
      1.2000     0.1599     0.1201
      1.2000     0.1413     0.1415
      1.2000     0.1198     0.1601
      1.2000     0.0943     0.1764
      1.2000     0.0651     0.1891
      1.2000     0.0333     0.1972
      1.2000     0.0000     0.2000
&BPNODE TNODE=3, TNPC=40, TINTC=3, &END
&SECT1 STX=0.0, STY=0.0, STZ=0.0, SCALE=1.0, ALF=0.0, THETA=0.0, INMODE=4,
 TNODS=0, TNPS=0, TINTS=0, &END
      1.2942     0.0000    -0.1994
      1.2942     0.0335    -0.1965
      1.2942     0.0653    -0.1884
      1.2942     0.0943    -0.1756
      1.2942     0.1198    -0.1594
      1.2942     0.1411    -0.1408
      1.2942     0.1596    -0.1194
      1.2942     0.1758    -0.0940
      1.2942     0.1885    -0.0649
      1.2942     0.1966    -0.0332
      1.2942     0.1994     0.0000
      1.2942     0.1965     0.0335
      1.2942     0.1884     0.0653
      1.2942     0.1756     0.0943
      1.2942     0.1594     0.1198
      1.2942     0.1408     0.1411
      1.2942     0.1194     0.1596
      1.2942     0.0940     0.1758
      1.2942     0.0649     0.1885
      1.2942     0.0332     0.1966
      1.2942     0.0000     0.1994
&BPNODE TNODE=3, TNPC=40, TINTC=3, &END
&SECT1 STX=0.0, STY=0.0, STZ=0.0, SCALE=1.0, ALF=0.0, THETA=0.0, INMODE=4,
 TNODS=0, TNPS=0, TINTS=0, &END
      1.3877     0.0000    -0.1975
      1.3877     0.0332    -0.1947
      1.3877     0.0646    -0.1867
      1.3877     0.0934    -0.1741
      1.3877     0.1185    -0.1580
      1.3877     0.1397    -0.1396
      1.3877     0.1582    -0.1182
      1.3877     0.1742    -0.0930
      1.3877     0.1868    -0.0643
      1.3877     0.1948    -0.0328
      1.3877     0.1975     0.0000
      1.3877     0.1947     0.0332
      1.3877     0.1867     0.0646
      1.3877     0.1741     0.0934
      1.3877     0.1580     0.1185
      1.3877     0.1396     0.1397
      1.3877     0.1182     0.1582
      1.3877     0.0930     0.1742
      1.3877     0.0643     0.1868
      1.3877     0.0328     0.1948
      1.3877     0.0000     0.1975
&BPNODE TNODE=3, TNPC=40, TINTC=3, &END
&SECT1 STX=0.0, STY=0.0, STZ=0.0, SCALE=1.0, ALF=0.0, THETA=0.0, INMODE=4,
 TNODS=0, TNPS=0, TINTS=0, &END
      1.4801     0.0000    -0.1945
      1.4801     0.0327    -0.1917
      1.4801     0.0637    -0.1837
      1.4801     0.0920    -0.1713
      1.4801     0.1168    -0.1554
      1.4801     0.1377    -0.1373
      1.4801     0.1557    -0.1165
      1.4801     0.1715    -0.0917
      1.4801     0.1838    -0.0633
```

```
 1.4801    0.1917   -0.0324
 1.4801    0.1945    0.0000
 1.4801    0.1917    0.0327
 1.4801    0.1837    0.0637
 1.4801    0.1713    0.0920
 1.4801    0.1554    0.1168
 1.4801    0.1373    0.1377
 1.4801    0.1165    0.1557
 1.4801    0.0917    0.1715
 1.4801    0.0633    0.1838
 1.4801    0.0324    0.1917
 1.4801    0.0000    0.1945
&BPNODE TNODE=3, TNPC=40, TINTC=3, &END
&SECT1 STX=0.0, STY=0.0, STZ=0.0, SCALE=1.0, ALF=0.0, THETA=0.0, INMODE=4,
 TNODS=0, TNPS=0, TINTS=0, &END
 1.5708    0.0000   -0.1902
 1.5708    0.0320   -0.1875
 1.5708    0.0623   -0.1797
 1.5708    0.0900   -0.1675
 1.5708    0.1143   -0.1520
 1.5708    0.1346   -0.1343
 1.5708    0.1523   -0.1139
 1.5708    0.1677   -0.0897
 1.5708    0.1798   -0.0620
 1.5708    0.1875   -0.0317
 1.5708    0.1902    0.0000
 1.5708    0.1875    0.0320
 1.5708    0.1797    0.0623
 1.5708    0.1675    0.0900
 1.5708    0.1520    0.1143
 1.5708    0.1343    0.1346
 1.5708    0.1139    0.1523
 1.5708    0.0897    0.1677
 1.5708    0.0620    0.1798
 1.5708    0.0317    0.1875
 1.5708    0.0000    0.1902
&BPNODE TNODE=3, TNPC=40, TINTC=3, &END
&SECT1 STX=0.0, STY=0.0, STZ=0.0, SCALE=1.0, ALF=0.0, THETA=0.0, INMODE=4,
 TNODS=0, TNPS=0, TINTS=0, &END
 1.6592    0.0000   -0.1848
 1.6592    0.0311   -0.1821
 1.6592    0.0604   -0.1746
 1.6592    0.0873   -0.1628
 1.6592    0.1109   -0.1478
 1.6592    0.1306   -0.1306
 1.6592    0.1480   -0.1105
 1.6592    0.1630   -0.0870
 1.6592    0.1747   -0.0601
 1.6592    0.1822   -0.0307
 1.6592    0.1848    0.0000
 1.6592    0.1821    0.0311
 1.6592    0.1746    0.0604
 1.6592    0.1628    0.0873
 1.6592    0.1478    0.1109
 1.6592    0.1306    0.1306
 1.6592    0.1105    0.1480
 1.6592    0.0870    0.1630
 1.6592    0.0601    0.1747
 1.6592    0.0307    0.1822
 1.6592    0.0000    0.1848
&BPNODE TNODE=3, TNPC=40, TINTC=3, &END
&SECT1 STX=0.0, STY=0.0, STZ=0.0, SCALE=1.0, ALF=0.0, THETA=0.0, INMODE=4,
 TNODS=0, TNPS=0, TINTS=0, &END
 1.7448    0.0000   -0.1782
 1.7448    0.0300   -0.1756
 1.7448    0.0584   -0.1683
 1.7448    0.0843   -0.1569
 1.7448    0.1071   -0.1424
 1.7448    0.1261   -0.1258
 1.7448    0.1427   -0.1067
 1.7448    0.1571   -0.0840
 1.7448    0.1685   -0.0580
 1.7448    0.1757   -0.0297
 1.7448    0.1782    0.0000
 1.7448    0.1756    0.0300
 1.7448    0.1683    0.0584
```



```
 1.7448    0.1569    0.0843
 1.7448    0.1424    0.1071
 1.7448    0.1258    0.1261
 1.7448    0.1067    0.1427
 1.7448    0.0840    0.1571
 1.7448    0.0580    0.1685
 1.7448    0.0297    0.1757
 1.7448    0.0000    0.1782
&BPNODE TNODE=3, TNPC=40, TINTC=3, &END
&SECT1 STX=0.0, STY=0.0, STZ=0.0, SCALE=1.0, ALF=0.0, THETA=0.0, INMODE=4,
 TNODS=0, TNPS=0, TINTS=0, &END
 1.8270    0.0000   -0.1705
 1.8270    0.0287   -0.1681
 1.8270    0.0558   -0.1611
 1.8270    0.0806   -0.1502
 1.8270    0.1023   -0.1364
 1.8270    0.1206   -0.1205
 1.8270    0.1366   -0.1020
 1.8270    0.1504   -0.0802
 1.8270    0.1612   -0.0554
 1.8270    0.1681   -0.0283
 1.8270    0.1705    0.0000
 1.8270    0.1681    0.0287
 1.8270    0.1611    0.0558
 1.8270    0.1502    0.0806
 1.8270    0.1364    0.1023
 1.8270    0.1205    0.1206
 1.8270    0.1020    0.1366
 1.8270    0.0802    0.1504
 1.8270    0.0554    0.1612
 1.8270    0.0283    0.1681
 1.8270    0.0000    0.1705
&BPNODE TNODE=3, TNPC=40, TINTC=3, &END
&SECT1 STX=0.0, STY=0.0, STZ=0.0, SCALE=1.0, ALF=0.0, THETA=0.0, INMODE=4,
 TNODS=0, TNPS=0, TINTS=0, &END
 1.9053    0.0000   -0.1618
 1.9053    0.0273   -0.1595
 1.9053    0.0530   -0.1528
 1.9053    0.0765   -0.1425
 1.9053    0.0972   -0.1293
 1.9053    0.1145   -0.1143
 1.9053    0.1296   -0.0968
 1.9053    0.1427   -0.0762
 1.9053    0.1530   -0.0526
 1.9053    0.1595   -0.0269
 1.9053    0.1618    0.0000
 1.9053    0.1595    0.0273
 1.9053    0.1528    0.0530
 1.9053    0.1425    0.0765
 1.9053    0.1293    0.0972
 1.9053    0.1143    0.1145
 1.9053    0.0968    0.1296
 1.9053    0.0762    0.1427
 1.9053    0.0526    0.1530
 1.9053    0.0269    0.1595
 1.9053    0.0000    0.1618
&BPNODE TNODE=3, TNPC=40, TINTC=3, &END
&SECT1 STX=0.0, STY=0.0, STZ=0.0, SCALE=1.0, ALF=0.0, THETA=0.0, INMODE=4,
 TNODS=0, TNPS=0, TINTS=0, &END
 1.9793    0.0000   -0.1520
 1.9793    0.0257   -0.1499
 1.9793    0.0499   -0.1436
 1.9793    0.0720   -0.1339
 1.9793    0.0914   -0.1215
 1.9793    0.1077   -0.1073
 1.9793    0.1217   -0.0910
 1.9793    0.1341   -0.0717
 1.9793    0.1437   -0.0495
 1.9793    0.1499   -0.0253
 1.9793    0.1520    0.0000
 1.9793    0.1499    0.0257
 1.9793    0.1436    0.0499
 1.9793    0.1339    0.0720
 1.9793    0.1215    0.0914
 1.9793    0.1073    0.1077
 1.9793    0.0910    0.1217
```

```
     1.9793    0.0717    0.1341
     1.9793    0.0495    0.1437
     1.9793    0.0253    0.1499
     1.9793    0.0000    0.1520
 &BPNODE TNODE=3, TNPC=40, TINTC=3, &END
 &SECT1 STX=0.0, STY=0.0, STZ=0.0, SCALE=1.0, ALF=0.0, THETA=0.0, INMODE=4,
  TNODS=0, TNPS=0, TINTS=0, &END
     2.0485    0.0000   -0.1414
     2.0485    0.0239   -0.1393
     2.0485    0.0464   -0.1336
     2.0485    0.0669   -0.1245
     2.0485    0.0850   -0.1130
     2.0485    0.1001   -0.0998
     2.0485    0.1132   -0.0846
     2.0485    0.1247   -0.0666
     2.0485    0.1337   -0.0460
     2.0485    0.1394   -0.0235
     2.0485    0.1414    0.0000
     2.0485    0.1393    0.0239
     2.0485    0.1336    0.0464
     2.0485    0.1245    0.0669
     2.0485    0.1130    0.0850
     2.0485    0.0998    0.1001
     2.0485    0.0846    0.1132
     2.0485    0.0666    0.1247
     2.0485    0.0460    0.1337
     2.0485    0.0235    0.1394
     2.0485    0.0000    0.1414
 &BPNODE TNODE=3, TNPC=40, TINTC=3, &END
 &SECT1 STX=0.0, STY=0.0, STZ=0.0, SCALE=1.0, ALF=0.0, THETA=0.0, INMODE=4,
  TNODS=0, TNPS=0, TINTS=0, &END
     2.1125    0.0000   -0.1298
     2.1125    0.0219   -0.1280
     2.1125    0.0426   -0.1227
     2.1125    0.0614   -0.1144
     2.1125    0.0780   -0.1038
     2.1125    0.0919   -0.0917
     2.1125    0.1041   -0.0776
     2.1125    0.1146   -0.0611
     2.1125    0.1228   -0.0422
     2.1125    0.1280   -0.0216
     2.1125    0.1298    0.0000
     2.1125    0.1280    0.0219
     2.1125    0.1227    0.0426
     2.1125    0.1144    0.0614
     2.1125    0.1038    0.0780
     2.1125    0.0917    0.0919
     2.1125    0.0776    0.1041
     2.1125    0.0611    0.1146
     2.1125    0.0422    0.1228
     2.1125    0.0216    0.1280
     2.1125    0.0000    0.1298
 &BPNODE TNODE=3, TNPC=40, TINTC=3, &END
 &SECT1 STX=0.0, STY=0.0, STZ=0.0, SCALE=1.0, ALF=0.0, THETA=0.0, INMODE=4,
  TNODS=0, TNPS=0, TINTS=0, &END
     2.1708    0.0000   -0.1175
     2.1708    0.0198   -0.1158
     2.1708    0.0385   -0.1110
     2.1708    0.0556   -0.1035
     2.1708    0.0705   -0.0940
     2.1708    0.0831   -0.0831
     2.1708    0.0942   -0.0702
     2.1708    0.1037   -0.0552
     2.1708    0.1111   -0.0382
     2.1708    0.1159   -0.0195
     2.1708    0.1175    0.0000
     2.1708    0.1158    0.0198
     2.1708    0.1110    0.0385
     2.1708    0.1035    0.0556
     2.1708    0.0940    0.0705
     2.1708    0.0831    0.0831
     2.1708    0.0702    0.0942
     2.1708    0.0552    0.1037
     2.1708    0.0382    0.1111
     2.1708    0.0195    0.1159
     2.1708    0.0000    0.1175
```



```
 &BPNODE TNODE=3, TNPC=40, TINTC=3, &END
 &SECT1 STX=0.0, STY=0.0, STZ=0.0, SCALE=1.0, ALF=0.0, THETA=0.0, INMODE=4,
  TNODS=0, TNPS=0, TINTS=0, &END
     2.2232    0.0000   -0.1045
     2.2232    0.0177   -0.1029
     2.2232    0.0343   -0.0987
     2.2232    0.0495   -0.0920
     2.2232    0.0628   -0.0835
     2.2232    0.0739   -0.0737
     2.2232    0.0837   -0.0624
     2.2232    0.0922   -0.0491
     2.2232    0.0988   -0.0339
     2.2232    0.1030   -0.0174
     2.2232    0.1045    0.0000
     2.2232    0.1029    0.0177
     2.2232    0.0987    0.0343
     2.2232    0.0920    0.0495
     2.2232    0.0835    0.0628
     2.2232    0.0737    0.0739
     2.2232    0.0624    0.0837
     2.2232    0.0491    0.0922
     2.2232    0.0339    0.0988
     2.2232    0.0174    0.1030
     2.2232    0.0000    0.1045
 &BPNODE TNODE=3, TNPC=40, TINTC=3, &END
 &SECT1 STX=0.0, STY=0.0, STZ=0.0, SCALE=1.0, ALF=0.0, THETA=0.0, INMODE=4,
  TNODS=0, TNPS=0, TINTS=0, &END
     2.2692    0.0000   -0.0908
     2.2692    0.0154   -0.0894
     2.2692    0.0298   -0.0857
     2.2692    0.0429   -0.0799
     2.2692    0.0545   -0.0726
     2.2692    0.0642   -0.0641
     2.2692    0.0728   -0.0541
     2.2692    0.0801   -0.0426
     2.2692    0.0858   -0.0294
     2.2692    0.0895   -0.0150
     2.2692    0.0908    0.0000
     2.2692    0.0894    0.0154
     2.2692    0.0857    0.0298
     2.2692    0.0799    0.0429
     2.2692    0.0726    0.0545
     2.2692    0.0641    0.0642
     2.2692    0.0541    0.0728
     2.2692    0.0426    0.0801
     2.2692    0.0294    0.0858
     2.2692    0.0150    0.0895
     2.2692    0.0000    0.0908
 &BPNODE TNODE=3, TNPC=40, TINTC=3, &END
 &SECT1 STX=0.0, STY=0.0, STZ=0.0, SCALE=1.0, ALF=0.0, THETA=0.0, INMODE=4,
  TNODS=0, TNPS=0, TINTS=0, &END
     2.3087    0.0000   -0.0765
     2.3087    0.0130   -0.0754
     2.3087    0.0251   -0.0722
     2.3087    0.0362   -0.0674
     2.3087    0.0459   -0.0612
     2.3087    0.0541   -0.0541
     2.3087    0.0614   -0.0456
     2.3087    0.0676   -0.0359
     2.3087    0.0724   -0.0248
     2.3087    0.0754   -0.0127
     2.3087    0.0765    0.0000
     2.3087    0.0754    0.0130
     2.3087    0.0722    0.0251
     2.3087    0.0674    0.0362
     2.3087    0.0612    0.0459
     2.3087    0.0541    0.0541
     2.3087    0.0456    0.0614
     2.3087    0.0359    0.0676
     2.3087    0.0248    0.0724
     2.3087    0.0127    0.0754
     2.3087    0.0000    0.0765
 &BPNODE TNODE=3, TNPC=40, TINTC=3, &END
 &SECT1 STX=0.0, STY=0.0, STZ=0.0, SCALE=1.0, ALF=0.0, THETA=0.0, INMODE=4,
  TNODS=0, TNPS=0, TINTS=0, &END
     2.3413    0.0000   -0.0618
```

```
     2.3413    0.0106   -0.0609
     2.3413    0.0203   -0.0583
     2.3413    0.0293   -0.0544
     2.3413    0.0371   -0.0494
     2.3413    0.0437   -0.0436
     2.3413    0.0496   -0.0368
     2.3413    0.0546   -0.0289
     2.3413    0.0584   -0.0200
     2.3413    0.0609   -0.0102
     2.3413    0.0618    0.0000
     2.3413    0.0609    0.0106
     2.3413    0.0583    0.0203
     2.3413    0.0544    0.0293
     2.3413    0.0494    0.0371
     2.3413    0.0436    0.0437
     2.3413    0.0368    0.0496
     2.3413    0.0289    0.0546
     2.3413    0.0200    0.0584
     2.3413    0.0102    0.0609
     2.3413    0.0000    0.0618
&BPNODE TNODE=3, TNPC=40, TINTC=3, &END
&SECT1 STX=0.0, STY=0.0, STZ=0.0, SCALE=1.0, ALF=0.0, THETA=0.0, INMODE=4,
 TNODS=0, TNPS=0, TINTS=0, &END
     2.3668    0.0000   -0.0467
     2.3668    0.0081   -0.0460
     2.3668    0.0155   -0.0440
     2.3668    0.0222   -0.0410
     2.3668    0.0282   -0.0372
     2.3668    0.0332   -0.0328
     2.3668    0.0374   -0.0278
     2.3668    0.0412   -0.0219
     2.3668    0.0441   -0.0151
     2.3668    0.0460   -0.0077
     2.3668    0.0467    0.0000
     2.3668    0.0460    0.0081
     2.3668    0.0440    0.0155
     2.3668    0.0410    0.0222
     2.3668    0.0372    0.0282
     2.3668    0.0328    0.0332
     2.3668    0.0278    0.0374
     2.3668    0.0219    0.0412
     2.3668    0.0151    0.0441
     2.3668    0.0077    0.0460
     2.3668    0.0000    0.0467
&BPNODE TNODE=3, TNPC=40, TINTC=3, &END
&SECT1 STX=0.0, STY=0.0, STZ=0.0, SCALE=1.0, ALF=0.0, THETA=0.0, INMODE=4,
 TNODS=0, TNPS=0, TINTS=0, &END
     2.3852    0.0000   -0.0313
     2.3852    0.0055   -0.0308
     2.3852    0.0104   -0.0295
     2.3852    0.0149   -0.0275
     2.3852    0.0188   -0.0250
     2.3852    0.0221   -0.0221
     2.3852    0.0252   -0.0185
     2.3852    0.0277   -0.0145
     2.3852    0.0296   -0.0100
     2.3852    0.0308   -0.0051
     2.3852    0.0313    0.0000
     2.3852    0.0308    0.0055
     2.3852    0.0295    0.0104
     2.3852    0.0275    0.0149
     2.3852    0.0250    0.0188
     2.3852    0.0221    0.0221
     2.3852    0.0185    0.0252
     2.3852    0.0145    0.0277
     2.3852    0.0100    0.0296
     2.3852    0.0051    0.0308
     2.3852    0.0000    0.0313
&BPNODE TNODE=3, TNPC=40, TINTC=3, &END
&SECT1 STX=0.0, STY=0.0, STZ=0.0, SCALE=1.0, ALF=0.0, THETA=0.0, INMODE=4,
 TNODS=0, TNPS=0, TINTS=0, &END
     2.3963    0.0000   -0.0157
     2.3963    0.0029   -0.0154
     2.3963    0.0053   -0.0148
     2.3963    0.0075   -0.0138
     2.3963    0.0095   -0.0125
```



```
     2.3963    0.0111   -0.0111
     2.3963    0.0127   -0.0092
     2.3963    0.0139   -0.0072
     2.3963    0.0149   -0.0049
     2.3963    0.0155   -0.0025
     2.3963    0.0157    0.0000
     2.3963    0.0154    0.0029
     2.3963    0.0148    0.0053
     2.3963    0.0138    0.0075
     2.3963    0.0125    0.0095
     2.3963    0.0111    0.0111
     2.3963    0.0092    0.0127
     2.3963    0.0072    0.0139
     2.3963    0.0049    0.0149
     2.3963    0.0025    0.0155
     2.3963    0.0000    0.0157
&BPNODE TNODE=3, TNPC=40, TINTC=3, &END
 &SECT1 STX=0.0, STY=0.0, STZ=0.0, SCALE=1.0, ALF=0.0, THETA=0.0, INMODE=4,
  TNODS=5, TNPS=0, TINTS=0, &END
     2.4000    0.0000    0.0000
     2.4000    0.0000    0.0000
     2.4000    0.0000    0.0000
     2.4000    0.0000    0.0000
     2.4000    0.0000    0.0000
     2.4000    0.0000    0.0000
     2.4000    0.0000    0.0000
     2.4000    0.0000    0.0000
     2.4000    0.0000    0.0000
     2.4000    0.0000    0.0000
     2.4000    0.0000    0.0000
     2.4000    0.0000    0.0000
     2.4000    0.0000    0.0000
     2.4000    0.0000    0.0000
     2.4000    0.0000    0.0000
     2.4000    0.0000    0.0000
     2.4000    0.0000    0.0000
     2.4000    0.0000    0.0000
     2.4000    0.0000    0.0000
     2.4000    0.0000    0.0000
     2.4000    0.0000    0.0000
 &BPNODE TNODE=3, TNPC=40, TINTC=3, &END

 &WAKE1   IDWAK=1,         IFLXW=1,         ITRFTZ= 0,       INTRW= 0,         &END
  Wake_1_Partial_Ring_at_x/c=0.99_closes_side_wakes
 &WAKE2   KWPACH=1,        KWSIDE=1,        KWLINE=39,        KWPAN1=25,
          KWPAN2=40,        NODEW=3,         INITIAL=0,                         &END
 &WAKE1   IDWAK=1,         IFLXW=1,         ITRFTZ= 0,       INTRW= 0,         &END
  Wake_2_117_deg_wake_from_x/c=0.50
 &WAKE2   KWPACH=1,        KWSIDE=2,        KWLINE=26,        KWPAN1=21,
          KWPAN2=38,        NODEW=5,         INITIAL=0,                         &END

 &ONSTRM  NONSL =1,  KPSL = 201,205,209,213,217,221,225,229,233,237,240,361,365,369,
373,377,381,385,389,393,397,400,601,605,609,613,617,621,625,629,634,637,600,761,765,7
69,773,777,781,785,789,793,797,800,1041,1045,1049,1053,1057,1061,1065,1069,1073,1077,
1080,1241,1245,1249,1253,1257,1261,
1265,1269,1273,1277,1280,       &END

&BLPARAM RN =7700000,     VISC = 0.000017143, NSLBL = 1,2,3,4,5,6,7,8,9,10,11,12,13,1
4,15,16,17,18,19,20,21,22,23,24,25,26,27,28,29,30,31,32,33,34,35,36,37,38,39,40,41,42
,43,44,45,46,47,48,49,50,51,52,53,54,55,56,57,58,59,60,61,62,63,64,65,
66,                        &END


 &VS1      NVOLR= 0,        NVOLC= 0,                                          &END
 &VS2      X0=     -0.1000, Y0=      1.5000, Z0=     -0.1000, INTVSR= 1,        &END
 &VS3      X1=     -0.1000, Y1=      1.5000, Z1=      0.1000, NPT1=  0,         &END
 &VS4      X2=     -0.1000, Y2=      1.5000, Z2=      0.1000, NPT2= 20,         &END
 &VS5      X3=      1.1000, Y3=      1.5000, Z3=     -0.1000, NPT3= 25,         &END

 &VS6      XR0=     2.0000, YR0=     2.0000, ZR0=     0.0000, INTVSC= 1,        &END
 &VS7      XR1=     4.0000, YR1=     2.0000, ZR1=     0.0000,
           XR2=     2.0000, YR2=     2.0000, ZR2=     1.0000,                   &END
 &VS8      R1=      0.1000, R2=      1.0000, PHI1=  0.0,      PHI2=360.0,       &END
 &VS9      NRAD=    5,      NPHI=   12,      NLEN=  3,                          &END
```

Jun 11 1997 05:33 **pr10w117.in** Page 15

```
&SLIN1   NSTLIN=0,                                                        &END
&SLIN2   SXO=   -2.0000, SYO=    1.0000, SZO=   -0.5000,
         SU=     0.0000, SD=    10.0000, DS=     0.2500, INTSL= 1,        &END
&SLIN2   SXO=   -2.0000, SYO=    1.0000, SZO=   -0.4000,
         SU=     0.0000, SD=    10.0000, DS=     0.2500, INTSL= 1,        &END
&SLIN2   SXO=   -2.0000, SYO=    1.0000, SZO=   -0.3000,
         SU=     0.0000, SD=    10.0000, DS=     0.2500, INTSL= 1,        &END
&SLIN2   SXO=   -2.0000, SYO=    1.0000, SZO=   -0.2000,
         SU=     0.0000, SD=    10.0000, DS=     0.2500, INTSL= 1,        &END
&SLIN2   SXO=   -2.0000, SYO=    1.0000, SZO=   -0.1000,
         SU=     0.0000, SD=    10.0000, DS=     0.2500, INTSL= 1,        &END
&SLIN2   SXO=   -2.0000, SYO=    1.0000, SZO=    0.0000,
         SU=     0.0000, SD=    10.0000, DS=     0.2500, INTSL= 1,        &END
```

APPENDIX G. CMARC/PMARC DATA EXTRACTION PROGRAM

Printed by pollard from hawkeye

Jun 20 1997 04:45 **postprolate.f** Page 1

```
program postprolate.exe   !..for CMARC Prolate output file
                          !..by Tuncer, 3/96 modified by Steve Pollard 2/97
                          !..Steve Pollard 5/97 to extract and normalize Prolate
                             Spheroid CMARC Data
     parameter (nmx=400 )
     dimension npanel(nmx)
     character yn*1,line*132,fname*20,fnamee*20, byte*8
     real x,y,z,phi
     integer q
     logical ok, out, tstep
     data  tstep,out /.false., .false./, fname /"post.d"/
     q=0
    >
        print*,' '
        print*, ' This program reads in CMARC.OUT file formats and'
        print*, ' pulls out panel #, xyz location, cp and velocity.'
        print*,' '
        print*,'The program requires the following steps: '
        print*,' '
        print*,'1) First the program checks for the file "post.d".'
        print*,'   Data will be harvested from the PMARC output file'
        print*,'   based on which panels are designated in "post.d".'
        print*,'   You need to create a file "post.d" and put it in'
        print*,'   this directory. The file has the following format:'
        print*,' '
        print*,'   First panel #      Last Panel #        Step Size'
        print*,' '
        print*,'2) Next, you will be asked to input a filename.  It '
        print*,'   should be a CMARC.OUT file.'
        print*,' '
        print*,'3) The program then promps you for which time step'
        print*,'   data should be harvested. Your choices are the'
        print*,'   first time step (0) or the last time step '
        print*,'   (usually 10). You should pick the last time '
        print*,'   state to approx steady state.'
        print*,' '
        print*,'4) Finally, the program harvests the PMARC data and'
        print*,'   outputs it into a file named "p<data file name>".'
        print*,' '
        print*,'   Program is starting:'
        print*,' '

   1 inquire(FILE='post.d',EXIST=ok)
     if( .not. ok ) then
        print*,' '
        print*, '   Input the filename containing the PMARC output  - ', fname,'- d
oes NOT exist.'
        print*,'                            Enter the file name :>'
        read(*,'(A20)') fname
        goto 1
     endif
     OPEN(1,FILE=FNAME,FORM='formatted',STATUS='OLD')
     np = 0
     do nr = 1,100
        read(1,*,end=2, err=2) ns,ne,ninc
        do n = ns,ne,ninc
        np = np+1
        npanel(np) = n
        enddo
        if( np .gt. nmx ) then
          print*, ' CHECK prog. dimensions '
          stop
        endif
     enddo
   2 close(1)

   5 print*,' '
     PRINT*,'  Enter the PMARC DATA file name :>'
     read(*,'(A20)') fname
     if( fname .eq. '') fname='out'
     inquire(FILE=fname,EXIST=ok)
     if( .not. ok ) then
        print*, '       ', fname, ' does NOT exist.'
        goto 5
     endif
```

Jun 20 1997 04:45 **postprolate.f** Page 2

```
     OPEN(2,FILE=FNAME,FORM='formatted',STATUS='OLD')

     fnamee = 'p'//fname
     print*, "      Output FileName: ", fnamee
     open(3,file=fnamee,form='formatted')  !..output file


  10 continue
     nline = nline+1
     read(2,'(a132)',end=100,err=10) line
     read(line,'(a8)') byte
c    print*, 'Line :',nline, byte
     IF( byte .eq. " TIME ST" ) then
        read(line,'(a12,i10)') byte, nstep
        out = .false.
        tstep = .true.
        nc = 1
     ELSEIF( tstep .and. byte .eq. " AERODYN" ) then
        print*, ' '
        print*, '  TIME STEP =',nstep
        print*, '     Output panel info?  [y/n]:> '
        read(*,'(A1)') yn
        if( yn .eq. "y" .and. tstep ) then
           out = .true.
        elseif( yn .eq. "q" ) then
           goto 100
        endif
        tstep = .false.
     ELSEIF( out .and. nc .le. np ) then
        read(line,*,err=10) ipanel,x,y,z,cp,vx,vy,vz,v,dub,dphI,xmach
        if ( npanel(nc) .eq. ipanel )  then
           phi=atan(y/(-z))*57.3
              if (phi .eq. 0) then
                 q=q+1
              endif
              if (phi .lt. 0) then
                 phi=180+phi
              endif
              if (phi .eq. 0) then
                    if (q .gt. 1) then
                      phi=180
                    endif
              endif
           x=x/2.4
           y=y/2.4
           z=z/2.4
           write(3,'(i5,6f11.4)') ipanel,phi,x,y,z,cp,v
           nc = nc+1
        endif
     ENDIF
     goto 10

 100 continue
     close(2)
     close(3)
        print*,' '
        print*,' '

        print*,'*** Note: The output file does not contain column'
        print*,'          headers, allowing the data to be easily'
        print*,'          loaded into MATLAB using the "load"'
        print*,'          command. '
        print*,'          The data has the following format:'
        print*,' '
        print*, '    #panel  phi(deg)  x/c    y/c    z/c    cp    v '
        print*,' '
        print*,' '



     STOP
     END
```

APPENDIX H. LOFTSMAN INPUT FILES

Jun 11 1997 05:39 **fogfusa.lft** Page 1

```
BOX MOLDLINES DATA TEMPLATE

File name: fogfusa
Last revision:  4/12/97

------------------------------------------------------------------------------
BOTTOM WATERLINE

Segments: 3

Fore end        0,6.5
Aft end         12,0     53.0,0  53.5,5.75
Corner          0,0      S       53.5,0
Curvature       .69              0.95
------------------------------------------------------------------------------
WAIST WATERLINE

Segments: 1

Fore end        0,6.5
Aft end         53.5,6.5
Corner          S
Curvature
------------------------------------------------------------------------------
TOP WATERLINE

Segments: 7

Fore end    0,6.5
Aft end     8,9.3   15.2,9.3   21.6,13.0   29.0,14.6   44.6,11.6   53.0,11.5   53.5,6.5

Corner      0,9.3        S          S      24.3,14.6   35.4,14.6       S       53.5,11.5
Curvature    0.7                             0.71          0.81                  .95
------------------------------------------------------------------------------
MAXIMUM BUTTLINE DISTANCE FROM PLANE OF SYMMETRY

Segments: 6

Fore end        0,0
Aft end         1,3      1,3      22,4.5     43.6,4.5   53.1,1.3     53.5,0
Corner          0,2.9     S          S          S          S         53.5,1.3
Curvature        .9                                       0.8          0.95
------------------------------------------------------------------------------
BOTTOM K FACTOR

Segments: 3

Fore end        0,0.93
Aft end         12.0,0.98      43.6,0.98      53.5,0.95
Corner          S               S              S
Curvature
------------------------------------------------------------------------------
TOP K FACTOR

Segments: 4

Fore end        0,0.90
Aft end         15.20,0.95       24,1.0       44.65,1.0     53.5,0.95
Corner          S                S              S              S
Curvature
------------------------------------------------------------------------------
BUTTLINE AT PLANE OF SYMMETRY

Segments: 0
```

```
NPS FROG UAV Main Wing - Loftsman Input File

Date: 5/29/97

Breaks: 5

Break 1

Axis: 24.65,0,13.1
Axis/chord: 0
Chord: 20.0
Incidence: 4.5
Cant: 0
Section file: N2415
T/C ratio: 0.1500
Spars: 0
Panel rib angles: 0,999.0000,0.0000

Break 2

Axis: 24.65,6,13.1
Axis/chord: 0
Chord: 20.0
Incidence: 4.5
Cant: 0
Section file: N2415
T/C ratio: 0.1500
Spars: 0
Panel rib angles: 0,999.0000,0.0000

Break 3

Axis: 24.65,31.5,13.1
Axis/chord: 0
Chord: 20.0
Incidence: 4.5
Cant: 0
Section file: N2415
T/C ratio: 0.1500
Spars: 0
Panel rib angles: 0,999.0000,0.0000

Break 4

Axis: 24.65,53.0,13.1
Axis/chord: 0
Chord: 20.0
Incidence: 4.5
Cant: 0
Section file: N2415
T/C ratio: 0.1500
Spars: 0
Panel rib angles: 0,999.0000,0.0000

Break 5

Axis: 24.65,61.0,13.1
Axis/chord: 0
Chord: 18.5
Incidence: 4.5
Cant: 0
Section file: N2415
T/C ratio: 0.1500
Spars: 0
```

```
FROG UAV ENGINE NACELLE

File name: fogenpod
Last revision:  4/13/97
------------------------------------------------------------------------------
BOTTOM WATERLINE

Segments: 4

Fore end        16.5,20.4
Aft end         18.2,18.6    21.0,16.8     31.0,15.75    43.0, 16.8
Corner          16.6,19.6    19.15,17.35   23.8,15.9     35.6,15.65
Curvature       0.79          0.83         0.72           0.73
------------------------------------------------------------------------------
WAIST WATERLINE

Segments: 1

Fore end        16.5,20.4
Aft end         43.0,16.8
Corner          S
Curvature
------------------------------------------------------------------------------
TOP WATERLINE

Segments: 4

Fore end        16.3,20.4
Aft end         18.45,22.1    27.0,21.75    35.0,19.8     43.0,16.8
Corner          16.75,21.3    21.4,22.5     30.4,21.3     38.3,18.75
Curvature       0.79             0.80          0.70          0.75
------------------------------------------------------------------------------
MAXIMUM BUTTLINE DISTANCE FROM PLANE OF SYMMETRY

Segments: 4

Fore end        16.5,0
Aft end         18.2,1.6     23.0,2.3     40.8,2.3      43.0,0
Corner          16.5,0.70    20.1,2.25    S             43.0,2.3
Curvature       0.72          0.75                       0.90
------------------------------------------------------------------------------
BOTTOM K FACTOR

Segments: 4

Fore end        16.5,0.707
Aft end         18.2,0.707    24.0,0.93      42.0,0.93     43.0,0.75
Corner          S               20,0.93              S            S
Curvature                       0.9
------------------------------------------------------------------------------
TOP K FACTOR

Segments: 4

Fore end        16.5,0.707
Aft end         18.45,0.707     24.5,0.93    42.0,0.93      43.0,0.75
Corner          S                20.3,0.93          S              S
Curvature                        0.9
------------------------------------------------------------------------------
BUTTLINE AT PLANE OF SYMMETRY
Segments: 0
```

```
FROG UAV ENGINE PYLON (Lofted as A-Body Type)

-Basic pylon model modified so as not to have a top and bottom
-Single strip which is the side of the pylon.

File name: FOGPYLO1
Last revision: 4/23/97

Strips: 1
Sym: Y

M1B

Segments: 1
 Fore end      25.8,0
   Aft end     37.7,0
    Corner     25.8,3.8
  K factor     0.71

M1W
Segments: 1

  Fore end     25.8,14.31
   Aft end     37.7,13.65
    Corner     31.0,15.45
  K factor     0.72

C1B

Segments: S

C1W

Segments: S

K1

Segments: S

M2B

Segments: =M1B

M2W

Segments: 1

 Fore end     25.8,16.01
   Aft end     37.7,16.1
    Corner     33.65,15.35
  K factor     0.65
```

FROG UAV Tail Boom

File name: frogboom
Last revision: 4/28/97

4/28: added rounded start and finish to close ends

BOTTOM WATERLINE

Segments: 3

Fore end	53.5,9.375		88.5,9.375
Aft end	54,8.5	88,8.5	88.5,8.5
Corner	53.5,8.5	S	0.707
Curvature	0.707		

WAIST WATERLINE

Segments: 1

Fore end	53.5,9.375
Aft end	88.5, 9.375
Corner	S
Curvature	

TOP WATERLINE

Segments: 3

Fore end	53.5,9.375		88.5,9.375
Aft end	54.0,10.25	88,10.25	88.5,10.25
Corner	53.5,10.25	S	0.707
Curvature	0.707		

MAXIMUM BUTTLINE DISTANCE FROM PLANE OF SYMMETRY

Segments: 3

Fore end	53.5,0		88.5,0
Aft end	54,0.875	88,0.875	88.5,0.875
Corner	53.5,0.875	S	0.707
Curvature	0.707		

BOTTOM K FACTOR

Segments: 1

Fore end	53.5,0.707
Aft end	88.5, 0.707
Corner	S
Curvature	

TOP K FACTOR

Segments: 1

Fore end	53.5,0.707
Aft end	88.5, 0.707
Corner	S
Curvature	

BUTTLINE AT PLANE OF SYMMETRY
Segments: 0

FROG Horizontal Tail

Date: 4/14/97

Breaks: 2

Break 1

Axis: 82.5,0,8.09
Axis/chord: 0
Chord: 13.5
Incidence: 0
Cant: 0
Section file: N0006
T/C ratio: 0.06
Spars: 0
Panel rib angles: 0,999.0000,0.0000

Break 2

Axis: 86.5,19.875,8.09
Axis/chord: 0
Chord: 9.55
Incidence: 0
Cant: 0
Section file: N0006
T/C ratio: 0.06
Spars: 0
Panel rib angles: 0,999.0000,0.0000

```
FROG UAV Vertical Tail - LOFTSMAN input file

Date: 4/14/97

Breaks: 2

Break 1

Axis: 77.5,0,10.4
Axis/chord: 0
Chord: 20
Incidence: 0
Cant: 90
Section file: N0006
T/C ratio: 0.06
Spars: 0
Panel rib angles: 90,0,999

Break 2

Axis: 92.35,0,25.15
Axis/chord: 0
Chord: 10
Incidence: 0
Cant: 90
Section file: N0006
T/C ratio: 0.06
Spars: 0
Panel rib angles: 90,0,999
```

APPENDIX I. FROG UAV CMARC INPUT FILE

Printed by pollard from hawkeye

Jun 11 1997 05:30 — froguav.in — Page 1

```
NPS FROG UAV CMARC/PMARCPANEL MODEL - Units = inches

Complete FROG UAV Model (3790 Patches)

Blended Wing/Fuselage Patches
Off-body Streamlines at Alpha/Static Probe Locations
Symmetric Calculations turned off - Symmetric patches selected.

Created by:  Steve Pollard  5/29/97
Revised:  6/10/97


&BINP2   LSTINP=2,    LSTOUT=0,    LSTFRQ=0,    LENRUN=0,    LPLTYP=1,     &END
&BINP3   LSTGEO=0,    LSTNAB=0,    LSTWAK=0,    LSTCPV=0,                  &END
&BINP4   MAXIT=400,    SOLRES=0.001,                                       &END
&BINP5   NTSTPS= 4,  DTSTEP=0.5,                                           &END
&BINP6   RSYM=1.0,    RGPR=0.0,    RFF=5.0,  RCORES=0.0080, RCOREW=0.0080, &END
&BINP7   VINF=1056.00,   VSOUND=13392.0,                                   &END
&BINP8   ALDEG= 0.00, YAWDEG=0.0,  PHIDOT=0.0,  THEDOT=0.0,  PSIDOT=0.0,   &END
&BINP8A  PHIMAX= 0.0, THEMAX= 0.0, PSIMAX=0.0,
         WRX=0.0,     WRY=0.0,     WRZ=0.0,                                &END
&BINP8B  DXMAX=0.0,   DYMAX=0.0,   DZMAX=0.0,
         WTX=0.0,     WTY=0.0,     WTZ=0.0,                                &END
&BINP9   CBAR=20,  SREF=2530.0, SSPAN= 62,
         RMPX=31.55,   RMPY=0.00,   RMPZ=8.57,                             &END
&BINP10  NORSET=0,    NBCHGE=0,    NCZONE=0,
         NCZPCH=0,    CZDUB=0.0,   VREF=0.0,                               &END
&BINP11  NORPCH=0,    NORF=0,      NORL=0,
         NOCF=0,      NOCL=0,      VNORM=0.0,                              &END
&BINP12  KPAN=0,      KSIDE=0,     NEWNAB=0,    NEWSID=0,                  &END
&BINP13  NBLIT=0,                                                          &END


&ASEM1   ASEMX=0.00,       ASEMY=0.00,       ASEMZ=0.00,
         ASCAL=1.00,       ATHET=0.00,       NODEA=5,                      &END
&ASEM2   APXX=0.00,        APYY=0.00,        APZZ=0.00,
         AHXX=0.00,        AHYY=1.00,        AHZZ=0.00,                    &END


&COMP1   COMPX= 0.0000,    COMPY= 0.0000,    COMPZ= 0.0000,
         CSCAL=  1.000,    CTHET=   0.0,     NODEC= 5,                     &END
&COMP2   CPXX= 0.0000,     CPYY= 0.0000,     CPZZ= 0.0000,
         CHXX= 0.0000,     CHYY=  1.000,     CHZZ= 0.0000,                 &END

&PATCH1 IREV=0, IDPAT=2, MAKE=0, KCOMP=1, KASS=1, IPATSYM=1, IPATCOP=0,
&END
  FUSELAGE_NOSE
&SECT1 STX=0.0, STY=0.0, STZ=0.0, SCALE=1.0, ALF=0.0, THETA=0.0, INMODE=4,
 TNODS=0, TNPS=0, TINTS=0, &END
   0.0000     0.0000     6.5000
   0.0000     0.0000     6.5000
   0.0000     0.0000     6.5000
   0.0000     0.0000     6.5000
   0.0000     0.0000     6.5000
   0.0000     0.0000     6.5000
   0.0000     0.0000     6.5000
   0.0000     0.0000     6.5000
   0.0000     0.0000     6.5000
   0.0000     0.0000     6.5000
   0.0000     0.0000     6.5000
   0.0000     0.0000     6.5000
   0.0000     0.0000     6.5000
   0.0000     0.0000     6.5000
   0.0000     0.0000     6.5000
   0.0000     0.0000     6.5000
&BPNODE TNODE=3, TNPC=0, TINTC=0, &END
&SECT1 STX=0.0, STY=0.0, STZ=0.0, SCALE=1.0, ALF=0.0, THETA=0.0, INMODE=4,
 TNODS=0, TNPS=0, TINTS=0, &END
   0.4894     0.0000     4.8456
   0.4894     0.9694     4.8472
   0.4894     1.8700     4.8569
   0.4894     2.4101     4.8828
   0.4894     2.6949     4.9422
   0.4894     2.8308     5.0656
   0.4894     2.8941     5.3171
   0.4894     2.9200     5.7981
```

Jun 11 1997 05:30 — froguav.in — Page 2

```
   0.4894     2.9252     6.5846
   0.4894     2.9005     6.9893
   0.4894     2.8237     7.2119
   0.4894     2.6669     7.3254
   0.4894     2.3672     7.3842
   0.4894     1.8372     7.4126
   0.4894     0.9694     7.4244
   0.4894     0.0000     7.4266
&BPNODE TNODE=3, TNPC=0, TINTC=0, &END
&SECT1 STX=0.0, STY=0.0, STZ=0.0, SCALE=1.0, ALF=0.0, THETA=0.0, INMODE=4,
 TNODS=0, TNPS=0, TINTS=0, &END
   1.9098     0.0000     3.2261
   1.9098     1.2120     3.2304
   1.9098     2.1514     3.2527
   1.9098     2.6464     3.3105
   1.9098     2.8844     3.4400
   1.9098     2.9946     3.7159
   1.9098     3.0431     4.2715
   1.9098     3.0617     5.2972
   1.9098     3.0650     6.5092
   1.9098     3.0481     7.3382
   1.9098     2.9862     7.8079
   1.9098     2.8504     8.0540
   1.9098     2.5827     8.1796
   1.9098     2.0806     8.2410
   1.9098     1.1960     8.2673
   1.9098     0.0000     8.2731
&BPNODE TNODE=3, TNPC=0, TINTC=0, &END
&SECT1 STX=0.0, STY=0.0, STZ=0.0, SCALE=1.0, ALF=0.0, THETA=0.0, INMODE=4,
 TNODS=0, TNPS=0, TINTS=0, &END
   4.1221     0.0000     1.8058
   4.1221     1.3792     1.8110
   4.1221     2.3922     1.8401
   4.1221     2.8791     1.9216
   4.1221     3.0873     2.1152
   4.1221     3.1756     2.5617
   4.1221     3.2104     3.4985
   4.1221     3.2210     4.8740
   4.1221     3.2230     6.2532
   4.1221     3.2129     7.5020
   4.1221     3.1635     8.2308
   4.1221     3.0419     8.6115
   4.1221     2.7927     8.7934
   4.1221     2.2900     8.8805
   4.1221     1.3537     8.9164
   4.1221     0.0000     8.9243
&BPNODE TNODE=3, TNPC=0, TINTC=0, &END
&SECT1 STX=0.0, STY=0.0, STZ=0.0, SCALE=1.0, ALF=0.0, THETA=0.0, INMODE=4,
 TNODS=0, TNPS=0, TINTS=0, &END
   6.9098     0.0000     0.7304
   6.9098     1.4829     0.7343
   6.9098     2.6474     0.7608
   6.9098     3.1478     0.8479
   6.9098     3.3299     1.0887
   6.9098     3.3948     1.7151
   6.9098     3.4159     3.0358
   6.9098     3.4209     4.5188
   6.9098     3.4221     6.0017
   6.9098     3.4168     7.4676
   6.9098     3.3779     8.4328
   6.9098     3.2701     8.9147
   6.9098     3.0302     9.1303
   6.9098     2.5077     9.2266
   6.9098     1.4679     9.2637
   6.9098     0.0000     9.2711
&BPNODE TNODE=3, TNPC=0, TINTC=0, &END
&SECT1 STX=0.0, STY=0.0, STZ=0.0, SCALE=1.0, ALF=0.0, THETA=0.0, INMODE=4,
 TNODS=0, TNPS=0, TINTS=0, &END
  10.0000     0.0000     0.1152
  10.0000     1.5156     0.1169
  10.0000     2.8805     0.1323
  10.0000     3.4347     0.2022
  10.0000     3.5900     0.4599
  10.0000     3.6311     1.2905
  10.0000     3.6402     2.7963
  10.0000     3.6423     4.3120
```

```
    10.0000     3.6428     5.8276
    10.0000     3.6400     7.3433
    10.0000     3.6087     8.4519
    10.0000     3.5110     8.9679
    10.0000     3.2695     9.1801
    10.0000     2.7005     9.2654
    10.0000     1.5113     9.2951
    10.0000     0.0000     9.3000
&BPNODE TNODE=3, TNPC=0, TINTC=0, &END
&SECT1 STX=0.0, STY=0.0, STZ=0.0, SCALE=1.0, ALF=0.0, THETA=0.0, INMODE=4,
 TNODS=0, TNPS=0, TINTS=0, &END
    13.0902     0.0000     0.0000
    13.0902     1.5138     0.0007
    13.0902     3.0061     0.0077
    13.0902     3.6868     0.0552
    13.0902     3.8313     0.3019
    13.0902     3.8583     1.3036
    13.0902     3.8623     2.8174
    13.0902     3.8633     4.3312
    13.0902     3.8636     5.8451
    13.0902     3.8614     7.3589
    13.0902     3.8344     8.5203
    13.0902     3.7416     9.0232
    13.0902     3.4903     9.2092
    13.0902     2.8478     9.2766
    13.0902     1.5130     9.2971
    13.0902     0.0000     9.3000
&BPNODE TNODE=3, TNPC=0, TINTC=0, &END
&SECT1 STX=0.0, STY=0.0, STZ=0.0, SCALE=1.0, ALF=0.0, THETA=0.0, INMODE=4,
 TNODS=0, TNPS=0, TINTS=0, &END
    15.8779     0.0000     0.0000
    15.8779     1.5558     0.0007
    15.8779     3.1041     0.0070
    15.8779     3.8653     0.0517
    15.8779     4.0270     0.2880
    15.8779     4.0569     1.2775
    15.8779     4.0614     2.8332
    15.8779     4.0624     4.3890
    15.8779     4.0627     5.9448
    15.8779     4.0612     7.5006
    15.8779     4.0415     8.8474
    15.8779     3.9629     9.4248
    15.8779     3.7146     9.6156
    15.8779     3.0056     9.6748
    15.8779     1.5544     9.6899
    15.8779     0.0000     9.6919
&BPNODE TNODE=3, TNPC=0, TINTC=0, &END
&SECT1 STX=0.0, STY=0.0, STZ=0.0, SCALE=1.0, ALF=0.0, THETA=0.0, INMODE=4,
 TNODS=0, TNPS=0, TINTS=0, &END
    18.0902     0.0000     0.0000
    18.0902     1.6509     0.0007
    18.0902     3.2889     0.0077
    18.0902     4.0453     0.0611
    18.0902     4.1913     0.3563
    18.0902     4.2164     1.5673
    18.0902     4.2198     3.2182
    18.0902     4.2206     4.8691
    18.0902     4.2207     6.5200
    18.0902     4.2195     8.1710
    18.0902     4.2094     9.8015
    18.0902     4.1567    10.6520
    18.0902     3.9490    10.8950
    18.0902     3.2238    10.9567
    18.0902     1.6504    10.9694
    18.0902     0.0000    10.9709
&BPNODE TNODE=3, TNPC=0, TINTC=0, &END
&SECT1 STX=0.0, STY=0.0, STZ=0.0, SCALE=1.0, ALF=0.0, THETA=0.0, INMODE=4,
 TNODS=0, TNPS=0, TINTS=0, &END
    19.5106     0.0000     0.0000
    19.5106     1.7043     0.0007
    19.5106     3.3938     0.0081
    19.5106     4.1553     0.0661
    19.5106     4.2955     0.3979
    19.5106     4.3184     1.7232
    19.5106     4.3214     3.4275
    19.5106     4.3221     5.1318
```

Printed by pollard from hawkeye


```
    19.5106     4.3222     6.8361
    19.5106     4.3214     8.5405
    19.5106     4.3169    10.2448
    19.5106     4.2840    11.4245
    19.5106     4.1133    11.7224
    19.5106     3.3665    11.7816
    19.5106     1.7041    11.7911
    19.5106     0.0000    11.7920
&BPNODE TNODE=3, TNPC=0, TINTC=0, &END
&SECT1 STX=0.0, STY=0.0, STZ=0.0, SCALE=1.0, ALF=0.0, THETA=0.0, INMODE=4,
 TNODS=3, TNPS=0, TINTS=0, &END
    20.0000     0.0000     0.0000
    20.0000     1.7202     0.0007
    20.0000     3.4256     0.0081
    20.0000     4.1917     0.0673
    20.0000     4.3314     0.4135
    20.0000     4.3535     1.7754
    20.0000     4.3564     3.4956
    20.0000     4.3571     5.2158
    20.0000     4.3571     6.9360
    20.0000     4.3565     8.6562
    20.0000     4.3532    10.3763
    20.0000     4.3272    11.6828
    20.0000     4.1713    12.0088
    20.0000     3.4117    12.0661
    20.0000     1.7202    12.0742
    20.0000     0.0000    12.0750
&BPNODE TNODE=3, TNPC=0, TINTC=0, &END

&PATCH1 IREV=0, IDPAT=2, MAKE=0, KCOMP=1, KASS=1, IPATSYM=1, IPATCOP=0, &END
  ROOT TRANSITION FORE STARBOARD
&SECT1 STX=0.0, STY=0.0, STZ=0.0, SCALE=1.0, ALF=0.0, THETA=0.0, INMODE=4,
 TNODS=0, TNPS=0, TINTS=0, &END
    20.0000     0.0000     0.0000
    20.0000     1.7202     0.0007
    20.0000     3.4256     0.0081
    20.0000     4.1917     0.0673
    20.0000     4.3314     0.4135
    20.0000     4.3535     1.7754
    20.0000     4.3564     3.4956
    20.0000     4.3571     5.2158
    20.0000     4.3571     6.9360
    20.0000     4.3565     8.6562
    20.0000     4.3532    10.3763
    20.0000     4.3272    11.6828
    20.0000     4.1713    12.0088
    20.0000     3.4117    12.0661
    20.0000     1.7202    12.0742
    20.0000     0.0000    12.0750
&BPNODE TNODE=3, TNPC=0, TINTC=0, &END
&SECT1 STX=0.0, STY=0.0, STZ=0.0, SCALE=1.0, ALF=0.0, THETA=0.0, INMODE=4,
 TNODS=0, TNPS=0, TINTS=0, &END
    20.4440     0.0000     0.0000
    20.4440     1.7171     0.0007
    20.4440     3.4241     0.0078
    20.4440     4.2151     0.0644
    20.4440     4.3616     0.3949
    20.4440     4.3850     1.7224
    20.4440     4.3881     3.4395
    20.4440     4.3888     5.1566
    20.4440     4.3889     6.8736
    20.4440     4.3885     8.5907
    20.4440     4.3865    10.3078
    20.4440     4.3707    11.8182
    20.4440     4.2485    12.2579
    20.4440     3.5302    12.3232
    20.4440     1.7837    12.3310
    20.4440     0.0000    12.3317
&BPNODE TNODE=3, TNPC=0, TINTC=0, &END
&SECT1 STX=0.0, STY=0.0, STZ=0.0, SCALE=1.0, ALF=0.0, THETA=0.0, INMODE=4,
 TNODS=0, TNPS=0, TINTS=0, &END
    21.6065     0.0000     0.0000
    21.6065     1.7392     0.0007
    21.6065     3.4719     0.0076
    21.6065     4.2930     0.0637
    21.6065     4.4441     0.3949
```

```
   21.6065    4.4680    1.7396
   21.6065    4.4711    3.4788
   21.6065    4.4718    5.2180
   21.6065    4.4719    6.9572
   21.6065    4.4717    8.6964
   21.6065    4.4711   10.4355
   21.6065    4.4667   12.1724
   21.6065    4.3976   12.9316
   21.6065    3.6877   12.9989
   21.6065    1.8477   13.0035
   21.6065    0.0000   13.0039
&BPNODE TNODE=3, TNPC=0, TINTC=0, &END
&SECT1 STX=0.0, STY=0.0, STZ=0.0, SCALE=1.0, ALF=0.0, THETA=0.0, INMODE=4,
 TNODS=0, TNPS=0, TINTS=0, &END
   23.0435    0.0000    0.0000
   23.0435    1.7813    0.0007
   23.0435    3.5493    0.0083
   23.0435    4.3384    0.0714
   23.0435    4.4761    0.4540
   23.0435    4.4967    1.9224
   23.0435    4.4994    3.7037
   23.0435    4.4999    5.4850
   23.0435    4.5000    7.2664
   23.0435    4.5000    9.0477
   23.0435    4.4999   10.8290
   23.0435    4.4993   12.6104
   23.0435    4.4647   13.6074
   23.0435    3.4428   13.6337
   23.0435    1.7214   13.6342
   23.0435    0.0000   13.6343
&BPNODE TNODE=3, TNPC=0, TINTC=0, &END
&SECT1 STX=0.0, STY=0.0, STZ=0.0, SCALE=1.0, ALF=0.0, THETA=0.0, INMODE=4,
 TNODS=0, TNPS=0, TINTS=0, &END
   24.2060    0.0000    0.0000
   24.2060    1.8135    0.0008
   24.2060    3.6032    0.0090
   24.2060    4.3543    0.0795
   24.2060    4.4793    0.5138
   24.2060    4.4972    2.0834
   24.2060    4.4995    3.8970
   24.2060    4.5000    5.7105
   24.2060    4.5000    7.5240
   24.2060    4.5000    9.3376
   24.2060    4.5000   11.1511
   24.2060    4.5000   12.9647
   24.2060    4.2423   13.9775
   24.2060    2.8282   13.9775
   24.2060    1.4141   13.9775
   24.2060    0.0000   13.9775
&BPNODE TNODE=3, TNPC=0, TINTC=0, &END
&SECT1 STX=0.0, STY=0.0, STZ=0.0, SCALE=1.0, ALF=0.0, THETA=0.0, INMODE=4,
 TNODS=3, TNPS=0, TINTS=0, &END
   24.6500    0.0000    0.0000
   24.6500    1.8258    0.0008
   24.6500    3.6231    0.0094
   24.6500    4.3600    0.0829
   24.6500    4.4804    0.5384
   24.6500    4.4973    2.1449
   24.6500    4.4995    3.9708
   24.6500    4.5000    5.7966
   24.6500    4.5000    7.6225
   24.6500    4.5000    9.4483
   24.6500    4.5000   11.2742
   24.6500    4.5000   13.1000
   24.6500    4.2213   14.0848
   24.6500    2.8142   14.0848
   24.6500    1.4071   14.0848
   24.6500    0.0000   14.0848
&BPNODE TNODE=3, TNPC=0, TINTC=0, &END

&PATCH_ 'REV=0, IDPAT=2, MAKE=0, KCOMP=1, KASS=1, IPATSYM=1, IPATCOP=0, &END
  ROC[illegible]OWER STARBOARD
&SECT1 STX=0.0, STY=0.0, STZ=0.0, SCALE=1.0, ALF=0.0, THETA=0.0, INMODE=4,
 TNODS=0, TNPS=0, TINTS=0, &END
   24.6500    0.0000    0.0000
   24.6500    1.8258    0.0008
```



```
   24.6500    3.6231    0.0094
   24.6500    4.3600    0.0829
   24.6500    4.4804    0.5384
   24.6500    4.4973    2.1449
   24.6500    4.4995    3.9708
   24.6500    4.5000    5.7966
   24.6500    4.5000    7.6225
   24.6500    4.5000    9.4483
   24.6500    4.5000   11.2742
   24.6500    4.5000   13.1000
&BPNODE TNODE=3, TNPC=0, TINTC=0, &END
&SECT1 STX=0.0, STY=0.0, STZ=0.0, SCALE=1.0, ALF=0.0, THETA=0.0, INMODE=4,
 TNODS=0, TNPS=0, TINTS=0, &END
   24.8679    0.0000    0.0000
   24.8679    1.7867    0.0007
   24.8679    3.5584    0.0084
   24.8679    4.3412    0.0727
   24.8679    4.4766    0.4634
   24.8679    4.4968    1.9491
   24.8679    4.4994    3.7357
   24.8679    4.4999    5.5224
   24.8679    4.5000    7.3091
   24.8679    4.5000    9.0958
   24.8679    4.5000   10.8824
   24.8679    4.5000   12.6691
&BPNODE TNODE=3, TNPC=0, TINTC=0, &END
&SECT1 STX=0.0, STY=0.0, STZ=0.0, SCALE=1.0, ALF=0.0, THETA=0.0, INMODE=4,
 TNODS=0, TNPS=0, TINTS=0, &END
   25.5119    0.0000    0.0000
   25.5119    1.7519    0.0007
   25.5119    3.4973    0.0076
   25.5119    4.3223    0.0646
   25.5119    4.4728    0.4048
   25.5119    4.4962    1.7750
   25.5119    4.4992    3.5269
   25.5119    4.4999    5.2788
   25.5119    4.5000    7.0306
   25.5119    4.5000    8.7825
   25.5119    4.5000   10.5344
   25.5119    4.5000   12.2862
&BPNODE TNODE=3, TNPC=0, TINTC=0, &END
&SECT1 STX=0.0, STY=0.0, STZ=0.0, SCALE=1.0, ALF=0.0, THETA=0.0, INMODE=4,
 TNODS=0, TNPS=0, TINTS=0, &END
   26.5541    0.0000    0.0000
   26.5541    1.7230    0.0007
   26.5541    3.4441    0.0070
   26.5541    4.3050    0.0585
   26.5541    4.4691    0.3614
   26.5541    4.4956    1.6308
   26.5541    4.4991    3.3539
   26.5541    4.4999    5.0769
   26.5541    4.5000    6.7999
   26.5541    4.5000    8.5229
   26.5541    4.5000   10.2460
   26.5541    4.5000   11.9690
&BPNODE TNODE=3, TNPC=0, TINTC=0, &END
&SECT1 STX=0.0, STY=0.0, STZ=0.0, SCALE=1.0, ALF=0.0, THETA=0.0, INMODE=4,
 TNODS=0, TNPS=0, TINTS=0, &END
   27.9487    0.0000    0.0000
   27.9487    1.7011    0.0006
   27.9487    3.4020    0.0066
   27.9487    4.2909    0.0542
   27.9487    4.4660    0.3314
   27.9487    4.4951    1.5215
   27.9487    4.4990    3.2226
   27.9487    4.4998    4.9237
   27.9487    4.5000    6.6249
   27.9487    4.5000    8.3260
   27.9487    4.5000   10.0272
   27.9487    4.5000   11.7283
&BPNODE TNODE=3, TNPC=0, TINTC=0, &END
&SECT1 STX=0.0, STY=0.0, STZ=0.0, SCALE=1.0, ALF=0.0, THETA=0.0, INMODE=4,
 TNODS=0, TNPS=0, TINTS=0, &END
   29.6349    0.0000    0.0000
   29.6349    1.6863    0.0006
   29.6349    3.3725    0.0063
```

```
    29.6349     4.2808     0.0515
    29.6349     4.4638     0.3122
    29.6349     4.4947     1.4471
    29.6349     4.4989     3.1333
    29.6349     4.4998     4.8196
    29.6349     4.5000     6.5059
    29.6349     4.5000     8.1922
    29.6349     4.5000     9.8784
    29.6349     4.5000    11.5647
&BPNODE TNODE=3, TNPC=0, TINTC=0, &END
&SECT1 STX=0.0, STY=0.0, STZ=0.0, SCALE=1.0, ALF=0.0, THETA=0.0, INMODE=4,
 TNODS=0, TNPS=0, TINTS=0, &END
    31.5390     0.0000     0.0000
    31.5390     1.6769     0.0006
    31.5390     3.3538     0.0061
    31.5390     4.2741     0.0499
    31.5390     4.4623     0.3007
    31.5390     4.4944     1.4001
    31.5390     4.4989     3.0770
    31.5390     4.4998     4.7539
    31.5390     4.5000     6.4308
    31.5390     4.5000     8.1077
    31.5390     4.5000     9.7845
    31.5390     4.5000    11.4614
&BPNODE TNODE=3, TNPC=0, TINTC=0, &END
&SECT1 STX=0.0, STY=0.0, STZ=0.0, SCALE=1.0, ALF=0.0, THETA=0.0, INMODE=4,
 TNODS=0, TNPS=0, TINTS=0, &END
    33.5777     0.0000     0.0000
    33.5777     1.6712     0.0006
    33.5777     3.3424     0.0060
    33.5777     4.2700     0.0489
    33.5777     4.4613     0.2939
    33.5777     4.4943     1.3718
    33.5777     4.4988     3.0430
    33.5777     4.4998     4.7142
    33.5777     4.5000     6.3855
    33.5777     4.5000     8.0567
    33.5777     4.5000     9.7279
    33.5777     4.5000    11.3991
&BPNODE TNODE=3, TNPC=0, TINTC=0, &END
&SECT1 STX=0.0, STY=0.0, STZ=0.0, SCALE=1.0, ALF=0.0, THETA=0.0, INMODE=4,
 TNODS=0, TNPS=0, TINTS=0, &END
    35.6619     0.0000     0.0000
    35.6619     1.6694     0.0006
    35.6619     3.3388     0.0060
    35.6619     4.2687     0.0486
    35.6619     4.4610     0.2918
    35.6619     4.4942     1.3627
    35.6619     4.4988     3.0321
    35.6619     4.4998     4.7015
    35.6619     4.5000     6.3708
    35.6619     4.5000     8.0402
    35.6619     4.5000     9.7096
    35.6619     4.5000    11.3790
&BPNODE TNODE=3, TNPC=0, TINTC=0, &END
&SECT1 STX=0.0, STY=0.0, STZ=0.0, SCALE=1.0, ALF=0.0, THETA=0.0, INMODE=4,
 TNODS=0, TNPS=0, TINTS=0, &END
    37.7006     0.0000     0.0000
    37.7006     1.6701     0.0006
    37.7006     3.3402     0.0060
    37.7006     4.2692     0.0487
    37.7006     4.4611     0.2926
    37.7006     4.4942     1.3663
    37.7006     4.4988     3.0365
    37.7006     4.4998     4.7066
    37.7006     4.5000     6.3767
    37.7006     4.5000     8.0468
    37.7006     4.5000     9.7170
    37.7006     4.5000    11.3871
&BPNODE TNODE=3, TNPC=0, TINTC=0, &END
&SECT1 STX=0.0, STY=0.0, STZ=0.0, SCALE=1.0, ALF=0.0, THETA=0.0, INMODE=4,
 TNODS=0, TNPS=0, TINTS=0, &END
    39.6047     0.0000     0.0000
    39.6047     1.6716     0.0006
    39.6047     3.3432     0.0060
    39.6047     4.2703     0.0490
```



```
    39.6047     4.4614     0.2944
    39.6047     4.4943     1.3737
    39.6047     4.4988     3.0452
    39.6047     4.4998     4.7168
    39.6047     4.5000     6.3884
    39.6047     4.5000     8.0600
    39.6047     4.5000     9.7316
    39.6047     4.5000    11.4032
&BPNODE TNODE=3, TNPC=0, TINTC=0, &END
&SECT1 STX=0.0, STY=0.0, STZ=0.0, SCALE=1.0, ALF=0.0, THETA=0.0, INMODE=4,
 TNODS=0, TNPS=0, TINTS=0, &END
    41.2909     0.0000     0.0000
    41.2909     1.6739     0.0006
    41.2909     3.3479     0.0061
    41.2909     4.2720     0.0494
    41.2909     4.4618     0.2971
    41.2909     4.4943     1.3854
    41.2909     4.4988     3.0593
    41.2909     4.4998     4.7332
    41.2909     4.5000     6.4072
    41.2909     4.5000     8.0811
    41.2909     4.5000     9.7550
    41.2909     4.5000    11.4290
&BPNODE TNODE=3, TNPC=0, TINTC=0, &END
&SECT1 STX=0.0, STY=0.0, STZ=0.0, SCALE=1.0, ALF=0.0, THETA=0.0, INMODE=4,
 TNODS=0, TNPS=0, TINTS=0, &END
    42.6855     0.0000     0.0000
    42.6855     1.6764     0.0006
    42.6855     3.3529     0.0061
    42.6855     4.2738     0.0498
    42.6855     4.4622     0.3001
    42.6855     4.4944     1.3979
    42.6855     4.4989     3.0743
    42.6855     4.4998     4.7507
    42.6855     4.5000     6.4272
    42.6855     4.5000     8.1036
    42.6855     4.5000     9.7800
    42.6855     4.5000    11.4565
&BPNODE TNODE=3, TNPC=0, TINTC=0, &END
&SECT1 STX=0.0, STY=0.0, STZ=0.0, SCALE=1.0, ALF=0.0, THETA=0.0, INMODE=4,
 TNODS=0, TNPS=0, TINTS=0, &END
    43.7277     0.0000     0.0000
    43.7277     1.6766     0.0007
    43.7277     3.3528     0.0067
    43.7277     4.2374     0.0530
    43.7277     4.4194     0.3099
    43.7277     4.4514     1.4174
    43.7277     4.4558     3.0940
    43.7277     4.4568     4.7706
    43.7277     4.4570     6.4472
    43.7277     4.4570     8.1238
    43.7277     4.4570     9.8004
    43.7277     4.4570    11.4770
&BPNODE TNODE=3, TNPC=0, TINTC=0, &END
&SECT1 STX=0.0, STY=0.0, STZ=0.0, SCALE=1.0, ALF=0.0, THETA=0.0, INMODE=4,
 TNODS=0, TNPS=0, TINTS=0, &END
    44.3717     0.0000     0.0000
    44.3717     1.6650     0.0009
    44.3717     3.3021     0.0097
    44.3717     4.0431     0.0680
    44.3717     4.2033     0.3596
    44.3717     4.2341     1.5030
    44.3717     4.2388     3.1680
    44.3717     4.2398     4.8331
    44.3717     4.2400     6.4981
    44.3717     4.2400     8.1631
    44.3717     4.2400     9.8282
    44.3717     4.2400    11.4932
&BPNODE TNODE=3, TNPC=0, TINTC=0, &END
&SECT1 STX=0.0, STY=0.0, STZ=0.0, SCALE=1.0, ALF=0.0, THETA=0.0, INMODE=4,
 TNODS=3, TNPS=0, TINTS=0, &END
    44.5909     0.0000     0.0000
    44.5909     1.6672     0.0010
    44.5909     3.2859     0.0111
    44.5909     3.9797     0.0752
    44.5909     4.1306     0.3843
```

```
  44.5909    4.1604    1.5597
  44.5909    4.1650    3.2268
  44.5909    4.1660    4.8940
  44.5909    4.1662    6.5612
  44.5909    4.1662    8.2284
  44.5909    4.1662    9.8955
  44.5909    4.1662   11.5627
&BPNODE TNODE=3, TNPC=0, TINTC=0, &END

&PATCH1 IREV=0, IDPAT=2, MAKE=0, KCOMP=1, KASS=1, IPATSYM=1, IPATCOP=0, &END
  ROOT UPPER STARBOARD
&SECT1 STX=0.0, STY=0.0, STZ=0.0, SCALE=1.0, ALF=0.0, THETA=0.0, INMODE=4,
 TNODS=0, TNPS=0, TINTS=0, &END
  24.6500    4.5000   13.1000
  24.6500    4.2213   14.0848
  24.6500    2.8142   14.0848
  24.6500    1.4071   14.0848
  24.6500    0.0000   14.0848
&BPNODE TNODE=3, TNPC=0, TINTC=0, &END
&SECT1 STX=0.0, STY=0.0, STZ=0.0, SCALE=1.0, ALF=0.0, THETA=0.0, INMODE=4,
 TNODS=0, TNPS=0, TINTS=0, &END
  24.8679    4.5000   13.5517
  24.8679    4.2213   14.1334
  24.8679    2.8142   14.1334
  24.8679    1.4071   14.1334
  24.8679    0.0000   14.1334
&BPNODE TNODE=3, TNPC=0, TINTC=0, &END
&SECT1 STX=0.0, STY=0.0, STZ=0.0, SCALE=1.0, ALF=0.0, THETA=0.0, INMODE=4,
 TNODS=0, TNPS=0, TINTS=0, &END
  25.5119    4.5000   13.9485
  25.5119    4.2213   14.2622
  25.5119    2.8142   14.2622
  25.5119    1.4071   14.2622
  25.5119    0.0000   14.2622
&BPNODE TNODE=3, TNPC=0, TINTC=0, &END
&SECT1 STX=0.0, STY=0.0, STZ=0.0, SCALE=1.0, ALF=0.0, THETA=0.0, INMODE=4,
 TNODS=0, TNPS=0, TINTS=0, &END
  26.5541    4.5000   14.2646
  26.5541    4.2213   14.4272
  26.5541    2.8142   14.4272
  26.5541    1.4071   14.4272
  26.5541    0.0000   14.4272
&BPNODE TNODE=3, TNPC=0, TINTC=0, &END
&SECT1 STX=0.0, STY=0.0, STZ=0.0, SCALE=1.0, ALF=0.0, THETA=0.0, INMODE=4,
 TNODS=0, TNPS=0, TINTS=0, &END
  27.9487    4.5000   14.4706
  27.9487    4.2213   14.5653
  27.9487    2.8142   14.5653
  27.9487    1.4071   14.5653
  27.9487    0.0000   14.5653
&BPNODE TNODE=3, TNPC=0, TINTC=0, &END
&SECT1 STX=0.0, STY=0.0, STZ=0.0, SCALE=1.0, ALF=0.0, THETA=0.0, INMODE=4,
 TNODS=0, TNPS=0, TINTS=0, &END
  29.6349    4.5000   14.5367
  29.6349    4.2213   14.5971
  29.6349    2.8142   14.5971
  29.6349    1.4071   14.5971
  29.6349    0.0000   14.5971
&BPNODE TNODE=3, TNPC=0, TINTC=0, &END
&SECT1 STX=0.0, STY=0.0, STZ=0.0, SCALE=1.0, ALF=0.0, THETA=0.0, INMODE=4,
 TNODS=0, TNPS=0, TINTS=0, &END
  31.5390    4.5000   14.4449
  31.5390    4.2213   14.5447
  31.5390    2.8142   14.5447
  31.5390    1.4071   14.5447
  31.5390    0.0000   14.5447
&BPNODE TNODE=3, TNPC=0, TINTC=0, &END
&SECT1 STX=0.0, STY=0.0, STZ=0.0, SCALE=1.0, ALF=0.0, THETA=0.0, INMODE=4,
 TNODS=0, TNPS=0, TINTS=0, &END
  33.5777    4.5000   14.2088
  33.5777    4.2213   14.3864
  33.5777    2.8142   14.3864
  33.5777    1.4071   14.3864
  33.5777    0.0000   14.3864
&BPNODE TNODE=3, TNPC=0, TINTC=0, &END
&SECT1 STX=0.0, STY=0.0, STZ=0.0, SCALE=1.0, ALF=0.0, THETA=0.0, INMODE=4,
```



```
 TNODS=0, TNPS=0, TINTS=0, &END
  35.6619    4.5000   13.8627
  35.6619    4.2213   14.0807
  35.6619    2.8142   14.0807
  35.6619    1.4071   14.0807
  35.6619    0.0000   14.0807
&BPNODE TNODE=3, TNPC=0, TINTC=0, &END
&SECT1 STX=0.0, STY=0.0, STZ=0.0, SCALE=1.0, ALF=0.0, THETA=0.0, INMODE=4,
 TNODS=0, TNPS=0, TINTS=0, &END
  37.7006    4.5000   13.4473
  37.7006    4.2213   13.6423
  37.7006    2.8142   13.6423
  37.7006    1.4071   13.6423
  37.7006    0.0000   13.6423
&BPNODE TNODE=3, TNPC=0, TINTC=0, &END
&SECT1 STX=0.0, STY=0.0, STZ=0.0, SCALE=1.0, ALF=0.0, THETA=0.0, INMODE=4,
 TNODS=0, TNPS=0, TINTS=0, &END
  39.6047    4.5000   12.9980
  39.6047    4.2213   13.1398
  39.6047    2.8142   13.1398
  39.6047    1.4071   13.1398
  39.6047    0.0000   13.1398
&BPNODE TNODE=3, TNPC=0, TINTC=0, &END
&SECT1 STX=0.0, STY=0.0, STZ=0.0, SCALE=1.0, ALF=0.0, THETA=0.0, INMODE=4,
 TNODS=0, TNPS=0, TINTS=0, &END
  41.2909    4.5000   12.5573
  41.2909    4.2213   12.6458
  41.2909    2.8142   12.6458
  41.2909    1.4071   12.6458
  41.2909    0.0000   12.6458
&BPNODE TNODE=3, TNPC=0, TINTC=0, &END
&SECT1 STX=0.0, STY=0.0, STZ=0.0, SCALE=1.0, ALF=0.0, THETA=0.0, INMODE=4,
 TNODS=0, TNPS=0, TINTS=0, &END
  42.6855    4.5000   12.1606
  42.6855    4.2213   12.2144
  42.6855    2.8142   12.2144
  42.6855    1.4071   12.2144
  42.6855    0.0000   12.2144
&BPNODE TNODE=3, TNPC=0, TINTC=0, &END
&SECT1 STX=0.0, STY=0.0, STZ=0.0, SCALE=1.0, ALF=0.0, THETA=0.0, INMODE=4,
 TNODS=0, TNPS=0, TINTS=0, &END
  43.7277    4.4570   11.8400
  43.7277    4.1900   11.8826
  43.7277    2.8142   11.8826
  43.7277    1.4071   11.8826
  43.7277    0.0000   11.8826
&BPNODE TNODE=3, TNPC=0, TINTC=0, &END
&SECT1 STX=0.0, STY=0.0, STZ=0.0, SCALE=1.0, ALF=0.0, THETA=0.0, INMODE=4,
 TNODS=0, TNPS=0, TINTS=0, &END
  44.3717    4.2400   11.6336
  44.3717    3.9900   11.6743
  44.3717    2.8142   11.6743
  44.3717    1.4071   11.6743
  44.3717    0.0000   11.6743
&BPNODE TNODE=3, TNPC=0, TINTC=0, &END
&SECT1 STX=0.0, STY=0.0, STZ=0.0, SCALE=1.0, ALF=0.0, THETA=0.0, INMODE=4,
 TNODS=3, TNPS=0, TINTS=0, &END
  44.5909    4.1662   11.5627
  44.5909    3.9300   11.6030
  44.5909    2.8142   11.6030
  44.5909    1.4071   11.6030
  44.5909    0.0000   11.6030
&BPNODE TNODE=3, TNPC=0, TINTC=0, &END

&PATCH1 IREV=0, IDPAT=2, MAKE=0, KCOMP=1, KASS=1, IPATSYM=1, IPATCOP=0, &END
  ROOT TRANSITION AFT STARBOARD
&SECT1 STX=0.0, STY=0.0, STZ=0.0, SCALE=1.0, ALF=0.0, THETA=0.0, INMODE=4,
 TNODS=0, TNPS=0, TINTS=0, &END
  44.5909    0.0000    0.0000
  44.5909    1.6672    0.0010
  44.5909    3.2859    0.0111
  44.5909    3.9797    0.[illegible]2
  44.5909    4.1306    0.3843
  44.5909    4.1604    1.5597
  44.5909    4.1650    3.2268
  44.5909    4.1660    4.8940
```

```
   44.5909     4.1662     6.5612
   44.5909     4.1662     8.2284
   44.5909     4.1662     9.8955
   44.5909     4.1662    11.5627
   44.5909     3.9300    11.6030
   44.5909     2.8142    11.6030
   44.5909     1.4071    11.6030
   44.5909     0.0000    11.6030
&BPNODE TNODE=3, TNPC=0, TINTC=0, &END
&SECT1 STX=0.0, STY=0.0, STZ=0.0, SCALE=1.0, ALF=0.0, THETA=0.0, INMODE=4,
 TNODS=0, TNPS=0, TINTS=0, &END
   44.9164     0.0000     0.0000
   44.9164     1.6527     0.0012
   44.9164     3.2292     0.0128
   44.9164     3.8750     0.0819
   44.9164     4.0206     0.4023
   44.9164     4.0505     1.5694
   44.9164     4.0553     3.2220
   44.9164     4.0564     4.8747
   44.9164     4.0566     6.5274
   44.9164     4.0566     8.1800
   44.9164     4.0566     9.8327
   44.9164     4.0562    11.4773
   44.9164     3.8438    11.5962
   44.9164     2.8142    11.5962
   44.9164     1.4071    11.5962
   44.9164     0.0000    11.5962
&BPNODE TNODE=3, TNPC=0, TINTC=0, &END
&SECT1 STX=0.0, STY=0.0, STZ=0.0, SCALE=1.0, ALF=0.0, THETA=0.0, INMODE=4,
 TNODS=0, TNPS=0, TINTS=0, &END
   45.7687     0.0000     0.0000
   45.7687     1.6149     0.0016
   45.7687     3.0609     0.0178
   45.7687     3.6006     0.1009
   45.7687     3.7321     0.4387
   45.7687     3.7625     1.5799
   45.7687     3.7679     3.1948
   45.7687     3.7692     4.8097
   45.7687     3.7695     6.4245
   45.7687     3.7695     8.0394
   45.7687     3.7693     9.6543
   45.7687     3.7674    11.2536
   45.7687     3.5600    11.5767
   45.7687     2.8142    11.5857
   45.7687     1.4071    11.5860
   45.7687     0.0000    11.5861
&BPNODE TNODE=3, TNPC=0, TINTC=0, &END
&SECT1 STX=0.0, STY=0.0, STZ=0.0, SCALE=1.0, ALF=0.0, THETA=0.0, INMODE=4,
 TNODS=0, TNPS=0, TINTS=0, &END
   46.8222     0.0000     0.0000
   46.8222     1.5638     0.0025
   46.8222     2.8199     0.0253
   46.8222     3.2590     0.1249
   46.8222     3.3765     0.4866
   46.8222     3.4068     1.5991
   46.8222     3.4128     3.1628
   46.8222     3.4143     4.7266
   46.8222     3.4146     6.2903
   46.8222     3.4146     7.8541
   46.8222     3.4142     9.4178
   46.8222     3.4111    10.9772
   46.8222     3.3229    11.5231
   46.8222     2.8650    11.5700
   46.8222     1.4071    11.5733
   46.8222     0.0000    11.5735
&BPNODE TNODE=3, TNPC=0, TINTC=0, &END
&SECT1 STX=0.0, STY=0.0, STZ=0.0, SCALE=1.0, ALF=0.0, THETA=0.0, INMODE=4,
 TNODS=0, TNPS=0, TINTS=0, &END
   47.6745     0.0000     0.0000
   47.6745     1.5223     0.0036
   47.6745     2.6098     0.0323
   47.6745     2.9827     0.1456
   47.6745     3.0895     0.5253
   47.6745     3.1192     1.6204
   47.6745     3.1255     3.1427
   47.6745     3.1271     4.6650
```



```
   47.6745     3.1275     6.1873
   47.6745     3.1275     7.7096
   47.6745     3.1269     9.2319
   47.6745     3.1232    10.7536
   47.6745     3.0838    11.4579
   47.6745     2.7717    11.5525
   47.6745     1.4071    11.5627
   47.6745     0.0000    11.5634
&BPNODE TNODE=3, TNPC=0, TINTC=0, &END
&SECT1 STX=0.0, STY=0.0, STZ=0.0, SCALE=1.0, ALF=0.0, THETA=0.0, INMODE=4,
 TNODS=3, TNPS=0, TINTS=0, &END
   48.0000     0.0000     0.0000
   48.0000     1.5058     0.0041
   48.0000     2.5263     0.0352
   48.0000     2.8769     0.1533
   48.0000     2.9802     0.5421
   48.0000     3.0094     1.6335
   48.0000     3.0158     3.1393
   48.0000     3.0175     4.6450
   48.0000     3.0179     6.1508
   48.0000     3.0178     7.6566
   48.0000     3.0172     9.1624
   48.0000     3.0134    10.6681
   48.0000     2.9761    11.4292
   48.0000     2.7054    11.5444
   48.0000     1.4071    11.5586
   48.0000     0.0000    11.5595
&BPNODE TNODE=3, TNPC=0, TINTC=0, &END

&PATCH1 IREV=0, IDPAT=2, MAKE=0, KCOMP=1, KASS=1, IPATSYM=1, IPATCOP=0,
&END
   FUSELAGE_AFT
&SECT1 STX=0.0, STY=0.0, STZ=0.0, SCALE=1.0, ALF=0.0, THETA=0.0, INMODE=4,
 TNODS=0, TNPS=0, TINTS=0, &END
   48.0000     0.0000     0.0000
   48.0000     1.5058     0.0041
   48.0000     2.5263     0.0352
   48.0000     2.8769     0.1533
   48.0000     2.9802     0.5421
   48.0000     3.0094     1.6335
   48.0000     3.0158     3.1393
   48.0000     3.0175     4.6450
   48.0000     3.0179     6.1508
   48.0000     3.0178     7.6566
   48.0000     3.0172     9.1624
   48.0000     3.0134    10.6681
   48.0000     2.9761    11.4292
   48.0000     2.7054    11.5444
   48.0000     1.5058    11.5586
   48.0000     0.0000    11.5595
&BPNODE TNODE=3, TNPC=0, TINTC=0, &END
&SECT1 STX=0.0, STY=0.0, STZ=0.0, SCALE=1.0, ALF=0.0, THETA=0.0, INMODE=4,
 TNODS=0, TNPS=0, TINTS=0, &END
   48.2093     0.0000     0.0000
   48.2093     1.5001     0.0045
   48.2093     2.4757     0.0375
   48.2093     2.8105     0.1604
   48.2093     2.9106     0.5614
   48.2093     2.9390     1.6667
   48.2093     2.9453     3.1668
   48.2093     2.9469     4.6669
   48.2093     2.9474     6.1670
   48.2093     2.9473     7.6670
   48.2093     2.9466     9.1671
   48.2093     2.9424    10.6669
   48.2093     2.9044    11.4175
   48.2093     2.6462    11.5397
   48.2093     1.4996    11.5559
   48.2093     0.0000    11.5570
&BPNODE TNODE=3, TNPC=0, TINTC=0, &END
&SECT1 STX=0.0, STY=0.0, STZ=0.0, SCALE=1.0, ALF=0.0, THETA=0.0, INMODE=4,
 TNODS=0, TNPS=0, TINTS=0, &END
   48.8055     0.0000     0.0000
   48.8055     1.4733     0.0060
   48.8055     2.3269     0.0446
   48.8055     2.6221     0.1829
```

```
    48.8055     2.7120     0.6123
    48.8055     2.7385     1.7484
    48.8055     2.7445     3.2309
    48.8055     2.7462     4.7134
    48.8055     2.7466     6.1959
    48.8055     2.7465     7.6784
    48.8055     2.7456     9.1609
    48.8055     2.7404    10.6408
    48.8055     2.7016    11.3810
    48.8055     2.4736    11.5252
    48.8055     1.4808    11.5480
    48.8055     0.0000    11.5499
&BPNODE TNODE=3, TNPC=0, TINTC=0, &END
&SECT1 STX=0.0, STY=0.0, STZ=0.0, SCALE=1.0, ALF=0.0, THETA=0.0, INMODE=4,
 TNODS=0, TNPS=0, TINTS=0, &END
    49.6976     0.0000     0.0000
    49.6976     1.3923     0.0085
    49.6976     2.0943     0.0564
    49.6976     2.3385     0.2185
    49.6976     2.4154     0.6980
    49.6976     2.4387     1.8818
    49.6976     2.4441     3.3356
    49.6976     2.4457     4.7894
    49.6976     2.4461     6.2432
    49.6976     2.4459     7.6970
    49.6976     2.4448     9.1508
    49.6976     2.4382    10.5961
    49.6976     2.3990    11.3282
    49.6976     2.2089    11.5012
    49.6976     1.4448    11.5354
    49.6976     0.0000    11.5393
&BPNODE TNODE=3, TNPC=0, TINTC=0, &END
&SECT1 STX=0.0, STY=0.0, STZ=0.0, SCALE=1.0, ALF=0.0, THETA=0.0, INMODE=4,
 TNODS=0, TNPS=0, TINTS=0, &END
    50.7500     0.0000     0.0000
    50.7500     1.2503     0.0119
    50.7500     1.8087     0.0723
    50.7500     2.0016     0.2624
    50.7500     2.0654     0.8001
    50.7500     2.0851     2.0280
    50.7500     2.0898     3.4449
    50.7500     2.0912     4.8618
    50.7500     2.0916     6.2787
    50.7500     2.0914     7.6956
    50.7500     2.0900     9.1125
    50.7500     2.0826    10.5181
    50.7500     2.0449    11.2629
    50.7500     1.8881    11.4705
    50.7500     1.3215    11.5194
    50.7500     0.0000    11.5268
&BPNODE TNODE=3, TNPC=0, TINTC=0, &END
&SECT1 STX=0.0, STY=0.0, STZ=0.0, SCALE=1.0, ALF=0.0, THETA=0.0, INMODE=4,
 TNODS=0, TNPS=0, TINTS=0, &END
    51.8024     0.0000     0.0000
    51.8024     1.0710     0.0155
    51.8024     1.5126     0.0897
    51.8024     1.6649     0.3144
    51.8024     1.7158     0.9210
    51.8024     1.7316     2.1843
    51.8024     1.7355     3.5578
    51.8024     1.7368     4.9313
    51.8024     1.7371     6.3049
    51.8024     1.7369     7.6784
    51.8024     1.7353     9.0519
    51.8024     1.7278    10.4187
    51.8024     1.6936    11.1932
    51.8024     1.5648    11.4376
    51.8024     1.1343    11.5024
    51.8024     0.0000    11.5143
&BPNODE TNODE=3, TNPC=0, TINTC=0, &END
&SECT1 STX=0.0, STY=0.0, STZ=0.0, SCALE=1.0, ALF=0.0, THETA=0.0, INMODE=4,
 TNODS=0, TNPS=0, TINTS=0, &END
    52.6945     0.0000     0.0000
    52.6945     0.8991     0.0186
    52.6945     1.2562     0.1053
    52.6945     1.3782     0.3607
```

Printed by pollard from hawkeye


```
    52.6945     1.4194     1.0318
    52.6945     1.4320     2.3099
    52.6945     1.4352     3.6427
    52.6945     1.4363     4.9756
    52.6945     1.4366     6.3084
    52.6945     1.4363     7.6413
    52.6945     1.4348     8.9741
    52.6945     1.4280    10.3058
    52.6945     1.3981    11.1267
    52.6945     1.2909    11.4083
    52.6945     0.9497    11.4877
    52.6945     0.0000    11.5036
&BPNODE TNODE=3, TNPC=0, TINTC=0, &END
&SECT1 STX=0.0, STY=0.0, STZ=0.0, SCALE=1.0, ALF=0.0, THETA=0.0, INMODE=4,
 TNODS=0, TNPS=0, TINTS=0, &END
    53.2907     0.0000     0.0142
    53.2907     0.7868     0.0350
    53.2907     1.0933     0.1303
    53.2907     1.1979     0.4106
    53.2907     1.2330     1.1338
    53.2907     1.2435     2.4132
    53.2907     1.2463     3.7174
    53.2907     1.2472     5.0216
    53.2907     1.2475     6.3259
    53.2907     1.2472     7.6301
    53.2907     1.2458     8.9343
    53.2907     1.2394    10.2385
    53.2907     1.2120    11.0812
    53.2907     1.1171    11.3809
    53.2907     0.8219    11.4693
    53.2907     0.0000    11.4876
&BPNODE TNODE=3, TNPC=0, TINTC=0, &END
&SECT1 STX=0.0, STY=0.0, STZ=0.0, SCALE=1.0, ALF=0.0, THETA=0.0, INMODE=4,
 TNODS=3, TNPS=0, TINTS=0, &END
    53.5000     0.0000     5.7500
    53.5000     0.0000     5.7539
    53.5000     0.0000     5.7578
    53.5000     0.0000     5.7852
    53.5000     0.0000     5.8447
    53.5000     0.0000     5.9043
    53.5000     0.0000     5.9639
    53.5000     0.0000     6.0234
    53.5000     0.0000     6.0830
    53.5000     0.0000     6.1426
    53.5000     0.0000     6.2021
    53.5000     0.0000     6.2617
    53.5000     0.0000     6.3213
    53.5000     0.0000     6.3809
    53.5000     0.0000     6.4404
    53.5000     0.0000     6.5000
&BPNODE TNODE=3, TNPC=0, TINTC=0, &END

&PATCH1 IREV=0, IDPAT=1, MAKE=0, KCOMP=1, KASS=1, IPATSYM=1, IPATCOP=0, &END
 WING_INBOARD
&SECT1 STX=0.0, STY=0.0, STZ=0.0, SCALE=1.0, ALF=0.0, THETA=0.0, INMODE=4,
 TNODS=0, TNPS=0, TINTS=0, &END
    44.5909     4.1662    11.5627
    44.3717     4.2400    11.4932
    43.7277     4.4570    11.4770
    42.6855     4.5000    11.4565
    41.2909     4.5000    11.4290
    39.6047     4.5000    11.4032
    37.7006     4.5000    11.3871
    35.6619     4.5000    11.3790
    33.5777     4.5000    11.3991
    31.5390     4.5000    11.4614
    29.6349     4.5000    11.5647
    27.9487     4.5000    11.7283
    26.5541     4.5000    11.9690
    25.5119     4.5000    12.2862
    24.8679     4.5000    12.6691
    24.6500     4.5000    13.1000
    24.8679     4.5000    13.5517
    25.5119     4.5000    13.9485
    26.5541     4.5000    14.2646
    27.9487     4.5000    14.4706
```

```
     29.6349     4.5000    14.5367
     31.5390     4.5000    14.4449
     33.5777     4.5000    14.2088
     35.6619     4.5000    13.8627
     37.7006     4.5000    13.4473
     39.6047     4.5000    12.9980
     41.2909     4.5000    12.5573
     42.6855     4.5000    12.1606
     43.7277     4.4570    11.8400
     44.3717     4.2400    11.6336
     44.5909     4.1662    11.5627
&BPNODE TNODE=3, TNPC=0, TINTC=0, &END
&SECT1 STX=0.0, STY=0.0, STZ=0.0, SCALE=1.0, ALF=0.0, THETA=0.0, INMODE=4,
 TNODS=0, TNPS=0, TINTS=0, &END
    44.5896     5.0188    11.5308
    44.3717     5.0188    11.4914
    43.7277     5.0188    11.4763
    42.6855     5.0188    11.4563
    41.2909     5.0188    11.4289
    39.6047     5.0188    11.4032
    37.7006     5.0188    11.3871
    35.6619     5.0188    11.3790
    33.5777     5.0188    11.3991
    31.5390     5.0188    11.4614
    29.6349     5.0188    11.5647
    27.9487     5.0188    11.7283
    26.5541     5.0188    11.9690
    25.5119     5.0188    12.2862
    24.8679     5.0188    12.6691
    24.6500     5.0188    13.1000
    24.8679     5.0188    13.5517
    25.5119     5.0188    13.9485
    26.5541     5.0188    14.2646
    27.9487     5.0188    14.4706
    29.6349     5.0188    14.5367
    31.5390     5.0188    14.4449
    33.5777     5.0188    14.2088
    35.6619     5.0188    13.8627
    37.7006     5.0188    13.4473
    39.6047     5.0188    12.9980
    41.2909     5.0188    12.5573
    42.6855     5.0188    12.1607
    43.7277     5.0188    11.8407
    44.3717     5.0188    11.6352
    44.5896     5.0188    11.5308
&BPNODE TNODE=3, TNPC=0, TINTC=0, &END
&SECT1 STX=0.0, STY=0.0, STZ=0.0, SCALE=1.0, ALF=0.0, THETA=0.0, INMODE=4,
 TNODS=0, TNPS=0, TINTS=0, &END
    44.5896     6.5553    11.5308
    44.3717     6.5553    11.4914
    43.7277     6.5553    11.4763
    42.6855     6.5553    11.4563
    41.2909     6.5553    11.4289
    39.6047     6.5553    11.4032
    37.7006     6.5553    11.3871
    35.6619     6.5553    11.3790
    33.5777     6.5553    11.3991
    31.5390     6.5553    11.4614
    29.6349     6.5553    11.5647
    27.9487     6.5553    11.7283
    26.5541     6.5553    11.9690
    25.5119     6.5553    12.2862
    24.8679     6.5553    12.6691
    24.6500     6.5553    13.1000
    24.8679     6.5553    13.5517
    25.5119     6.5553    13.9485
    26.5541     6.5553    14.2646
    27.9487     6.5553    14.4706
    29.6349     6.5553    14.5367
    31.5390     6.5553    14.4449
    33.5777     6.5553    14.2088
    35.6619     6.5553    13.8627
    37.7006     6.5553    13.4473
    39.6047     6.5553    12.9980
    41.2909     6.5553    12.5573
    42.6855     6.5553    12.1607
```



```
    43.7277     6.5553    11.8407
    44.3717     6.5553    11.6352
    44.5896     6.5553    11.5308
&BPNODE TNODE=3, TNPC=0, TINTC=0, &END
&SECT1 STX=0.0, STY=0.0, STZ=0.0, SCALE=1.0, ALF=0.0, THETA=0.0, INMODE=4,
 TNODS=0, TNPS=0, TINTS=0, &END
    44.5896     9.0503    11.5308
    44.3717     9.0503    11.4914
    43.7277     9.0503    11.4763
    42.6855     9.0503    11.4563
    41.2909     9.0503    11.4289
    39.6047     9.0503    11.4032
    37.7006     9.0503    11.3871
    35.6619     9.0503    11.3790
    33.5777     9.0503    11.3991
    31.5390     9.0503    11.4614
    29.6349     9.0503    11.5647
    27.9487     9.0503    11.7283
    26.5541     9.0503    11.9690
    25.5119     9.0503    12.2862
    24.8679     9.0503    12.6691
    24.6500     9.0503    13.1000
    24.8679     9.0503    13.5517
    25.5119     9.0503    13.9485
    26.5541     9.0503    14.2646
    27.9487     9.0503    14.4706
    29.6349     9.0503    14.5367
    31.5390     9.0503    14.4449
    33.5777     9.0503    14.2088
    35.6619     9.0503    13.8627
    37.7006     9.0503    13.4473
    39.6047     9.0503    12.9980
    41.2909     9.0503    12.5573
    42.6855     9.0503    12.1607
    43.7277     9.0503    11.8407
    44.3717     9.0503    11.6352
    44.5896     9.0503    11.5308
&BPNODE TNODE=3, TNPC=0, TINTC=0, &END
&SECT1 STX=0.0, STY=0.0, STZ=0.0, SCALE=1.0, ALF=0.0, THETA=0.0, INMODE=4,
 TNODS=0, TNPS=0, TINTS=0, &END
    44.5896    12.4081    11.5308
    44.3717    12.4081    11.4914
    43.7277    12.4081    11.4763
    42.6855    12.4081    11.4563
    41.2909    12.4081    11.4289
    39.6047    12.4081    11.4032
    37.7006    12.4081    11.3871
    35.6619    12.4081    11.3790
    33.5777    12.4081    11.3991
    31.5390    12.4081    11.4614
    29.6349    12.4081    11.5647
    27.9487    12.4081    11.7283
    26.5541    12.4081    11.9690
    25.5119    12.4081    12.2862
    24.8679    12.4081    12.6691
    24.6500    12.4081    13.1000
    24.8679    12.4081    13.5517
    25.5119    12.4081    13.9485
    26.5541    12.4081    14.2646
    27.9487    12.4081    14.4706
    29.6349    12.4081    14.5367
    31.5390    12.4081    14.4449
    33.5777    12.4081    14.2088
    35.6619    12.4081    13.8627
    37.7006    12.4081    13.4473
    39.6047    12.4081    12.9980
    41.2909    12.4081    12.5573
    42.6855    12.4081    12.1607
    43.7277    12.4081    11.8407
    44.3717    12.4081    11.6352
    44.5896    12.4081    11.5308
&BPNODE TNODE=3, TNPC=0, TINTC=0, &END
&SECT1 STX=0.0, STY=0.0, STZ=0.0, SCALE=1.0, ALF=0.0, THETA=0.0, INMODE=4,
 TNODS=0, TNPS=0, TINTS=0, &END
    44.5896    16.4996    11.5308
    44.3717    16.4996    11.4914
```

```
 43.7277   16.4996   11.4763
 42.6855   16.4996   11.4563
 41.2909   16.4996   11.4289
 39.6047   16.4996   11.4032
 37.7006   16.4996   11.3871
 35.6619   16.4996   11.3790
 33.5777   16.4996   11.3991
 31.5390   16.4996   11.4614
 29.6349   16.4996   11.5647
 27.9487   16.4996   11.7283
 26.5541   16.4996   11.9690
 25.5119   16.4996   12.2862
 24.8679   16.4996   12.6691
 24.6500   16.4996   13.1000
 24.8679   16.4996   13.5517
 25.5119   16.4996   13.9485
 26.5541   16.4996   14.2646
 27.9487   16.4996   14.4706
 29.6349   16.4996   14.5367
 31.5390   16.4996   14.4449
 33.5777   16.4996   14.2088
 35.6619   16.4996   13.8627
 37.7006   16.4996   13.4473
 39.6047   16.4996   12.9980
 41.2909   16.4996   12.5573
 42.6855   16.4996   12.1607
 43.7277   16.4996   11.8407
 44.3717   16.4996   11.6352
 44.5896   16.4996   11.5308
&BPNODE TNODE=3, TNPC=0, TINTC=0, &END
&SECT1 STX=0.0, STY=0.0, STZ=0.0, SCALE=1.0, ALF=0.0, THETA=0.0, INMODE=4,
 TNODS=0, TNPS=0, TINTS=0, &END
 44.5896   21.1675   11.5308
 44.3717   21.1675   11.4914
 43.7277   21.1675   11.4763
 42.6855   21.1675   11.4563
 41.2909   21.1675   11.4289
 39.6047   21.1675   11.4032
 37.7006   21.1675   11.3871
 35.6619   21.1675   11.3790
 33.5777   21.1675   11.3991
 31.5390   21.1675   11.4614
 29.6349   21.1675   11.5647
 27.9487   21.1675   11.7283
 26.5541   21.1675   11.9690
 25.5119   21.1675   12.2862
 24.8679   21.1675   12.6691
 24.6500   21.1675   13.1000
 24.8679   21.1675   13.5517
 25.5119   21.1675   13.9485
 26.5541   21.1675   14.2646
 27.9487   21.1675   14.4706
 29.6349   21.1675   14.53(.
 31.5390   21.1675   14.4449
 33.5777   21.1675   14.2088
 35.6619   21.1675   13.8627
 37.7006   21.1675   13.4473
 39.6047   21.1675   12.9980
 41.2909   21.1675   12.5573
 42.6855   21.1675   12.1607
 43.7277   21.1675   11.8407
 44.3717   21.1675   11.6352
 44.5896   21.1675   11.5308
&BPNODE TNODE=3, TNPC=0, TINTC=0, &END
&SECT1 STX=0.0, STY=0.0, STZ=0.0, SCALE=1.0, ALF=0.0, THETA=0.0, INMODE=4,
 TNODS=0, TNPS=0, TINTS=0, &END
 44.5896   26.2326   11.5308
 44.3717   26.2326   11.4914
 43.7277   26.2326   11.4763
 42.6855   26.2326   11.4563
 41.2909   26.2326   11.4289
 39.6047   26.2326   11.4032
 37.7006   26.2326   11.3871
 35.6619   26.2326   11.3790
 33.5777   26.2326   11.3991
 31.5390   26.2326   11.4614
```



```
 29.6349   26.2326   11.5647
 27.9487   26.2326   11.7283
 26.5541   26.2326   11.9690
 25.5119   26.2326   12.2862
 24.8679   26.2326   12.6691
 24.6500   26.2326   13.1000
 24.8679   26.2326   13.5517
 25.5119   26.2326   13.9485
 26.5541   26.2326   14.2646
 27.9487   26.2326   14.4706
 29.6349   26.2326   14.5367
 31.5390   26.2326   14.4449
 33.5777   26.2326   14.2088
 35.6619   26.2326   13.8627
 37.7006   26.2326   13.4473
 39.6047   26.2326   12.9980
 41.2909   26.2326   12.5573
 42.6855   26.2326   12.1607
 43.7277   26.2326   11.8407
 44.3717   26.2326   11.6352
 44.5896   26.2326   11.5308
&BPNODE TNODE=3, TNPC=0, TINTC=0, &END
&SECT1 STX=0.0, STY=0.0, STZ=0.0, SCALE=1.0, ALF=0.0, THETA=0.0, INMODE=4,
 TNODS=3, TNPS=0, TINTS=0, &END
 44.5896   31.5000   11.5308
 44.3717   31.5000   11.4914
 43.7277   31.5000   11.4763
 42.6855   31.5000   11.4563
 41.2909   31.5000   11.4289
 39.6047   31.5000   11.4032
 37.7006   31.5000   11.3871
 35.6619   31.5000   11.3790
 33.5777   31.5000   11.3991
 31.5390   31.5000   11.4614
 29.6349   31.5000   11.5647
 27.9487   31.5000   11.7283
 26.5541   31.5000   11.9690
 25.5119   31.5000   12.2862
 24.8679   31.5000   12.6691
 24.6500   31.5000   13.1000
 24.8679   31.5000   13.5517
 25.5119   31.5000   13.9485
 26.5541   31.5000   14.2646
 27.9487   31.5000   14.4706
 29.6349   31.5000   14.5367
 31.5390   31.5000   14.4449
 33.5777   31.5000   14.2088
 35.6619   31.5000   13.8627
 37.7006   31.5000   13.4473
 39.6047   31.5000   12.9980
 41.2909   31.5000   12.5573
 42.6855   31.5000   12.1607
 43.7277   31.5000   11.8407
 44.3717   31.5000   11.6352
 44.5896   31.5000   11.5308
&BPNODE TNODE=3, TNPC=0, TINTC=0, &END

&PATCH1 IREV=0, IDPAT=1, MAKE=0, KCOMP=1, KASS=1, IPATSYM=1, IPATCOP=0, &END
  WING_MID_AILERON
&SECT1 STX=0.0, STY=0.0, STZ=0.0, SCALE=1.0, ALF=0.0, THETA=0.0, INMODE=4,
 TNODS=0, TNPS=0, TINTS=0, &END
 44.5896   31.5000   11.5308
 44.3717   31.5000   11.4914
 43.7277   31.5000   11.4763
 42.6855   31.5000   11.4563
 41.2909   31.5000   11.4289
 39.6047   31.5000   11.4032
 37.7006   31.5000   11.3871
 35.6619   31.5000   11.3790
 33.5777   31.5000   11.3991
 31.5390   31.5000   11.4614
 29.6349   31.5000   11.5647
 27.9487   31.5000   11.7283
 26.5541   31.5000   11.9690
 25.5119   31.5000   12.2862
 24.8679   31.5000   12.6691
```

```
   24.6500   31.5000   13.1000
   24.8679   31.5000   13.5517
   25.5119   31.5000   13.9485
   26.5541   31.5000   14.2646
   27.9487   31.5000   14.4706
   29.6349   31.5000   14.5367
   31.5390   31.5000   14.4449
   33.5777   31.5000   14.2088
   35.6619   31.5000   13.8627
   37.7006   31.5000   13.4473
   39.6047   31.5000   12.9980
   41.2909   31.5000   12.5573
   42.6855   31.5000   12.1607
   43.7277   31.5000   11.8407
   44.3717   31.5000   11.6352
   44.5896   31.5000   11.5308
&BPNODE TNODE=3, TNPC=0, TINTC=0, &END
&SECT1 STX=0.0, STY=0.0, STZ=0.0, SCALE=1.0, ALF=0.0, THETA=0.0, INMODE=4,
 TNODS=0, TNPS=0, TINTS=0, &END
   44.5896   35.8000   11.5308
   44.3717   35.8000   11.4914
   43.7277   35.8000   11.4763
   42.6855   35.8000   11.4563
   41.2909   35.8000   11.4289
   39.6047   35.8000   11.4032
   37.7006   35.8000   11.3871
   35.6619   35.8000   11.3790
   33.5777   35.8000   11.3991
   31.5390   35.8000   11.4614
   29.6349   35.8000   11.5647
   27.9487   35.8000   11.7283
   26.5541   35.8000   11.9690
   25.5119   35.8000   12.2862
   24.8679   35.8000   12.6691
   24.6500   35.8000   13.1000
   24.8679   35.8000   13.5517
   25.5119   35.8000   13.9485
   26.5541   35.8000   14.2646
   27.9487   35.8000   14.4706
   29.6349   35.8000   14.5367
   31.5390   35.8000   14.4449
   33.5777   35.8000   14.2088
   35.6619   35.8000   13.8627
   37.7006   35.8000   13.4473
   39.6047   35.8000   12.9980
   41.2909   35.8000   12.5573
   42.6855   35.8000   12.1607
   43.7277   35.8000   11.8407
   44.3717   35.8000   11.6352
   44.5896   35.8000   11.5308
&BPNODE TNODE=3, TNPC=0, TINTC=0, &END
&SECT1 STX=0.0, STY=0.0, STZ=0.0, SCALE=1.0, ALF=0.0, THETA=0.0, INMODE=4,
 TNODS=0, TNPS=0, TINTS=0, &END
   44.5896   40.1000   11.5308
   44.3717   40.1000   11.4914
   43.7277   40.1000   11.4763
   42.6855   40.1000   11.4563
   41.2909   40.1000   11.4289
   39.6047   40.1000   11.4032
   37.7006   40.1000   11.3871
   35.6619   40.1000   11.3790
   33.5777   40.1000   11.3991
   31.5390   40.1000   11.4614
   29.6349   40.1000   11.5647
   27.9487   40.1000   11.7283
   26.5541   40.1000   11.9690
   25.5119   40.1000   12.2862
   24.8679   40.1000   12.6691
   24.6500   40.1000   13.1000
   24.8679   40.1000   13.5517
   25.5119   40.1000   13.9485
   26.5541   40.1000   14.2646
   27.9487   40.1000   14.4706
   29.6349   40.1000   14.5367
   31.5390   40.1000   14.4449
   33.5777   40.1000   14.2088
```



```
   35.6619   40.1000   13.8627
   37.7006   40.1000   13.4473
   39.6047   40.1000   12.9980
   41.2909   40.1000   12.5573
   42.6855   40.1000   12.1607
   43.7277   40.1000   11.8407
   44.3717   40.1000   11.6352
   44.5896   40.1000   11.5308
&BPNODE TNODE=3, TNPC=0, TINTC=0, &END
&SECT1 STX=0.0, STY=0.0, STZ=0.0, SCALE=1.0, ALF=0.0, THETA=0.0, INMODE=4,
 TNODS=0, TNPS=0, TINTS=0, &END
   44.5896   44.4000   11.5308
   44.3717   44.4000   11.4914
   43.7277   44.4000   11.4763
   42.6855   44.4000   11.4563
   41.2909   44.4000   11.4289
   39.6047   44.4000   11.4032
   37.7006   44.4000   11.3871
   35.6619   44.4000   11.3790
   33.5777   44.4000   11.3991
   31.5390   44.4000   11.4614
   29.6349   44.4000   11.5647
   27.9487   44.4000   11.7283
   26.5541   44.4000   11.9690
   25.5119   44.4000   12.2862
   24.8679   44.4000   12.6691
   24.6500   44.4000   13.1000
   24.8679   44.4000   13.5517
   25.5119   44.4000   13.9485
   26.5541   44.4000   14.2646
   27.9487   44.4000   14.4706
   29.6349   44.4000   14.5367
   31.5390   44.4000   14.4449
   33.5777   44.4000   14.2088
   35.6619   44.4000   13.8627
   37.7006   44.4000   13.4473
   39.6047   44.4000   12.9980
   41.2909   44.4000   12.5573
   42.6855   44.4000   12.1607
   43.7277   44.4000   11.8407
   44.3717   44.4000   11.6352
   44.5896   44.4000   11.5308
&BPNODE TNODE=3, TNPC=0, TINTC=0, &END
&SECT1 STX=0.0, STY=0.0, STZ=0.0, SCALE=1.0, ALF=0.0, THETA=0.0, INMODE=4,
 TNODS=0, TNPS=0, TINTS=0, &END
   44.5896   48.7000   11.5308
   44.3717   48.7000   11.4914
   43.7277   48.7000   11.4763
   42.6855   48.7000   11.4563
   41.2909   48.7000   11.4289
   39.6047   48.7000   11.4032
   37.7006   48.7000   11.3871
   35.6619   48.7000   11.3790
   33.5777   48.7000   11.3991
   31.5390   48.7000   11.4614
   29.6349   48.7000   11.5647
   27.9487   48.7000   11.7283
   26.5541   48.7000   11.9690
   25.5119   48.7000   12.2862
   24.8679   48.7000   12.6691
   24.6500   48.7000   13.1000
   24.8679   48.7000   13.5517
   25.5119   48.7000   13.9485
   26.5541   48.7000   14.2646
   27.9487   48.7000   14.4706
   29.6349   48.7000   14.5367
   31.5390   48.7000   14.4449
   33.5777   48.7000   14.2088
   35.6619   48.7000   13.8627
   37.7006   48.7000   13.4473
   39.6047   48.7000   12.9980
   41.2909   48.7000   12.5573
   42.6855   48.7000   12.1607
   43.7277   48.7000   11.8407
   44.3717   48.7000   11.6352
   44.5896   48.7000   11.5308
```

Printed by pollard from hawkeye

Jun 11 1997 05:30 **froguav.in** Page 21

```
&BPNODE TNODE=3, TNPC=0, TINTC=0, &END
&SECT1 STX=0.0, STY=0.0, STZ=0.0, SCALE=1.0, ALF=0.0, THETA=0.0, INMODE=4,
 TNODS=3, TNPS=0, TINTS=0, &END
  44.5896   53.0000   11.5308
  44.3717   53.0000   11.4914
  43.7277   53.0000   11.4763
  42.6855   53.0000   11.4563
  41.2909   53.0000   11.4289
  39.6047   53.0000   11.4032
  37.7006   53.0000   11.3871
  35.6619   53.0000   11.3790
  33.5777   53.0000   11.3991
  31.5390   53.0000   11.4614
  29.6349   53.0000   11.5647
  27.9487   53.0000   11.7283
  26.5541   53.0000   11.9690
  25.5119   53.0000   12.2862
  24.8679   53.0000   12.6691
  24.6500   53.0000   13.1000
  24.8679   53.0000   13.5517
  25.5119   53.0000   13.9485
  26.5541   53.0000   14.2646
  27.9487   53.0000   14.4706
  29.6349   53.0000   14.5367
  31.5390   53.0000   14.4449
  33.5777   53.0000   14.2088
  35.6619   53.0000   13.8627
  37.7006   53.0000   13.4473
  39.6047   53.0000   12.9980
  41.2909   53.0000   12.5573
  42.6855   53.0000   12.1607
  43.7277   53.0000   11.8407
  44.3717   53.0000   11.6352
  44.5896   53.0000   11.5308
&BPNODE TNODE=3, TNPC=0, TINTC=0, &END

&PATCH1 IREV=0, IDPAT=1, MAKE=0, KCOMP=1, KASS=1, IPATSYM=1, IPATCOP=0, &END
  WING_OUTBOARD_TAPER
&SECT1 STX=0.0, STY=0.0, STZ=0.0, SCALE=1.0, ALF=0.0, THETA=0.0, INMODE=4,
 TNODS=0, TNPS=0, TINTS=0, &END
  44.5896   53.0000   11.5308
  44.3717   53.0000   11.4914
  43.7277   53.0000   11.4763
  42.6855   53.0000   11.4563
  41.2909   53.0000   11.4289
  39.6047   53.0000   11.4032
  37.7006   53.0000   11.3871
  35.6619   53.0000   11.3790
  33.5777   53.0000   11.3991
  31.5390   53.0000   11.4614
  29.6349   53.0000   11.5647
  27.9487   53.0000   11.7283
  26.5541   53.0000   11.9690
  25.5119   53.0000   12.2862
  24.8679   53.0000   12.6691
  24.6500   53.0000   13.1000
  24.8679   53.0000   13.5517
  25.5119   53.0000   13.9485
  26.5541   53.0000   14.2646
  27.9487   53.0000   14.4706
  29.6349   53.0000   14.5367
  31.5390   53.0000   14.4449
  33.5777   53.0000   14.2088
  35.6619   53.0000   13.8627
  37.7006   53.0000   13.4473
  39.6047   53.0000   12.9980
  41.2909   53.0000   12.5573
  42.6855   53.0000   12.1607
  43.7277   53.0000   11.8407
  44.3717   53.0000   11.6352
  44.5896   53.0000   11.5308
&BPNODE TNODE=3, TNPC=0, TINTC=0, &END
&SECT1 STX=0.0, STY=0.0, STZ=0.0, SCALE=1.0, ALF=0.0, THETA=0.0, INMODE=4,
 TNODS=0, TNPS=0, TINTS=0, &END
  43.8419   57.0000   11.5897
```

Jun 11 1997 05:30 **froguav.in** Page 22

```
  43.6322   57.0000   11.5517
  43.0123   57.0000   11.5372
  42.0092   57.0000   11.5180
  40.6669   57.0000   11.4916
  39.0439   57.0000   11.4668
  37.2112   57.0000   11.4513
  35.2490   57.0000   11.4436
  33.2429   57.0000   11.4629
  31.2806   57.0000   11.5229
  29.4480   57.0000   11.6223
  27.8250   57.0000   11.7798
  26.4827   57.0000   12.0114
  25.4796   57.0000   12.3168
  24.8597   57.0000   12.6853
  24.6500   57.0000   13.1000
  24.8597   57.0000   13.5348
  25.4796   57.0000   13.9167
  26.4827   57.0000   14.2209
  27.8250   57.0000   14.4192
  29.4480   57.0000   14.4828
  31.2806   57.0000   14.3944
  33.2429   57.0000   14.1673
  35.2490   57.0000   13.8341
  37.2112   57.0000   13.4342
  39.0439   57.0000   13.0018
  40.6669   57.0000   12.5777
  42.0092   57.0000   12.1959
  43.0123   57.0000   11.8879
  43.6322   57.0000   11.6901
  43.8419   57.0000   11.5897
&BPNODE TNODE=3, TNPC=0, TINTC=0, &END
&SECT1 STX=0.0, STY=0.0, STZ=0.0, SCALE=1.0, ALF=0.0, THETA=0.0, INMODE=4,
 TNODS=0, TNPS=0, TINTS=0, &END
  43.2945   59.9282   11.6327
  43.0908   59.9282   11.5959
  42.4885   59.9282   11.5818
  41.5141   59.9282   11.5631
  40.2100   59.9282   11.5375
  38.6334   59.9282   11.5134
  36.8530   59.9282   11.4983
  34.9467   59.9282   11.4908
  32.9978   59.9282   11.5096
  31.0915   59.9282   11.5679
  29.3111   59.9282   11.6644
  27.7344   59.9282   11.8174
  26.4304   59.9282   12.0424
  25.4560   59.9282   12.3391
  24.8537   59.9282   12.6971
  24.6500   59.9282   13.1000
  24.8537   59.9282   13.5224
  25.4560   59.9282   13.8934
  26.4304   59.9282   14.1890
  27.7344   59.9282   14.3815
  29.3111   59.9282   14.4433
  31.0915   59.9282   14.3575
  32.9978   59.9282   14.1368
  34.9467   59.9282   13.8132
  36.8530   59.9282   13.4247
  38.6334   59.9282   13.0046
  40.2100   59.9282   12.5926
  41.5141   59.9282   12.2217
  42.4885   59.9282   11.9225
  43.0908   59.9282   11.7303
  43.2945   59.9282   11.6327
&BPNODE TNODE=3, TNPC=0, TINTC=0, &END
&SECT1 STX=0.0, STY=0.0, STZ=0.0, SCALE=1.0, ALF=0.0, THETA=0.0, INMODE=4,
 TNODS=3, TNPS=0, TINTS=0, &END
  43.0941   61.0000   11.6485
  42.8926   61.0000   11.6120
  42.2968   61.0000   11.5981
  41.332[illegible]   61.0000   11.5796
  40.04[illegible]   61.0000   11.5543
  38.4831   61.0000   11.5304
  36.7218   61.0000   11.5156
  34.8360   61.0000   11.5081
  32.9081   61.0000   11.5267
```

```
   31.0223    61.0000    11.5843
   29.2610    61.0000    11.6799
   27.7013    61.0000    11.8312
   26.4113    61.0000    12.0538
   25.4473    61.0000    12.3473
   24.8515    61.0000    12.7014
   24.6500    61.0000    13.1000
   24.8515    61.0000    13.5178
   25.4473    61.0000    13.8848
   26.4113    61.0000    14.1773
   27.7013    61.0000    14.3678
   29.2610    61.0000    14.4289
   31.0223    61.0000    14.3440
   32.9081    61.0000    14.1257
   34.8360    61.0000    13.8055
   36.7218    61.0000    13.4212
   38.4831    61.0000    13.0057
   40.0428    61.0000    12.5980
   41.3329    61.0000    12.2311
   42.2968    61.0000    11.9351
   42.8926    61.0000    11.7451
   43.0941    61.0000    11.6485
 &BPNODE TNODE=3, TNPC=0, TINTC=0, &END

&PATCH1  IREV=  0, IDPAT= 1, MAKE=   17, KCOMP= 1, KASS= 1, IPATSYM=1,
         IPATCOP=0,                                                  &END
WING_TIP_Half_Round
 &PATCH2  ITYP=  2,    TNODS= 3,    TNPS=   4,   TINTS= 3,      &END


 &PATCH1 IREV=0, IDPAT=1, MAKE=0, KCOMP=1, KASS=1, IPATSYM=1, IPATCOP=0, &END
   FOG_HORIZONTAL_TAIL
 &SECT1 STX=0.0, STY=0.0, STZ=0.0, SCALE=1.0, ALF=0.0, THETA=0.0, INMODE=4,
  TNODS=0, TNPS=0, TINTS=0, &END
   96.0000    0.0000    8.0900
   95.7266    0.0000    8.0641
   94.9285    0.0000    8.0097
   93.6703    0.0000    7.9337
   92.0541    0.0000    7.8478
   90.2106    0.0000    7.7664
   88.2894    0.0000    7.7063
   86.4459    0.0000    7.6850
   84.8297    0.0000    7.7154
   83.5715    0.0000    7.8000
   82.7734    0.0000    7.9302
   82.5000    0.0000    8.0900
   82.7734    0.0000    8.2498
   83.5715    0.0000    8.3800
   84.8297    0.0000    8.4646
   86.4459    0.0000    8.4950
   88.2894    0.0000    8.4737
   90.2106    0.0000    8.4136
   92.0541    0.0000    8.3322
   93.6703    0.0000    8.2463
   94.9285    0.0000    8.1703
   95.7266    0.0000    8.1159
   96.0000    0.0000    8.0900
 &BPNODE TNODE=3, TNPC=0, TINTC=0, &END
 &SECT1 STX=0.0, STY=0.0, STZ=0.0, SCALE=1.0, ALF=0.0, THETA=0.0, INMODE=4,
  TNODS=0, TNPS=0, TINTS=0, &END
   96.0012    0.4864    8.0900
   95.7298    0.4864    8.0643
   94.9374    0.4864    8.0103
   93.6882    0.4864    7.9348
   92.0835    0.4864    7.8495
   90.2533    0.4864    7.7687
   88.3458    0.4864    7.7091
   86.5156    0.4864    7.6879
   84.9109    0.4864    7.7180
   83.6618    0.4864    7.8021
   82 86[illegible]4    0.4864    7.9313
   82.[illegible]97[illegible]    0.4864    8.0900
   82.8694    0.4864    8.2487
   83.6618    0.4864    8.3779
   84.9109    0.4864    8.4620
   86.5156    0.4864    8.4921
```



```
   88.3458    0.4864    8.4709
   90.2533    0.4864    8.4113
   92.0835    0.4864    8.3305
   93.6882    0.4864    8.2452
   94.9374    0.4864    8.1697
   95.7298    0.4864    8.1157
   96.0012    0.4864    8.0900
 &BPNODE TNODE=3, TNPC=0, TINTC=0, &END
 &SECT1 STX=0.0, STY=0.0, STZ=0.0, SCALE=1.0, ALF=0.0, THETA=0.0, INMODE=4,
  TNODS=0, TNPS=0, TINTS=0, &END
   96.0048    1.8979    8.0900
   95.7390    1.8979    8.0648
   94.9632    1.8979    8.0120
   93.7402    1.8979    7.9381
   92.1691    1.8979    7.8545
   90.3772    1.8979    7.7755
   88.5096    1.8979    7.7170
   86.7177    1.8979    7.6963
   85.1466    1.8979    7.7258
   83.9236    1.8979    7.8081
   83.1477    1.8979    7.9347
   82.8820    1.8979    8.0900
   83.1477    1.8979    8.2453
   83.9236    1.8979    8.3719
   85.1466    1.8979    8.4542
   86.7177    1.8979    8.4837
   88.5096    1.8979    8.4630
   90.3772    1.8979    8.4045
   92.1691    1.8979    8.3255
   93.7402    1.8979    8.2419
   94.9632    1.8979    8.1680
   95.7390    1.8979    8.1152
   96.0048    1.8979    8.0900
 &BPNODE TNODE=3, TNPC=0, TINTC=0, &END
 &SECT1 STX=0.0, STY=0.0, STZ=0.0, SCALE=1.0, ALF=0.0, THETA=0.0, INMODE=4,
  TNODS=0, TNPS=0, TINTS=0, &END
   96.0103    4.0964    8.0900
   95.7534    4.0964    8.0657
   95.0034    4.0964    8.0146
   93.8211    4.0964    7.9432
   92.3023    4.0964    7.8624
   90.5701    4.0964    7.7859
   88.7647    4.0964    7.7295
   87.0324    4.0964    7.7094
   85.5136    4.0964    7.7380
   84.3313    4.0964    7.8175
   83.5814    4.0964    7.9398
   83.3244    4.0964    8.0900
   83.5814    4.0964    8.2402
   84.3313    4.0964    8.3625
   85.5136    4.0964    8.4420
   87.0324    4.0964    8.4706
   88.7647    4.0964    8.4505
   90.5701    4.0964    8.3941
   92.3023    4.0964    8.3176
   93.8211    4.0964    8.2368
   95.0034    4.0964    8.1654
   95.7534    4.0964    8.1143
   96.0103    4.0964    8.0900
 &BPNODE TNODE=3, TNPC=0, TINTC=0, &END
 &SECT1 STX=0.0, STY=0.0, STZ=0.0, SCALE=1.0, ALF=0.0, THETA=0.0, INMODE=4,
  TNODS=0, TNPS=0, TINTS=0, &END
   96.0173    6.8666    8.0900
   95.7715    6.8666    8.0667
   95.0541    6.8666    8.0178
   93.9231    6.8666    7.9495
   92.4702    6.8666    7.8723
   90.8131    6.8666    7.7991
   89.0861    6.8666    7.7451
   87.4290    6.8666    7.7259
   85.9762    6.8666    7.7532
   84.8452    6.8666    7.8293
   84.1277    6.8666    7.9464
   83.8820    6.8666    8.0900
   84.1277    6.8666    8.2336
   84.8452    6.8666    8.3507
```

```
 85.9762    6.8666    8.4268
 87.4290    6.8666    8.4541
 89.0861    6.8666    8.4349
 90.8131    6.8666    8.3809
 92.4702    6.8666    8.3077
 93.9231    6.8666    8.2305
 95.0541    6.8666    8.1622
 95.7715    6.8666    8.1133
 96.0173    6.8666    8.0900
&BPNODE TNODE=3, TNPC=0, TINTC=0, &END
&SECT1 STX=0.0, STY=0.0, STZ=0.0, SCALE=1.0, ALF=0.0, THETA=0.0, INMODE=4,
 TNODS=0, TNPS=0, TINTS=0, &END
 96.0250    9.9375    8.0900
 95.7916    9.9375    8.0679
 95.1102    9.9375    8.0215
 94.0361    9.9375    7.9566
 92.6563    9.9375    7.8832
 91.0826    9.9375    7.8138
 89.4424    9.9375    7.7625
 87.8687    9.9375    7.7442
 86.4889    9.9375    7.7702
 85.4148    9.9375    7.8424
 84.7334    9.9375    7.9536
 84.5000    9.9375    8.0900
 84.7334    9.9375    8.2264
 85.4148    9.9375    8.3376
 86.4889    9.9375    8.4098
 87.8687    9.9375    8.4358
 89.4424    9.9375    8.4175
 91.0826    9.9375    8.3662
 92.6563    9.9375    8.2968
 94.0361    9.9375    8.2234
 95.1102    9.9375    8.1585
 95.7916    9.9375    8.1121
 96.0250    9.9375    8.0900
&BPNODE TNODE=3, TNPC=0, TINTC=0, &END
&SECT1 STX=0.0, STY=0.0, STZ=0.0, SCALE=1.0, ALF=0.0, THETA=0.0, INMODE=4,
 TNODS=0, TNPS=0, TINTS=0, &END
 96.0327   13.0084    8.0900
 95.8117   13.0084    8.0691
 95.1664   13.0084    8.0251
 94.1492   13.0084    7.9637
 92.8424   13.0084    7.8942
 91.3520   13.0084    7.8284
 89.7987   13.0084    7.7798
 88.3083   13.0084    7.7625
 87.0016   13.0084    7.7871
 85.9844   13.0084    7.8555
 85.3391   13.0084    7.9608
 85.1180   13.0084    8.0900
 85.3391   13.0084    8.2192
 85.9844   13.0084    8.3245
 87.0016   13.0084    8.3929
 88.3083   13.0084    8.4175
 89.7987   13.0084    8.4002
 91.3520   13.0084    8.3516
 92.8424   13.0084    8.2858
 94.1492   13.0084    8.2163
 95.1664   13.0084    8.1549
 95.8117   13.0084    8.1109
 96.0327   13.0084    8.0900
&BPNODE TNODE=3, TNPC=0, TINTC=0, &END
&SECT1 STX=0.0, STY=0.0, STZ=0.0, SCALE=1.0, ALF=0.0, THETA=0.0, INMODE=4,
 TNODS=0, TNPS=0, TINTS=0, &END
 96.0397   15.7786    8.0900
 95.8298   15.7786    8.0701
 95.2171   15.7786    8.0284
 94.2512   15.7786    7.9700
 93.0103   15.7786    7.9040
 91.5951   15.7786    7.8416
 90.1201   15.7786    7.7955
 88.7049   15.7786    7.7790
 87.4641   15.7786    7.8024
 86.4982   15.7786    7.8674
 85.8855   15.7786    7.9673
 85.6756   15.7786    8.0900
```



```
 85.8855   15.7786    8.2127
 86.4982   15.7786    8.3126
 87.4641   15.7786    8.3776
 88.7049   15.7786    8.4010
 90.1201   15.7786    8.3845
 91.5951   15.7786    8.3384
 93.0103   15.7786    8.2760
 94.2512   15.7786    8.2100
 95.2171   15.7786    8.1516
 95.8298   15.7786    8.1099
 96.0397   15.7786    8.0900
&BPNODE TNODE=3, TNPC=0, TINTC=0, &END
&SECT1 STX=0.0, STY=0.0, STZ=0.0, SCALE=1.0, ALF=0.0, THETA=0.0, INMODE=4,
 TNODS=0, TNPS=0, TINTS=0, &END
 96.0452   17.9771    8.0900
 95.8442   17.9771    8.0710
 95.2573   17.9771    8.0310
 94.3321   17.9771    7.9751
 93.1436   17.9771    7.9119
 91.7880   17.9771    7.8521
 90.3752   17.9771    7.8079
 89.0197   17.9771    7.7921
 87.8312   17.9771    7.8145
 86.9060   17.9771    7.8767
 86.3191   17.9771    7.9725
 86.1180   17.9771    8.0900
 86.3191   17.9771    8.2075
 86.9060   17.9771    8.3033
 87.8312   17.9771    8.3655
 89.0197   17.9771    8.3879
 90.3752   17.9771    8.3721
 91.7880   17.9771    8.3279
 93.1436   17.9771    8.2681
 94.3321   17.9771    8.2049
 95.2573   17.9771    8.1490
 95.8442   17.9771    8.1090
 96.0452   17.9771    8.0900
&BPNODE TNODE=3, TNPC=0, TINTC=0, &END
&SECT1 STX=0.0, STY=0.0, STZ=0.0, SCALE=1.0, ALF=0.0, THETA=0.0, INMODE=4,
 TNODS=0, TNPS=0, TINTS=0, &END
 96.0488   19.3886    8.0900
 95.8534   19.3886    8.0715
 95.2831   19.3886    8.0326
 94.3841   19.3886    7.9783
 93.2291   19.3886    7.9169
 91.9119   19.3886    7.8588
 90.5390   19.3886    7.8158
 89.2218   19.3886    7.8006
 88.0668   19.3886    7.8223
 87.1678   19.3886    7.8828
 86.5975   19.3886    7.9758
 86.4021   19.3886    8.0900
 86.5975   19.3886    8.2042
 87.1678   19.3886    8.2972
 88.0668   19.3886    8.3577
 89.2218   19.3886    8.3794
 90.5390   19.3886    8.3642
 91.9119   19.3886    8.3212
 93.2291   19.3886    8.2631
 94.3841   19.3886    8.2017
 95.2831   19.3886    8.1474
 95.8534   19.3886    8.1085
 96.0488   19.3886    8.0900
&BPNODE TNODE=3, TNPC=0, TINTC=0, &END
&SECT1 STX=0.0, STY=0.0, STZ=0.0, SCALE=1.0, ALF=0.0, THETA=0.0, INMODE=4,
 TNODS=3, TNPS=0, TINTS=0, &END
 96.0500   19.8750    8.0900
 95.8566   19.8750    8.0717
 95.2920   19.8750    8.0332
 94.4020   19.8750    7.9795
 93.2586   19.8750    7.9186
 91.9546   19.8[illegible]    7.8611
 90.5954   19.8750    7.8186
 89.2914   19.8750    7.8035
 88.1480   19.8750    7.8250
 87.2580   19.8750    7.8848
```

```
   86.6934    19.8750     7.9770
   86.5000    19.8750     8.0900
   86.6934    19.8750     8.2030
   87.2580    19.8750     8.2952
   88.1480    19.8750     8.3550
   89.2914    19.8750     8.3765
   90.5954    19.8750     8.3614
   91.9546    19.8750     8.3189
   93.2586    19.8750     8.2614
   94.4020    19.8750     8.2005
   95.2920    19.8750     8.1468
   95.8566    19.8750     8.1083
   96.0500    19.8750     8.0900
&BPNODE TNODE=3, TNPC=0, TINTC=0, &END


&PATCH1 IREV=0, IDPAT=1, MAKE=0, KCOMP=1, KASS=1, IPATSYM=0, IPATCOP=0, &END
  FOG_VERTICAL_TAIL
&SECT1 STX=0.0, STY=0.0, STZ=0.0, SCALE=1.0, ALF=0.0, THETA=0.0, INMODE=4,
 TNODS=0, TNPS=0, TINTS=0, &END
   97.5000     0.0000    10.4000
   96.8969     0.0548    10.4000
   95.1604     0.1657    10.4000
   92.5000     0.3161    10.4000
   89.2365     0.4671    10.4000
   85.7635     0.5752    10.4000
   82.5000     0.5942    10.4000
   79.8396     0.4945    10.4000
   78.1031     0.2842    10.4000
   77.5000     0.0000    10.4000
   78.1031    -0.2842    10.4000
   79.8396    -0.4945    10.4000
   82.5000    -0.5942    10.4000
   85.7635    -0.5752    10.4000
   89.2365    -0.4671    10.4000
   92.5000    -0.3161    10.4000
   95.1604    -0.1657    10.4000
   96.8969    -0.0548    10.4000
   97.5000     0.0000    10.4000
&BPNODE TNODE=3, TNPC=0, TINTC=0, &END
&SECT1 STX=0.0, STY=0.0, STZ=0.0, SCALE=1.0, ALF=0.0, THETA=0.0, INMODE=4,
 TNODS=0, TNPS=0, TINTS=0, &END
   97.6846     0.0000    10.9614
   97.0930     0.0537    10.9614
   95.3896     0.1625    10.9614
   92.7797     0.3101    10.9614
   89.5783     0.4582    10.9614
   86.1715     0.5643    10.9614
   82.9700     0.5829    10.9614
   80.3602     0.4851    10.9614
   78.6568     0.2788    10.9614
   78.0652     0.0000    10.9614
   78.6568    -0.2788    10.9614
   80.3602    -0.4851    10.9614
   82.9700    -0.5829    10.9614
   86.1715    -0.5643    10.9614
   89.5783    -0.4582    10.9614
   92.7797    -0.3101    10.9614
   95.3896    -0.1625    10.9614
   97.0930    -0.0537    10.9614
   97.6846     0.0000    10.9614
&BPNODE TNODE=3, TNPC=0, TINTC=0, &END
&SECT1 STX=0.0, STY=0.0, STZ=0.0, SCALE=1.0, ALF=0.0, THETA=0.0, INMODE=4,
 TNODS=0, TNPS=0, TINTS=0, &END
   98.2103     0.0000    12.5601
   97.6514     0.0508    12.5601
   96.0420     0.1536    12.5601
   93.5764     0.2929    12.5601
   90.5518     0.4329    12.5601
   87.3332     0.5331    12.5601
   84.3086     0.5507    12.5601
   81.8430     0.4583    12.5601
   80.2336     0.2634    12.5601
   79.6747     0.0000    12.5601
   80.2336    -0.2634    12.5601
```

Printed by pollard from hawkeye


```
   81.8430    -0.4583    12.5601
   84.3086    -0.5507    12.5601
   87.3332    -0.5331    12.5601
   90.5518    -0.4329    12.5601
   93.5764    -0.2929    12.5601
   96.0420    -0.1536    12.5601
   97.6514    -0.0508    12.5601
   98.2103     0.0000    12.5601
&BPNODE TNODE=3, TNPC=0, TINTC=0, &END
&SECT1 STX=0.0, STY=0.0, STZ=0.0, SCALE=1.0, ALF=0.0, THETA=0.0, INMODE=4,
 TNODS=0, TNPS=0, TINTS=0, &END
   98.9970     0.0000    14.9527
   98.4870     0.0463    14.9527
   97.0185     0.1401    14.9527
   94.7686     0.2673    14.9527
   92.0088     0.3950    14.9527
   89.0718     0.4864    14.9527
   86.3119     0.5025    14.9527
   84.0621     0.4182    14.9527
   82.5936     0.2404    14.9527
   82.0836     0.0000    14.9527
   82.5936    -0.2404    14.9527
   84.0621    -0.4182    14.9527
   86.3119    -0.5025    14.9527
   89.0718    -0.4864    14.9527
   92.0088    -0.3950    14.9527
   94.7686    -0.2673    14.9527
   97.0185    -0.1401    14.9527
   98.4870    -0.0463    14.9527
   98.9970     0.0000    14.9527
&BPNODE TNODE=3, TNPC=0, TINTC=0, &END
&SECT1 STX=0.0, STY=0.0, STZ=0.0, SCALE=1.0, ALF=0.0, THETA=0.0, INMODE=4,
 TNODS=0, TNPS=0, TINTS=0, &END
   99.9250     0.0000    17.7750
   99.4727     0.0411    17.7750
   98.1703     0.1243    17.7750
   96.1750     0.2371    17.7750
   93.7274     0.3503    17.7750
   91.1226     0.4314    17.7750
   88.6750     0.4456    17.7750
   86.6797     0.3709    17.7750
   85.3773     0.2132    17.7750
   84.9250     0.0000    17.7750
   85.3773    -0.2132    17.7750
   86.6797    -0.3709    17.7750
   88.6750    -0.4456    17.7750
   91.1226    -0.4314    17.7750
   93.7274    -0.3503    17.7750
   96.1750    -0.2371    17.7750
   98.1703    -0.1243    17.7750
   99.4727    -0.0411    17.7750
   99.9250     0.0000    17.7750
&BPNODE TNODE=3, TNPC=0, TINTC=0, &END
&SECT1 STX=0.0, STY=0.0, STZ=0.0, SCALE=1.0, ALF=0.0, THETA=0.0, INMODE=4,
 TNODS=0, TNPS=0, TINTS=0, &END
  100.8530     0.0000    20.5973
  100.4584     0.0358    20.5973
   99.3222     0.1084    20.5973
   97.5814     0.2068    20.5973
   95.4459     0.3056    20.5973
   93.1735     0.3764    20.5973
   91.0381     0.3888    20.5973
   89.2973     0.3236    20.5973
   88.1610     0.1860    20.5973
   87.7664     0.0000    20.5973
   88.1610    -0.1860    20.5973
   89.2973    -0.3236    20.5973
   91.0381    -0.3888    20.5973
   93.1735    -0.3764    20.5973
   95.4459    -0.3056    20.5973
   97.5814    -0.2068    20.5973
   99.3222    -0.1084    20.5973
  100.4584    -0.0358    20.5973
  100.8530     0.0000    20.5973
&BPNODE TNODE=3, TNPC=0, TINTC=0, &END
&SECT1 STX=0.0, STY=0.0, STZ=0.0, SCALE=1.0, ALF=0.0, THETA=0.0, INMODE=4,
```

```
 TNODS=0, TNPS=0, TINTS=0, &END
 101.6397    0.0000   22.9899
 101.2940    0.0314   22.9899
 100.2986    0.0950   22.9899
  98.7736    0.1812   22.9899
  96.9029    0.2677   22.9899
  94.9121    0.3297   22.9899
  93.0414    0.3406   22.9899
  91.5164    0.2835   22.9899
  90.5210    0.1629   22.9899
  90.1753    0.0000   22.9899
  90.5210   -0.1629   22.9899
  91.5164   -0.2835   22.9899
  93.0414   -0.3406   22.9899
  94.9121   -0.3297   22.9899
  96.9029   -0.2677   22.9899
  98.7736   -0.1812   22.9899
 100.2986   -0.0950   22.9899
 101.2940   -0.0314   22.9899
 101.6397    0.0000   22.9899
&BPNODE TNODE=3, TNPC=0, TINTC=0, &END
&SECT1 STX=0.0, STY=0.0, STZ=0.0, SCALE=1.0, ALF=0.0, THETA=0.0, INMODE=4,
 TNODS=0, TNPS=0, TINTS=0, &END
 102.1654    0.0000   24.5886
 101.8524    0.0284   24.5886
 100.9511    0.0860   24.5886
  99.5703    0.1641   24.5886
  97.8764    0.2424   24.5886
  96.0738    0.2986   24.5886
  94.3800    0.3084   24.5886
  92.9991    0.2567   24.5886
  92.0978    0.1475   24.5886
  91.7848    0.0000   24.5886
  92.0978   -0.1475   24.5886
  92.9991   -0.2567   24.5886
  94.3800   -0.3084   24.5886
  96.0738   -0.2986   24.5886
  97.8764   -0.2424   24.5886
  99.5703   -0.1641   24.5886
 100.9511   -0.0860   24.5886
 101.8524   -0.0284   24.5886
 102.1654    0.0000   24.5886
&BPNODE TNODE=3, TNPC=0, TINTC=0, &END
&SECT1 STX=0.0, STY=0.0, STZ=0.0, SCALE=1.0, ALF=0.0, THETA=0.0, INMODE=4,
 TNODS=3, TNPS=0, TINTS=0, &END
 102.3500    0.0000   25.1500
 102.0485    0.0274   25.1500
 101.1802    0.0828   25.1500
  99.8500    0.1580   25.1500
  98.2182    0.2335   25.1500
  96.4818    0.2876   25.1500
  94.8500    0.2971   25.1500
  93.5198    0.2473   25.1500
  92.6515    0.1421   25.1500
  92.3500    0.0000   25.1500
  92.6515   -0.1421   25.1500
  93.5198   -0.2473   25.1500
  94.8500   -0.2971   25.1500
  96.4818   -0.2876   25.1500
  98.2182   -0.2335   25.1500
  99.8500   -0.1580   25.1500
 101.1802   -0.0828   25.1500
 102.0485   -0.0274   25.1500
 102.3500    0.0000   25.1500
&BPNODE TNODE=3, TNPC=0, TINTC=0, &END


&PATCH1 IREV=0, IDPAT=2, MAKE=0, KCOMP=1, KASS=1, IPATSYM=1, IPATCOP=0, &END
  FOG_PYLON
&SECT1 STX=0.0, STY=0.0, STZ=0.0, SCALE=1.0, ALF=0.0, THETA=0.0, INMODE=4,
 TNODS=0, TNPS=0, TINTS=0, &END
  25.8000    0.0000   14.3100
  25.8000    0.0000   14.3516
  25.8000    0.0000   14.5358
  25.8000    0.0000   14.7201
  25.8000    0.0000   14.9044
```



```
  25.8000    0.0000   15.0886
  25.8000    0.0000   15.2729
  25.8000    0.0000   15.4572
  25.8000    0.0000   15.6415
  25.8000    0.0000   15.8257
  25.8000    0.0000   16.0100
&BPNODE TNODE=3, TNPC=0, TINTC=0, &END
&SECT1 STX=0.0, STY=0.0, STZ=0.0, SCALE=1.0, ALF=0.0, THETA=0.0, INMODE=4,
 TNODS=0, TNPS=0, TINTS=0, &END
  25.9300    0.5302   14.3377
  25.9300    0.5302   14.3753
  25.9300    0.5302   14.5558
  25.9300    0.5302   14.7362
  25.9300    0.5302   14.9167
  25.9300    0.5302   15.0971
  25.9300    0.5302   15.2776
  25.9300    0.5302   15.4581
  25.9300    0.5302   15.6385
  25.9300    0.5302   15.8190
  25.9300    0.5302   15.9995
&BPNODE TNODE=3, TNPC=0, TINTC=0, &END
&SECT1 STX=0.0, STY=0.0, STZ=0.0, SCALE=1.0, ALF=0.0, THETA=0.0, INMODE=4,
 TNODS=0, TNPS=0, TINTS=0, &END
  26.3144    0.9601   14.4108
  26.3144    0.9601   14.4384
  26.3144    0.9601   14.6089
  26.3144    0.9601   14.7793
  26.3144    0.9601   14.9497
  26.3144    0.9601   15.1201
  26.3144    0.9601   15.2905
  26.3144    0.9601   15.4609
  26.3144    0.9601   15.6313
  26.3144    0.9601   15.8017
  26.3144    0.9601   15.9721
&BPNODE TNODE=3, TNPC=0, TINTC=0, &END
&SECT1 STX=0.0, STY=0.0, STZ=0.0, SCALE=1.0, ALF=0.0, THETA=0.0, INMODE=4,
 TNODS=0, TNPS=0, TINTS=0, &END
  26.9363    1.2810   14.5052
  26.9363    1.2810   14.5199
  26.9363    1.2810   14.6773
  26.9363    1.2810   14.8348
  26.9363    1.2810   14.9922
  26.9363    1.2810   15.1496
  26.9363    1.2810   15.3070
  26.9363    1.2810   15.4644
  26.9363    1.2810   15.6219
  26.9363    1.2810   15.7793
  26.9363    1.2810   15.9367
&BPNODE TNODE=3, TNPC=0, TINTC=0, &END
&SECT1 STX=0.0, STY=0.0, STZ=0.0, SCALE=1.0, ALF=0.0, THETA=0.0, INMODE=4,
 TNODS=0, TNPS=0, TINTS=0, &END
  27.7687    1.4893   14.5940
  27.7687    1.4893   14.[illegible]034
  27.7687    1.4893   14.[illegible]408
  27.7687    1.4893   14.8859
  27.7687    1.4893   15.0309
  27.7687    1.4893   15.1759
  27.7687    1.4893   15.3210
  27.7687    1.4893   15.4660
  27.7687    1.4893   15.6110
  27.7687    1.4893   15.7561
  27.7687    1.4893   15.9011
&BPNODE TNODE=3, TNPC=0, TINTC=0, &END
&SECT1 STX=0.0, STY=0.0, STZ=0.0, SCALE=1.0, ALF=0.0, THETA=0.0, INMODE=4,
 TNODS=0, TNPS=0, TINTS=0, &END
  28.7750    1.5866   14.6549
  28.7750    1.5866   14.6638
  28.7750    1.5866   14.7837
  28.7750    1.5866   14.9196
  28.7750    1.5866   15.0555
  28.7750    1.5866   15.[illegible]914
  28.7750    1.5866   15.[illegible]73
  28.7750    1.5866   15.4632
  28.7750    1.5866   15.5991
  28.7750    1.5866   15.7351
  28.7750    1.5866   15.8710
```

```
&BPNODE TNODE=3, TNPC=0, TINTC=0, &END
&SECT1 STX=0.0, STY=0.0, STZ=0.0, SCALE=1.0, ALF=0.0, THETA=0.0, INMODE=4,
 TNODS=0, TNPS=0, TINTS=0, &END
  29.9113     1.5803    14.6732
  29.9113     1.5803    14.6818
  29.9113     1.5803    14.7940
  29.9113     1.5803    14.9260
  29.9113     1.5803    15.0580
  29.9113     1.5803    15.1900
  29.9113     1.5803    15.3220
  29.9113     1.5803    15.4540
  29.9113     1.5803    15.5860
  29.9113     1.5803    15.7180
  29.9113     1.5803    15.8500
&BPNODE TNODE=3, TNPC=0, TINTC=0, &END
&SECT1 STX=0.0, STY=0.0, STZ=0.0, SCALE=1.0, ALF=0.0, THETA=0.0, INMODE=4,
 TNODS=0, TNPS=0, TINTS=0, &END
  31.1281     1.4826    14.6416
  31.1281     1.4826    14.6504
  31.1281     1.4826    14.7667
  31.1281     1.4826    14.9009
  31.1281     1.4826    15.0351
  31.1281     1.4826    15.1694
  31.1281     1.4826    15.3036
  31.1281     1.4826    15.4379
  31.1281     1.4826    15.5721
  31.1281     1.4826    15.7063
  31.1281     1.4826    15.8406
&BPNODE TNODE=3, TNPC=0, TINTC=0, &END
&SECT1 STX=0.0, STY=0.0, STZ=0.0, SCALE=1.0, ALF=0.0, THETA=0.0, INMODE=4,
 TNODS=0, TNPS=0, TINTS=0, &END
  32.3719     1.3110    14.5598
  32.3719     1.3110    14.5691
  32.3719     1.3110    14.7023
  32.3719     1.3110    14.8450
  32.3719     1.3110    14.9877
  32.3719     1.3110    15.1304
  32.3719     1.3110    15.2731
  32.3719     1.3110    15.4158
  32.3719     1.3110    15.5585
  32.3719     1.3110    15.7012
  32.3719     1.3110    15.8439
&BPNODE TNODE=3, TNPC=0, TINTC=0, &END
&SECT1 STX=0.0, STY=0.0, STZ=0.0, SCALE=1.0, ALF=0.0, THETA=0.0, INMODE=4,
 TNODS=0, TNPS=0, TINTS=0, &END
  33.5886     1.0866    14.4337
  33.5886     1.0866    14.4475
  33.5886     1.0866    14.6044
  33.5886     1.0866    14.7614
  33.5886     1.0866    14.9184
  33.5886     1.0866    15.0754
  33.5886     1.0866    15.2324
  33.5886     1.0866    15.3894
  33.5886     1.0866    15.5464
  33.5886     1.0866    15.7034
  33.5886     1.0866    15.8604
&BPNODE TNODE=3, TNPC=0, TINTC=0, &END
&SECT1 STX=0.0, STY=0.0, STZ=0.0, SCALE=1.0, ALF=0.0, THETA=0.0, INMODE=4,
 TNODS=0, TNPS=0, TINTS=0, &END
  34.7250     0.8337    14.2747
  34.7250     0.8337    14.3074
  34.7250     0.8337    14.4831
  34.7250     0.8337    14.6589
  34.7250     0.8337    14.8347
  34.7250     0.8337    15.0105
  34.7250     0.8337    15.1863
  34.7250     0.8337    15.3621
  34.7250     0.8337    15.5379
  34.7250     0.8337    15.7137
  34.7250     0.8337    15.8895
&BPNODE TNODE=3, TNPC=0, TINTC=0, &END
&SECT1 STX=0.0, STY=0.0, STZ=0.0, SCALE=1.0, ALF=0.0, THETA=0.0, INMODE=4,
 TNODS=0, TNPS=0, TINTS=0, &END
  35.7313     0.5784    14.0992
  35.7313     0.5784    14.1537
  35.7313     0.5784    14.3510
```



```
  35.7313     0.5784    14.5484
  35.7313     0.5784    14.7457
  35.7313     0.5784    14.9430
  35.7313     0.5784    15.1403
  35.7313     0.5784    15.3377
  35.7313     0.5784    15.5350
  35.7313     0.5784    15.7323
  35.7313     0.5784    15.9296
&BPNODE TNODE=3, TNPC=0, TINTC=0, &END
&SECT1 STX=0.0, STY=0.0, STZ=0.0, SCALE=1.0, ALF=0.0, THETA=0.0, INMODE=4,
 TNODS=0, TNPS=0, TINTS=0, &END
  36.5637     0.3462    13.9276
  36.5637     0.3462    14.0041
  36.5637     0.3462    14.2235
  36.5637     0.3462    14.4428
  36.5637     0.3462    14.6622
  36.5637     0.3462    14.8815
  36.5637     0.3462    15.1009
  36.5637     0.3462    15.3203
  36.5637     0.3462    15.5396
  36.5637     0.3462    15.7590
  36.5637     0.3462    15.9783
&BPNODE TNODE=3, TNPC=0, TINTC=0, &END
&SECT1 STX=0.0, STY=0.0, STZ=0.0, SCALE=1.0, ALF=0.0, THETA=0.0, INMODE=4,
 TNODS=0, TNPS=0, TINTS=0, &END
  37.1856     0.1609    13.7823
  37.1856     0.1609    13.8781
  37.1856     0.1609    14.1173
  37.1856     0.1609    14.3565
  37.1856     0.1609    14.5957
  37.1856     0.1609    14.8349
  37.1856     0.1609    15.0741
  37.1856     0.1609    15.3134
  37.1856     0.1609    15.5526
  37.1856     0.1609    15.7918
  37.1856     0.1609    16.0310
&BPNODE TNODE=3, TNPC=0, TINTC=0, &END
&SECT1 STX=0.0, STY=0.0, STZ=0.0, SCALE=1.0, ALF=0.0, THETA=0.0, INMODE=4,
 TNODS=0, TNPS=0, TINTS=0, &END
  37.5700     0.0413    13.6845
  37.5700     0.0413    13.7951
  37.5700     0.0413    14.0488
  37.5700     0.0413    14.3025
  37.5700     0.0413    14.5562
  37.5700     0.0413    14.8099
  37.5700     0.0413    15.0636
  37.5700     0.0413    15.3173
  37.5700     0.0413    15.5710
  37.5700     0.0413    15.8247
  37.5700     0.0413    16.0784
&BPNODE TNODE=3, TNPC=0, TINTC=0, &END
&SECT1 STX=0.0, STY=0.0, STZ=0.0, SCALE=1.0, ALF=0.0, THETA=0.0, INMODE=4,
 TNODS=3, TNPS=0, TINTS=0, &END
  37.7000     0.0000    13.6500
  37.7000     0.0000    13.7663
  37.7000     0.0000    14.0256
  37.7000     0.0000    14.2849
  37.7000     0.0000    14.5442
  37.7000     0.0000    14.8035
  37.7000     0.0000    15.0628
  37.7000     0.0000    15.3221
  37.7000     0.0000    15.5814
  37.7000     0.0000    15.8407
  37.7000     0.0000    16.1000
&BPNODE TNODE=3, TNPC=0, TINTC=0, &END


&PATCH1 IREV=0, IDPAT=2, MAKE=0, KCOMP=1, KASS=1, IPATSYM=1, IPATCOP=0, &END
  FOG_ENGINE_POD
&SECT1 STX=0.0, STY=0.0, STZ=0.0, SCALE=1.0, ALF=0.0, THETA=0.0, INMODE=4,
 TNODS=0, TNPS=0, TINTS=0, &END
  16.5000     0.0000    20.4000
  16.5000     0.0000    20.4000
  16.5000     0.0000    20.4000
  16.5000     0.0000    20.4000
```

Printed by pollard from hawkeye


```
     16.5000     0.0000    20.4000
     16.5000     0.0000    20.4000
     16.5000     0.0000    20.4000
     16.5000     0.0000    20.4000
     16.5000     0.0000    20.4000
     16.5000     0.0000    20.4000
     16.5000     0.0000    20.4000
 &BPNODE TNODE=3, TNPC=0, TINTC=0, &END
 &SECT1 STX=0.0, STY=0.0, STZ=0.0, SCALE=1.0, ALF=0.0, THETA=0.0, INMODE=4,
  TNODS=0, TNPS=0, TINTS=0, &END
     16.7895     0.0000    19.7036
     16.7895     0.1802    19.7381
     16.7895     0.3338    19.8311
     16.7895     0.4530    19.9692
     16.7895     0.5342    20.1491
     16.7895     0.5642    20.3542
     16.7895     0.5363    20.5590
     16.7895     0.4556    20.7374
     16.7895     0.3349    20.8747
     16.7895     0.1800    20.9661
     16.7895     0.0000    20.9995
 &BPNODE TNODE=3, TNPC=0, TINTC=0, &END
 &SECT1 STX=0.0, STY=0.0, STZ=0.0, SCALE=1.0, ALF=0.0, THETA=0.0, INMODE=4,
  TNODS=0, TNPS=0, TINTS=0, &END
     17.6455     0.0000    18.9621
     17.6455     0.4134    19.0316
     17.6455     0.7696    19.2229
     17.6455     1.0398    19.5042
     17.6455     1.2183    19.8707
     17.6455     1.2728    20.2955
     17.6455     1.1966    20.7383
     17.6455     1.0093    21.1240
     17.6455     0.7418    21.4169
     17.6455     0.3972    21.6150
     17.6455     0.0000    21.6870
 &BPNODE TNODE=3, TNPC=0, TINTC=0, &END
 &SECT1 STX=0.0, STY=0.0, STZ=0.0, SCALE=1.0, ALF=0.0, THETA=0.0, INMODE=4,
  TNODS=0, TNPS=0, TINTS=0, &END
     19.0305     0.0000    17.6702
     19.0305     0.7979    17.7380
     19.0305     1.3113    17.9554
     19.0305     1.6163    18.3439
     19.0305     1.7872    18.9932
     19.0305     1.8434    19.9738
     19.0305     1.7865    20.8477
     19.0305     1.5906    21.4633
     19.0305     1.2554    21.8603
     19.0305     0.7367    22.0950
     19.0305     0.0000    22.1718
 &BPNODE TNODE=3, TNPC=0, TINTC=0, &END
 &SECT1 STX=0.0, STY=0.0, STZ=0.0, SCALE=1.0, ALF=0.0, THETA=0.0, INMODE=4,
  TNODS=0, TNPS=0, TINTS=0, &END
     20.8840     0.0000    16.8347
     20.8840     1.3042    16.8570
     20.8840     1.8746    16.9602
     20.8840     2.0812    17.2524
     20.8840     2.1525    18.0117
     20.8840     2.1689    19.5462
     20.8840     2.1572    21.0957
     20.8840     2.0882    21.8715
     20.8840     1.8780    22.1653
     20.8840     1.3111    22.2650
     20.8840     0.0000    22.2869
 &BPNODE TNODE=3, TNPC=0, TINTC=0, &END
 &SECT1 STX=0.0, STY=0.0, STZ=0.0, SCALE=1.0, ALF=0.0, THETA=0.0, INMODE=4,
  TNODS=0, TNPS=0, TINTS=0, &END
     23.1250     0.0000    16.3511
     23.1250     1.4033    16.3708
     23.1250     2.0127    16.4691
     23.1250     2.2204    16.7715
     23.1250     2.2[illegible]    17.5999
     23.1250     [illegible]    19.2276
     23.1250     2.2915    20.8939
     23.1250     2.2329    21.7791
     23.1250     2.0307    22.0844
     23.1250     1.4246    22.1766
```



```
     23.1250     0.0000    22.1945
 &BPNODE TNODE=3, TNPC=0, TINTC=0, &END
 &SECT1 STX=0.0, STY=0.0, STZ=0.0, SCALE=1.0, ALF=0.0, THETA=0.0, INMODE=4,
  TNODS=0, TNPS=0, TINTS=0, &END
     25.6555     0.0000    16.0481
     25.6555     1.4141    16.0679
     25.6555     2.0188    16.1668
     25.6555     2.2226    16.4703
     25.6555     2.2870    17.3089
     25.6555     2.2999    18.9446
     25.6555     2.2912    20.6132
     25.6555     2.2327    21.5039
     25.6555     2.0316    21.8124
     25.6555     1.4305    21.9057
     25.6555     0.0000    21.9240
 &BPNODE TNODE=3, TNPC=0, TINTC=0, &END
 &SECT1 STX=0.0, STY=0.0, STZ=0.0, SCALE=1.0, ALF=0.0, THETA=0.0, INMODE=4,
  TNODS=0, TNPS=0, TINTS=0, &END
     28.3650     0.0000    15.8494
     28.3650     1.4144    15.8682
     28.3650     2.0199    15.9622
     28.3650     2.2237    16.2532
     28.3650     2.2875    17.0611
     28.3650     2.3000    18.6632
     28.3650     2.2900    20.2862
     28.3650     2.2287    21.1215
     28.3650     2.0240    21.4109
     28.3650     1.4190    21.4999
     28.3650     0.0000    21.5175
 &BPNODE TNODE=3, TNPC=0, TINTC=0, &END
 &SECT1 STX=0.0, STY=0.0, STZ=0.0, SCALE=1.0, ALF=0.0, THETA=0.0, INMODE=4,
  TNODS=0, TNPS=0, TINTS=0, &END
     31.1350     0.0000    15.7474
     31.1350     1.3961    15.7637
     31.1350     2.0103    15.8456
     31.1350     2.2203    16.1006
     31.1350     2.2865    16.8111
     31.1350     2.3000    18.3044
     31.1350     2.2888    19.8200
     31.1350     2.2242    20.5497
     31.1350     2.0130    20.8000
     31.1350     1.3979    20.8773
     31.1350     0.0000    20.8925
 &BPNODE TNODE=3, TNPC=0, TINTC=0, &END
 &SECT1 STX=0.0, STY=0.0, STZ=0.0, SCALE=1.0, ALF=0.0, THETA=0.0, INMODE=4,
  TNODS=0, TNPS=0, TINTS=0, &END
     33.8445     0.0000    15.8093
     33.8445     1.3627    15.8218
     33.8445     1.9940    15.8864
     33.8445     2.2152    16.0907
     33.8445     2.2852    16.6649
     33.8445     2.3000    17.9747
     33.8445     2.2868    19.3038
     33.8445     2.2166    19.8875
     33.8445     1.9942    20.0845
     33.8445     1.3615    20.1457
     33.8445     0.0000    20.1575
 &BPNODE TNODE=3, TNPC=0, TINTC=0, &END
 &SECT1 STX=0.0, STY=0.0, STZ=0.0, SCALE=1.0, ALF=0.0, THETA=0.0, INMODE=4,
  TNODS=0, TNPS=0, TINTS=0, &END
     36.3750     0.0000    15.9892
     36.3750     1.3053    15.9975
     36.3750     1.9691    16.0428
     36.3750     2.2080    16.1903
     36.3750     2.2835    16.6129
     36.3750     2.3000    17.6647
     36.3750     2.2844    18.7297
     36.3750     2.2062    19.1542
     36.3750     1.9627    19.2941
     36.3750     1.2912    19.3366
     36.3750     0.0000    19.3443
 &BPNODE TNODE=3, TNPC=0, TINTC=0, &END
 &SECT1 STX=0.0, STY=0.0, STZ=0.0, SCALE=1.0, ALF=0.0, THETA=0.0, INMODE=4,
  TNODS=0, TNPS=0, TINTS=0, &END
     38.6160     0.0000    16.2138
     38.6160     1.1972    16.2181
```

```
  38.6160    1.9280    16.2456
  38.6160    2.1972    16.3400
  38.6160    2.2813    16.6192
  38.6160    2.3000    17.3609
  38.6160    2.2827    18.1311
  38.6160    2.1968    18.4163
  38.6160    1.9293    18.5068
  38.6160    1.2029    18.5335
  38.6160    0.0000    18.5378
&BPNODE TNODE=3, TNPC=0, TINTC=0, &END
&SECT1 STX=0.0, STY=0.0, STZ=0.0, SCALE=1.0, ALF=0.0, THETA=0.0, INMODE=4,
 TNODS=0, TNPS=0, TINTS=0, &END
  40.4695    0.0000    16.4386
  40.4695    1.0541    16.4404
  40.4695    1.8638    16.4540
  40.4695    2.1814    16.5048
  40.4695    2.2786    16.6646
  40.4695    2.3000    17.1216
  40.4695    2.2796    17.6011
  40.4695    2.1790    17.7620
  40.4695    1.8677    17.8097
  40.4695    1.0610    17.8229
  40.4695    0.0000    17.8247
&BPNODE TNODE=3, TNPC=0, TINTC=0, &END
&SECT1 STX=0.0, STY=0.0, STZ=0.0, SCALE=1.0, ALF=0.0, THETA=0.0, INMODE=4,
 TNODS=0, TNPS=0, TINTS=0, &END
  41.8545    0.0000    16.6286
  41.8545    0.8776    16.6291
  41.8545    1.7102    16.6332
  41.8545    2.1282    16.6520
  41.8545    2.2589    16.7231
  41.8545    2.2846    16.9507
  41.8545    2.2559    17.1850
  41.8545    2.1229    17.2486
  41.8545    1.7061    17.2659
  41.8545    0.8776    17.2699
  41.8545    0.0000    17.2703
&BPNODE TNODE=3, TNPC=0, TINTC=0, &END
&SECT1 STX=0.0, STY=0.0, STZ=0.0, SCALE=1.0, ALF=0.0, THETA=0.0, INMODE=4,
 TNODS=0, TNPS=0, TINTS=0, &END
  42.7105    0.0000    16.7554
  42.7105    0.6609    16.7566
  42.7105    1.2924    16.7619
  42.7105    1.7606    16.7743
  42.7105    2.0332    16.7974
  42.7105    2.1274    16.8434
  42.7105    2.0340    16.8795
  42.7105    1.7674    16.9014
  42.7105    1.3047    16.9135
  42.7105    0.6710    16.9187
  42.7105    0.0000    16.9198
&BPNODE TNODE=3, TNPC=0, TINTC=0, &END
&SECT1 STX=0.0, STY=0.0, STZ=0.0, SCALE=1.0, ALF=0.0, THETA=0.0, INMODE=4,
 TNODS=3, TNPS=0, TINTS=0, &END
  43.0000    0.0000    16.8000
  43.0000    0.0000    16.8000
  43.0000    0.0000    16.8000
  43.0000    0.0000    16.8000
  43.0000    0.0000    16.8000
  43.0000    0.0000    16.8000
  43.0000    0.0000    16.8000
  43.0000    0.0000    16.8000
  43.0000    0.0000    16.8000
  43.0000    0.0000    16.8000
  43.0000    0.0000    16.8000
&BPNODE TNODE=3, TNPC=0, TINTC=0, &END


&PATCH1 IREV=0, IDPAT=2, MAKE=0, KCOMP=1, KASS=1, IPATSYM=1, IPATCOP=0, &END
 FOG_UAV_BOOM (10X12) CLOSED ENDS
&SECT1 STX=0.0, STY=0.0, STZ=0.0, SCALE=1.0, ALF=0.0, THETA=0.0. INMODE=4,
 TNODS=0, TNPS=0, TINTS=0, &END
  53.5000    0.0000    9.3750
  53.5000    0.0000    9.3750
  53.5000    0.0000    9.3750
  53.5000    0.0000    9.3750
```



```
  53.5000    0.0000    9.3750
  53.5000    0.0000    9.3750
  53.5000    0.0000    9.3750
  53.5000    0.0000    9.3750
  53.5000    0.0000    9.3750
  53.5000    0.0000    9.3750
  53.5000    0.0000    9.3750
&BPNODE TNODE=3, TNPC=0, TINTC=0, &END
&SECT1 STX=0.0, STY=0.0, STZ=0.0, SCALE=1.0, ALF=0.0, THETA=0.0, INMODE=4,
 TNODS=0, TNPS=0, TINTS=0, &END
  53.5000    0.0000    8.5178
  53.5000    0.2731    8.5625
  53.5000    0.5094    8.6857
  53.5000    0.6900    8.8665
  53.5000    0.8127    9.1024
  53.5000    0.8572    9.3738
  53.5000    0.8121    9.6495
  53.5000    0.6885    9.8855
  53.5000    0.5074   10.0658
  53.5000    0.2712   10.1882
  53.5000    0.0000   10.2322
&BPNODE TNODE=3, TNPC=0, TINTC=0, &END
&SECT1 STX=0.0, STY=0.0, STZ=0.0, SCALE=1.0, ALF=0.0, THETA=0.0, INMODE=4,
 TNODS=0, TNPS=0, TINTS=0, &END
  55.1002    0.0000    8.5000
  55.1002    0.2785    8.5455
  55.1002    0.5195    8.6711
  55.1002    0.7046    8.8564
  55.1002    0.8296    9.0971
  55.1002    0.8750    9.3739
  55.1002    0.8290    9.6548
  55.1002    0.7031    9.8956
  55.1002    0.5175   10.0804
  55.1002    0.2766   10.2051
  55.1002    0.0000   10.2500
&BPNODE TNODE=3, TNPC=0, TINTC=0, &END
&SECT1 STX=0.0, STY=0.0, STZ=0.0, SCALE=1.0, ALF=0.0, THETA=0.0, INMODE=4,
 TNODS=0, TNPS=0, TINTS=0, &END
  57.1102    0.0000    8.5000
  57.1102    0.2785    8.5455
  57.1102    0.5195    8.6711
  57.1102    0.7046    8.8564
  57.1102    0.8296    9.0971
  57.1102    0.8750    9.3739
  57.1102    0.8290    9.6548
  57.1102    0.7031    9.8956
  57.1102    0.5175   10.0804
  57.1102    0.2766   10.2051
  57.1102    0.0000   10.2500
&BPNODE TNODE=3, TNPC=0, TINTC=0, &END
&SECT1 STX=0.0, STY=0.0, STZ=0.0, SCALE=1.0, ALF=0.0, THETA=0.0, INMODE=4,
 TNODS=0, TNPS=0, TINTS=0, &END
  59.9757    0.0000    8.5000
  59.9757    0.2785    8.5455
  59.9757    0.5195    8.6711
  59.9757    0.7046    8.8564
  59.9757    0.8296    9.0971
  59.9757    0.8750    9.3739
  59.9757    0.8290    9.6548
  59.9757    0.7031    9.8956
  59.9757    0.5175   10.0804
  59.9757    0.2766   10.2051
  59.9757    0.0000   10.2500
&BPNODE TNODE=3, TNPC=0, TINTC=0, &END
&SECT1 STX=0.0, STY=0.0, STZ=0.0, SCALE=1.0, ALF=0.0, THETA=0.0, INMODE=4,
 TNODS=0, TNPS=0, TINTS=0, &END
  63.8927    0.0000    8.5000
  63.8927    0.2785    8.5455
  63.8927    0.5195    8.6711
  63.8927    0.7046    8.8564
  63.8927    0.8296    9.0971
  63.8927    0.8750    9.3739
  63.8927    0.8290    9.6548
  63.8927    0.7031    9.8956
  63.8927    0.5175   10.0804
  63.8927    0.2766   10.2051
```

```
 63.8927     0.0000    10.2500
&BPNODE TNODE=3, TNPC=0, TINTC=0, &END
&SECT1 STX=0.0, STY=0.0, STZ=0.0, SCALE=1.0, ALF=0.0, THETA=0.0, INMODE=4,
 TNODS=0, TNPS=0, TINTS=0, &END
  71.0000    0.0000    8.5000
  71.0000    0.2785    8.5455
  71.0000    0.5195    8.6711
  71.0000    0.7046    8.8564
  71.0000    0.8296    9.0971
  71.0000    0.8750    9.3739
  71.0000    0.8290    9.6548
  71.0000    0.7031    9.8956
  71.0000    0.5175   10.0804
  71.0000    0.2766   10.2051
  71.0000    0.0000   10.2500
&BPNODE TNODE=3, TNPC=0, TINTC=0, &END
&SECT1 STX=0.0, STY=0.0, STZ=0.0, SCALE=1.0, ALF=0.0, THETA=0.0, INMODE=4,
 TNODS=0, TNPS=0, TINTS=0, &END
  78.1073    0.0000    8.5000
  78.1073    0.2785    8.5455
  78.1073    0.5195    8.6711
  78.1073    0.7046    8.8564
  78.1073    0.8296    9.0971
  78.1073    0.8750    9.3739
  78.1073    0.8290    9.6548
  78.1073    0.7031    9.8956
  78.1073    0.5175   10.0804
  78.1073    0.2766   10.2051
  78.1073    0.0000   10.2500
&BPNODE TNODE=3, TNPC=0, TINTC=0, &END
&SECT1 STX=0.0, STY=0.0, STZ=0.0, SCALE=1.0, ALF=0.0, THETA=0.0, INMODE=4,
 TNODS=0, TNPS=0, TINTS=0, &END
  82.0243    0.0000    8.5000
  82.0243    0.2785    8.5455
  82.0243    0.5195    8.6711
  82.0243    0.7046    8.8564
  82.0243    0.8296    9.0971
  82.0243    0.8750    9.3739
  82.0243    0.8290    9.6548
  82.0243    0.7031    9.8956
  82.0243    0.5175   10.0804
  82.0243    0.2766   10.2051
  82.0243    0.0000   10.2500
&BPNODE TNODE=3, TNPC=0, TINTC=0, &END
&SECT1 STX=0.0, STY=0.0, STZ=0.0, SCALE=1.0, ALF=0.0, THETA=0.0, INMODE=4,
 TNODS=0, TNPS=0, TINTS=0, &END
  84.8898    0.0000    8.5000
  84.8898    0.2785    8.5455
  84.8898    0.5195    8.6711
  84.8898    0.7046    8.8564
  84.8898    0.8296    9.0971
  84.8898    0.8750    9.3739
  84.8898    0.8290    9.6548
  84.8898    0.7031    9.8956
  84.8898    0.5175   10.0804
  84.8898    0.2766   10.2051
  84.8898    0.0000   10.2500
&BPNODE TNODE=3, TNPC=0, TINTC=0, &END
&SECT1 STX=0.0, STY=0.0, STZ=0.0, SCALE=1.0, ALF=0.0, THETA=0.0, INMODE=4,
 TNODS=0, TNPS=0, TINTS=0, &END
  86.8998    0.0000    8.5000
  86.8998    0.2785    8.5455
  86.8998    0.5195    8.6711
  86.8998    0.7046    8.8564
  86.8998    0.8296    9.0971
  86.8998    0.8750    9.3739
  86.8998    0.8290    9.6548
  86.8998    0.7031    9.8956
  86.8998    0.5175   10.0804
  86.8998    0.2766   10.2051
  86.8998    0.0000   10.2500
&BPNODE TNODE=3, TNPC=0, TINTC=0, &END
&SECT1 STX=0.0, STY=0.0, STZ=0.0, SCALE=1.0, ALF=0.0, THETA=0.0, INMODE=4,
 TNODS=0, TNPS=0, TINTS=0, &END
  88.5002    0.0000    8.5178
  88.5002    0.2731    8.5625
```



```
  88.5002    0.5094    8.6857
  88.5002    0.6900    8.8665
  88.5002    0.8127    9.1024
  88.5002    0.8572    9.3738
  88.5002    0.8121    9.6495
  88.5002    0.6885    9.8855
  88.5002    0.5074   10.0658
  88.5002    0.2712   10.1882
  88.5002    0.0000   10.2322
&BPNODE TNODE=3, TNPC=0, TINTC=0, &END
&SECT1 STX=0.0, STY=0.0, STZ=0.0, SCALE=1.0, ALF=0.0, THETA=0.0, INMODE=4,
 TNODS=5, TNPS=0, TINTS=0, &END
  88.5000    0.0000    9.3750
  88.5000    0.0000    9.3750
  88.5000    0.0000    9.3750
  88.5000    0.0000    9.3750
  88.5000    0.0000    9.3750
  88.5000    0.0000    9.3750
  88.5000    0.0000    9.3750
  88.5000    0.0000    9.3750
  88.5000    0.0000    9.3750
  88.5000    0.0000    9.3750
  88.5000    0.0000    9.3750
&BPNODE TNODE=3, TNPC=0, TINTC=0, &END


&WAKE1   IDWAK=1,        IFLXW=1,       ITRFTZ= 1,     INTRW= 0,       &END
 RIGHT_WING_WAKE
 &WAKE2   KWPACH=17,      KWSIDE=4,      KWLINE=1,      KWPAN1=0,
          KWPAN2=0,      NODEW=0,       INITIAL=0,                      &END
 &WAKE2   KWPACH=15,      KWSIDE=4,      KWLINE=1,      KWPAN1=0,
          KWPAN2=0,      NODEW=0,       INITIAL=0,                      &END
 &WAKE2   KWPACH=13,      KWSIDE=4,      KWLINE=1,      KWPAN1=0,
          KWPAN2=0,      NODEW=3,       INITIAL=0,                      &END

 &WAKE1   IDWAK=1,        IFLXW=1,       ITRFTZ= 1,     INTRW= 0,       &END
  LEFT_WING_WAKE
 &WAKE2   KWPACH=18,      KWSIDE=4,      KWLINE=1,      KWPAN1=0,
          KWPAN2=0,      NODEW=0,       INITIAL=0,                      &END
 &WAKE2   KWPACH=16,      KWSIDE=4,      KWLINE=1,      KWPAN1=0,
          KWPAN2=0,      NODEW=0,       INITIAL=0,                      &END
 &WAKE2   KWPACH=14,      KWSIDE=4,      KWLINE=1,      KWPAN1=0,
          KWPAN2=0,      NODEW=3,       INITIAL=0,                      &END


 &WAKE1   IDWAK=1,        IFLXW=1,       ITRFTZ= 1,     INTRW= 0,       &END
  RIGHT_HORIZ_TAIL_WAKE
 &WAKE2   KWPACH=21,      KWSIDE=4,      KWLINE=1,      KWPAN1=0,
          KWPAN2=0,      NODEW=3,       INITIAL=0,                      &END

 &WAKE1   IDWAK=1,        IFLXW=1,       ITRFTZ= 1,     INTRW= 0,       &END
 LEFT_HORIZ_TAIL_WAKE
 &WAKE2   KWPACH=22,      KWSIDE=4,      KWLINE=1,      KWPAN1=0,
          KWPAN2=0,      NODEW=3,       INITIAL=0,                      &END

 &WAKE1   IDWAK=1,        IFLXW=1,       ITRFTZ= 1,     INTRW= 1,       &END
  VERT_TAIL_WAKE
 &WAKE2   KWPACH=23,      KWSIDE=4,      KWLINE=1,      KWPAN1=0,
          KWPAN2=0,      NODEW=5,       INITIAL=0,                      &END

 &WAKE1   IDWAK=1,        IFLXW=1,       ITRFTZ= 1,     INTRW= 1,       &END
  ENGINE_PYLON_WAKE
 &WAKE2   KWPACH=24,      KWSIDE=3,      KWLINE=0,      KWPAN1=0,
          KWPAN2=0,      NODEW=3,       INITIAL=0,                      &END


 &WAKE1   IDWAK=1,        IFLXW=0,       ITRFTZ= 1,     INTRW= 1,       &END
  LEFT_ENGINE_POD_WAKE
 &WAKE2   KWPACH=27,      KWSIDE=1,      KWLINE=15,     KWPAN1=6,
          KWPAN2=10,     NODEW=5,       INITIAL=0,                       &END


 &WAKE1   IDWAK=1,        IFLXW=0,       ITRFTZ= 1,     INTRW= 1,       &END
  RIGHT_ENGINE_POD_WAKE
 &WAKE2   KWPACH=26,      KWSIDE=1,      KWLINE=15,     KWPAN1=6,
          KWPAN2=10,     NODEW=3,       INITIAL=0,                       &END
```

```
&ONSTRM  NONSL =0,  KPSL =
1,2,3,4,5,6,7,8,9,10,11,117,115,113,111,109,107,105,103,102,197,195,193,191,
189,187,185,183,1937,1938,1939,1940,1941,2890,2908,2926,2944,2962,2980,
2998,1073,1045,1017,989,961,933,905,2638,2616,2594,2572,2550,2528,2506,2584,     &EN
D

&BLPARAM RN =929000,    VISC = 0.022641, NSLBL = 1,2,3,4,5,6,7,8,9,10,11,
12,13,14,15,16,17,18,19,20,21,22,23,24,25,26,27,28,29,30,31,32,33,34,35,36,37,38,
39,40,41,42,43,44,45,46,47,48,49,50,51,52,53,54,55,      &END

&VS1      NVOLR= 0,        NVOLC= 0,                                      &END
&VS2      X0=    -0.1000, Y0=     1.5000, Z0=    -0.1000, INTVSR= 1,      &END
&VS3      X1=    -0.1000, Y1=     1.5000, Z1=     0.1000, NPT1=  0,       &END
&VS4      X2=    -0.1000, Y2=     1.5000, Z2=     0.1000, NPT2= 20,       &END
&VS5      X3=     1.1000, Y3=     1.5000, Z3=    -0.1000, NPT3= 25,       &END

&VS6      XR0=    2.0000, YR0=    2.0000, ZR0=    0.0000, INTVSC= 1,      &END
&VS7      XR1=    4.0000, YR1=    2.0000, ZR1=    0.0000,
          XR2=    2.0000, YR2=    2.0000, ZR2=    1.0000,                 &END
&VS8      R1=     0.1000, R2=     1.0000, PHI1=  0.0,     PHI2=360.0,     &END
&VS9      NRAD=   5,       NPHI=  12,      NLEN=  3,                      &END

&SLIN1    NSTLIN=4,                                                       &END
&SLIN2    SX0=   -6.5000, SY0=    2.50000, SZ0=   7.5000,
          SU=     2.0000, SD=    2.0000, DS=     0.100, INTSL= 1,        &END
&SLIN2    SX0=   -8.25000, SY0=    0.00000, SZ0=   7.5000,
          SU=     2.0000, SD=    2.0000, DS=     0.100, INTSL= 1,        &END
&SLIN2    SX0=   -6.5000, SY0=    2.50000, SZ0=   7.5000,
          SU=    15.0000, SD=    100.0000, DS=     0.500, INTSL= 1,        &END
&SLIN2    SX0=   -8.25000, SY0=    0.00000, SZ0=   7.5000,
          SU=    15.0000, SD=    100.0000, DS=     0.500, INTSL= 1,        &END
```

LIST OF REFERENCES

1. Papageorgiou, E., "*Development of a Dynamic Model for a UAV*," Master's Thesis, Naval Postgraduate School, Monterey, CA, March 1997.

2. Garrison, P., and Pinella, D., *CMARC User's Guide*, AeroLogic, Inc, http://www.iac.net/~aerol, 1996.

3. Bertin, J. J., and Smith, M. L., *Aerodynamics for Engineers*, Prentice Hall, 1989.

4. Ashby, D. L., Dudley, M. R., Iguchi, S. K., Browne, L., and Katz, J., *Potential Flow Theory and Operation Guide for the Panel Code PMARC_12*, NASA TM-102851, Ames Research Center, Moffet Field, CA., December 1992.

5. Anderson, J. D., *Fundamentals of Aerodynamics*, McGraw-Hill, Inc., 1991.

6. Lambert, M. A., *Evaluation of the NASA-AMES Panel Method (PMARC) for Aerodynamic Missile Design*, Master's Thesis, Naval Postgraduate School, CA, September, 1995.

7. Tuncer, I. H., and Platzer, M. F., *PMARC Potential Flow Solutions with Wakes Over an Ogive Cylinder at High Incidence*, AIAA Paper No. 97-1968, American Institute of Aeronautics and Astronautics, June 1997.

8. Cebeci, T., "*Computation of Three-Dimensional Boundary Layers Including Separation*," VKI Lecture Series, Douglas Aircraft Company, April 1986.

9. Young, A. D., *Boundary Layers*, American Institute of Aeronautics, 1989.

10. Jones, K. D., and Center, K. B., "*Numerical Wake Visualization for Airfoils Undergoing Forced and Aeroelastic Motions*," AIAA Paper No. 96-0055, January 1996.

11 Nowak, L. M., *Computational Investigations of a NACA 0012 Airfoil in Low Reynolds Number Flows*, Master's Thesis, Naval Postgraduate School, Monterey, CA, September 1992.

12. Kreplin, H. P., "Three-Dimensional Boundary Layer and Flow Field Data of an Inclined Prolate Spheroid," *AGARD Advisory Report No. 303: A Selection of Experimental Test Cases for the Validation of CFD Codes*, Volumes I and II, North Atlantic Treaty Organization, August 1994.

13. *Performance Phase Textbook-Volume I,* USAF Test Pilot School, Edwards AFB, CA., June 1988.

14. Nicolai, L. M., *Fundamentals of AIRCRAFT DESIGN,* METs, Inc., 1984.

15. Walden, A. B., van Dam, C. P., and Brandon, J. M., *Modeling of the Interaction Between a Lifting Wing and a Following Aircraft and Comparison with Experimental Results,* AIAA 96-0771, 34th Aerospace Sciences Meeting and Exhibit, Reno, NV, January 1996.

INITIAL DISTRIBUTION LIST

1. Defense Technical Information Center 2
   8725 John J. Kingman Road, Ste 0944
   Ft. Belvoir, VA 22060-6218

2. Dudley Knox Library 2
   Naval Postgraduate School
   411 Dyer Rd.
   Monterey, CA 93943-5101

3. Chairman 1
   Department of Aeronautics and Astronautics, Code AA
   Naval Postgraduate School
   699 Dyer Road, Room 137
   Monterey, CA 93943-5106

4. Dr. Max F. Platzer 5
   Department of Aeronautics and Astronautics, Code AA/PL
   Naval Postgraduate School
   699 Dyer Road, Room 137
   Monterey, CA 93943-5106

5. Dr. Ismail H. Tuncer 1
   Department of Aeronautics and Astronautics, Code AA
   Naval Postgraduate School
   699 Dyer Road, Room 137
   Monterey, CA 93943-5106

6. Dr. Kevin Jones 1
   Department of Aeronautics and Astronautics, Code AA
   Naval Postgraduate School
   699 Dyer Road, Room 137
   Monterey, CA 93943-5106

7. LCDR Stephen J. Pollard 2
   Department of Aviation Safety
   Naval Postgraduate School
   1 University Circle
   Monterey, CA 93943-5106

8. Peter Garrison 1
AeroLogic, Inc.
1613 Altivo Way
Los Angeles, CA 90026